

University of Nottingham
UK | CHINA | MALAYSIA



Investigating *agr* Quorum Sensing and Autoinducing Peptide Biosynthesis in *Staphylococcus aureus*

Thesis submitted to the University of Nottingham for the degree of Doctor of Philosophy

Isobel Blower

February 2023

Declaration

I hereby declare that, unless otherwise acknowledged, the work presented in this thesis is my own. None of this work has been submitted in whole or in part for another degree at the University of Nottingham or any other institute of learning.

Isobel Blower, 2023

Covid Impact Statement

This project was adversely affected by the COVID-19 pandemic as outlined below.

Chapter 3 of this thesis outlines the development of bioluminescent reporters for monitoring *agr* activation and inhibition in *Staphylococcus aureus*. This work was performed at the beginning of the PhD project which commenced in September 2019. The original aim of this thesis was to develop these reporters further and to test these in *in vivo* models, using these to develop real time reporters for *agr* activation and inhibition. However, in March 2020, the laboratory closed for 6 months and no lab work could be performed in this time. On return to the lab, shift work was employed with work allowed in the laboratory between the hours of 6am-2pm. This continued for a further 12 months until late July 2021. A three month extension was granted to complete the project however due to this severe disruption in lab work, the aim of this PhD changed. There was no possibility of commencing *in vivo* animal work at this time and so the project shifted to focus on investigating *agr* protein interactions *in vitro*. This work is continued in Chapters 4, 5 and 6. This is the reason behind the lack of continuation developing the *agr* bioreporters and the shift in the focus between Chapter 3 and the other results chapters.

Abstract

Staphylococcus aureus is a high priority pathogen which has generated resistance to multiple antibiotics meaning it is difficult to treat. Due to this, novel treatments for *S. aureus* infections are being investigated including the development of virulence factor inhibitors. Inhibiting the virulence of the bacterium will assist immune clearance, reducing the need for exposure to bactericidal antibiotics which provide pressure for resistance to emerge. In *S. aureus* virulence is largely controlled by the *agr* quorum sensing (QS) system. This is a means of bacterial communication via the release and detection of a signal molecule autoinducing peptide (AIP).

AIPs are produced by post-translational processing of precursor peptide AgrD by cytoplasmic endopeptidase AgrB. AgrD is directed to the cell membrane via the N-terminal amphipathic leader. Here, AgrB recognises AgrD and facilitates cleavage of the C-terminus and formation of a thiolactone ring which is essential for AIP function. Subsequent removal of the AgrD N-terminus releases the mature AIP. Once released externally, AIP binds to histidine kinase AgrC on neighbouring cells activating a signal transduction pathway via AgrA, upregulating AIP biosynthesis and virulence gene expression. The exact mechanism of AgrD processing, however, is poorly understood. Research into this pathway will aid the development of inhibitors which target AIP biosynthesis which can be used as alternative therapies to prevent *S. aureus* infections.

The present study sought to develop bioreporters for *agr* QS activation and inhibition. Novel luciferases *Gaussia* luciferase and NanoLuc were shown to be effective reporters for *agr* expression in *S. aureus* through evaluation of chemical agent-mediated activation and inhibition of *agr.* These reporters enabled quantitative analysis of *agr* inhibition and can be used to screen for *agr* QS inhibitors.

This study also sought to explore the mechanism of biosynthesis of AIP, the pheromone of the *agr* QS system. This is produced by post-translational processing of precursor peptide AgrD by integral membrane protease AgrB. AgrB dimerization was posited to be essential for AgrD processing from analysis of computational modelling of AgrB and AgrD interactions in a lipid membrane. Oligomerization of AgrB was also demonstrated in living cells through the use of novel NanoBRET and NanoBiT assays developed to show protein proximity in live cells. This is the first confirmation of AgrB oligomerisation in living cells which it is thought to be essential for AgrD processing.

Additionally, an *agrBD* expression construct was developed to increase understanding of AIP maturation. An AgrBD enzyme bound intermediate was discovered to form in *E. coli* membranes which was detectable by Western blot against AgrB. This intermediate was found to be essential in the processing of AgrB to form AIP. This complex was analysed with a range of inactivating mutations in AgrB identifying residues in AgrB which are essential for recognition of AgrD. It was also analysed in the presence of protease inhibitors including the natural product ambuic acid and several ambuic acid analogues and enabled insights into the mechanism of action of these compounds.

To investigate AIP processing further, AgrB was purified and was shown to be able to perform C-terminal but not N-terminal cleavage of AgrD. MroQ, another protease which has been reported recently to have a potential role in AgrD processing was also purified and, in the presence of purified AgrB and MroQ, mature AIP was formed. This provided evidence for the function of MroQ in the N-terminal cleavage of AgrD, releasing mature AIP.

Acknowledgements

Firstly, I would like to thank my supervisors Dr. Phil Hill, Professor Paul Williams and Dr. Jeni Luckett for all their support and guidance throughout my PhD. Thank you for supporting me throughout my project and helping me to build my confidence.

I would like to say a special thank you to Dr. Ewan Murray without whom this project would not have been possible. Thank you for all the help guiding my project and for not letting me get worked up when things weren't going to plan. I couldn't have done it without all your help.

I am very grateful for the generous funding from the Wellcome Trust and the University of Nottingham, which made this work possible. To all the amazing colleagues I have had who have helped me during the last 4 years, both in the staph group and the C-floor labs. Particularly I would like to thank Dr Phil Bardelang for all the help with protein purification and for advising on my project. I would also like to thank my friends Maria, Marina, Dean, Claire and Sam for the endless coffees and drinks venting about work and supporting each other.

I would also like to thank my family who have no idea what I'm doing, but have fully supported me the whole way and have told me they will read this thesis... Finally, I would like to thank my fiancé Alistair who has been there for me throughout the last 4 years, has been forced to listen to endless presentations, has comforted me through *agr* induced melt downs and has never lost faith in me. Thank you for your support I couldn't have done it without you.

Publications

Blower I., Tong C., Sun X., Murray E., Luckett J., Chan W., Williams P., Hill P. **Gaussia Luciferase as a Reporter for Quorum Sensing in Staphylococcus aureus.** Sensors (Basel). 2020;20(15). DOI: 10.3390/s20154305

Bardelang P., Murray E., Blower I., Zandomeneghi S., Goode A., Hussain R., Kumari D., Siligardi G., Inoue K., Luckett J., Doutch J., Emsley J. Chan W., Hill P., Williams P., Bonev B. **Conformational analysis and interaction of the Staphylococcus aureus transmembrane peptidase AgrB with its AgrD propeptide substrate.** Frontiers in Chemistry. 2023;11. DOI: 10.3389/fchem.2023.1113885

List of key presentations

Blower I., Murray E., Bardelang P., Luckett J., Hill P., Williams P. **Autoinducing Peptide Biosynthesis and Quorum Sensing Inhibition in *Staphylococcus aureus*.** Microbiology Society Annual Conference, Belfast, 2022 – Poster presentation

Blower I., Murray E., Bardelang P., Luckett J., Hill P., Williams P. **Autoinducing Peptide Biosynthesis and Quorum Sensing Inhibition in *Staphylococcus aureus*.** Cell–Cell Communication in Bacteria: Fundamental and Applied Aspects, Cambridge, 2022 – Flash talk and poster presentation

Blower I., Murray E., Bardelang P., Luckett J., Hill P., Williams P. **Autoinducing Peptide Biosynthesis and Quorum Sensing Inhibition in *Staphylococcus aureus*.** Biosciences Symposium, University of Nottingham, 2022 – Poster presentation. Prize: Prof GSAB Steward Communication prize

Abbreviations

°C	Degrees Celsius
agr	Accessory gene regulator
AIP	Autoinducing peptide
APS	Ammonium persulphate
BHI	Brain heart infusion
bp	Base pair
BRET	Bioluminescence resonance energy transfer
BSA	Bovine serum albumin
CTZ	Coelenterazine
dH_2O	Deionised water
DMF	Dimethylformamide
DMSO	Dimethyl sulphoxide
DNA	Deoxyribonucleic acid
dNTP	Deoxyribonucleic triphosphate
E. coli	*Escherichia coli*
EDTA	Ethylenediaminetetraacetic acid
g	Gram
GLuc	*Gaussia* luciferase
h	Hours
Hi-Fi	High fidelity
HRP	Horseradish peroxidase
IC_{50}	Half maximal inhibitory concentration
IMAC	Immobilised metal affinity chromatography
IPTG	Isopropyl β- d-1-thiogalactopyranoside
kb	Kilobase
kDa	KiloDalton
L	Litre
LB	Luria broth
LC-MS	Liquid chromatography mass spectrometry

M	Molar
MBP	Maltose binding protein
mBU	Milli BRET units
mg	Milligram
min	Minute
mL	Millilitres
mM	Millimolar
mol	Moles
MSSA	Methicillin susceptible *Staphylococcus aureus*
MRSA	Methicillin resistant *Staphylococcus aureus*
mw	Molecular weight
NanoBRET	NanoLuc bioluminescence resonance energy transfer
NanoLuc	NanoLuciferase
NanoBiT	NanoLuc binary technology
nM	Nanomolar
nm	Nanometers
OD_{600}	Optical density at a wavelength of 600 nm
PAGE	Polyacrylamide gel electrophoresis
PBS	Phosphate buffered saline
PCR	Polymerase chain reaction
PMSF	Phenylmethylsulfonyl fluoride
PRSA	Penicillin resistant *Staphylococcus aureus*
PVDF	Polyvinylidene fluoride
QS	Quorum sensing
RBS	Ribosome binding site
RLU	Relative light units
ROS	Reactive oxygen species
Rot	Repressor of toxins
rpm	Revolutions per minute
S. aureus	*Staphylococcus aureus*

SDS	Sodium dodecyl sulphate
SEC	Size exclusion chromatography
s	Seconds
S. epidermidis	*Staphylococcus epidermidis*
SpA	Staphylococcal protein A
SSTI	Skin and soft tissue infection
TB	Terrific broth
TBS	Tris buffered saline
TCEP	Tris(2-carboxyethyl)phosphine
TEMED	Tetramethylethylenediamine
TSB	Tryptone soy broth
VISA	Vancomycin intermediate *Staphylococcus aureus*
VRSA	Vancomycin resistant *Staphylococcus aureus*
WHO	World Health Organisation
% (v/v)	Percentage volume per volume
% (w/v)	Percentage weight per volume
μg	Microgram
μL	Microlitre
μM	Micromolar

Table of Contents

1. Introduction *25*

1.1. Antibiotic resistance 25

1.2. Staphylococcus aureus 25

1.2.1. Epidemiology and antibiotic resistance 25

1.2.2. Therapeutic approaches to treatment 28

1.2.3. Virulence factors 30

1.3. Quorum sensing 31

1.3.1. Overview of the *agr* QS system 32

1.3.2. *agr* subgroups 34

1.3.3. AgrD processing 36

1.3.4. Effect of *agr* activation 39

1.3.5. Regulation of *agr* quorum sensing 41

1.4. Inhibition of virulence and *agr* quorum sensing 43

1.4.1. Inhibitors of *agr* activation 48

1.4.2. Investigating *agr* activation experimentally 49

1.5. Luciferases as bioreporters 50

1.5.1. *Gaussia* luciferase 52

1.5.2. NanoLuciferase 54

1.6. Aims 56

2. Methods 57

2.1 Bacterial strains and growth conditions 57

2.2 Molecular biology techniques for DNA manipulation 59

2.2.1 Oligonucleotide primers used in this study 59

2.2.2 DNA sequence of *agr*P3-NanoLuc oligonucleotide purchased from Eurofins 63

2.2.3 DNA sequences of amplified AgrB and AgrD 64

2.2.4 Plasmids used in this study 65

2.2.5 Plasmid isolation from *E. coli* 68

2.2.6 Plasmid isolation from *S. aureus* 69

2.2.7 Genomic DNA extraction from staphylococci 69

2.2.8 Polymerase Chain Reaction (PCR) 69

2.2.9 DNA separation using agarose gel electrophoresis 69

2.2.10 DNA ligation and dialysis 70
2.2.11 HiFi DNA assembly 70
2.3 Generation of electrocompetent *E. coli* cells 70
2.4 Transformation of *E. coli* cells by electroporation 71
2.5 Generation of electrocompetent *S. aureus* cells 71
2.6 Transformation of *S. aureus* cells by electroporation 71
2.7 Phage transduction 72
2.7.1 Generation of phage lysate 72
2.7.2 Transduction 73
2.8 Detection of AIP-1 using bioreporter *S. aureus* ROJ143 73
2.9 GLuc and NanoLuc bioluminescence assays 74
2.9.1 Measuring *agr*P3 promoter activity using GLuc and NanoLuc bioluminescence 74
2.9.2 Measuring *agr*P3 activity with respect to growth phase using GLuc 74
2.9.3 Testing the effect of *agr* inhibitors and activators with *agr*P3-GLuc and *agr*P3-NanoLuc strains 75
2.10 NanoBiT assays 75
2.10.1 NanoBiT strains 75
2.10.2 Detection of NanoBiT bioluminescence using a Tecan Infinite F200 microplate reader 77
2.11 Protein induction from pCDFDuet-1 77
2.12 Membrane preparation 78
2.13 NanoBRET assay using Tecan Infinite F200 microplate reader 78
2.14 Preparing samples for visualisation of NanoBRET by confocal laser scanning microscopy 79
2.14.1 Confocal laser scanning microscopy 79
2.15 Cell free AgrB assay 79
2.16 SDS-PAGE 81
2.17 Western blot 83
2.18 Purification of recombinant AgrB 85

2.19 MBP-MroQ purification and size exclusion chromatography 87

3. Developing bioluminescent reporters for monitoring agrP3 expression in Staphylococcus aureus *90*

3.1 Introduction 90

3.2 Aims 91

3.3 Comparison of growth between *S. aureus* USA300 and *S. aureus* USA300 *agr*P3-GLuc 92

3.4 Detecting GLuc expression in cells compared with supernatant fractions 93

3.5 GLuc bioluminescence correlates with growth phase consistent with *agr* induction 95

3.6 Activation of *agr*P3-GLuc bioluminescence with synthetic AIP-1 96

3.7 Inhibition of *agr*P3-GLuc bioluminescence using competitive AgrC antagonist AIP-95 97

3.8 Growth in the presence of inhibitors and activators 98

3.9 Inhibition of *S. aureus* USA300 *agr*P3-GLuc bioluminescence using inhibitors of other components of the *agr* system 99

3.10 Construction of *S. aureus agr*P3-NanoLuc reporters 101

3.11 Reduction in bioluminescence after addition of substrate from GLuc compared to NanoLuc 103

3.12 Inhibition of *agr*P3-NanoLuc bioluminescence using competitive AgrC antagonists 105

3.13 Detecting NanoLuc expression in cells compared with cell free supernatants 106

3.14 Improvement of NanoLuc secretion 107

3.15 NanoLuc codon optimisation 108

3.16 Discussion and conclusions 110

4. Using bioluminescent tools to investigate AgrB and AgrD protein-protein interactions in live bacteria 115

4.1 Introduction 115

4.2 Aims 117

4.3 Computational modelling of AgrBB and AgrBD interactions 117

4.4 Development of a NanoBRET system to investigate presence of AgrB1 dimer in an *E. coli* expression model 120

4.4.1 Creation of constructs in *E. coli* and expression of Nanoluc 121

4.4.2 Western blot to show translational fusion of NanoLuc to AgrB1 122

4.4.3 Demonstration that AgrB fused to NanoLuc is functional 124

4.4.4 Bioluminescence from membrane and cytosolic fractions 125

4.4.5 Optimisation of signal from NanoLuc linked to AgrB 126

4.4.6 Introduction of Halo-AgrB to MCS2 of pCDFDuet-1 128

4.4.7 Detection of NanoBRET using a Tecan plate reader 129

4.4.8 NanoBRET detected by confocal laser scanning microscopy 131

4.5 Development of a NanoBiT system to monitor AgrBB and AgrBD interactions in *S. aureus* 132

4.5.1 AgrB1D1 interaction 134

4.5.2 AgrBB dimerization 137

4.6 Discussion 139

5. Identification and analysis of an AgrBD intermediate required for AIP biosynthesis in vitro *142*

5.1 Introduction 142

5.2 Aims 143

5.3 Construction of an *agrB1D1* expression vector 143

5.4 Expression of *agrB1D1* from *E. coli* C41 (DE3) and detection of AIP-1 145

5.5 Detection of AgrD1 by Western blot 146

5.6 Detection of AgrB1 by Western blot 147

5.7 Confirmation of AgrB1D1 complex formation with synthetic linear T7-AgrD1 149

5.8 AIP-1 production from AgrB1 membrane fractions incubated with T7-AgrD1. 151

5.9 AgrBD complex formation with N-terminal AgrD1 152

5.10 Dynamics of AgrB1D1 complex formation 153

5.11 AgrB1D1 complex formation with increasing concentrations of T7-AgrD1 155

5.12 Stability of the AgrB1D1 complex 155

5.13 AgrBD complex formation with different *agr* subgroups..... 157

5.14 AgrBD complex formation with AgrD2 from *Staphylococcus epidermidis* 164

5.15 Identification of residues in AgrB necessary for AgrBD complex formation 167

5.16 Effect of protease inhibitors on AgrB1D1 complex formation 171

5.17 Discussion..... 176

6. Evaluating the mechanism of action of AIP biosynthesis inhibitors and the function of protease MroQ..... 184

6.1 Introduction 184

6.2 Aims 185

6.3 AgrB1D1 complex formation with ambuic acid 185

6.4 Impact of ambuic acid analogues on AgrBD complex formation 189

6.5 Purification of recombinant AgrB1 193

6.6 Incubation of purified AgrB1 with T7-AgrD1..... 196

6.7 Incubation of purified AgrB1 with T7-AgrD1 and ambuic acid 199

6.8 Purification of MroQ 201

6.9 AIP-1 production with purified AgrB1 and MroQ..... 204

6.10 Analysis of the processing of T7-AgrD1 by AgrB1 and MroQ 206
6.11 AIP-1 production from MroQ with N-terminal AgrD1 208
6.12 Discussion and conclusions 209
7. Summary and Future Directions 214
7.1 Development of *agr* QS reporters 214
7.2 AgrB oligomerization and AgrBD interactions 216
7.3 Development of screening pathway for AgrB inhibitors 219
8. References 223

Table of Figures

Figure 1-1. Timeline of the introduction of antibiotics with the emergence of resistant *S. aureus* strains taken from McGuinness et al. 2017 (20)..... 28
Figure 1-2. Schematic of a production of a selection of virulence factors from *S. aureus.* 31
Figure 1-3. Schematic of the *agr* quorum sensing system adapted from Novick and Geisinger, 2008 (54). 33
Figure 1-4. Structure of AIP molecules from *S. aureus agr* groups 1-4. ... 35
Figure 1-5. Outline of proteolysis steps involved in processing of AgrD. Adapted from Zhao et al. 2022 (69). 36
Figure 1-6. Schematic of the processing of AgrD to form AIP..... 37
Figure 1-7. Known regulators of the *agr* system adapted from Marroquin et al. 2019 (48, 75, 80). 42
Figure 1-8. Production of light from *Gaussia* luciferase with substrate coelenterazine (142)..... 52
Figure 1-9. Production of light from NanoLuc with substrate furimazine. From England et al. 2016 (148)..... 54
Figure 3-1. Outline of the staphylococcal *agr* system and the *agr*P3-GLuc reporter. 92
Figure 3-2. Comparison of growth of *S. aureus* USA300 and USA300 *agr*P3-GLuc. 93
Figure 3-3. The difference in bioluminescence in the supernatant and cell pellet of *S. aureus* USA300 *agr*P3-GLuc and USA300 ∆*agr agr*P3-GLuc. 94
Figure 3-4. OD_{600} and relative bioluminescence from *S. aureus* USA300 *agr*P3 GLuc over 12 h. 96
Figure 3-5. The impact of addition of exogenous AIP-1 on bioluminescence produced by *S. aureus* USA300 ∆*agr agr*P3-GLuc pSKermP2-*agrAC*. 97
Figure 3-6. Impact of 100 nM AIP-95 on relative bioluminescence output from *S. aureus* USA300 *agr*P3-GLuc. 98
Figure 3-7. Growth of *S. aureus* USA300 *agr*P3-GLuc in the presence of AIP-1 and AIP-96. 99

Figure 3-8. Impact of the addition of ambuic acid and apicidin on bioluminescence output from *S. aureus* USA300 *agr*P3-GLuc. 100
Figure 3-9. Schematic of the *agr*P3-SpA-NanoLuc oligonucleotide purchased from Eurofins. 101
Figure 3-10. Bioluminescence produced by *S. aureus* ROJ143 after growth for 3.5 h with supernatants from overnight cultures of test strains. 102
Figure 3-11. Reduction in bioluminescence over 10 min from GLuc and NanoLuc after addition of CTZ of NanoGlo as substrate. 104
Figure 3-12. Impact of the addition of competitive *agr* inhibitors (Ala^5)AIP-1 and AIP-95 on bioluminescence output from *S. aureus* USA300 *agr*P3-NanoLuc. 105
Figure 3-13. Comparison of bioluminescence output from supernatant and cell pellet of *S. aureus* USA300 *agr*P3-NanoLuc. 106
Figure 3-14. Comparison of bioluminescence from *agr*P3-NanoLuc strains with and without codon optimisation..... 109
Figure 3-15. Impact of 100 nM AIP-95 and Ala^5(AIP-1) on bioluminescence output from *S. aureus* USA300 *agr*P3-SasD-NanoLuc. 110
Figure 4-1. Atom MD-annealed homology model of AgrB1 in a membrane at the end of 500 ns all atom trajectory in hydrated membranes of 4:1 POPG/POPE. 118
Figure 4-2. Conformation of the $(AgrB)_2$/AgrD complex at the end of 500 ns atomistic MD simulations..... 119
Figure 4-3. Schematic of NanoBRET used to detect AgrB1 dimer formation. 121
Figure 4-4. *E. coli* C41 (DE3) pCDFDuet-1 *nanoluc-agrB1* streaked on LB with 500 μM IPTG and visualised with a long exposure camera..... 122
Figure 4-5. Western blots showing translational fusion of NanoLuc to AgrB1. 123
Figure 4-6. AIP-1 production from *E. coli* C41 (DE3) with pCDFDuet-1 *nanoluc-agrB1 agrD1*. 124

Figure 4-7. Bioluminescence produced by membrane and cytosolic fractions of *E. coli* C41 (DE3) pCDFDuet-1 *nanoluc-agrB1 agrD1*. 125
Figure 4-8. AIP-1 production from *E. coli* C41 (DE3) with pCDFDuet-1 *nanoluc-agrB1 agrD1* and pCDFDuet-1 *agrB1-nanoluc agrD1* with a 3 or 15 amino acid linker between NanoLuc and AgrB. 127
Figure 4-9. Bioluminescence produced by membrane fractions of *E. coli* C41 (DE3) pCDFDuet-1 *nanoluc-agrB1 agrD1* (N-terminal) and pCDFDuet-1 *agrB1-nanoluc agrD1* (C-terminal) with 3 or 15 amino acid linkers. 128
Figure 4-10. Plasmid map of pCDFDuet-1 *agrB1-nanoluc HaloTag-agrB1* used for NanoBRET. 129
Figure 4-11. Corrected BRET ratio from test and control strain. 130
Figure 4-12. AgrB dimerization in *E. coli* C41 (DE3) visualised by NanoBRET using confocal microscopy. 132
Figure 4-13. Schematic of the NanoBiT assay used to monitor AgrBD protein interaction. 133
Figure 4-14. Schematic of an example NanoBiT strain used to investigate AgrB1 AgrD1 interaction. 134
Figure 4-15. Bioluminescence from NanoBiT strains with AgrB1 on the chromosome and AgrD1 on plasmid pSK5630. 136
Figure 4-16. Bioluminescence from *S. aureus* SH1000 *agr*P2-AgrB1 C-terminal SmBit pSK5630 *agrD1 C-terminal LgBiT* (AgrBCS pAgrDCL) in the presence of AIP-95. 137
Figure 4-17. Bioluminescence from NanoBiT strains with AgrB1 on the chromosome and AgrB1 on plasmid pSK5630. 138
Figure 5-1. Vector map of expression vector pCDFDuet-1 *agrB1 agrD1*. 144
Figure 5-2. Bioluminescence from *S. aureus* ROJ143 representing AIP-1 production after induction of proteins in *E. coli* C41 (DE3). 145
Figure 5-3. Detection of AgrD1 from *E. coli* C41 (DE3) in membrane and cytosolic fractions. 147

Figure 5-4. Detection of AgrB1 from *E. coli* C41 (DE3) in membrane and cytosolic fractions. 148
Figure 5-5. Schematic of synthetic linear T7-AgrD1 149
Figure 5-6. Western blots of membrane assay with AgrB1 and synthetic linear T7-AgrD1. 150
Figure 5-7. Bioluminescence output from *S. aureus* ROJ143 confirming AIP-1 production after incubation of *E. coli* C41 (DE3) pCDFDuet-1 *agrB1* membrane fractions with T7-AgrD1 151
Figure 5-8. Schematic of synthetic alfa AgrD1 lacking the C-terminus ... 152
Figure 5-9. AgrB1D1 complex formation and AIP-1 production with N-terminally tagged AgrD1 peptide. 153
Figure 5-10. AgrB1D1 complex formation and AIP-1 production over time. 154
Figure 5-11. AgrB1D1 complex formation with membrane fractions of *E. coli* C41 (DE3) pCDFDuet-1 *agrB1* incubated with T7-AgrD1 at increasing concentrations. 155
Figure 5-12. AgrB1D1 complex stability in increasing reducing environment. 156
Figure 5-13. AgrB1D1 complex stability after boiling. 157
Figure 5-14. Western blot with AgrB nanobody 2ABE10 to detect AgrB1, AgrB2 and AgrB3. 159
Figure 5-15. Reactivity of AgrB1 with AgrD of different subgroups. 160
Figure 5-16. AgrB1 and T7-AgrD2 with and without β-mercaptoethanol. 161
Figure 5-17. Cross reactivity of AgrB2 with AgrD of different subgroups. 161
Figure 5-18. Cross reactivity of AgrB3 with AgrD of different subgroups. 162
Figure 5-19. AIP-1 production from AgrB2 and AgrB3 with T7-AgrD1. ... 163
Figure 5-20. Clustal Omega alignment of AgrD C-termini. 164
Figure 5-21. AgrBD complex formation with *S. aureus* AgrB1 and *S. epidermidis* AgrD2. 165
Figure 5-22. Clustal Omega alignment of AgrD C-termini from *S. aureus* group I and *S. epidermidis* group II. 166

Figure 5-23. Schematic of the role of Cys84 AgrB and Cys28 AgrD..... 167
Figure 5-24. AIP-1 production and AgrB1D1 complex formation with site specific mutations in AgrB1 C84 and AgrD1 C28..... 168
Figure 5-25. AIP-1 production and AgrBD complex formation with *E. coli* C41 (DE3) after induction of pCDFDuet-1 *agrB1D1* with inactivating point mutations..... 170
Figure 5-26. AIP-1 production and AgrBD complex formation with membrane fractions of induced *E. coli* C41(DE3) pCDFDuet-1 *agrB1D1* H77A. 171
Figure 5-27. AIP-1 production from *E. coli* BL21 pCold *agrB1* incubated with T7-AgrD1..... 172
Figure 5-28. Effect of protease inhibitors on AgrB1D1 complex formation where inhibitors were added before T7-AgrD1..... 173
Figure 5-29. AgrB1D1 complex formation in the presence of protease inhibitors with inhibitors added simultaneously to T7-AgrD1..... 174
Figure 5-30. AgrB1D1 complex formation in the presence of 100 μM pefabloc..... 175
Figure 5-31. AgrB1D1 complex formation in the presence of protease inhibitors with inhibitors added after T7-AgrD1. 176
Figure 6-1. Effect of increasing concentrations of ambuic acid on (a) AgrB1D1 complex formation and (b) AIP-1 production. 186
Figure 6-2. AIP-1 production from membrane fractions of induced *E. coli* C41(DE3) pCDFDuet-1 *agrB1* incubated with T7-AgrD1 and ambuic acid characterized using (a) *S. aureus* ROJ143 and (b) LC-MS..... 187
Figure 6-3. AIP-1 production from membrane fractions of induced *E. coli* C41(DE3) pCDFDuet-1 *agrB3* incubated with T7-AgrD1 and DMSO or ambuic acid. 189
Figure 6-4. Chemical structures of ambuic acid and analogues tested. . 190
Figure 6-5. Effect of ambuic acid analogues on (a) AgrB1D1 complex formation and (b) AIP-1 production. 192
Figure 6-6. Effect of ambuic acid analogues on AgrB1 dimer formation. 193

Figure 6-7. Western blot of *E. coli* C41 (DE3) after induction of AgrB1 expression from pCold *agrB1* before purification. 194
Figure 6-8. Coomassie stained gel showing AgrB1 purification. 195
Figure 6-9. Coomassie stained gel of AgrB1 purification after desalting. 196
Figure 6-10. Coomassie stained gel of purified AgrB1 incubated with T7-AgrD1. 197
Figure 6-11. Western blot of purified AgrB1 incubated with T7-AgrD1. .. 198
Figure 6-12. AIP-1 production from purified AgrB1 incubated with T7-AgrD1. 199
Figure 6-13. Impact of the addition of ambuic acid and LB276 on complex formation of AgrB in *E. coli* membrane and purified (*) AgrB with T7-AgrD. 200
Figure 6-14. AIP-1 production from *E. coli* membrane fractions with AgrB1 and purified AgrB1 incubated with T7-AgrD1 in the presence and of ambuic acid. 201
Figure 6-15. Coomassie stained gel showing MBP-MroQ purification. ... 202
Figure 6-16. Size exclusion chromatography peak from AKTApure. 203
Figure 6-17. Coomassie stained gel of MBP-MroQ purification after size exclusion chromatography. 203
Figure 6-18. AIP-1 production and AgrB1D1 complex formation with purified AgrB1 and T7-AgrD1 with increasing concentrations of MroQ..... 204
Figure 6-19. AIP-1 production from purified AgrB1 with T7-AgrD1 and MroQ in the presence of AFC characterized using (a) LC-MS and (b) *S. aureus* ROJ143. 205
Figure 6-20. AgrBD complex formation with purified AgrB1, T7-AgrD1 and 2 μM MroQ in the presence of AFC. 206
Figure 6-21. Processing of T7-AgrD1 by AgrB1 and MroQ. 207
Figure 6-22. AIP-1 production from purified MroQ and AgrB1 with alfa-AgrD1 characterized using (a) *S. aureus* ROJ143 and (b) LC-MS..... 209
Figure 6-23. Schematic of processing of AgrD by AgrB and MroQ. 212

Figure 7-1. Flow chart demonstrating screening pathway for AgrB inhibitors using methods developed in this thesis..... 220

Table of Tables

Table 1-1. Virulence mechanisms which can be targeted in *S. aureus*. ... 43
Table 2-1. Bacterial strains used in this study. ... 58
Table 2-2. Primers used in this study. ... 59
Table 2-3. Plasmids used in this study ... 65
Table 2-4. Split luciferase strains used for NanoBiT. ... 75
Table 3-1. Percentage bioluminescence from supernatant and cell pellet of *S. aureus* USA300 *agr*P3-signal peptide-NanoLuc strains after overnight growth ... 108
Table 3-2. Percentage bioluminescence from supernatant and cell pellet of *S. aureus* USA300 *agr*P3-signal peptide-NanoLuc strains with codon optimisation after overnight growth. ... 109

1. Introduction

1.1. Antibiotic resistance

Antibiotics are one of the most successful drug categories in the improvement of human health and have been enormously successful in the treatment and prevention of infectious diseases (1, 2). The introduction of antibiotics in the 20th century transformed modern medicine, saving millions of lives by changing the outcome of bacterial infections. The emergence of drug resistant strains however, is now endangering the efficacy of these drugs, affecting practice in every field of medicine (3).

Almost all antibiotics in clinical use belong to classes discovered in the 'golden age' of antibiotic discovery from the late 1960s to the early 1980s (3-5). Currently the discovery of novel antibiotics is unable to keep up with the increase in antibiotic resistance meaning that infectious diseases remain a major threat to human health (2). The overuse and misuse of potent antimicrobials in medical and agricultural practices has led to the rise of multiantibiotic resistant bacteria and clinically significant antibiotic resistance has now evolved against almost all antibiotics in use (6, 7).

Due to this there is an urgent need to research and develop antimicrobials with novel targets which are effective against resistant strains and against which resistance cannot easily emerge. Alternative therapies are being considered such as those which target functions essential for infection, for example virulence factor production, without affecting bacterial growth. These will provide less pressure for development of resistance (7, 8).

1.2. Staphylococcus aureus

1.2.1. Epidemiology and antibiotic resistance

Staphylococcus aureus is a Gram-positive bacterium which has been identified by the World Health Organisation as a high priority pathogen (9).

S. aureus is both a human pathogen and a commensal bacterium, harmlessly colonising around 30% of the healthy human population (10, 11). It is one of the most common causes of bacterial infections in the hospital and in the community (12). Nosocomial infections are commonly transmitted by healthcare workers or as a result of invasive procedures such as surgery and implantation of medical devices (13).

S. aureus typically colonises the skin and mucous membranes such as the nasopharynx and is transmitted by direct contact (14). Once across the skin or mucosal membrane *S. aureus* can cause infection due to production of a range of virulence factors. These include cell surface associated proteins such as Protein A, coagulase, and fibronectin binding proteins as well as secreted exoproteins, haemolysins, toxic shock syndrome toxin-1 and Panton-Valentine toxin (15, 16). It can survive in the blood or tissues causing a variety of infections ranging from minor skin infections to life threatening acute and chronic infections such as bacteraemia or endocarditis (10, 16). *S. aureus* is the primary cause of both community and hospital acquired skin and soft tissue infections (SSTIs) (17). *S. aureus* infections often manifest as abscesses, these are a common presentation of SSTIs and can be difficult to treat (18). Abscesses can also form in deeper tissues such as muscle and organ systems (19).

S. aureus is able to acquire resistance to multiple antibiotics which can make treatment difficult (20, 21). *S. aureus* has acquired resistance to antibiotics largely through acquisition of genes by horizontal gene transfer of mobile genetic elements (20). Resistance can also emerge through, for example, mutations which alter the drug binding site or which increase expression of endogenous efflux pumps causing removal of the drug (22). The emergence of new strain lineages also adds to the challenge of treatment as the pathogen evolves rapidly. For example, the expansion of hypervirulent USA300 in the United States which is commonly associated with community

acquired infections (23, 24). USA300 exhibits increased virulence factor production and more efficient transmission than other strains and therefore became the most common source of antibiotic resistant *S. aureus* infections in North America (25). Infection with resistant *S. aureus* strains leads to increased hospital stays and hospital related morbidity resulting in large economic burden (13).

In the pre-antibiotic era, the fatality rate for *S. aureus* bacteraemia was around 80% however this was immediately reduced by the introduction of antibiotics to treat these infections (10). The mortality rate for *S. aureus* bacteraemia is currently between 10-30% (26). β-lactam antibiotics such as penicillin and methicillin introduced in the 20th century were effective against *S. aureus* however resistance emerged rapidly and methicillin resistant *Staphylococcus aureus* (MRSA) remains a threat to global health (22, 27). MRSA accounts for a high proportion of hospital associated *S. aureus* infections which have high morbidity and mortality rates (28). Consequently physicians are turning increasingly to antibiotics of last resort, such as the glycopeptide vancomycin, for treatment of MRSA infections and resistance to these is spreading (20). Vancomycin resistant strains have emerged over the last 20 years and are increasingly isolated among community-acquired *S. aureus* infections (20, 29). A timeline of the emergence of resistant *S. aureus* strains is outlined in **Figure 1-1**.

The increasing prevalence of drug resistant strains complicates treatment as empirical antibiotic treatment regimens may be ineffective resulting in a limited choice of therapies. This highlights the importance of the development of antibiotics with novel targets which are effective against these strains (7).

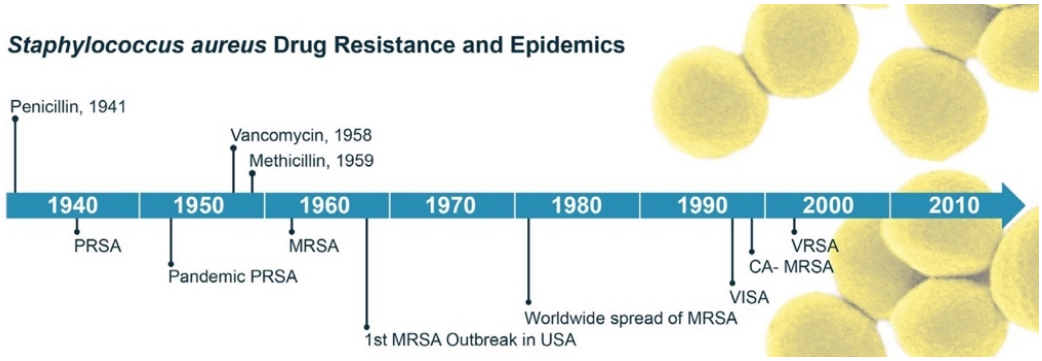


Figure 1-1. Timeline of the introduction of antibiotics with the emergence of resistant *S. aureus* strains taken from McGuinness et al. 2017 (20). Resistant strains include penicillin resistant *S. aureus* (PRSA), methicillin resistant *S. aureus* (MRSA), vancomycin resistant *S. aureus* (VRSA), vancomycin intermediate *S. aureus* (VISA) and community acquired MRSA (CA-MRSA).

1.2.2. Therapeutic approaches to treatment

Traditionally, infections caused by *S. aureus* were treated with penicillin which was introduced in the 1940s, however, quickly after its introduction, resistance to penicillin was observed (30, 31). Penicillin is a β-lactam antibiotic which targets penicillin binding protein 2 (PBP2) in *S. aureus*, interfering with peptidoglycan synthesis and so inhibiting bacterial cell wall biosynthesis. Penicillin resistant strains express a β-lactamase, encoded by *blaZ*, which destroys the drug's β-lactam bond and inactivates it (22). The *blaZ* gene is widespread and is carried on transposon Tn*552* or Tn*552* like elements on a plasmid or encoded on the chromosome. Indeed, the rate of resistance to penicillin is now greater than 90% in human *S. aureus* isolates rendering the drug essentially ineffective (32, 33).

Due to the increase in penicillin resistant *S. aureus*, analogues of this were made, including methicillin, which was introduced into the clinic in 1959, and oxacillin (22). Methicillin resistant *S. aureus* (MRSA) strains were already identified from hospitals in the UK by July-October 1960 (32). Resistance to

methicillin and oxacillin is due to the acquisition of a homologue of PBP2 called PBP2a which is not susceptible to the drug's action (34, 35). The active site of PBP2a is not accessible to the antibiotic therefore cannot be inhibited and this protein takes over peptidoglycan biosynthesis. PBP2a is encoded by *mecA* which is carried on a mobile genetic element SCC*mec* (22, 36). Methicillin resistance can also be conferred by $PBP2A_{LGA}$ encoded on *mecC*, which was identified in 2012, this is also responsible for cross linking peptidoglycan in the cell wall (37).

Methicillin is no longer used clinically due to widespread resistance in the hospital and community. New β-lactam antibiotics have been introduced such as ceftaroline which binds to PBP2a however clinical use of this has also led to emergence of resistance (38). The term MRSA is still used although methicillin is not in use and MRSA strains confer resistance to virtually all β-lactam antibiotics. MRSA strains can also acquire resistance to other antibiotics such as vancomycin, further complicating treatment (32).

Vancomycin is a glycopeptide antibiotic used to treat serious infections caused by MRSA in hospital settings. In 1997 the first vancomycin intermediate *S. aureus* (VISA) strain was identified in Japan with an increased MIC against vancomycin (39). This was closely followed by the first vancomycin resistant *S. aureus* (VRSA) strain isolated in 2002 in the USA (36). VRSA strains acquire resistance by conjugal transfer of the *vanA* operon from *Enterococcus faecalis*. VISA strains appear to acquire multiple mutations causing, for example, altered peptidoglycan biosynthesis, which leads to reduced susceptibility to vancomycin (33, 36). Vancomycin is one of the first line drugs used to treat MRSA and the emergence of clinical isolates of VISA and VRSA over the last 20 years has become a public health concern (36).

S. aureus is naturally susceptible to virtually all antibiotics developed however it is able to acquire resistance to almost any antibiotic (40). Therefore, novel, and alternative therapies which do not provide such pressure for resistance to emerge are being investigated. Phage therapies are being developed. These use bacteriophages which are lytic viruses that infect and kill bacteria with high specificity however none have yet made it through clinical trials (41). Extensive research has also been performed into development of *S. aureus* vaccinations however, again, none have been successful so far (42). Combination antibiotic therapies are being employed such as using daptomycin, a cyclic peptide, in combination with β-lactam antibiotics as MRSA strains resistant to daptomycin can become sensitive to β-lactams (43). Alternative antibiotics are being trialled as well as combination therapies however there is an urgent need to discover antimicrobial agents with novel mechanisms of action. New drug targets are being investigated such as targeting fatty acid biosynthesis or modification or inhibition of genes associated with bacterial virulence (33). Virulence factor inhibitors will not kill or inhibit the growth of the bacteria so are thought to provide less pressure for resistance to emerge.

1.2.3. Virulence factors

S. aureus is a very versatile organism, it can exist harmlessly as a commensal bacterium on the skin and can cause a variety of acute and chronic infections. This versatility is due to the production and control of a range of virulence factors which enable evasion of host defences, spread around the host degrading host tissues and adherence to surfaces (11).

S. aureus employs different virulence factors depending on the growth phase. In the early stages of infection *S. aureus* produces cell wall associated virulence factors associated with tissue attachment, adhesion, and evasion of the host immune system. This enables the bacteria to accumulate and can enable it to form a biofilm (44). Biofilms are aggregated

communities of bacteria encased in a matrix composed of protein, DNA and polysaccharide. Growth in biofilms enables evasion of host defences and increased tolerance to antibiotics making infections hard to treat (13). As the bacterial population increases, the production of adhesins is downregulated and a variety of secreted exoproteins are released. These include proteases, haemolysins, superantigens and nucleases which both convert local host tissues to nutrients for bacterial growth and inhibit the host immune response (45, 46). Virulence factor production in *S. aureus* is represented in **Figure 1-2**. The two phases of the *S. aureus* infection cycle, adhesion and invasion are largely controlled by quorum sensing. This is a means of cell to cell communication in bacterial populations through release and detection of a signalling molecule (46).

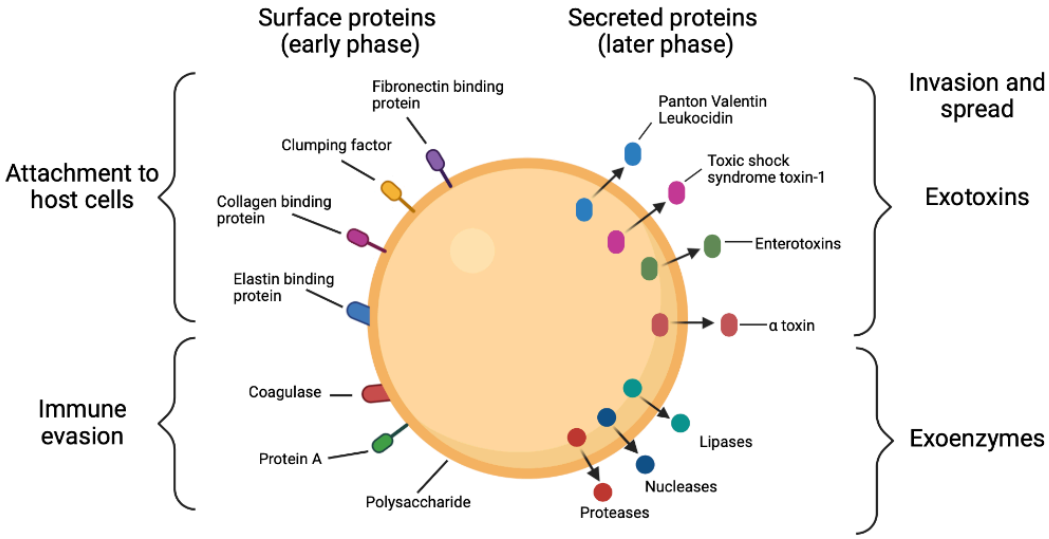


Figure 1-2. Schematic of a production of a selection of virulence factors from *S. aureus.* Surface associated factors are produced in the early stages of infection and secreted proteins in the later stages.

1.3. Quorum sensing

Quorum sensing (QS) is a means of cell-to-cell communication in bacterial populations. It coordinates cooperative behaviour and in some cases can enable bacteria to respond to altered environments caused, for example, by

cellular stress, altered nutrient levels and immune defences (47). Bacteria communicate using secreted signal molecules. When the extracellular concentration of the signal molecule reaches a threshold, a signal transduction pathway is activated leading to target gene activation and downstream effects (15). In some cases the production of the signal molecule is increased on QS activation, here the phenomenon is called autoinduction (48).

As mentioned in section 1.2.3, in *S. aureus* virulence is largely controlled by quorum sensing, in particular by the accessory gene regulator (*agr*) QS system which is a global regulator of virulence factor production (12, 15). Activation of the *agr* system leads to upregulation of secreted virulence factors such as exoproteases and downregulation of proteins involved in biofilm formation and surface attachment (49). Activation of the *agr* system has been shown to be essential for *S. aureus* virulence in multiple animal infection models (11, 15, 50).

1.3.1. Overview of the *agr* QS system

The staphylococcal *agr* operon consists of a ~3 kb locus with two divergent transcriptional subunits under the control of promoters P2 and P3 (47, 49). The P2 operon encodes *agrBDCA*, a two-component signal transduction system and its activating ligand (51). The P3 transcript is RNAIII which is the major effector of the *agr* system leading to upregulation of secreted virulence factors and downregulation of surface associated factors (52, 53). The *agr* system is outlined in **Figure 1-3**.

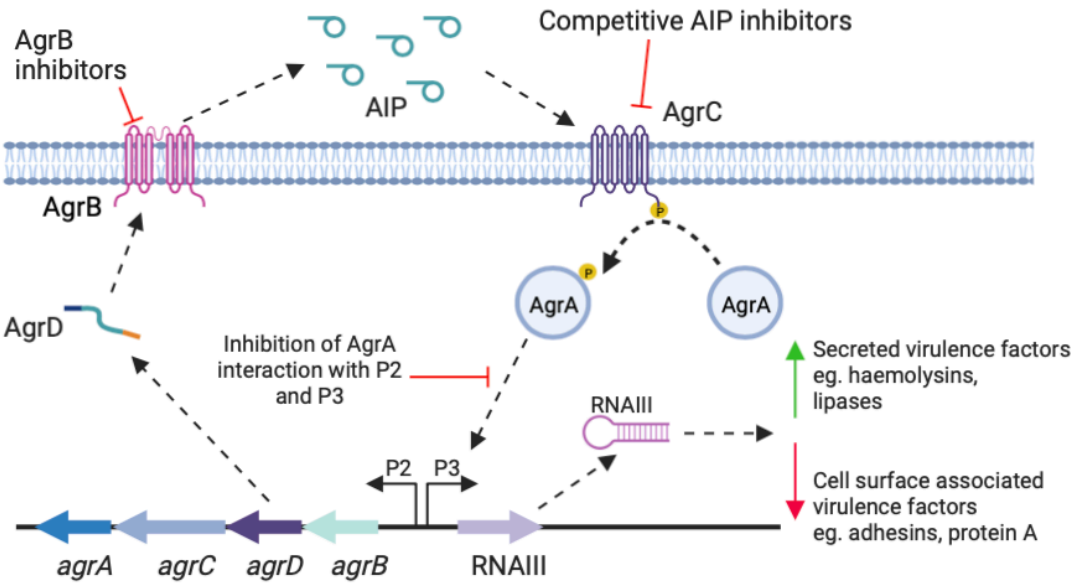


Figure 1-3. Schematic of the *agr* quorum sensing system adapted from Novick and Geisinger, 2008 (54). Precursor peptide AgrD is post-translationally processed, partially by AgrB, and forms mature AIP which leaves the cell. AIP accumulates outside the cell and when this reaches a threshold concentration it binds to and activates AgrC. This phosphorylates on AIP binding and in turn phosphorylates AgrA which upregulates expression from P2 and P3 leading to exponential *agr* activation and activation of RNAIII, the effector of the system. This system can be targeted with inhibitors and components which are amenable to inhibition are indicated by blunt arrows.

The autoinducer of the *agr* system as with other Gram-positive bacteria is a peptide termed an 'autoinducing peptide' (AIP) (51). This is produced by post-translational N- and C- terminal processing of precursor peptide AgrD to form a 7-9 amino acid peptide with a unique thiolactone ring. The thiolactone ring is essential for AIP activity and is conserved among all AIP molecules across species with one exception in *Staphylococcus intermedius* where a lactone ring is present (11, 54). AgrB is an integral membrane

protease which is responsible for the initial stages of processing of AgrD involving cleavage of the C-terminus and thiolactone ring formation (55, 56).

Once an AIP reaches a threshold concentration outside the cell, it binds to and activates AgrC in the membrane. AgrC is a histidine kinase which auto phosphorylates in response to AIP binding and in turn phosphorylates AgrA, the response regulator (57). AgrC and AgrA make up the two-component signal transduction system. Phosphorylated AgrA dimerises and binds to and activates P2 and P3 upregulating *agrBDCA* and RNAIII transcription (11, 49). The AIP molecule is encoded on the *agr* operon therefore this is a positive feedback loop leading to exponential *agr* activation via autoinduction (54).

1.3.2. *agr* subgroups

The *agr* system is present in a wide variety of Gram-positive bacteria including *Staphylococci*, *Clostridia*, *Listeria*, *Lactococci* and *Enterococci*. There are interspecies differences however the *agr* system is highly conserved throughout *Staphylococci*. There are though variations in AgrB, AgrD and AgrC and these variations have resulted in four *agr* subgroups in *S. aureus* (11). There has also been one or more *agr* subgroup described in all other species of *Staphylococci* (54).

The *agr* subgroups differ in the hypervariable region of the *agr* locus. The N-terminal third of AgrB and the C-terminal region of AgrC are highly conserved and the intervening sequences make up the hypervariable region (11). AgrA and RNAIII are also highly conserved (58).

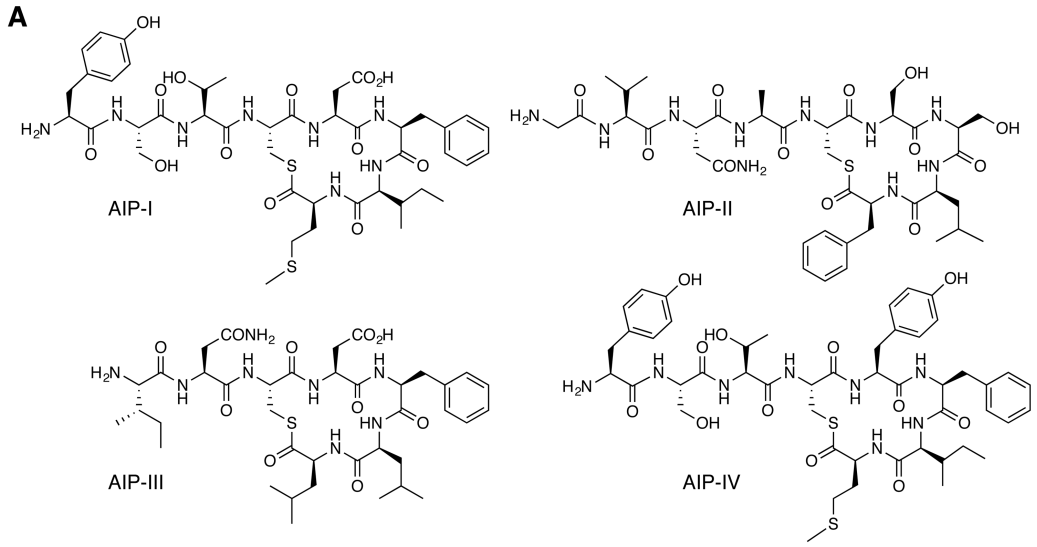


Figure 1-4. Structure of AIP molecules from *S. aureus agr* groups 1-4. Taken from Tal-Gan et al. 2013 (59).

AIP molecules are highly specific for their cognate AgrC receptor and molecules of different groups display inhibitory activity, this is known as *'agr* interference' (60). The ability of an AIP to activate its cognate receptor is highly specific and is dictated by the structure of the AIP molecule. The only exception to this is groups I and IV where the AIP molecules are very closely related and inter-group activation is seen (46). The structures of AIP molecules from the four *agr* subgroups in *S. aureus* are shown in **Figure 1-4**. AIP molecules from different species can also inhibit the *agr* system indicating this is not a cooperative but a competitive phenotype (11, 61).

There is a correlation between *agr* subgroup and infection type (46). Clinical isolates from a single infection site rarely contain a variety of *agr* subgroups and studies have shown that *agr* group I is the most commonly isolated methicillin sensitive *S. aureus* (MSSA) strain (62, 63). Group III strains are associated with menstrual toxic shock syndrome, and necrotising pneumonia (60, 64). Group II strains are associated with bloodstream infections and most VISA strains isolated are *agr* group II (58, 65). Group IV strains are associated with exfoliative syndromes and group II and IV show

increased biofilm formation (58, 66). There are also differences in the timing of *agr* activation with agr groups I and IV activating earliest and group III latest (46).

1.3.3. AgrD processing

As mentioned in section 1.3.1, the autoinducer of the *agr* system is autoinducing peptide (AIP). AIPs are produced by post translational processing of precursor peptide AgrD and exported from the cell via an unknown mechanism (46). AgrD consists of a N-terminal amphipathic leader (24 amino acids), the AIP molecule (7-9 amino acids) and the negatively charged C-terminal tail (14 amino acids) (67). Generation of mature AIP involves two proteolysis reactions, the cleavage of the C-terminus by AgrB and thiolactone ring formation and the subsequent cleavage of the N-terminus to release mature AIP, this is outlined in **Figure 1-5** (68).

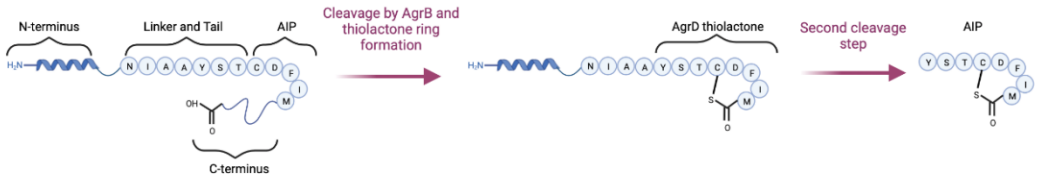


Figure 1-5. Outline of proteolysis steps involved in processing of AgrD. Adapted from Zhao et al. 2022 (69). In the first cleavage step, full length AgrD is C-terminally cleaved by AgrB and the thiolactone ring forms. In the second cleavage step the AgrD intermediate is N-terminally cleaved to produce the mature AIP molecule.

The exact method of AgrD processing is not completely understood however the current model is as follows. The AgrD pro-peptide is directed to the cell membrane after translation by the N-terminal amphipathic leader (70). This leader is necessary for association with the cell membrane and AIP formation (70). At the membrane, AgrD is recognised by AgrB via the C-terminal recognition sequence which is cleaved by AgrB (71). Following

cleavage of the C-terminus, an AgrB-AgrD acyl-enzyme intermediate is suggested to form with AgrD bound through a thioester bond to cysteine 84 of AgrB (67, 68, 72). AgrD cysteine 28 catalyses thioester exchange and allows a thiolactone ring to form (67). The thiolactone ring forms by covalent linking of the central cysteine, Cys28, to the C-terminal amino carboxylate as shown in **Figure 1-5**. This ring is essential for the function of the AIP molecule (54, 68). Following thiolactone ring formation, AgrD is released from AgrB. The N-terminus is cleaved potentially involving MroQ and signal peptidase I (SpsB) and the mature thiolactone is released from the cell (69, 73). This processing pathway is outlined in **Figure 1-6**.

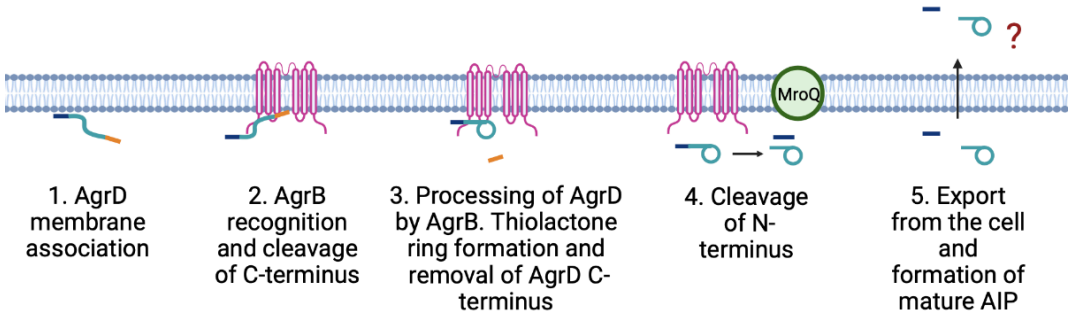


Figure 1-6. Schematic of the processing of AgrD to form AIP. AgrD associates to the membrane via the N-terminus. Here, it is recognised by AgrB and the C-terminus is cleaved before thiolactone ring formation. The N-terminus is then cleaved likely by MroQ and the mature AIP molecule leaves the cell. It is currently unclear whether N-terminal cleavage occurs inside or outside the cell.

AgrB is a 22 kDa integral membrane endopeptidase which is located in the cytoplasmic membrane (56, 71). It is thought to form at least dimers in the membrane and is only functional within a lipid membrane (68). It is predicted to have 6 transmembrane α-helices however as yet no high-resolution structures of AgrB are available. AgrB is involved in the C-terminal cleavage of AgrD and analysis has revealed His77 and Cys84 to be necessary for the

endopeptidase activities. These are thought to form a catalytic centre and are conserved among *agr* subgroups (71). Cys84 in AgrB attacks the cleavage site in AgrD between M32 and D33 giving a linear peptide which is bound to AgrB. This is then cyclised by intramolecular transthioesterification giving the AgrD thiolactone. Formation of the thiolactone ring has been shown to be reversible. The AgrD C-terminus is turned over by an additional protease ClpP, which is thought to recognise this fragment via a conserved motif (68).

After thiolactone ring formation, the N-terminal amphipathic helix is cleaved. Previous studies suggested a role here for the signal peptidase, SpsB, which is anchored to the outer face of the membrane. AgrD was suggested to be transported out of the cell where SpsB would cleave the N-terminus releasing mature AIP (73). Recent studies, however, have argued against a major role for SpsB, showing that deletion of SpsB in *S. aureus* has no effect on the production of mature AIP. Evidence has been put forward for the involvement of another protease, MroQ (69, 74). MroQ is a putative integral membrane type II CAAX protease, located upstream of the *agr* operon (75, 76).

MroQ was identified in a virulence screen where MroQ and *agr* mutants displayed similar phenotypes such as a decrease in haemolysis and secretion of virulence factors such as PVL along with increased expression of SpA (75). MroQ was originally thought to be involved in the regulation of *agr* quorum sensing through interaction with AgrC, however it is now thought to be involved in AgrD processing (75, 76). Deletion of MroQ leads to an accumulation of an AIP processing intermediate at the membrane which coincides with a loss in secreted mature AIP (76).

It has been proposed that MroQ could also have a direct or indirect role in translocation of AIP across the membrane. Previously it has been

hypothesised that AgrD is translocated across the membrane before N-terminal cleavage. One proposed mechanism involves insertion of AgrD N-terminus into the membrane in an orientation which enables processing by an AgrB-MroQ complex followed by passive diffusion of AIP out of the cell (76). Interestingly the N-terminal fraction of AgrD has been detected extracellularly in fibrils in biofilms and in planktonic supernatants of *S. aureus* cultures. It has been shown to display similar properties to phenol soluble modulins (PSMs) with cytolytic activity against human cells and proinflammatory properties (77, 78). This demonstrates that N-terminal AgrD is outside the cell and implies that either N-terminal cleavage may occur after AgrD leaves the cell or both N-AgrD and AIP cross the cell membrane independently.

1.3.4. Effect of *agr* activation

On phosphorylation by AgrC, AgrA binds to and activates *agr*P2 and *agr*P3, upregulating RNAII and RNAIII expression. AgrA also directly binds to the promoter region of phenol soluble modulins (PSMs) which facilitate immune evasion. AgrA binding to PSM promoter regions upregulates their expression (12). Despite this, RNAIII is the major effector of the *agr* system. It is a regulatory RNA which also encodes the delta haemolysin gene (*hld*), translation of which is delayed after RNAIII transcription (79). RNAIII primarily functions through base pairing with 5' ends of mRNAs, suppressing translation of proteins involved in adhesion and de-repressing proteins involved in invasion and spread (46). Many virulence factors are upregulated by RNAIII including, alpha toxin (involved in SSTIs, pneumonia and endovascular infections), serine proteases, cysteine proteases and gamma-haemolysin. Virulence factors downregulated by RNAIII include those involved in cell adhesion such as adhesins, cell wall secretory protein and some surface receptors (80).

RNAIII is a large regulatory RNA with a complex secondary structure which can promote or inhibit gene expression through post-translational regulation (80). For example, RNAIII binds *hla* mRNA enabling access to a ribosome and therefore upregulating translation of alpha toxin (81). It also binds *spa* mRNA, preventing access to a ribosome to the ribosome binding site and therefore preventing translation and leading to downregulation of staphylococcal protein A (SpA) which is involved in immune evasion (82). RNAIII can directly affect gene expression in this way however it exerts many of its effects indirectly through global regulator, repressor of toxins (Rot). Rot acts as a repressor for multiple secreted virulence factors such as enterotoxin B and alpha toxin and also acts as a positive regulator for many cell surface associated factors such as SpA. RNAIII controls Rot expression through blocking the ribosome binding site, preventing Rot translation. Therefore, when the *agr* system is active, RNAIII prevents translation of Rot leading to downstream effects including upregulation of secreted virulence factors and downregulation of cell surface associated virulence factors (80, 83).

Due to the dual activity of the *agr* operon, *agr* is temporally expressed during infection. Low *agr* activity at the start of infection allows high Rot activity. This enables expression of immune evasion proteins and adhesins leading to accumulation of bacteria and evasion of the host response. For example, expression of Protein A which binds to IgG may help form a walled off infection site leading to abscess formation (46, 84). Abscesses are common presentations of *S. aureus* infections. After initial infection, an immune response is typically raised resulting in the recruitment of neutrophils, these are killed by the pathogen and host tissue fibrosis occurs (85). This leads to formation of an abscess consisting of a staphylococcal abscess community at the centre of a lesion surrounded by fibrin deposits (86).

The *agr* system is activated later in infection when the population density is higher, and the infection site is depleted in nutrients. Activation of *agr* leads to RNAIII transcription which inhibits Rot translation and leads to expression of secreted virulence factors and degradative enzymes enabling bacteria to acquire nutrients from host tissue and escape the abscess or infection site, spreading to secondary infection sites (46, 84, 87).

1.3.5. Regulation of *agr* quorum sensing

The *agr* system controls the production of a range of virulence factors therefore it is under tight control. This is affected by numerous metabolic and environmental factors such as pH and glucose and nutrient availability (87, 88). Both acidic and alkaline pH have been shown to inhibit *agr,* with near neutral pH resulting in maximal *agr* activity. Reactive oxygen species (ROS) released by neutrophils can also affect *agr* activity by oxidising AIP molecules rendering them ineffective (80). Oxidative stress caused by ROS can also induce disulphide bond formation in AgrA resulting in impaired binding to promoter regions therefore reduced *agr* induction and reduced expression of secreted virulence factors (89).

There is a basal level of transcription from both the *agr*P2 and *agr*P3 promoters, this is at a much slower rate from the *agr*P3 promoter. The basal level of *agr*P2 transcription is thought to enable *S. aureus* to respond to signals such as cell density leading to rapid upregulation of *agr* QS and virulence gene expression (51, 90).

Two of the key transcription factors which regulate *agr* are AgrA itself and staphylococcal accessory regulator A (SarA) (47). Phosphorylated AgrA dimerises and binds in the intergenic region between *agr*P2 and *agr*P3 upregulating transcription (91). AgrA binds even when its level is very low demonstrating this is important in the initiation of the QS pathway (47). SarA is a DNA binding protein which also binds in the intergenic region between

*agr*P2 and *agr*P3 stimulating transcription of RNAII and RNAIII (92). Other transcription factors including MgrA, which is involved in multidrug resistance and cell wall turnover, SarU and SarZ, contribute to *agr* upregulation by modulating expression of regulators that bind to the promoter region (23, 47, 93).

Interestingly, MgrA also promotes the expression of SarX, an *agr* repressor for 'switching off' the *agr* system (94). Other negative regulators of the *agr* system include CodY, a global regulator which senses nutritional signals and indirectly represses *agrBDCA* operon and RNAIII transcription in exponential growth in rich medium. This is thought to be responsible for growth phase regulation of *agr* (95). Additionally, SarR can compete with SarA, displacing it and so repressing *agr* upregulation (91).

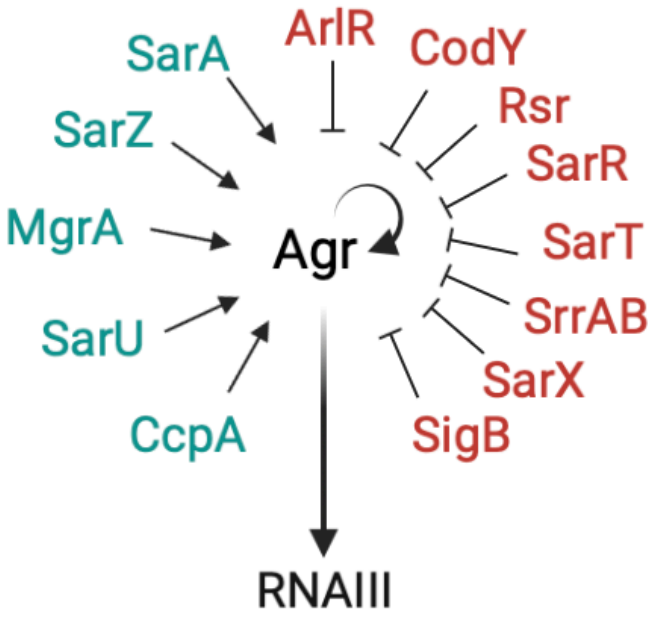


Figure 1-7. Known regulators of the *agr* system adapted from Marroquin et al. 2019 (48, 75, 80). *agr* activators are shown in green with arrows and inhibitors are shown in red with blunt arrows.

Many of the transcription factors involved in up or down regulation of *agr* QS respond to environmental and metabolic factors such as pH, reactive oxygen species and nutrient availability (23). This means the *agr* system is under tight control in response to the environment.

1.4. Inhibition of virulence and *agr* quorum sensing

The increase in the prevalence of antibiotic resistant *S. aureus* has resulted in increased research into novel drug targets including targeting the virulence of the bacterium. This will reduce the ability of the bacteria to cause infection without targeting processes essential for its growth and survival. This will provide less selective pressure for resistance to emerge and will allow it to be cleared by the immune system. A number of antivirulence strategies against *S. aureus* are outlined in **Table 1-1**.

Table 1-1. Virulence mechanisms which can be targeted in *S. aureus*.

Target	Function	Treatment strategy	Ref.
Sortase A	Surface attachment of proteins including those involved in virulence and immune evasion such as SpA	Inhibition of sortase A prevents attachment of surface proteins such as SpA	(96, 97)
ClpP	Protease involved in protein quality control. Involved in virulence regulation.	Activate ClpP to initiate degradation of essential proteins leading to inhibition of cell division and eventual cell death	(98, 99)

Direct target of toxins	Eg. PVL and α-haemolysin involved in virulence	Target chemically or with neutralising monoclonal antibodies	(100, 101)
Carotenoid biosynthetic pathway	Carotenoid pigment of *S. aureus* promotes resistance to ROS and neutrophil killing but has little impact on *ex vivo* survival	Inhibition of this pathway reduces *S. aureus* survival under oxidative stress, leading to increased neutrophil clearance	(102, 103)
Regulatory pathways eg. MgrA,	MgrA is a key transcriptional regulator involved in virulence	Block MgrA binding DNA prevents upregulation of virulence factors	(104)
agr system	Global regulator of *Staphylococcal* virulence	Inhibiting *agr* signalling inhibits production of a range of virulence factors	(88)

The *agr* QS system is a global regulator of virulence, therefore this is of interest when investigating virulence factor inhibitors (7, 15). Control of the *agr* QS system would enable inhibition of secreted virulence factor production without providing selective pressure for development of resistance making this an attractive drug target (15, 46).

Bacterial signalling systems are prime drug targets for combatting antimicrobial resistant infections. The *agr* QS system is an interesting antivirulence target with *agr* inhibitors being shown to delay infections and reduce *S. aureus* abscess size in multiple mouse skin infection models (105-109). *S. aureus* is the primary cause of SSTIs and *agr* activation is often associated with these therefore this is a very interesting avenue of research. Moreover, 90% of *S. aureus* infections are SSTIs therefore limiting antibiotic

use for these would have a major impact preserving antibiotics for invasive or systemic infections (105).

Virulence factor inhibitors can attenuate infection without affecting bacterial growth. This will allow the immune system to clear the infection without providing pressure for resistance to emerge (6). They could also be used as adjuncts to existing antibiotics or with therapies which boost the immune response to clear *S. aureus* infections (48). Antivirulence strategies which target *agr* QS could be used prophylactically, as inhibiting *agr* early in infection could limit disease development. Attenuating infection early on would allow the host immune system to respond and clear the avirulent pathogen before establishment of infection, sparing exposure to antibiotics (47). Inhibition of *agr* early in infection will limit the spread of invasive infections however, it will also increase *S. aureus* cell adherence and immune evasion through upregulation of surface associated proteins such as SpA. This may allow the bacteria to aggregate and could help the infection to establish. In order to circumvent this problem, multiple virulence pathways could be inhibited simultaneously. Inhibition of *agr* will reduce expression of secreted toxins such as α-toxin however will increase expression of SpA. Simultaneous inhibition of Sortase A would prevent attachment of SpA to the cell surface therefore would prevent the increase in immune evasion caused by *agr* inhibition allowing clearance of the pathogen by the immune system (98).

Studies have demonstrated that *agr* inhibitors such as apicidin, savirin and ω-hydroxyemodin aid immune clearance of infection as well as inhibiting *agr* signalling (105, 107, 110). This is thought to be due to the inhibition of expression of virulence factors which target innate and adaptive immune cells. For example, α-haemolysin, which is upregulated by *agr* activation, enables *S. aureus* survival in macrophages and induces apoptosis in T cells, B cells and monocytes. Additionally, PSMs, upregulated by AgrA are highly

cytotoxic to a number of cell types including phagocytes such as neutrophils which are important in the initial phase of host defence against pathogens (111). Therefore, inhibition of virulence factor production increases survival of immune cells which promote pathogen clearance protecting the host from excessive tissue damage (105, 110). Due to the reliance on the immune response when treating with anti-*agr* therapies it may be necessary to ascertain the immune status of the patient before treatment (112).

The *agr* system is employed in many Gram-positive bacteria as well as *S. aureus* such as *Enterococcus faecalis* and *Clostridium difficile*. These pathogens represent some of the most common causes of healthcare associated infections resulting in significant morbidity and mortality (47). Antivirulence strategies which target the *agr* system and are effective across species, such as ambuic acid which inhibits QS in *S. aureus* and *Enterococcus faecalis,* could therefore, have a significant impact on human health (47, 113).

The *agr* system is also employed, however, by commensal bacteria such as *Staphylococcus epidermidis* and *Staphylococcus hominis*. *S. epidermidis* is thought to benefit the host by competing with *S. aureus* for colonisation. Additionally, AIPs from *S. epidermidis* have been shown to inhibit *S. aureus agr* QS. Therefore, to avoid affecting the host microbiota, the cross reactivity of *agr* inhibitors with commensal strains such as this must be determined (105, 110). Therapeutics could be targeted to components of the *agr* system which are not conserved between species or could be shown not to affect commensal strains. Examples of these include savirin, an AgrA inhibitor, and ambuic acid an AgrB inhibitor which have both been shown to have no effect on quorum sensing in multiple commensal strains including *S. epidermidis* (105, 107).

Inhibitors of *agr* will not, however, be useful against all manifestations of *S. aureus* infection. The contribution of *agr* to infection has been demonstrated in SSTIs however *agr* dysfunction has been shown to be associated with other disease manifestations such as persistent bacteriaemia and in some infection models *agr* does not seem to be necessary for the development of disease (15, 114, 115). There have also been several reports of *agr* defective strains isolated from human infections. These have non-haemolytic phenotypes due to mutations in the *agr* locus (50). *agr* defective strains are associated with increased hospitalisation rates and increased resistance to glycopeptides such as vancomycin (116, 117). It is thought that mutations in *agr* may be adaptive for survival *in vivo,* giving a short-term survival and growth advantage. Indeed, it has been demonstrated that *agr* functional populations exhibit cell death, which is not noted in *agr* dysfunctional populations, giving *agr* dysfunctional cells a fitness advantage (118). *agr* defective strains, however, only represent a minority of clinical cases and strains with a functional *agr* system are favoured in transmission (47, 117, 119). It has been shown that dysfunctional *agr* strains develop by mutation during infection and are unable to initiate infection (50). Additionally, it is thought that not all *agr* mutations may be completely inactivating but may modify the timing and strength of *agr* induction (49). This demonstrates that the efficacy of *agr* inhibitors will depend on the infection being treated and the timing of the inhibition of *agr* may be critical in order for it to be effective (120).

Disruption of *agr* is also associated with increased biofilm formation due to increased expression of cell surface associated factors involved in cell adhesion when *agr* is inhibited (115). *S. aureus* biofilms can form readily on host tissues and implanted medical devices causing chronic infections with high tolerance to antibiotics (6). Therefore anti-QS therapeutics may not be suitable for the treatment of device related infections however they may be

useful as adjuncts to existing antibiotics or as prophylactic treatment preventing the spread of infection.

1.4.1. Inhibitors of *agr* activation

The *agr* system can be targeted for inhibition at a number of different points for example inhibition of AgrC, inhibition of AgrA-DNA interactions and inhibition of AIP biosynthesis through targeting AgrB (**Figure 1-3**) (6, 107). Examples of *agr* inhibitors which have been shown to be effective include AgrA inhibitors savirin and its analogue staquorsin, AIP analogues which block AgrC, ambuic acid which inhibits AgrB and ω-hydroxyemodin, an AgrA inhibitor (105-107, 110, 121).

AgrA has been identified as an antivirulence target with a number of inhibitors having been developed against it. AgrA is part of the two-component signal transduction system which leads to upregulation of promoters *agr*P2 and *agr*P3. Blocking binding of phosphorylated AgrA to *agr*P2 and *agr*P3 will prevent *agr* upregulation, reducing expression of secreted virulence factors leading to increasing immune clearance (88). Savirin was reported in 2014 by Sully et al. to inhibit AgrA with minimal impact on growth and little effect on QS in commensal bacteria such as *S. epidermidis* (105). An analogue of savirin, staquorsin was reported in 2021 to have improved efficacy over savirin. This was also shown to decrease virulence in a mouse abscess model of infection with no resistance seen (106). Additionally, ω-hydroxyemodin was shown to bind directly to AgrA preventing its interaction with the *agr*P2 promoter. Treatment with ω-hydroxyemodin also reduced dermonecrosis and led to increased bacterial clearance in a mouse skin infection model (110). More recently, apicidin, a fungal derived metabolite, was reported in 2019 to target AgrA, reducing the ability of AgrA to upregulate *agr*P3 and reducing virulence in mouse abscess models of infection (108).

It is known that AIP molecules of different *agr* subgroups and different species can inhibit *agr* QS (60). Considering this, synthetic AIP analogues have been made which inhibit *agr* QS by preventing signalling via AgrC. One such example is Ala^5(AIP-1), this is an AIP analogue which is a potent *agr* QS inhibitor against all *S. aureus agr* subgroups (66). Solonamide B has also been identified as an AgrC inhibitor and a number of analogues have been synthesised which reduce *agr* associated virulence (112, 122).

AgrC is hypermutable which suggests that resistance to AgrC inhibitors may develop quickly therefore there are concerns as to whether AgrC is an effective target for potential therapeutics. *agr* QS can also be inhibited by preventing synthesis of AIP. AIP biosynthesis can be inhibited by targeting AgrB which is more conserved than AgrC, therefore could represent a good potential drug target. AgrB inhibitors could be for example, peptide analogues which compete for the AgrB active site or compounds which prevent recognition and cleavage of AgrD by changing the structure of AgrB (47, 88). Ambuic acid, a fungal metabolite has been identified as a putative AgrB inhibitor, reducing AIP production, with reduction in pathology in murine abscess models of infection (107, 113). Ambuic acid has also been shown to have little effect on QS in multiple commensal bacteria making it a good anti-virulence candidate (107).

1.4.2. Investigating *agr* activation experimentally

Studying *agr* controlled virulence factor expression and inhibition *in vitro* is relatively straightforward however studying the regulation of QS and gene expression *in vivo* is much more complex. Genes which are expressed during infection *in vivo* may be shut-off or non-essential in laboratory conditions. Regulation of the QS response is also highly dependent on the environment and the presence of immune cells and regulators which may not be present *in vitro* (87). For example, apolipoprotein B, which is present in blood at acute infection sites, sequesters AIP preventing *agr* activation

(123). AIP can also be inactivated by oxidants such as NADPH which is released by phagocytes (124). Additionally, mutations which affect the timing and strength of *agr* induction can occur (49). Therefore, it is important to assess *agr* expression *in vivo* (49, 84, 87, 116). This will further our understanding of factors which contribute to infection severity and will enable design of antivirulence factors (27, 49).

To investigate temporal *agr* expression and *agr* inhibition it is important to develop real time methods of monitoring *agr* expression in *in vivo* models (23). This can be performed using bioluminescent or fluorescent reporters linked to promoters of the *agr* system (116, 125). Bioluminescent reporters have been generated with the *Photorhabdus luminescens lux* operon linked to the *agr*P3 promoter. The *agr*P3-*lux* reporter has been used to measure temporal *agr* activation in infection models and assess *agr* inhibitors *in vivo* (107, 109). Fluorescent reporters have also been generated with, for example, GFP linked to the *agr*P3 promoter, and these have been used to screen for *agr* inhibitors (120, 125, 126).

1.5. Luciferases as bioreporters

Bioluminescence is a naturally occurring phenomenon and luciferase-based bioluminescence has become a key tool for monitoring of biological processes. Bioluminescence is found across a range of life including bacteria, insects, fungi, and marine organisms (127). It typically occurs when a luciferase enzyme oxidises a photon emitting substrate releasing light. This can be observed visually using biophotonic imaging or quantified using a luminometer (128). Luciferases are often used as biological reporters due to their high sensitivity, broad dynamic range, and operational simplicity. Luciferases have been used to monitor multiple cellular processes such as gene expression and protein interactions as well as tracking bacterial and viral infections (129, 130).

Bioluminescence is widely exploited for *in vivo* optical imaging, it enables non-invasive molecular imaging with low background compared to fluorescence and high sensitivity (130, 131). Bioluminescence imaging is a powerful tool for analysing infectious diseases in animal models. It enables real time monitoring of spatial and temporal progression of infection in the same animal. Imaging also enables visualisation of the spread of infection around the body. Pathogens can be engineered to express more than one luciferase enzyme or a luciferase in combination with a fluorescent protein, enabling monitoring of multiple processes simultaneously (132).

Fluorescence is another phenomenon widely used for *in vivo* imaging and analysis. This occurs when a substance absorbs light and immediately emits light at a different wavelength. Bioluminescence, however, can be advantageous over fluorescence for a number of reasons. Although fluorescence does not require a substrate, which bioluminescence does, fluorescence does require excitation light which can cause photobleaching and phototoxicity (133). Fluorescence also has higher background signal *in vivo* than bioluminescence giving it a higher signal to noise ratio meaning decreased sensitivity (134, 135). Additionally, fluorescent proteins have a long half-life, this means that temporal gene regulation is difficult to monitor with these proteins as the signal degrades slowly leading to accumulation (136).

Different luciferases are useful for different applications due to their individual properties for example, for high throughput drug screening, the luciferase would need to be stable with high light output to enable monitoring of drug activity in real time (137). Traditionally luciferases such as firefly, Renilla and bacterial luciferases have been used however these are limited due to their size, stability, and efficiency. They also require ATP therefore impact on the energy source of the bacteria. Therefore, researchers are beginning to develop and focus on novel luciferases such as *Gaussia*

luciferase and NanoLuc which are smaller and brighter giving high sensitivity.

1.5.1. *Gaussia* luciferase

Gaussia luciferase (GLuc) is a naturally secreted enzyme from the marine copepod *Gaussia princeps.* It is a 185 amino acid, 19.9 kDa luciferase which catalyses oxidative decarboxylation of substrate coelenterazine (CTZ) producing coelenteramide and emitting blue light at 480 nm as displayed in **Figure 1-8** (138). It is a highly sensitive reporter, 1000 times brighter than traditional luciferases firefly or Renilla and is 20,000 times more sensitive than secreted alkaline phosphatase (137, 139, 140). GLuc is non-toxic and is naturally secreted from the cell therefore is useful for monitoring biological processes in real time. GLuc does not require ATP as a cofactor for light production unlike many luciferases therefore poses less of a metabolic burden on the cell and is not restricted to intracellular use (141). GLuc is a useful reporter due to its small size and high light intensity giving high sensitivity. It is also stable at a wide range of pH and is resistant to heat and oxidative stress giving it a wide functional range (140).

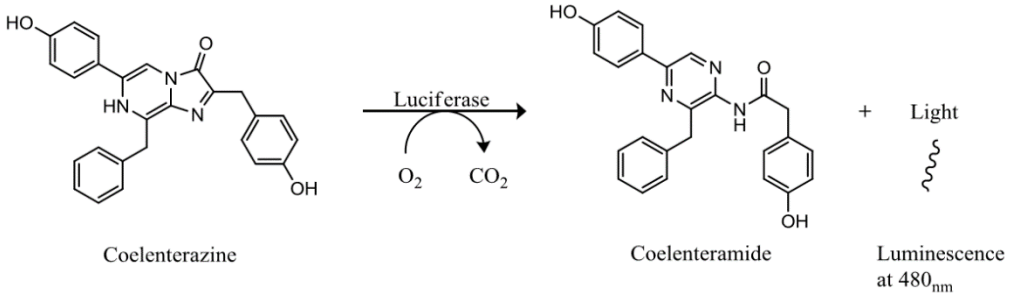


Figure 1-8. Production of light from *Gaussia* luciferase with substrate coelenterazine (142).

GLuc is a sensitive reporter which has been used to study a variety of biological processes such as gene expression, promoter activity, protein-protein interactions and tumour cell growth (137). It is a secreted luciferase therefore kinetics of biological processes can be measured in real time using

in vivo models. Secreted luciferases can be detected in small volumes of blood or mouse urine from murine models enabling non-invasive, *ex vivo* monitoring of *in vivo* processes (139, 143). This complements *in vivo* bioluminescence imaging which can be used to localise the signal following intravenous injection of CTZ into a mouse (143). The half-life of GLuc in the blood is approximately 20 min, this enables multiple measurements to be taken in a short period of time without accumulation of signal (143, 144).



GLuc is widely used as a biological reporter in eukaryotes and has also been shown to be effective as a reporter in bacteria such as *Salmonella enterica* and *Mycobaterium smegmatis* (140, 145). However, use in *E. coli* has been shown to be complicated due to the 10 cysteine residues which form disulphide bonds (141). Use in *S. aureus* has not been demonstrated before.

GLuc is a useful reporter however it does have some limitations. It is a flash luciferase, with the bioluminescent signal dropping off rapidly over the course of 10 min after addition of CTZ substrate (139). Mutations have been generated to increase the half-life of the bioluminescent signal however it is necessary to use a luminometer with a built-in injector to measure bioluminescence making the assays time consuming (137, 146). Furthermore, the use of GLuc *in vivo* is limited due to the peak emission at 480 nM. This blue light is absorbed by pigmented molecules in the blood such as haemoglobin and melanin (144). Additionally, CTZ can bind to serum proteins and is cleared rapidly from the bloodstream. It can also be degraded by auto-oxidation in serum providing high levels of background luminescence. Due to this and the flash-type kinetics of the luciferase when

imaging the signal needs to be acquired immediately after administration of substrate (139). Despite this, GLuc has been used for *in vivo* imaging as light can be detected after addition of CTZ and the rapid degradation of the substrate can be advantageous allowing multiple images without accumulation of signal. GLuc bioluminescence can also be detected *ex vivo* from blood samples enabling real time assaying of biological processes demonstrating the usefulness of this luciferase (143, 146).

1.5.2. NanoLuciferase

NanoLuciferase (NanoLuc) is another novel luciferase which is derived from the deep-sea shrimp *Oplophorus gracilirostris*. The native luciferase has a heteromeric structure which was optimised by Promega to produce NanoLuc (129, 147). NanoLuc is 19.1 kDa and reacts with substrate furimazine, a CTZ analogue, to produce high intensity glow-type bioluminescence with a half-life exceeding 2 h as shown in **Figure 1-9** (129, 148). It has a number of advantages over established bioluminescent reporter systems including enhanced stability, smaller size and high light output (147). It is also ATP independent so poses little metabolic burden on the cell and can be employed for extracellular use. The NanoLuc system is extremely versatile, it can be used for monitoring protein-protein and protein-ligand interactions, exploring gene regulation and cell signalling, monitoring protein stability and bioluminescence imaging (148).

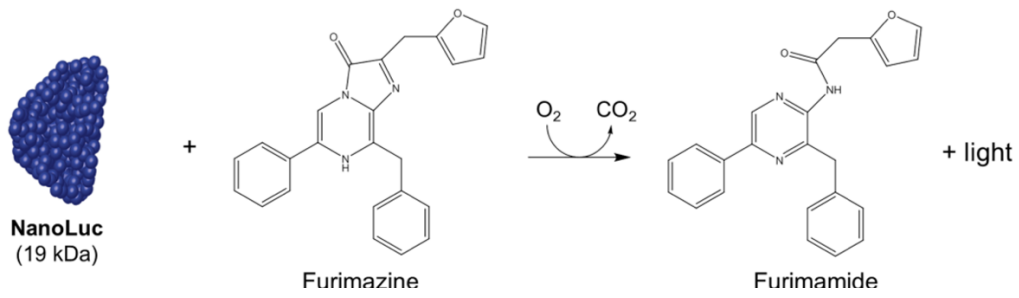


Figure 1-9. Production of light from NanoLuc with substrate furimazine. From England et al. 2016 (148).

The glow-type bioluminescence provides an advantage over GLuc as it allows a larger window for *in vivo* imaging and acquisition of bioluminescence readings. Furimazine can be injected intravenously and has been shown to display enhanced stability and lower background activity compared to CTZ (148). NanoLuc can also be secreted by inserting a signal sequence upstream of the NanoLuc sequence. Secreted NanoLuc has been detected from the serum of *in vivo* models demonstrating that this can be used as an *ex vivo* biomarker (149).

Although NanoLuc does not have optimal spectral emission for *in vivo* imaging with peak emission at 460 nm, it has been used for *in vivo* imaging techniques, including for the monitoring of disease progression (148, 149). Use of NanoLuc has been demonstrated for tracking disease progression caused by group A *Streptococcus in vivo* with correlation seen between the NanoLuc signal and the number of viable bacteria (150). This shows that NanoLuc is a useful reporter for use in prokaryotes *in vivo*. Imaging with NanoLuc has also been demonstrated in superficial and deep tissues although sensitivity of detection from deep tissues was lower due to absorption and scattering of light (149).

1.6. Aims

The aims of this study were to investigate *agr* quorum sensing in *S. aureus* through:

- Development and validation of novel luciferase reporters for monitoring *agr* activation and inhibition
- Development of novel bioluminescent techniques to investigate *agr* protein-protein interactions in live *S. aureus* and *E. coli* cells
- Investigation of AIP biosynthesis through monitoring of AgrBD interactions *in vitro* in *E. coli* membranes
- Use of an AgrB1D1 intermediate to probe the mechanism of action of AgrB inhibitors
- Purification of AgrB1 and MroQ and analysis of AIP-1 biosynthesis in a cell free model

2. Methods

2.1 Bacterial strains and growth conditions

Staphylococcal strains were cultured in tryptic soy broth (TSB; Oxoid) and maintained on TSB agar unless stated otherwise. To make TSB, 30 g TSB powder as purchased was added to 1 L distilled water and media was sterilised by autoclaving at 121°C for 15 min.

For selection and plasmid maintenance in *S. aureus* antibiotics were added at the following concentrations: chloramphenicol 10 μg/mL, kanamycin 100 μg/mL, tetracycline 2.5 μg/mL and erythromycin 10 μg/mL. Antibiotic stocks were dissolved in the appropriate diluent to the following concentrations; chloramphenicol 25 mg/mL 100% ethanol, kanamycin 100 mg/mL dH_2O, tetracycline 2.5 mg/mL 50% ethanol and erythromycin 10 mg/mL 100% ethanol. Antibiotics were filter sterilised using a 0.2 μM syringe filter before use.

E. coli strains were cultured in lysogeny broth (LB; Oxoid) and maintained on LB agar. To make LB, 25 g LB powder as purchased was added to 1 L distilled water and media was sterilised by autoclaving at 121°C for 15 min.

For selection and plasmid maintenance in *E. coli* antibiotics were added at the following concentrations: spectinomycin 100 μg/mL and kanamycin 100 μg/mL. Spectinomycin stock was made to 100 mg/mL in dH_2O.

Liquid cultures were grown at 37°C with aeration by shaking at 200 rpm and agar plates were incubated at 37°C statically. Liquid culture growth was monitored by measuring optical density at 600 nm (OD_{600}) using a spectrophotometer. All strains used are outlined in **Table 2-1**.

Stocks of bacterial strains were made in 10 % (v/v) glycerol and stored at -80°C.

Table 2-1. Bacterial strains used in this study.

Bacterial strain	Characteristics	Source/Reference
Staphylococcus aureus		
USA300 JE2	*S. aureus* clinical isolate	(151)
USA300 JE2 *agr*P3-GLuc	*attB2:P3-SpA leader-GLuc kan^R*	(152)
USA300 JE2 Δ*agr* *agr*P3-GLuc	*attB2:P3-SpA leader-GLuc Δagr kan^{R}ery^R*	(152)
USA300 JE2 *agr*P3-NanoLuc	*attB2:P3-SpA leader-NanoLuc kan^R*	This study
USA300 JE2 Δ*agr* *agr*P3-NanoLuc	*attB2:P3-SpA leader-NanoLuc Δagr kan^{R}ery^R*	This study
ROJ143	RN4220 Δ*agr* P3-*luxCDABE* pSKERM P2-*agrCA-1 cm^R*	(153)
RN4220	Cloning intermediate attB2 *cm^R*	(154)
USA300 JE2 *agr*P3-SpA-NanoLuc codon optimised	*attB2:P3-SpA leader-RBS-NanoLuc kan^R* NanoLuc codon optimised for *S. aureus*	This study
USA300 JE2 *agr*P3-ClfA-NanoLuc codon optimised	*attB2:P3-ClfA leader-RBS-NanoLuc kan^R* NanoLuc codon optimised for *S. aureus*	This study

USA300 JE2 *agr*P3-SasD-NanoLuc codon optimised	*attB2:P3-SasD leader-RBS-NanoLuc kan^R* NanoLuc codon optimised for *S. aureus*	This study
USA300 JE2 *agr*P3-IsdC-NanoLuc codon optimised	*attB2:P3-IsdC leader-RBS-NanoLuc kan^R* NanoLuc codon optimised for *S. aureus*	This study
SH1000	Derivative of *S. aureus* NCTC 8325-4	(155)
Staphylococcus epidermidis		
1457	*agr g*roup 2 strain used in biofilm research	(156)
Escherichia coli		
DC10B	*dcm*$^-$ cloning strain	(157)
C41 (DE3)	Expression strain optimised for expression of membrane proteins	(158)

2.2 Molecular biology techniques for DNA manipulation

2.2.1 Oligonucleotide primers used in this study

Oligonucleotide primers used are outlined in **Table 2-2**. All primers were sourced from Sigma-Aldrich.

Table 2-2. Primers used in this study.

Primer name	Sequence (5'-3')	Description
agrP3-Nano F	cttacccgtcttactgtcggctcactgtcattatacg atttagtacaatc	Amplify *agr*P3-nanoluc oligo with overhangs for

agrP3-Nano R	cccgggtaccgagctcgaatctcaggagagcgttcacc	HiFi cloning into pLL102
pLL102 F	attcgagctcggtacccg	Amplify pLL102 for HiFi cloning
pLL102 R	ccgacagtaagacgggtaag	
OU9R10	catactacatatcaacgaaatcag	Check integration from of pLL102 into *S. aureus* RN4220
OU9R7	atgggtggtaaaacacaaatttc	
agrP3 F	ctcactgtcattatacgatttagt	For sequencing *agr*P3-ss-NanoLuc
ClfA-F	cagtgcttgtaggtacgttaatcggttttggactactcagcagtaaagaagcagatgcagtcttcacactcgaagatttcgt	Replace SpA with ClfA leader in agrP3-SpA-NanoLuc
ClfA-R	aagccacgccaatcgatttttttccgaattgcgtgtttttctttttttcttcatattcatatgtttttcctcctactagtctctg	
IsdC-F	ttaattatcatcatcgcgacattcagtaattctgcaaatgccgtcttcacactcgaagatttcgt	Replace SpA with IsdC leader in agrP3-SpA-NanoLuc
IsdC-R	cgctaaaatcgttgtattaaaaacttttaaaatatttttcaaatgtttttcctcctactagtctctg	
SasD-F	actttagtattctcaagtatgccttttcaaaatgcgcatgccgtcttcacactcgaagatttcgt	Replace SpA with SasD leader in agrP3-SpA-NanoLuc
SasD-R	gcttgttacaattaaagaacctactgttgctaatttttcatatgtttttcctcctactagtctctg	
pLL102 F all	aacgcagaagcggtctgataaaac	Amplify pLL102 agrP3-ss-NanoLuc for HiFi cloning
pLL102 SpA R	agcatttgcagctggtgttac	
pLL102 ClfA R	tgcatctgcttctttactgc	
pLL102 SasD R	ggcatgcgcattttgaaaag	
pLL102 IsdC R	ggcatttgcagaattactgaatgtc	
NanoLuc SpA F	taacaccagctgcaaatgctgttttcaccctagaggatttc	Amplify codon optimised NanoLuc

NanoLuc ClfA F	gcagtaaagaagcagatgcagttttcaccctagaggatttc	with overhangs for HiFi cloning into pLL102 agrP3-ss-NanoLuc
NanoLuc SasD F	cttttcaaaatgcgcatgccgttttcaccctagaggatttc	
NanoLuc IsdC F	tcagtaattctgcaaatgccgttttcaccctagaggatttc	
Nanoluc all R	tatcagaccgcttctgcgttttatgctaaaattctttcacataaac	
pCDF MCS1 F	agccaggatccgaattcg	HiFi cloning to place AgrB1 in MCS1 of pCDFDuet-1
pCDF MCS1 R	gtggtgatgatggtgatg	
AgrB F	gccatcaccatcatcaccacttgaattattttgataataaaattgacc	
AgrB R	ctcgaattcggatcctggcttcattttaagtcctccttaataaag	
pCDF MCS2 F	gcagatctcaattggatatc	HiFi cloning to place AgrD1 in MCS2 of pCDFDuet-1
pCDF MCS2 R	catatgtatatctccttcttatacttaac	
AgrD F	aagaaggagatatacatatgaatacattatttaacttatttttgattttattac	
AgrD R	gatatccaattgagatctgcttcgtgtaattgtgttaattc	
AgrB C84S F	cttctttttggtcttatgtagaaagt	Mutate C84 in AgrB1 to serine
AgrB C84S R	aaggtgcatgtgcaccat	
AgrB R70A F	ttatttaatagcaagacatgcacatggtg	Mutate R70 in AgrB1 to alanine
AgrB R70A R	aatgttaaattcgtaattaacg	
AgrB G75A F	catgcacatgctgcacatgcac	Mutate G75 in AgrB1 to alanine
AgrB G75A R	tcttcttattaaataaaatgttaaattcgtaattaac	
AgrB H77A F	acatggtgcagctgcaccttcttc	Mutate H77 in AgrB1 to alanine
AgrB H77A R	gcatgtcttcttattaaataaaatg	
AgrB KKK-AAA F	agcacccattcctgtgcgactt	Mutate KKK129-131 in AgrB1 to alanine

AgrB KKK-AAA R	gctgcagttgctgcaggagcatata	
pCDF agrB2 F	agccaggatccgaattc	Remove AgrD2 from pCDFDuet-1 *agrB2D2*
pCDF agrB2 R	ttaatcctccttagggaaa	
agrD epi F	aagaaggagatatacatatgatgaatttattaggtggcttac	Amplify *agrD2* from *S. epidermidis* 1457 gDNA with overhangs for HiFi cloning into pCDFDuet-1 *agrB1*
agrD epi R	gatatccaattgagatctgcctactcatctagtttagttaattcttc	
pCDF agrB F	ttgaattattttgataataaaattgacc	HiFi cloning to place NanoLuc N-terminal to *agrB1* in pCDFDuet-1
pCDF agrB R	gtggtgatgatggtgatggctgctgc	
pCDF nano agrB F	gcagcagccatcaccatcatcaccacggttctgcggtcttcacactcgaagatttcgttg	
pCDF nano agrB R	ttttattatcaaaataattcaacgcagaacccgccagaatgcgttcgcac	
pCDF nano colony F	ggagatataccatgggcagcag	For colony PCR to check insertion of *NanoLuc* N-terminal to *agrB1*
pCDF nano colony R	ctcgaattcggatcctggct	
pCDF agrB F	agccaggatccgaattcg	HiFi cloning to place *NanoLuc* C-terminal to *agrB* in pCDFDuet-1 *agrB1*
pCDF agrB R	ttttaagtcctccttaataaagaaaatagg	
C term agrB nano F	ttattaaggaggacttaaaaggttctgcggtcttcacactcgaagatttcg	
C term agrB nano R	ctcgaattcggatcctggcttcacgccagaatgcgttc	
N term Nano B link F	gcgtctggttctgcggcgttgaattattttgataataaaattgaccagtttgc	Increase linker between NanoLuc-AgrB to 15 amino acids
N term Nano B link R	agaaccacccgcaccagacgcagaacccgccagaatgcgttcg	
C term Nano B link F	gttctgcgtctggttctgcggcggtcttcacactcgaagatttc	

C term Nano B link R	cacccgcaccagacgcagaacctttaagtcctc cttaataaagaaa	Increase linker between AgrB-NanoLuc to 15 amino acids
Halo-AgrB F	ataagaaggagatatacatatgatggcagaaat cggtactgg	Insert HaloTag N-terminal to AgrB1 to MCS2 of pCDFDuet-1
Halo-AgrB R	ccgatatccaattgagatctgctcattttaagtcctc cttaataaag	

2.2.2 DNA sequence of *agr*P3-NanoLuc oligonucleotide purchased from Eurofins (5'-3')

tcactgtcattatacgatttagtacaatcttttatcattatattgcctaactgtaggaaataaatacttaactgtt
aaatgtaatttgtatttaatattttaacataaaaaaaattacagttaagaataaaaaacgactagttaaga
aaaattggaaaataaatgcttttagcatgttttaatataactagatcacagagatgtgatggaaaatagtt
gatgatgactttacaaatacatacaggggtattaatttgaaaaagaaaaacatttattcaattcgtaaa
ctaggtgtaggtattgcatctgtaactttaggtacattacttatatctggtggcgtaacaccagctgcaaat
gctgtcttcacactcgaagatttcgttggggactggcgacagacagccggctacaacctggaccaagt
ccttgaacagggaggtgtgtccagtttgtttcagaatctcggggtgtccgtaactccgatccaaaggattg
tcctgagcggtgaaaatgggctgaagatcgacatccatgtcatcatcccgtatgaaggtctgagcggc
gaccaaatgggccagatcgaaaaaatttttaaggtggtgtaccctgtggatgatcatcactttaaggtga
tcctgcactatggcacactggtaatcgacggggttacgccgaacatgatcgactatttcggacggccgt
atgaaggcatcgccgtgttcgacggcaaaaagatcactgtaacagggaccctgtggaacggcaaca
aaattatcgacgagcgcctgatcaaccccgacggctccctgctgttccgagtaaccatcaacggagtg
accggctggcggctgtgcgaacgcattctggcgtaaaacgcagaagcggtctgataaaacagaattt
gcctggcgggtggtcccacctgaccccatgccgaactcagaagtgaaacgccgtagcgccgatggt
agtgtggggtctccccatgcgagagtagggaactgccaggcatcaaataaaacgaaaggctcagtc
gaaagactgggcctttcgttttatctgttgtttgtcggtgaacgctctcctgag

2.2.3 DNA sequences of amplified AgrB and AgrD

AgrB1 from *S. aureus* USA300 JE2 (5'-3'):

ttgaattattttgataataaaattgaccagtttgccacgtatcttcaaaagagaaataacttagatcatattc
aatttttgcaagtacgattagggatgcaggtcttagctaaaaatataggtaaattaattgttatgtatactatt
gcctatattttaaacatttttctgtttacgttaattacgaatttaacattttatttaataagaagacatgcacatg
gtgcacatgcaccttcttctttttggtgttatgtagaaagtattatactatttatacttttaccttagtaatagtaa
attttcatattaacttttttaattatgattattttaacagttatttctttaggtgtaatctcagtatatgctcctgcagc
aactaaaaagaagcccattcctgtgcgacttattaaacgaaaaaaatattatgcgattattgttagtttaa
ccctttttcattatcacacttatcatcaaagagccatttgcccaattcattcaattaggcatcataatagaagc
tattacattattacctattttctttattaaggaggacttaaaatga

AgrB2 from *S. aureus* NRS149 (5'-3'):

ttgaattattttgataacaaaattgaccagtttgccacgtatcttcaaaagagaaataacttagatcatattc
aatttttgcaagtacgtttagggatgcaaattatagttggtaatttttttaaaatacttgtaacatatagtatttct
atattcttaagtgtatttttgtttaccttagttacacacttatcctatatgttaatacgctataatgcacatggtgct
catgcaaagtcttcgatactttgttacatacaaagtattttaacatttgtatttgtaccttattttctaattaatata
gacattaattttacttatttactggccttatctattataggattgatttccgttgttatttatgcacctgcagcaac
gaaaaagcaacctataccaataaaattagtaaaacgtaaaaagtatttatctataattatgtatttattagt
tttgattctatccttaataatacatccattttatgctcaatttatgttattaggaattttagtggaatctattacatta
ttacctatttttttccctaaggaggattaa

AgrB3 from *S. aureus* MRSA 252 (5'-3'):

ttgaattattttgataacaaaattgaccagtttgccacgtatcttcaaaagagaaataacttagatcatattc
aatttttgcaagtacgattagggatgcaggtcttagctaaaaatataggaaaactgattgttatgtatactc
ttgcctatattttaaacatttttatcttcactttaattactaatatatcgttttatctaattagaaggtatgcacatg
gtgcacatgcaccttcatctttttggtgttatatagaaagcattacacttttattgttctacctctattagtacta
cattttcatattaatgaaacactaatgatgtttttagcattattaagtgttggcgtagtgattaaatatgcacct
gcagctactaagaagaagcctatcccggcaaggcttgtaaagcaaaaaagatatttttcaattataatt
agtacaattcttttcattatcacacttttttgtaaaggaaccatatacccaatttattcaactgggtattattatac
aagctattacattactaccaatatactattcaaaggaggactaa

AgrD1 from *S. aureus* USA300 JE2 (5'-3'):
aatacattatttaacttatttttttgattttattactgggattttaaaaaacattggtaacatcgcagcttatagtac
ttgtgacttcataatggatgaagttgaagtaccaaaagaattaacacaattacacgaa

AgrD2 from *S. aureus* NRS149 (5'-3'):
atgaatacacttgttaatatgttttttgattttataattaaattagctaaagcaatcggaattgtcggtggcgta
aacgcttgcagcagtttatttgatgaacctaaagtacccgctgaattaacgaatttatacgacaaatag

S. epidermidis AgrD2, from *S. epidermidis* 1457 (5'-3'):
atgaatttattaggtggcttacttttaaaaatttttttcaaactttatggcagtaattggtaacgcatcaaaatac
aacccttgtagtaattatctcgatgagccacaagtgccagaagaattaactaaactagatgagta

2.2.4 Plasmids used in this study

All plasmids used in this study are outlined in **Table 2-3**.

Table 2-3. Plasmids used in this study

Plasmid	Characteristics	Source/Reference
pMK-RQ *agr*P3-SpA NanoLuc	Vector from Eurofins with synthesised *agr*P3 SpA NanoLuc sequence. *Kan^R*	Eurofins
pLL102	Single copy integration vector for *Staphylococcus aureus*	(154)
pUNK NanoLuc	NanoLuc codon optimised for *S. aureus*	Carmen Tong, unpublished
pLL102 *agr*P3-SpA NanoLuc	*attP2:P3-SpA leader-NanoLuc kan^R*	This study
pLL102 *agr*P3-ClfA NanoLuc	*attP2:P3-ClfA leader-NanoLuc kan^R*	This study

pLL102 *agr*P3-SasD NanoLuc	*attP2:P3-SasD leader-NanoLuc kan*^{R}	This study
pLL102 *agr*P3-IsdC NanoLuc	*attP2:P3-IsdC leader-NanoLuc kan*^{R}	This study
pSKERM *agr*P2-*agrAC*	AgrAC complementation vector	(153)
pCDFDuet-1	Expression vector with two MCS for co-expression of two genes	Novagen
pCDFDuet-1 *agrB1*	Vector for expression of AgrB1 from MCS1	This study
pCDFDuet-1 *agr1I agrD1*	Vector for expression of AgrB1 from MCS1 and AgrD1 from MCS2	This study
pCDFDuet-1 *agrB1D1*	Vector for expression of AgrB1 and AgrD1 from MCS1	Ewan Murray
pCDFDuet-1 *nanoluc-agrB1*	Vector for expression of NanoLuc N-terminal to AgrB1 from MCS1	This study
pCDFDuet-1 *nanoluc-agrB1 agrD1*	Vector for expression of NanoLuc N-terminal to AgrB1 from MCS1 and AgrD1 from MCS2	This study
pCDFDuet-1 *agr1I-nanoluc*	Vector for expression of NanoLuc C-terminal to AgrB1 from MCS1	This study
pCDFDuet-1 *nanoluc-agrB1 agrD1*	Vector for expression of NanoLuc C-terminal to AgrB1 from MCS1 and AgrD1 from MCS2	This study

pCDFDuet-1 *nanoluc-agrB1 15 link*	Vector for expression of NanoLuc N-terminal to AgrB1 from MCS1 15 aa linker	This study
pCDFDuet-1 *nanoluc-agrB1 agrD1 15 link*	Vector for expression of NanoLuc N-terminal to AgrB1 from MCS1 and AgrD1 from MCS2 15 aa linker	This study
pCDFDuet-1 *agrB1-nanoluc 15 link*	Vector for expression of NanoLuc C-terminal to AgrB1 from MCS1 15 aa linker	This study
pCDFDuet-1 *nanoluc-agrB1 agrD1 15 link*	Vector for expression of NanoLuc C-terminal to AgrB1 from MCS1 and AgrD1 from MCS2 15 aa linker	This study
pCDFDuet-1 *agrB1-nanoluc halotag-agrB1 15 link*	Vector for expression of NanoLuc C-terminal to AgrB1 from MCS1 with a 15 aa linker and HaloTag N-terminal to AgrB1 from MCS2. Used for NanoBRET	This study
pCDFDuet-1 *halotag-agrB1*	Vector for expression of HaloTag N-terminal to AgrB1 from MCS2. A control for NanoBRET	This study
pCDFDuet-1 *agrB2*	Vector for expression of AgrB2 from MCS1	This study
pCDFDuet-1 *agrB2agrD2*	Vector for expression of AgrB2 and AgrD2 from MCS1	Ewan Murray
pCDFDuet-1 *agrB3*	Vector for expression of AgrB3 from MCS1	Ewan Murray

pCDFDuet-1 *agrB1 epiagr2*	Vector for expression of *S. aureus* AgrB1 from MCS1 and *S. epidermidis* AgrD2 from MCS2	This study
pCDFDuet-1 *agrB1 C84S agrD1*	Vector for expression of AgrB1 C84S and AgrD1 both from MCS1	This study
pCDFDuet-1 *agrB1 agrD1 C28S*	Vector for expression of AgrB1 and AgrD1 C28S both from MCS1	Ewan Murray
pCDFDuet-1 *agrB1 R70A agrD1*	Vector for expression of AgrB1 R70A and AgrD1 both from MCS1	This study
pCDFDuet-1 *agrB1 G75A agrD1*	Vector for expression of AgrB1 G75A and AgrD1 both from MCS1	This study
pCDFDuet-1 *agrB1 KKK129-131AAA agrD1*	Vector for expression of AgrB1KKK129-131AAA and AgrD1 both from MCS1	This study
pCDFDuet-1 *agrB1 H77A*	Vector for expression of AgrB1 H77A from MCS1	This study
pCold His10-*agrB1*	Vector for expression of AgrB1 for purification	Philip Bardelang
pCold *malE-mroQ*	Vector for expression of maltose binding protein-MroQ for purification	Philip Bardelang

2.2.5 Plasmid isolation from *E. coli*

Plasmids were isolated from *E. coli* using a GenElute Plasmid Miniprep kit (Sigma-Aldrich) following manufacturer guidelines. Plasmid DNA was eluted in 60 μL dH_2O and stored at -20°C.

2.2.6 Plasmid isolation from *S. aureus*

Plasmids were isolated from *S. aureus* using a GenElute Plasmid MiniPrep kit (Sigma-Aldrich). *S. aureus* cells from 5 mL overnight culture were pelleted and resuspended in resuspension solution with 50 μg/mL lysostaphin (Sigma-Aldrich). This was incubated at 37°C statically for 30 min after which the protocol was continued as per manufacturer guidelines. Plasmid DNA was eluted in 60 μL dH_2O and stored at -20°C.

2.2.7 Genomic DNA extraction from staphylococci

Genomic DNA was extracted from staphylococci spp. using a GenElute Bacterial Genomic DNA kit (Sigma-Aldrich) following the manufacturer guidelines for DNA extraction from Gram-positive bacteria. Genomic DNA was eluted in 100 μL dH_2O and stored at -20°C.

2.2.8 Polymerase Chain Reaction (PCR)

Standard PCR was performed using High Fidelity Q5 DNA polymerase (NEB). Colony PCR was performed with DreamTaq Green PCR master mix (ThermoFisher). All reactions were set up and run as per manufacturer guidelines. All primers used are listed in **Table 2-2**.

All constructs and strains were sequenced by Sanger DNA sequencing performed by Source BioScience, Nottingham NG8 6PX.

2.2.9 DNA separation using agarose gel electrophoresis

DNA fragments were separated and visualised using agarose gel electrophoresis. Agarose gels were prepared with 1 % agarose (w/v) in 1 x TAE buffer (40 mM Tris base pH 8.0, 50 mM EDTA, 0.1142 % glacial acetic acid (v/v)) with 0.01 % SYBR® Safe DNA stain (ThermoFisher). Samples were added to gel loading dye, purple (6x) (NEB) and run alongside a 1 kb

DNA ladder (NEB). Agarose gels were run at 90 V for 50 min and visualised using a UV transilluminator (BioRad).

2.2.10 DNA ligation and dialysis

DNA ligations were carried out using T4 DNA ligase (NEB). Before ligation plasmids were treated with T4 polynucleotide kinase (PNK). Reaction mixtures contained 2 μL plasmid or PCR product, 2 μL T4 ligase buffer, 1 μL T4 PNK and 15 μL water. This was incubated at 37°C for 30 min followed by 65°C for 20 min. For DNA ligation 2 μL ligase buffer and 1 μL T4 ligase were added to the PNK reaction and incubated at 16°C for 16 h.

Before transformation to *E. coli* electrocompetent cells, ligation reactions were dialysed using a 0.025 μM membrane filter (Merck) balanced on dH_2O for 15 min.

2.2.11 HiFi DNA assembly

Primers were designed using NEBuilder (159) and fragments with appropriate overhangs were amplified by PCR using Q5 polymerase. For plasmid assembly, 5 μL NEBuilder® HiFi DNA Assembly Master Mix (NEB) was added with 0.5 μL insert DNA, 1 μL vector DNA and 3.5 μL nuclease free water. The reaction was incubated at 50°C for 30 min before dialysis as described in section 2.2.10 and transformation into electrocompetent *E. coli* cells by electroporation.

2.3 Generation of electrocompetent *E. coli* cells

A 5 mL overnight culture of *E. coli* was diluted 1 in 100 in 100 mL fresh LB and incubated at 37°C, 200 rpm until the culture reached OD_{600} 0.6-0.8. The culture was cooled on ice for 30 min before cells were pelleted by centrifugation in a pre-chilled centrifuge (4°C) at 7,500 x g for 10 min. Cells were then washed three times in ice cold 10 % glycerol (v/v) before final

resuspension in 1 mL ice cold 10% glycerol. Cells were stored at -80°C in 100 μL aliquots.

2.4 Transformation of *E. coli* cells by electroporation

Aliquots of electrocompetent cells were thawed on ice. Cells were transferred to chilled 1 mm electroporation cuvettes (SLS) and 0.5-10 μL DNA was added and mixed gently. This was electroporated at 1.75 kV, 25 μF, 200 Ω and 1 mL LB was added to the cuvette. The cuvette was incubated at 37°C, 200 rpm for 1 hour before plating on LB with appropriate antibiotics for selection.

2.5 Generation of electrocompetent *S. aureus* cells

A 5 mL overnight culture of *S. aureus* was diluted 1 in 100 in 100 mL TSB and incubated at 37°C, 200 rpm until the culture reached OD_{600} 0.4-0.6. The culture was pelleted by centrifugation in a centrifuge with a swing out rotor at 4,000 x g for 10 min at room temperature. Cells were washed three times in room temperature 10 % glycerol (v/v). Cells were suspended in 30 mL 10 % glycerol (v/v) and left to stand at room temperature for 30 min. Finally, cells were suspended in 1 mL 10 % glycerol and stored at -80°C in 100 μL aliquots if not used immediately.

2.6 Transformation of *S. aureus* cells by electroporation

Fresh electrocompetent cells were used where possible or frozen aliquots were thawed on ice. 5-10 μL plasmid DNA was added to *S. aureus* electrocompetent cells, gently mixed and left to incubate at room temperature for 10 min. The mixture was then added to a 1 mm electroporation cuvette (SLS) and electroporated at 1.75 kV, 25 μF, 200 Ω. 1 mL brain heart infusion broth (BHI) was added immediately, and the total volume transferred to a universal containing 2 mL fresh BHI medium. This was incubated at 37°C, 200 rpm for 3 h before plating on BHI agar with

antibiotics for selection. To make BHI, 37 g BHI powder as purchased was added to 1 L distilled water and media was sterilised by autoclaving at 121°C for 15 min.

2.7 Phage transduction

Bioluminescent reporter strains used in this study were generated using phage transduction using phage Φ11. *agr* mutant strains were generated using phage RN6911 (160). This replaces the full *agr* operon with a tetracycline resistance cassette.

2.7.1 Generation of phage lysate

Donor *S. aureus* strains were grown overnight at 37°C, 200 rpm in 5 mL LK broth with suitable antibiotics. 0.25 mL overnight donor culture was added to 2.5 mL phage buffer and 2.5 mL LK broth without antibiotics in a 100 mL flask. Phage Φ11 was added at volumes of 0 μL, 50 μL, 100 μL and 200 μL and flasks were incubated at 37°C with intermittent swirling until the solutions became clear (5-6 h to overnight). Phage lysate was collected by filter sterilisation of the solutions using a 0.2 μM syringe filter. Lysates were stored at 4°C. This process was repeated to increase phage titre.

LK broth

Tryptone	5 g
Yeast extract	2.5 g
Potassium chloride	5 g

Components were dissolved in 500 mL Milli-Q purified water and autoclaved at 121°C for 15 min.

Phage buffer

$MgSO_4$	1 mM
$CaCl_2$	4 mM
Tris-Base (pH 7.8)	50 mM
NaCl	0.6 % (w/v)
Gelatin	0.01% (w/v)

Components were dissolved in Milli-Q purified water and autoclaved at 121°C for 15 min.

2.7.2 Transduction

The recipient *S. aureus* strain was grown overnight in 5 mL LK broth. 0.5 mL of the overnight culture was added to 1.5 mL LK broth with 10 mM $CaCl_2$ and volumes of phage lysate; 0 μL, 100 μL and 200 μL. Reactions were incubated at 37°C statically for 25 min then at 37°C with shaking at 200 rpm for 15 min. After incubation, 1 mL ice cold 20 mM sodium citrate was added, and the reactions incubated on ice for 5 min. The reactions were then centrifuged at 7,600 x g and cells resuspended in 1 mL 20 mM sodium citrate. Cells were incubated on ice for 4-5 h and plated on TSA supplemented with 20 mM sodium citrate and antibiotics for selection.

2.8 Detection of AIP-1 using bioreporter *S. aureus* ROJ143

A previously described protocol was used in this study to detect AIP-1 production using an *S. aureus* ROJ143 reporter strain (153). Overnight culture of ROJ143 was diluted 1/200 in BHI and 200 μL added to wells of a flat, black, clear-bottomed 96 well plate (Greiner). Supernatant of test cultures was separated from cells by centrifugation and 2 μL was added to ROJ143 in the 96 well plate in triplicate. The OD_{600} and relative light units (RLU; integration time 4000 ms) were recorded every 15 min for 16 h in a Tecan Infinite F200 microplate reader. The highest light output over the time period for each experiment was plotted and is displayed in the results, this was usually after incubation for between 3 and 4 h.

2.9 GLuc and NanoLuc bioluminescence assays

2.9.1 Measuring *agr*P3 promoter activity using GLuc and NanoLuc bioluminescence

A single colony of a test strain was cultured overnight at 37°C, 200 rpm in 5 mL TSB with antibiotics for selection. After overnight growth, supernatant was separated from cells by centrifugation twice at 13,000 x g for 2 min and the cell pellet was washed 3 times in TSB. 100 μL of each sample was loaded into a black, flat, clear-bottomed 96 well plate (Greiner). Bioluminescence (relative light units; RLU) was recorded after injection of 50 μL 20 μM coelenterazine (CTZ) substrate at 200 μL/s using a 96 well plate reader and injector (Infinite F200 Tecan). CTZ was injected into each well and RLU read in turn. RLU was read with an integration time of 100 ms after a wait time of 1 s. 3 technical repeats were recorded for each sample and statistical analysis performed using an unpaired t-test with Welch's correction.

2.9.2 Measuring *agr*P3 activity with respect to growth phase using GLuc

When testing bioluminescence output from GLuc over time, a single colony of the test strain was used to inoculate 50 mL TSB. This was incubated at 37°C, 200 rpm. A 1 mL sample and OD_{600} reading was taken every hour for 12 h. The supernatant fraction was separated from cells by centrifugation twice at 13,000 x g for 2 min. Supernatant fractions were stored at -20°C prior to analysis. Freeze thawing has been shown to have no effect on the stability of *Gaussia* luciferase (161). Samples were thawed at room temperature and loaded into a flat, black, clear-bottomed 96 well plate and RLU read using a Tecan Infinite F200 microplate reader as described previously.

2.9.3 Testing the effect of *agr* inhibitors and activators with *agr*P3-GLuc and *agr*P3-NanoLuc strains

When testing bioluminescence output from GLuc and NanoLuc in the presence of inhibitors and activators, a single colony of the test strain was used to inoculate 5 mL TSB with test compounds at the desired concentrations. Cultures were incubated at 37°C at 200 rpm overnight and samples were taken after 16 h. RLU was recorded as described previously.

2.10 NanoBiT assays

2.10.1 NanoBiT strains

All test strains were constructed in *S. aureus* SH1000 by Dr. Ewan Murray. Strains have AgrB1 with N- or C-terminal LargeBiT or SmallBiT integrated on the chromosome at the *attB2* site, and AgrB1 or AgrD1 with N- or C-terminal LargeBiT or SmallBiT on plasmid pSK5360. AgrB and AgrD are under the control of the *agr*P2 promoter, and the strain has a native *agr* system. Strains constructed are outlined in **Table 2-4**.

Table 2-4. Split luciferase strains used for NanoBiT. Strains are all *S. aureus* SH1000 with chromosomal integration as outlined and plasmid pSK5630. We were unable to construct the C-terminal SmBiT fusion to AgrD.

attB2 site on chromosome	Plasmid pSK5630
AgrBD strains	
*agr*P2-AgrB C terminal LgBiT	*agr*P2-AgrD N terminal SmBiT
*agr*P2-AgrB C terminal LgBiT	*agr*P2-AgrD C terminal LgBiT
*agr*P2-AgrB C terminal LgBiT	*agr*P2 N terminal LgBiT
*agr*P2-AgrB C terminal LgBiT	*agr*P2-AgrD N terminal LgBiT
*agr*P2-AgrB C terminal LgBiT	*agr*P2 N terminal SmBiT
*agr*P2-AgrB C terminal SmBiT	*agr*P2-AgrD N terminal LgBiT
*agr*P2-AgrB C terminal SmBiT	*agr*P2-AgrD N terminal SmBiT
*agr*P2-AgrB C terminal SmBiT	*agr*P2- N terminal LgBiT

*agr*P2-AgrB C terminal SmBiT	*agr*P2-AgrD C terminal LgBiT
*agr*P2-AgrB N terminal LgBiT	*agr*P2- N terminal LgBiT
*agr*P2-AgrB N terminal LgBiT	*agr*P2-AgrD N terminal SmBiT
*agr*P2-AgrB N terminal LgBiT	*agr*P2-AgrD N terminal LgBiT
*agr*P2-AgrB N terminal LgBiT	*agr*P2- N terminal SmBiT
*agr*P2-AgrB N terminal SmBiT	*agr*P2- N terminal LgBiT
*agr*P2-AgrB N terminal SmBiT	*agr*P2-AgrD N terminal SmBiT
*agr*P2-AgrB N terminal SmBiT	*agr*P2- N terminal SmBiT
*agr*P2-AgrB N terminal SmBiT	*agr*P2-AgrD C terminal LgBiT
*agr*P2-AgrB N terminal SmBiT	*agr*P2-AgrD N terminal LgBiT
*agr*P2-AgrB N terminal SmBiT	N/A
AgrBB strains	
*agr*P2-AgrB C terminal LgBiT	*agr*P2-AgrB N terminal LgBiT
*agr*P2-AgrB C terminal LgBiT	*agr*P2-AgrB N terminal SmBiT
*agr*P2-AgrB C terminal LgBiT	*agr*P2-AgrB C terminal LgBiT
*agr*P2-AgrB C terminal LgBiT	*agr*P2-AgrB C terminal SmBiT
*agr*P2-AgrB N terminal LgBiT	*agr*P2-AgrB N terminal LgBiT
*agr*P2-AgrB N terminal LgBiT	*agr*P2-AgrB C terminal SmBiT
*agr*P2-AgrB N terminal LgBiT	*agr*P2-AgrB C terminal LgBiT
*agr*P2-AgrB N terminal LgBiT	*agr*P2-AgrB N terminal SmBiT
*agr*P2-AgrB N terminal SmBiT	*agr*P2-AgrB N terminal LgBiT
*agr*P2-AgrB N terminal SmBiT	*agr*P2-AgrB N terminal SmBiT
*agr*P2-AgrB N terminal SmBiT	*agr*P2-AgrB C terminal LgBiT
*agr*P2-AgrB N terminal SmBiT	*agr*P2-AgrB C terminal SmBiT
*agr*P2-AgrB C terminal SmBiT	*agr*P2-AgrB N terminal LgBiT
*agr*P2-AgrB C terminal SmBiT	*agr*P2-AgrB C terminal LgBiT
*agr*P2-AgrB C terminal SmBiT	*agr*P2-AgrB N terminal SmBiT
*agr*P2-AgrB C terminal SmBiT	*agr*P2-AgrB C terminal SmBiT

2.10.2 Detection of NanoBiT bioluminescence using a Tecan Infinite F200 microplate reader

Overnight cultures were grown in 5 mL TSB with antibiotics for selection. After overnight growth 1 mL of each culture was washed twice in 1 mL TSB before resuspension in 1 mL TSB. This was diluted 1/300 in 6 mL TSB and grown at 37°C, 200 rpm for approximately 2.5 h until the culture reached OD_{600} 0.6-0.8. 100 μL culture was added to a white, flat bottomed 96 well plate in triplicate and 25 μL 5 x NanoGlo live cell assay reagent (Promega) was added. RLU was read with integration time 4000 ms on a Tecan Infinite F200 microplate reader.

A 5 x stock of NanoGlo live cell assay reagent was made by diluting NanoGlo live cell substrate in NanoGlo live cell buffer as per manufacturer's instructions (Promega).

2.11 Protein induction from pCDFDuet-1

Induction of protein expression from pCDFDuet-1 was performed in *E. coli* C41 (DE3). Plasmids were transformed into this strain for each induction. Overnight cultures were grown in 5 mL terrific broth (TB) with 100 μg/mL spectinomycin. A 1/200 dilution of overnight culture was created in 30 mL TB and was incubated at 37°C with shaking at 200 rpm to mid-exponential phage (OD_{600} ~0.8). 500 μM IPTG was added, and cultures incubated with shaking at 37°C for a further 3 h. Cells and supernatant were separated by centrifugation. The cell pellet was stored at -80°C and supernatant at -20°C.

Terrific broth

Tryptone	12 g
Yeast extract	24 g
Glycerol	4 mL
dH_2O	To 900 mL

10 x Terrific broth buffer solution

KH_2PO_4	2.13 g
K_2HPO_4	12.54 g
dH_2O	To 100 mL

Broth and buffer were sterilised by autoclaving prior to use.

2.12 Membrane preparation

E. coli C41 (DE3) cell pellets were resuspended in cOmplete protease inhibitor (Sigma-Aldrich) and lysed using an MP-FastPrep at 6.0 m/s for 30 s for two cycles. Samples were centrifuged at 13,500 x g for 5 min to remove lysis beads and transferred to ultracentrifuge tubes. Samples were centrifuged at 100,000 x g for 1 h at 4°C to pellet the membrane fraction. The cytosolic fraction was removed, and cell membrane fraction resuspended in PBS. Samples were stored at -20°C.

2.13 NanoBRET assay using Tecan Infinite F200 microplate reader

Test vectors were constructed using HiFi cloning and transformed by electroporation into expression strain *E. coli* C41 (DE3) as described previously (section 2.4). 10 mL cultures were grown for 2 hours at 37°C, and protein expression induced with 500 μM IPTG. After induction, 0.5 mL of culture was washed in PBS and resuspended in PBS with TMR-Direct (Promega) ligand. This was incubated at room temperature for 30 min before cells were washed twice in PBS and 100 μL added to wells of a clear bottomed, 96 well black Tecan plate (Greiner). NanoGlo reagent was prepared as per the manufacturer instructions (Promega) and 25 μL added to each well. Dual bioluminescence was read with a blue filter reading RLU between 400-475 nm and a green filter reading RLU between 500-600 nm.

2.14 Preparing samples for visualisation of NanoBRET by confocal laser scanning microscopy

pCDFDuet-1 *agrB1-nanoluc halotag-agrB1* was transformed by electroporation into expression strain *E. coli* C41 (DE3) as described previously (section 2.4). 10 mL cultures were grown in TB for 2 hours at 37°C, and protein expression induced with 500 μM IPTG. After induction 1 mL culture was washed in PBS and resuspended in PBS with TMR-Direct (Promega) ligand. This was incubated at room temperature for 30 min. Labelled cells were resuspended in soft top agar, pipetted onto a slide into a well formed with a silicon mould and sealed with a cover slip. Cells were imaged without addition of NanoGlo with excitation at 555 nm and emission at 585 nm. 2 x NanoGlo substrate (Promega) was pipetted on top, and cells imaged again with excitation at 350 nm and emission at 585 nm. 350 nm is sufficiently out of the range of excitation for TMRDirect that this is representative of no artificial excitation of the ligand.

2.14.1 Confocal laser scanning microscopy

Cells were mounted on slides in soft top agar, covered with a coverslip and imaged using a Zeiss LSM 700 confocal laser scanning microscope controlled by the ZEN 2009 software platform. The acquisition settings were based on the fluorescence of the sample and were kept consistent across each experiment.

2.15 Cell free AgrB assay

For the cell free AgrB assay, when using membrane preparations 30 mL *E. coli* C41 (DE3) pCDFDuet-1 *agrB1* was induced as described previously and the cell pellet resuspended in 1 mL AgrB buffer. AgrB buffer consists of 20 mM Tris-HCl pH 7.4, 5 mM $MgSO_4$. Lysis and membrane preparation was continued as described in section 2.12. T7-AgrD (Peptide Synthetics) stock solutions were made up in 10 % DMF at 0.2 mg/mL with 2 mM TCEP. alfa-AgrD (Peptide Synthetics) stock was made up in DMSO with

2 mM TCEP. Synthetic AgrD peptides were stored at -80°C. Amino acid sequences of the peptides and are displayed below.

T7-AgrD1:

MASMTGGQQMGRIQMNTLFNLFFDFITGILKNIGNIAAYSTCDFIMDEVEVPKELTQLHE

T7-tag N-terminus AIP C-terminus

T7-AgrD2:

MASMTGGQQMGRIQMNTLVNMFFDFIIKLAKAIGIVGGVNACSSLFDEPKVPAELTNLYDK

T7-tag N-terminus AIP C-terminus

T7-AgrD3:

MASMTGGQQMGRIQMKKLLNKVIELLVDFFNSIGYRAAYINCDFLLDEAEVPKELTQLHE

T7-Tag N-terminus AIP C-terminus

Alfa-AgrD1:

MPSRLEEELRRRLTEPMNTLFNLFFDFITGILKNIGNIAAYSTCDFIM

Alfa tag N-terminus AIP

Dioleoyl phosphatidylglycerol (DOPG) was prepared by evaporation of chloroform under nitrogen gas and resuspension in AgrB buffer to 10 mg/mL. DOPG was sonicated in a water bath for 30 min to create liposomes.

50 μL reactions were set up as follows. Components added depend on the experiment performed.

Membrane prep or DOPG	5 μL
5 mM DDM in AgrB buffer	5 μL
Purified AgrB (20 μM)	5 μL
T7-AgrD (20 μM)	5 μL
Purified MroQ (20 μM)	5 μL
Protease inhibitors	To required concentration
AgrB buffer	Up to 50 μL

Reactions were incubated at 37°C for 2 h and the reaction then stopped by addition of cOmplete protease inhibitor (Sigma-Aldrich) and heating to 70°C for 10 min. Reactions were added to 2 x Novex Tris-Glycine SDS sample buffer, heated to 55°C for 5 min and run on a 14 % Tris-Glycine gel (ThermoFisher) as described below.

Reporter assays were set up to monitor AIP-1 production using *S. aureus* ROJ143. This was performed as described previously with 10 μL reaction added to 190 μL *S. aureus* ROJ143. Samples were given to Nigel Halliday for analysis by liquid chromatography-mass spectrometry (LC-MS) to detect AIP-1.

2.16 SDS-PAGE

SDS-PAGE was used to separate proteins by size. Samples were added to loading buffer and heated to 55°C for 5 min before running alongside a Color prestained protein standard, broad range (NEB) on a 15% acrylamide gel. Gels were run at 200 V for 50 min in SDS running buffer.

4 x Loading buffer

Tris HCl pH 6.8	250 mM
SDS	8 % (w/v)
Bromophenol blue	0.2 % (w/v)
Glycerol	40 % (v/v)
β-mercaptoethanol	20 % (v/v)

Stacking gel

0.5 M Tris HCl pH 6.8	1.25 mL
10 % SDS	50 μL
30 % acrylamide	800 μL
Water	3.475 mL
10 % APS	50 μL
TEMED	7.5 μL

15 % Separating gel

1.5 M Tris HCl pH 8.8	2.5 mL
10 % SDS	100 μL
30 % acrylamide	5 mL
Water	2.3 mL
10 % APS	100 μL
TEMED	15 μL

When using precast gels, samples were added to 2 x Novex Tris-Glycine SDS sample buffer (ThermoFisher), heated to 55°C for 5 min and run alongside a Color prestained protein standard, broad range (NEB). Samples were run on Invitrogen Novex 14 % Tris-Glycine gels (ThermoFisher) at 200 V for 45 min in SDS running buffer.

SDS running buffer

Tris Base	30 g
Glycine	144 g
SDS	10 g
dH_2O	To 1 L

For separating proteins of low molecular weight, 16 % Tricine gels (ThermoFisher) were used. Samples were added to 2 x Novex Tricine SDS sample buffer (ThermoFisher), heated to 55°C for 5 min and run alongside a spectra multicolor low range protein ladder (ThermoFisher). Gels were run at 125 V for 1 hour in Novex Tricine SDS running buffer (ThermoFisher).

SDS-PAGE gels were stained with Coomassie blue stain for 45 min with gentle agitation at room temperature and de-stained with Coomassie blue de-stain for 2 h with gentle agitation at room temperature or until the bands were visible.

Coomassie blue stain

Coomassie	1.2 g/L
Methanol	50 %
Acetic acid	10 %

Coomassie blue de-stain

Methanol	25 %
Acetic acid	10 %

2.17 Western blot

SDS-PAGE gels were transferred to 0.2 μM polyvinylidene fluoride (PVDF) membrane overnight at 26 V, 4°C in transfer buffer.

10 x Membrane transfer buffer

Tris Base	30 g
Glycine	144 g
dH_2O	To 1 L

10 x TBS buffer

Tris HCl pH 7.6	500 mM
NaCl	1.5 M

To detect AgrD linked to an S-tag, PVDF membrane was blocked overnight at 4°C in 3 % bovine serum albumin (BSA; Sigma-Aldrich) in 25 mL TBST (1 x TBS buffer with 0.1% Tween20) with gentle agitation. S-tag antibody (Sigma-Aldrich) was used at a 1:5,000 dilution and incubated with PVDF membrane for 1 hour at room temperature with gentle agitation. The membrane was washed 4 times for 5 min each in TBST with gentle agitation. Secondary antibody was anti-mouse IgG HRP secondary antibody (Sigma-Aldrich). This was used at a 1:10,000 dilution and incubated with membrane for 45 min at room temperature with gentle agitation.

To detect AgrB, PVDF membrane was blocked overnight at 4°C in 3 % BSA in 25 mL TBST with gentle agitation. Primary nanobody used was 2ABE10, a nanobody raised in a llama against AgrB. 2ABE10 was cloned and expressed in *E. coli* and purified by Dr. Philip Bardelang. This was used at a 1:1,000 dilution and incubated with membrane for 1 hour at room temperature with gentle agitation. The membrane was washed 4 times for 5 min each in TBST with gentle agitation. Secondary antibody was HA-tag monoclonal antibody, HRP conjugated (Stratech Scientific). This was used at a 1:10,000 dilution and was incubated with membrane for 45 min at room temperature with gentle agitation.

To detect the T7 tag, the PVDF membrane was blocked overnight at 4°C in 5 % non-fat dry milk (AppliChem) in 25 mL TBST with gentle agitation. The membrane was incubated with T7 tag antibody HRP conjugate (Sigma-Aldrich) at a 1:10,000 dilution for 1.5 h at room temperature with gentle agitation.

To detect NanoLuc, the PVDF membrane was blocked overnight at 4°C in BSA in 25 mL TBST with gentle agitation. The membrane was incubated with anti-NanoLuc monoclonal antibody (Promega) at a 1 in 1,000 dilution.

Membrane was washed 4 times for 5 min each in TBST with gentle agitation. Secondary antibody was anti-mouse IgG HRP secondary antibody (Sigma-Aldrich). This was used at a 1:10,000 dilution and was incubated with membrane for 45 min at room temperature with gentle agitation.

After incubation with antibodies, all blots were washed 6 times for 5 min each in TBST at room temperature with gentle agitation. Protein bands were detected using Amersham ECL western blotting detection reagent (SLS) and Amersham hyperfilm ECL (SLS).

2.18 Purification of recombinant AgrB

AgrB was induced from *E. coli* C41 (DE3) pCold His10-*agrB1*. 3 mL overnight culture in TB was added to 500 mL TB in two 1 L flasks, giving a total of 1 L culture. This was grown at 37°C 200 rpm to OD_{600} 0.7-0.8 and 500 μM IPTG was added for induction of protein expression. Protein expression was induced at 20°C 180 rpm overnight. Cells were separated from supernatant by centrifugation at 3,000 x g for 15 min at 8°C and washed in cold PBS before resuspension in Tris buffer and storage at -80°C.

The cell pellet was thawed on ice and cells were lysed by sonication on ice at 15 amps for 6 min total. After lysis, samples were spun at 10,000 x g for 10 min at 8°C to remove unlysed cells. The supernatant was collected and centrifuged at 200,000 x g for 1 hour at 4°C. Pellets were resuspended in extraction buffer and incubated at 30°C 200 rpm for 3 h. The sample was then centrifuged at 100,000 x g for 25 mins at 10°C.

Talon cobalt IMAC columns (GE Healthcare) were prepared with 1.5 mL slurry in each of 3 columns. Columns were washed with 20 mM MES pH 5.0, 3 nM NaCl then de-ionized water then extraction buffer without DDM to equalise the salt concentration in the sample and the column. Samples from

the ultracentrifuge were split between the 3 columns. Columns were washed with 10 mL wash buffer and protein eluted with 2 mL elution buffer.

Samples were spin concentrated with a Vivaspin 6, 30,000 MwCO spun at 7,800 x g for 15 min at 15°C until the volume was reduced to <5 mL. For desalting, PD-10 prepacked columns (GE Healthcare) were used. Column was run through with desalting buffer before addition of sample and additional run through with desalting buffer. Elutions were collected and concentration tested on a NanoDrop spectrophotometer. Concentrations were calculated using $A = \varepsilon cl$ with ε for AgrB1 18910 $M^{-1}cm^{-1}$. Aliquots of AgrB1 were stored at -80°C prior to use.

Tris buffer

Tris-HCl pH 7.5	20 mM
Glycerol	10%
Mg^{2+}	5 mM

Extraction buffer

DDM	2 %
Sodium phosphate buffer pH 7.4	20 mM
NaCl	100 mM

Wash buffer

DDM	0.4 %
BME	4 mM
NaCl	100 mM
Sodium phosphate buffer pH 7.1	20 mM

Elution buffer

DDM	0.4 %
TCEP	1 mM
NaCl	100 mM
Sodium phosphate buffer pH 7.1	20 mM
Imidazole	0.6 M

Desalting buffer

DDM	0.4 %
$KHPO_4$ pH 7.4	20 mM
NaCl	100 mM
EDTA	0.5 mM

2.19 MBP-MroQ purification and size exclusion chromatography

MBP-MroQ was purified as described previously (69). MBP-MroQ was induced from *E. coli* C41 (DE3) pCold *malE-mroQ*. 250 mL culture was grown, induced, washed, and the cell pellet stored at -80°C in Tris buffer as described in section 2.18. The cell pellet was resuspended in 40 mL lysis buffer with 10 μL Benzonase (Sigma Aldrich) to break down DNA. Cell pellet was lysed using a French press at 800 psi, 1000 psi and 1200 psi (x3). The samples were centrifuged to remove cell debris and supernatants transferred to ultracentrifuge tubes before centrifuging at 200,000 x g for 2 h at 4°C to pellet the bacterial membrane fraction. Membrane pellets were resuspended in extraction buffer with 20 mg PMSF before incubation rolling at 4°C overnight.

HisPur Ni-NTA Resin (ThermoFisher) was washed sequentially in ethanol, water and extraction buffer. Samples were centrifuged at 100,000 x g for 30 min and the solubilised fraction was added to washed resin and incubated rolling at 4°C for 2 h. Resin and sample was added to a column and flow through collected before washing twice and elution.

Lysis buffer

NaCl	50 mM
PMSF	1 mM
Tris HCl pH 7.5	20 mM

Extraction buffer

Tris HCl pH 7.5	20 mM
NaCl	100 mM
TCEP	2 mM
Foscholine 12	2 %

Wash buffer 1

Tris HCl pH 7.5	20 mM
NaCl	500 mM
TCEP	1 mM
Foscholine 14	0.05 %
Imidazole	20 mM

Wash buffer 2

Tris HCl pH 7.5	20 mM
NaCl	100 mM
TCEP	1 mM
Foscholine 14	0.05 %
Imidazole	30 mM

Elution buffer

Tris HCl pH 7.5	20 mM
NaCl	100 mM
TCEP	1 mM
Foscholine 14	0.05 %
Imidazole	300 mM

Purified MBP-MroQ in elution buffer was spin concentrated with a Vivaspin 6 30,000 MwCO to reduce volume to <1.5 mL for size exclusion chromatography (SEC). The AKTApure was washed with degassed SEC buffer and sample was run through a HiLoad 16/600 SuperDex 200 pg SEC column (GE Healthcare). 2 mL fractions were collected, and concentration quantified using a NanoDrop spectrophotometer. Concentrations were

calculated as for AgrB1 with ε for MBP-MroQ 97750 $M^{-1}cm^{-1}$. Aliquots of MBP-MroQ were stored at -80°C.

SEC buffer

Tris HCl pH 7.5	20 mM
NaCl	100 mM
TCEP	50 mM
Foscholine 14	0.05 %

3. Developing bioluminescent reporters for monitoring *agr*P3 expression in *Staphylococcus aureus*

3.1 Introduction

The *agr* quorum sensing system is an interesting potential antivirulence target. There is increasing evidence to suggest that blocking *S. aureus* virulence gene expression attenuates infection in certain experimental animal infection models (107, 109). Attenuating virulence early in infection could allow the host immune system to respond and clear the pathogen without the need for exposure to conventional antibiotics (47). Virulence inhibitors could also be used as adjuvants with existing antibiotics or with therapies which boost the immune response (105, 110).

To aid the development of *agr* inhibitors it is important to know exactly when and where staphylococcal *agr* is expressed in the infection site. This will give insights into whether inhibitors will be used against established infections or as prophylactics to prevent infection. To investigate temporal *agr* expression and *agr* inhibition it is important to develop methods for real time monitoring of *agr* expression which can be used *in vivo* (23). This can be performed using bioluminescent reporters linked to the P3 promoter of the *agr* system (116).

Previously, *agr* reporters have been developed with bacterial luciferase from *Photorhabdus luminescens* encoded by the *luxABCDE* operon transcriptionally fused to the *agr*P3 promoter (109, 162). This is a useful reporter for measuring temporal *agr* activation *in vitro* and *in vivo* and for assessing *agr* inhibition (107, 109). This does have some limitations however, for example the requirement for ATP and FMNH2 for bioluminescence imposes a metabolic burden on the cell. Additionally, when

screening inhibitors, some of these may have off target effects inhibiting bioluminescence from the *lux* operon (163). Therefore, it is useful to develop novel reporters which can be used in tandem or in the place of the bacterial luciferase to screen for *agr* QS inhibitors.

Bacterial luciferase is also restricted to intracellular use due to the dependence on ATP and FMNH2. Research has shown that the use of secreted luciferases for *in vivo* work can be advantageous. Secreted luciferases can be detected in the blood or urine of murine models enabling real time monitoring of *in vivo* processes without the need to euthanise cohorts of animals (132, 147). This will result in the use of fewer animals and, as samples can be taken from a tail vein or from urine, fewer anaesthetic events for each animal. This will lead to a reduction in costs and will enable monitoring of *agr* activation and inhibition in real time.

Novel luciferases, including GLuc and NanoLuc have been shown to be useful as secreted reporters in *in vivo* studies. These have a number of advantages over bacterial luciferases including smaller size and higher light output. This allows high sensitivity with lower metabolic burden on the cell due to the lack of dependence on ATP and FMNH2 for bioluminescence (146, 148). The use of GLuc and NanoLuc should also avoid false positive results observed with bacterial luciferases when screening for QS inhibitors and so offer an alternative screen for inhibitors *in vitro* and *in vivo*. Both of these reporters have been shown to be effective previously but their use in *S. aureus* has not been demonstrated.

3.2 Aims

The aim of this chapter was to evaluate the use of novel luciferases GLuc and NanoLuc as reporters in *S. aureus* for monitoring activation and inhibition of the *agr* quorum sensing system. GLuc and NanoLuc will be placed under the control of the *agr*P3 promoter to detect *agr* activation in

real time. Their potential will also be assessed as secreted reporters which are useful as bioluminescence can be detected from the serum of *in vivo* models enabling real time *ex vivo* monitoring of *in vivo* processes (147). The *agr* system controlling *Gaussia* luciferase activation and secretion is outlined in **Figure 3-1**.

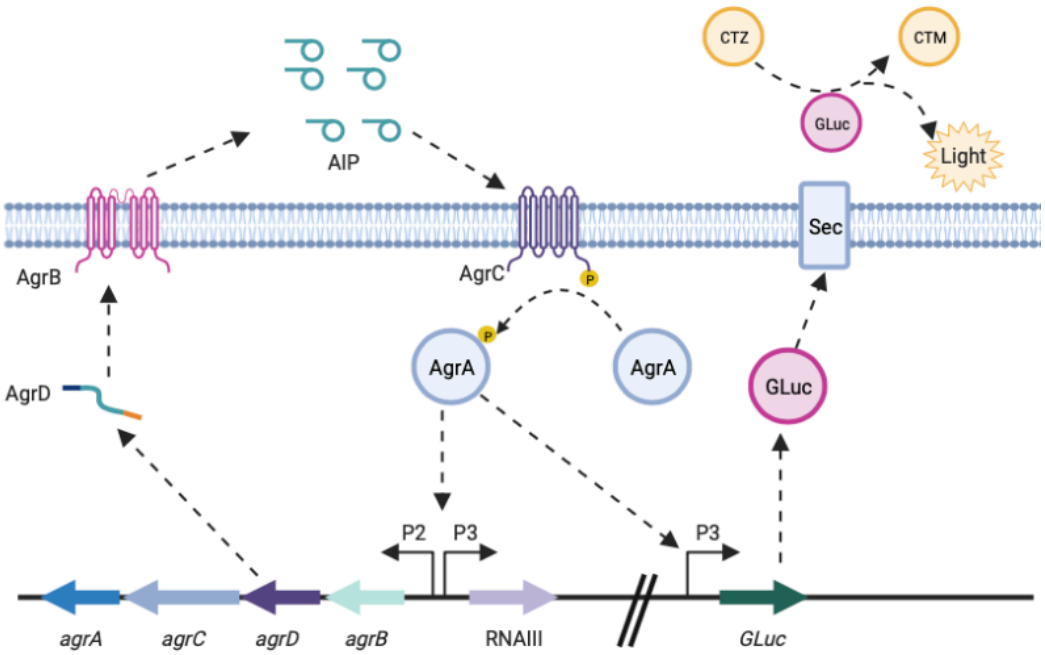


Figure 3-1. Outline of the staphylococcal *agr* system and the *agr*P3-GLuc reporter. The *agr* system is presented as outlined previously. *agr*P3-GLuc is incorporated on the chromosome at the *attB2* site. Activation of AgrA by AIP binding to AgrC will lead to upregulation of GLuc via *agr*P3. GLuc is secreted via the Sec pathway and on addition of CTZ, light is produced.

3.3 Comparison of growth between *S. aureus* USA300 and *S. aureus* USA300 *agr*P3-GLuc

Strains were constructed previously by Dr. Carmen Tong with *Gaussia* luciferase (GLuc) encoded chromosomally under the control of the *agr*P3 promoter in a *S. aureus* USA300 JE2 background (152). *S. aureus* USA300

belongs to *agr* group I and was chosen as the model strain as this is a highly virulent clinical strain with a hyperactive *agr* system which has been studied extensively in the lab (25). To demonstrate that the incorporation of GLuc into the chromosome did not affect the growth of *S. aureus* USA300, growth was compared in the wild type and the *agr*P3-GLuc strain over 15 h. Overnight culture was diluted 1/200 and grown in a Tecan plate reader at 37°C with OD_{600} read every 15 min for 15 h. As shown in Figure 3-2, there was no growth attenuation in *S. aureus* USA300 with incorporation of *agr*P3-GLuc on the chromosome compared to the wild type.

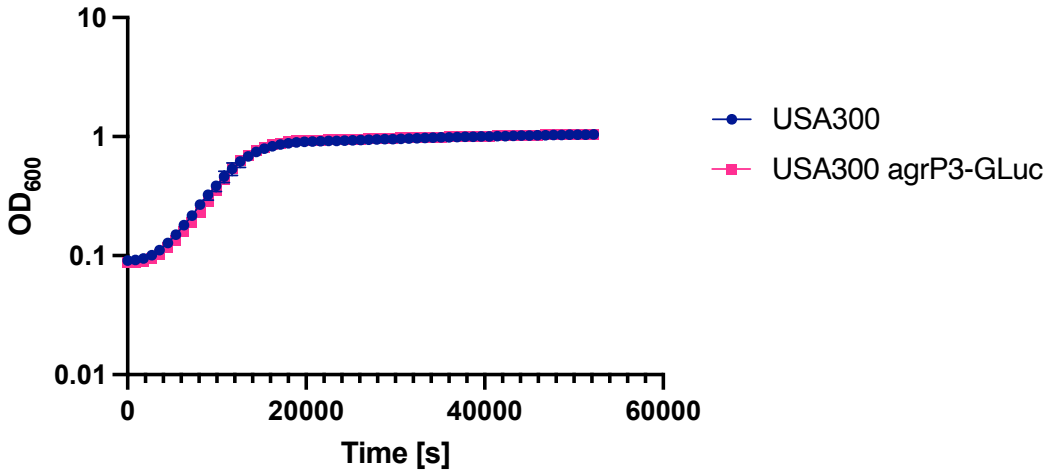


Figure 3-2. Comparison of growth of *S. aureus* USA300 and USA300 *agr*P3-GLuc. Data represents OD_{600} recorded every 15 min for 15 h. Data are representative of three technical repeats recorded for each sample with error bars displaying standard deviation.

3.4 Detecting GLuc expression in cells compared with supernatant fractions

When constructing the reporter strain, a staphylococcal Protein A (SpA) leader was engineered upstream of GLuc, after the *agr*P3 promoter, to direct the translated protein to the Sec pathway for secretion. To demonstrate that GLuc was being secreted, the cell pellet and supernatant fractions of overnight cultures were separated and the bioluminescence from each

fraction tested. The bioluminescence in the supernatant representing the secreted luciferase and the bioluminescence in the cell pellet representing the intracellular luciferase. As shown in Figure 3-3, the level of bioluminescence in the supernatant fraction was more than 1,000 times higher than in the cell pellet demonstrating effective secretion of the luciferase.

S. aureus USA300 Δ*agr agr*P3-GLuc was also constructed. This has *agr*P3-GLuc inserted on the chromosome however the *agr* system has been knocked out. The Δ*agr* strain was made by phage transduction with previously prepared Δ*agr* Φ11 phage lysate (152). As shown in Figure 3-3, a low level of bioluminescence was observed compared to the strain with a WT background. This is considered the background level of bioluminescence as the strain has no active *agr* system.

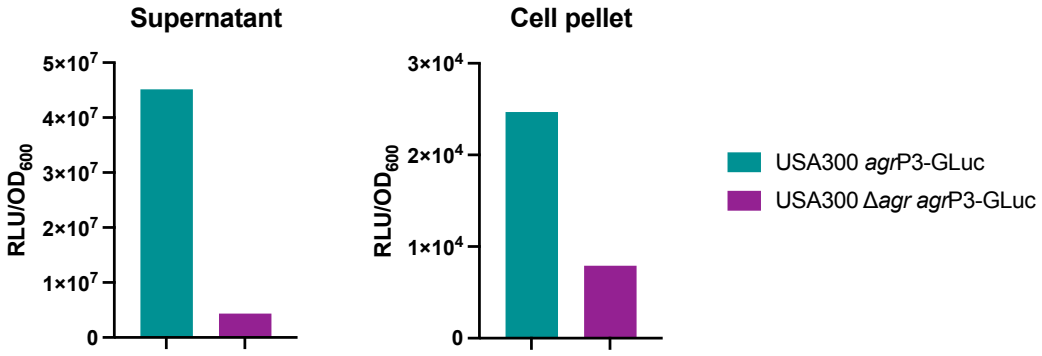


Figure 3-3. The difference in bioluminescence in the supernatant and cell pellet of *S. aureus* USA300 *agr*P3-GLuc and USA300 Δ*agr agr*P3-GLuc. After overnight growth the cells were separated from the supernatant by centrifugation and washed in PBS. This graph represents bioluminescence output (as relative light units: RLU) divided by population density (OD_{600}) after growth for 16 h. Data represent 3 technical repeats.

3.5 GLuc bioluminescence correlates with growth phase consistent with *agr* induction

In *Staphylococci*, *agr*-dependent QS is activated at high cell population densities when the concentration of signalling molecule AIP reaches a threshold concentration. This occurs in the late-exponential stage of growth *in vitro* (49). When AIP reaches the threshold concentration, signal transduction occurs through AgrC and AgrA leading to activation of *agr*P2 and *agr*P3 promoters therefore GLuc expression should be activated. To determine the profile of GLuc bioluminescence with respect to growth phase, bioluminescence and OD_{600} were quantified over 12 h using *S. aureus* USA300 *agr*P3-GLuc.

As shown in Figure 3-4, light output was low for the first 5 h of growth as the cells were in early exponential phase. From 5-7 h the level of bioluminescence increased from ~4.83 x 10^5 to ~8.74 x 10^6 RLU/OD_{600} as the cells reached late exponential and early stationary phases of growth. The increase in bioluminescence reached a plateau after 10 h at ~2.7 x 10^7 RLU/OD_{600}, this was representative of *agr* induction in real time.

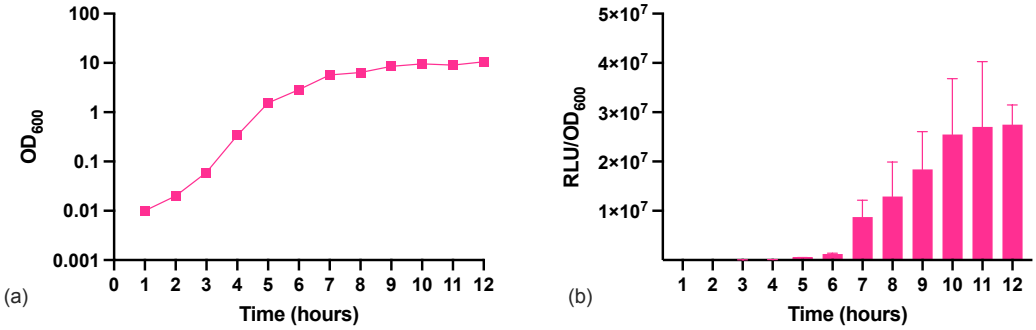


Figure 3-4. OD_{600} and relative bioluminescence from *S. aureus* USA300 *agr*P3 GLuc over 12 h. (a) OD_{600} (b) RLU recorded every hour for 12 h after inoculation of a single colony of *S. aureus* USA300 *agr*P3 GLuc into 50 mL TSB. Data are representative of three technical repeats recorded for each sample and error bars displaying standard deviation. The experiment was performed in biological triplicate.

3.6 Activation of *agr*P3-GLuc bioluminescence with synthetic AIP-1

To demonstrate that the *S. aureus* USA300 GLuc reporter responds to *agr* activation, *agrA* and *agrC*, which make up the two-component signal transduction system, were used to complement *S. aureus* USA300 Δ*agr* *agr*P3-GLuc on plasmid pSKermP2-*agrAC* (153). AgrA and AgrC are under the control of the *agr*P2 promoter. Complementation of AgrA and AgrC enables the strain to respond to exogenous AIP-1 via signal transduction though AgrC and AgrA which leads to *agr*P3 activation. Therefore, on addition of exogenous AIP-1, *agr*P3-GLuc will be activated leading to production of bioluminescence. Due to the lack of AgrB and AgrD the complemented Δ*agr* strain will not create its own AIP-1.

100 nM synthetic AIP-1 or 0.01% DMSO was added to overnight cultures of *S. aureus* USA300 Δ*agr* *agr*P3-GLuc pSKermP2-*agrAC* and *S. aureus*

USA300 Δ*agr* *agr*P3-GLuc without the complementation plasmid. Bioluminescence and OD_{600} were quantified after overnight growth.

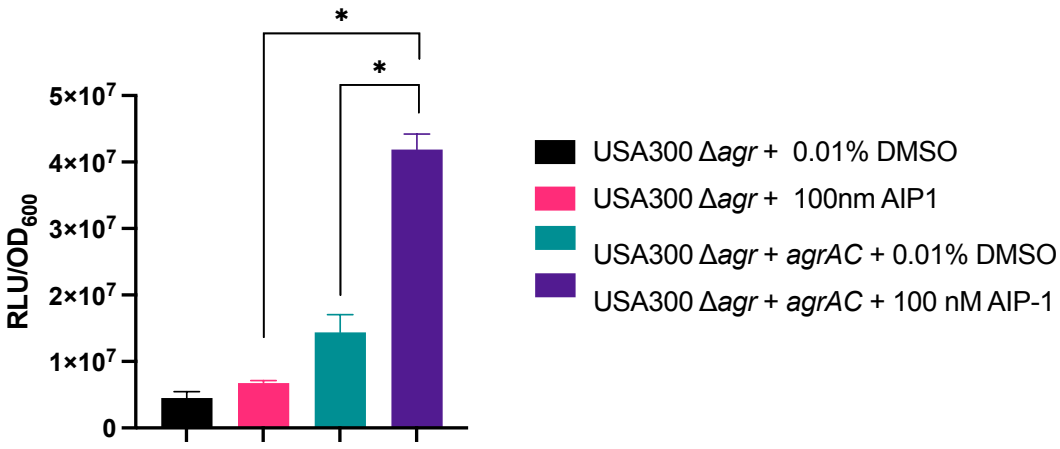


Figure 3-5. The impact of addition of exogenous AIP-1 on bioluminescence produced by *S. aureus* USA300 Δ*agr* *agr*P3-GLuc pSKermP2-*agrAC*. The data represent three technical repeats and three biological repeats for each sample with error bars displaying standard deviation. *p<0.0001.

As shown in Figure 3-5, after incubation with 100 nM AIP-1, the level of bioluminescence in the Δ*agr* strain was ~6.78 x 10^6 RLU/OD_{600}, this is similar to background levels observed after overnight incubation (Figure 3-3). This demonstrates that AIP-1 cannot activate the *agr* system in the knockout strain. With complementation of AgrA and AgrC, the DMSO control shows bioluminescence of ~1.4 x 10^7 RLU/OD_{600} and with addition of 100 nM AIP-1 this increases to ~4.19 x 10^7 RLU/OD_{600}. This is a significant increase showing that the strain is able to respond to exogenous AIP-1, activating *agr*P3-Gluc. This validates that GLuc is under the control of the *agr*-P3 promoter.

3.7 Inhibition of *agr*P3-GLuc bioluminescence using competitive AgrC antagonist AIP-95

To demonstrate further that GLuc expression is under the control of the *agr*P3 promoter, the strains were tested with AIP-95, a competitive

antagonist of the *agr* system. AIP-95 is a competitive analogue of AIP-1 which inhibits AIP-1 binding to AgrC1 and therefore prevents activation of the system. 0.01% DMSO was added as a solvent control.

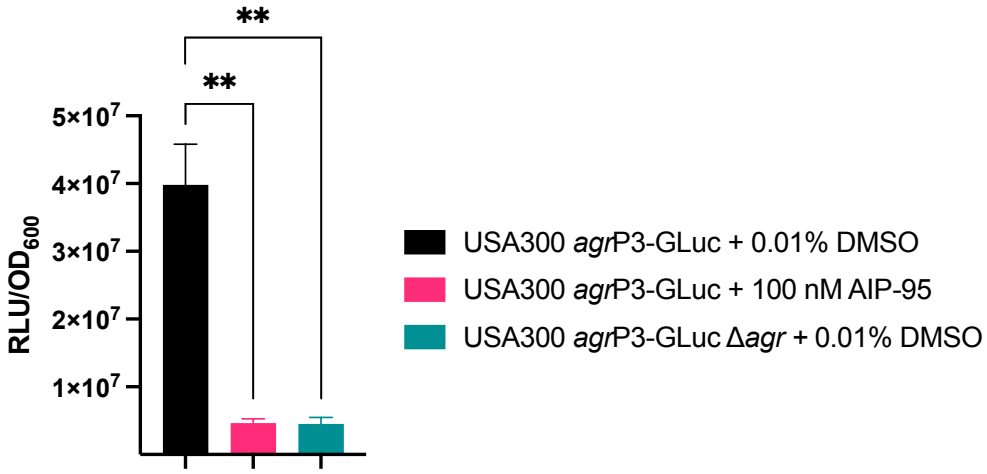


Figure 3-6. Impact of 100 nM AIP-95 on relative bioluminescence output from *S. aureus* USA300 *agr*P3-GLuc. The data represent three technical repeats and three biological repeats for each sample with error bars displaying standard deviation. ** $p<0.01$.

As shown in Figure 3-6, for *S. aureus* USA300 *agr*P3-GLuc, relative bioluminescence was high after overnight growth in the presence of DMSO (~3.98 x 10^7 RLU/OD_{600}) but was reduced ~10 fold to the level of the *agr* knockout strains after overnight growth in the presence of AIP-95 (~4.65 x 10^6 RLU/OD_{600}). This indicates that the bioluminescence recorded in the presence of AIP-95 represents background bioluminescence and no activation of the *agr*P3 promoter is detected. This shows that GLuc bioluminescence can be inhibited using an antagonist of the *agr* quorum sensing system confirming that it is under the control of *agr*P3.

3.8 Growth in the presence of inhibitors and activators

To ensure that the inhibitor and activator were not affecting growth of *S. aureus* USA300 *agr*P3-GLuc, growth was monitored over 7 h in the presence of these compounds. A single colony was added to 10 mL TSB

and incubated for 7 h with OD_{600} recorded every hour. As shown in **Figure 3-7**, growth was not attenuated after addition of either of the test compounds.

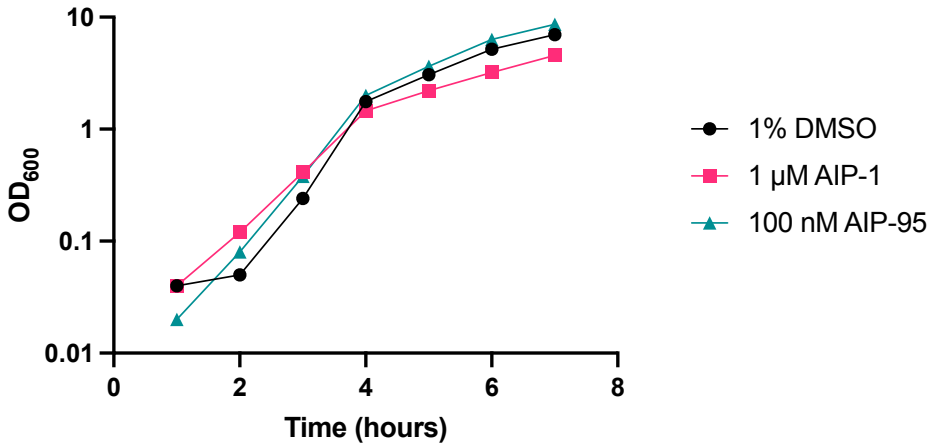


Figure 3-7. Growth of *S. aureus* USA300 *agr*P3-GLuc in the presence of AIP-1 and AIP-96. OD_{600} was recorded every hour for 7 h. Data shown are from one experiment and is representative of duplicate biological repeats.

3.9 Inhibition of *S. aureus* USA300 *agr*P3-GLuc bioluminescence using inhibitors of other components of the *agr* system

It has been demonstrated that *S. aureus* USA300 *agr*P3-GLuc produces bioluminescence in response to *agr* activation and that this bioluminescence can be inhibited with competitive AgrC antagonist AIP-95. Inhibitors have been developed against many different protein targets within the *agr* system as displayed in **Figure 1-3**. Therefore, to verify whether this reporter can be used to report inhibition of different proteins within the *agr* system, other inhibitors were tested. These were, ambuic acid, a signal biosynthesis inhibitor which targets AgrB and apicidin, an AgrA inhibitor (107, 108).

Ambuic acid and apicidin have both been shown to inhibit *agr* using an *agr*P3-*lux* reporter and have been shown to reduce lesion size in mouse models of infection (107, 108). To verify that the *agr*P3-GLuc reporter can be used to screen for inhibitors of different proteins within the *agr* system, these compounds were tested in overnight culture with *S. aureus* USA300 *agr*P3-GLuc.

Addition of ambuic acid at 40 μM significantly reduced bioluminescence, by almost 4-fold, compared with the DMSO control. Apicidin was tested at a range of concentrations and was shown to reduce bioluminescence at concentrations over 20 μM. This reduction, although statistically significant, is not close to the background level and indicates only partial inhibition of *agr* at high concentrations of the compound. Together this demonstrates that this reporter can be used to screen for *agr* inhibitors which target different *agr* proteins.

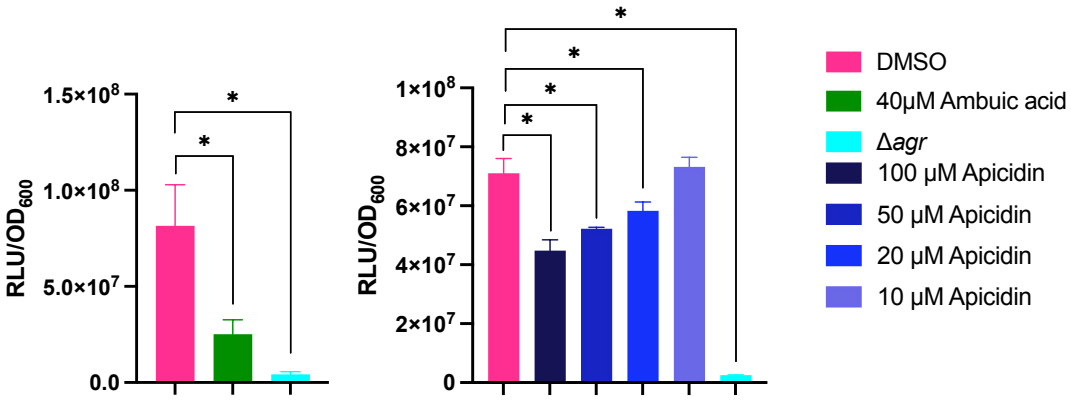


Figure 3-8. Impact of the addition of ambuic acid and apicidin on bioluminescence output from *S. aureus* USA300 *agr*P3-GLuc. The data represents three technical repeats with error bars showing standard deviation. The assay testing ambuic acid was performed in biological triplicate. *p<0.05.

3.10 Construction of *S. aureus agr*P3-NanoLuc reporters

Here it has been demonstrated that an *S. aureus agr*P3-GLuc reporter is useful for monitoring *agr* activity *in vitro* (163). NanoLuciferase (NanoLuc) is another novel luciferase which has a number of advantages over GLuc. It is a smaller protein and is brighter with glow-type bioluminescence. Its use has also been validated in *in vivo* studies (147). Due to this, strains were constructed with NanoLuc under the control of the *agr*P3 promoter to test whether this can be used as an improved reporter for *agr* activation in *S. aureus*.

An oligonucleotide was purchased from Eurofins consisting of the *agr*P3 promoter, an SpA leader to direct NanoLuc to the sec pathway for secretion in *S. aureus,* the NanoLuc sequence and a transcriptional terminator sequence (Figure 3-9). The DNA sequence of this is shown in the methods in section 2.2.2. This was cloned into plasmid pLL102, a vector with an *attP2* site which integrates specifically into an engineered *attB2* site in the chromosome of an *S. aureus* RN4220 strain (154). Phage transduction was performed to move the sequence into the chromosome of *S. aureus* USA300 JE2. Phage transduction was also performed using phage RN6911 to obtain an *agr* knockout strain to use as a control. This uses allelic replacement to replace the full *agr* operon with a tetracycline resistance cassette giving a Δ*agr* strain (160).

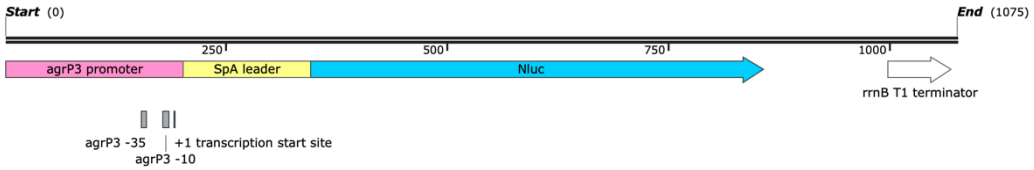


Figure 3-9. Schematic of the *agr*P3-SpA-NanoLuc oligonucleotide purchased from Eurofins. The *agr*P3 promoter is located upstream of an SpA leader to direct NanoLuc for secretion in *S. aureus* and the NanoLuc sequence. This is followed by a ribosomal terminator sequence.

To confirm the *agr* knockout, AIP production was assayed from *S. aureus* USA300 JE2 Δ*agr* *agr*P3-NanoLuc using *S. aureus* ROJ143 (164). *S. aureus* ROJ143 is derived from a *S. aureus* RN4220 Δ*agr* background with a chromosomally encoded *agr*P3-*lux* reporter and plasmid pSKermP2 encoding *agrC1* and *agrA1.* This can respond to exogenous AIP-1 producing light but does not make AIP-1 itself (153). Supernatant fractions from overnight cultures of test strains were added to *S. aureus* ROJ143 in a 96 well plate and grown at 37°C.

As shown in Figure 3-10, after 3.5 h of growth, the light output from *S. aureus* ROJ143 with supernatant from *S. aureus* USA300 JE2 *agr*P3-NanoLuc was comparable with that of supernatant from the wild type strain. This demonstrates that expression of NanoLuc has no effect on the ability of the strain to make AIP. No bioluminescence was recorded from the Δ*agr* strain demonstrating no AIP is made indicating a successful knockout of the *agr* QS system.

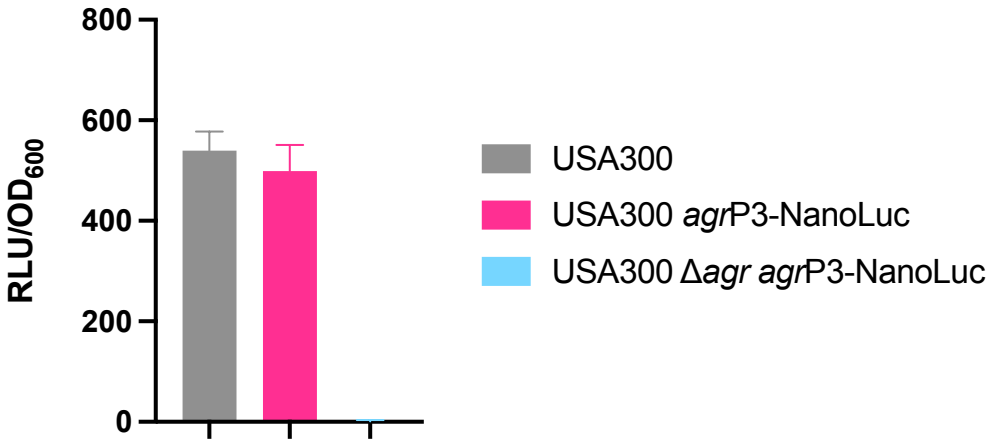


Figure 3-10. Bioluminescence produced by *S. aureus* ROJ143 after growth for 3.5 h with supernatants from overnight cultures of test strains. The data represent the mean with error bars displaying standard deviation of three biological repeats.

3.11 Reduction in bioluminescence after addition of substrate from GLuc compared to NanoLuc

One reason NanoLuc was chosen as an alternative to GLuc is because GLuc is a flash luciferase with the signal dropping off rapidly over 1 min after addition of the coelenterazine (CTZ) substrate (139). This means that the signal has to be captured with a luminometer with a built-in injector. NanoLuc is a glow type luciferase which makes it easier to work with (148). To quantify the differences in bioluminescence output from the different luciferases, bioluminescence from *S. aureus* USA300 SpA *agr*P3-NanoLuc and *S. aureus* USA300 SpA *agr*P3-GLuc was measured every 60 s for 10 min after addition of substrate. The NanoLuc strain was tested with both NanoGlo, the substrate for NanoLuc which is an analogue of CTZ with which the bioluminescence half-life should exceed 2 h, and CTZ.

As shown in **Figure 3-11**, bioluminescence output from NanoLuc with NanoGlo substrate was almost 600 times lower than from NanoLuc or GLuc with CTZ. However, the bioluminescence over 10 min was more stable with the NanoGlo substrate indicating an improved signal half-life. The signal from GLuc with CTZ substrate decreased rapidly, falling by almost 50% from ~7.3 x 10^6 RLU to ~3.9 x 10^6 in 60 s. The reduction in signal from NanoLuc with CTZ was less pronounced. This demonstrated that the half-life of bioluminescence from NanoLuc was extended over that of GLuc with both CTZ and NanoGlo substrates.

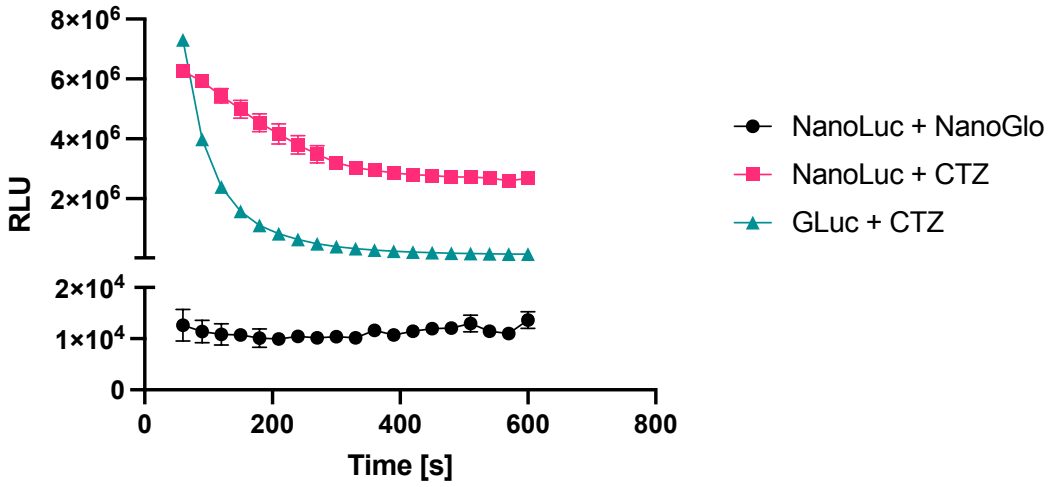


Figure 3-11. Reduction in bioluminescence over 10 min from GLuc and NanoLuc after addition of CTZ of NanoGlo as substrate. The data represent the mean with error bars displaying standard deviation of three technical repeats.

The low level of bioluminescence from NanoLuc with NanoGlo substrate was unexpected. NanoGlo is the optimised furimazine substrate for NanoLuc sold by Promega therefore would be expected to produce higher bioluminescence with NanoLuc than CTZ. Additionally, NanoLuc would be expected to be at least as bright as GLuc. The concentration of CTZ added to GLuc was optimised by Dr Carmen Tong (PhD thesis, University of Nottingham) to give the highest light output whereas NanoGlo was added as per the manufacturer's recommendations (152). It may be that the CTZ is in excess, saturating the enzyme whereas there may be a deficit of NanoGlo, not enabling the luciferase to saturate resulting in lower bioluminescence. Increasing the concentration of NanoGlo could increase the bioluminescence output from NanoLuc. Additionally, the NanoGlo reagent may have degraded. Promega state that the NanoGlo luciferase buffer can be freeze thawed at least 10 times without change in performance. However, the reagent was used by multiple lab users meaning that it may have been through many more freeze thaw cycles, which could have degraded components in the buffer leading to reduced light output from

NanoLuc. To test this, a new NanoGlo substrate and buffer should be used. This was not performed here due to cost and time constraints.

3.12 Inhibition of *agr*P3-NanoLuc bioluminescence using competitive AgrC antagonists

As described previously in section 3.7 with *agr*P3-GLuc, to demonstrate that NanoLuc expression was under the control of the *agr*P3 promoter, the strains were grown in the presence of two competitive AgrC inhibitors, AIP-95 and (Ala^5)AIP-1 (66). These are both cross group AgrC inhibitors and are analogues of AIP-1. Bioluminescence signal and OD_{600} were recorded after overnight incubation with the inhibitors.

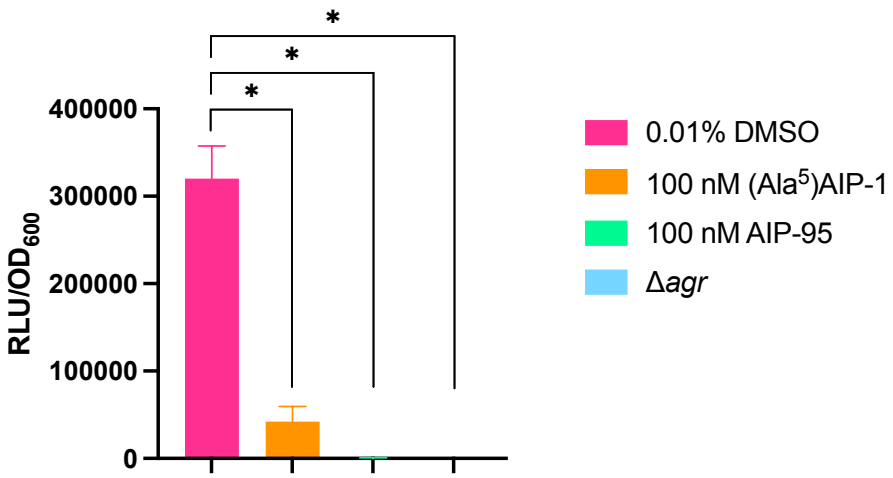


Figure 3-12. Impact of the addition of competitive *agr* inhibitors (Ala^5)AIP-1 and AIP-95 on bioluminescence output from *S. aureus* USA300 *agr*P3-NanoLuc. Data represent the bioluminescence output after overnight growth of test strain with inhibitors. RLU was read after injection of 50 μL 20 μM CTZ. Data represent the mean with error bars showing standard deviation of three biological repeats. *p<0.0001.

As shown in Figure 3-12, after incubation with either inhibitor, there was a significant decrease in bioluminescence. This demonstrates that bioluminescence from these strains can be inhibited with addition of

competitive AgrC inhibitors showing that bioluminescence correlates with *agr* activation.

3.13 Detecting NanoLuc expression in cells compared with cell free supernatants

When constructing the reporter, an SpA leader was generated upstream of NanoLuc to direct the translated protein to the Sec pathway for secretion as for the GLuc reporter. To check the level of secretion of NanoLuc, bioluminescence was tested after overnight growth in both the cells and supernatant fractions. As shown in Figure 3-13, the level of bioluminescence in the supernatant was significantly lower than in the cell pellet. This indicates that NanoLuc was not being efficiently secreted via Sec.

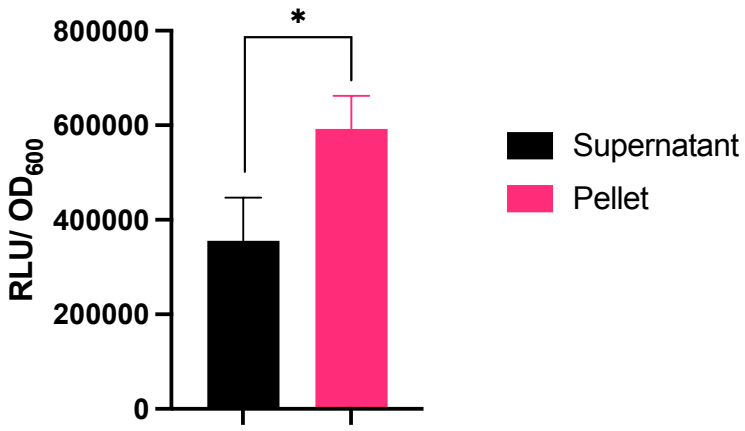


Figure 3-13. Comparison of bioluminescence output from supernatant and cell pellet of *S. aureus* USA300 *agr*P3-NanoLuc. After overnight growth OD_{600} was recorded and cells separated from supernatant by centrifugation. Cells were washed in PBS before bioluminescence was recorded. Bioluminescence was quantified after injection of 50 μL 20 μM CTZ. Data represents the mean with error bars displaying standard deviation of three biological repeats. *p<0.0001.

3.14 Improvement of NanoLuc secretion

It was hypothesised that changing the leader signal peptide could improve the efficiency of secretion. It has been reported previously that the use of different signal peptides can result in different levels of secretion of the same protein. It therefore can be important to find signal peptides which are optimal for each protein to be secreted (165, 166). In *S. aureus,* surface proteins are sent to two distinct destinations in the bacterial envelope. Proteins which have a YSIRK/GS motif in the N-terminal signal peptide such as SpA are distributed in a ring around the cell. Proteins with no YSIRK/GS in the signal peptide are directed to discrete assembly sites (167, 168). The SpA signal sequence does contain a YSIRK motif therefore signal peptides without this may improve secretion. The predicted likelihood of NanoLuc secretion via the Sec pathway with a variety of signal peptides was determined using SignalP (169). SignalP analyses the amino acid sequence input and uses this to predict the likelihood of secretion in the category chosen, here via the Sec pathway in Gram-positive bacteria (170). The predicted likelihood of secretion via Sec with the SpA leader was 0.7999. The best predicted signal peptides were chosen to be tested experimentally, these were; ClfA (0.9193), SasD (0.9819) and IsdC (0.9726). ClfA does contain a YSIRK motif whereas SasD and IsdC do not (167).

These signal peptides were amplified by PCR and inserted in the place of SpA in the vector pMK-RQ. These sequences were cloned into integration vector pLL102 using HiFi cloning and integrated into *S. aureus* RN4220. Phage transduction was again performed to incorporate the *agr*P3-signal peptide-NanoLuc sequence into the chromosome of *S. aureus* USA300 JE2.

Strains were grown overnight and the OD_{600} noted. The bioluminescence was recorded from cells and supernatant fraction after injection of 50 μL 20 μM CTZ and the percentage secretion of the luciferase was calculated

as shown in **Table 3-1**. The SasD leader was shown to direct the highest level of secretion with 60% NanoLuc signal secreted, however this is still far lower than the secretion observed for GLuc where 99% signal was detected in the culture supernatant.

Table 3-1. Percentage bioluminescence from supernatant and cell pellet of *S. aureus* USA300 *agr*P3-signal peptide-NanoLuc strains after overnight growth.

Signal peptide	Percentage bioluminescence	
	Supernatant	Pellet
SpA	24.42	75.58
ClfA	35.23	64.77
SasD	60.48	39.52
IsdC	24.81	75.19

3.15 NanoLuc codon optimisation

To attempt to improve expression and secretion of NanoLuc further, a *S. aureus* codon optimised version of the gene was used. This was cloned as described previously and inserted into the chromosome of *S. aureus* USA300 JE2 by phage transduction. As shown in **Figure 3-14**, bioluminescence was improved for all constructs with the codon optimised version of NanoLuc compared with the generic sequence.

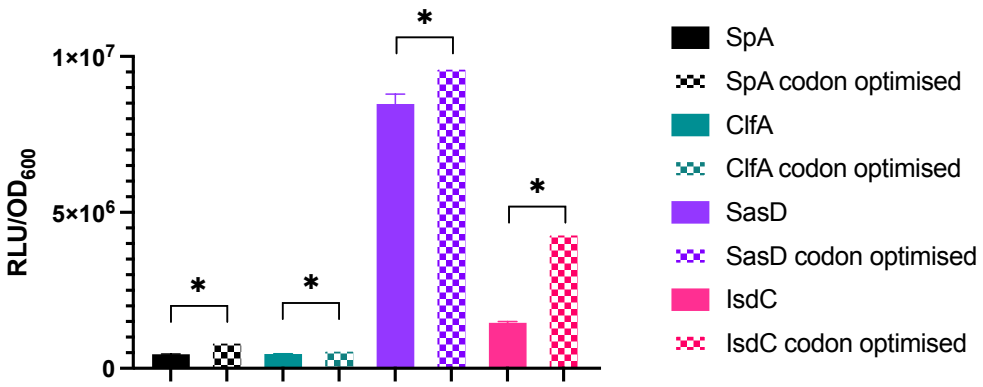


Figure 3-14. Comparison of bioluminescence from *agr*P3-NanoLuc strains with and without codon optimisation. Bioluminescence after overnight growth of *S. aureus* USA300 *agr*P3-NanoLuc with different signal peptide leaders. Bioluminescence was read after injection of 50 μL 20 μM CTZ. Data represents the mean with error bars displaying standard deviation of three technical repeats. *p<0.05.

To determine whether codon optimisation of NanoLuc allowed improved secretion from *S. aureus* USA300, bioluminescence from the cell pellet and supernatant was determined as previously after overnight growth. As shown in **Table 3-2**, the percentage bioluminescence was higher in the supernatant with signal peptides ClfA, SasD and IsdC indicating that more than 50% of the luciferase is being secreted. This is an improvement from the previous construct.

Table 3-2. Percentage bioluminescence from supernatant and cell pellet of *S. aureus* USA300 *agr*P3-signal peptide-NanoLuc strains with codon optimisation after overnight growth.

Signal peptide	% Bioluminescence	
	Supernatant	Cell pellet
SpA	49.27	50.73
ClfA	57.20	42.80
SasD	73.15	26.85
IsdC	67.55	32.45

As previously, the SasD signal peptide leader allowed the best secretion of NanoLuc as predicted by SigP. There is also the highest overall bioluminescence with this leader peptide (**Figure 3-14**). This construct was tested with *agr* competitive inhibitors AIP-95 and Ala^5(AIP-1) to determine whether the signal could be inhibited by *agr* antagonists. As shown in **Figure 3-15**, bioluminescence from *S. aureus* USA300 *agr*P3-SasD-NanoLuc decreased on addition of *agr* inhibitors. This shows that NanoLuc signal can be inhibited using *agr* QS antagonists and demonstrated that it is under the control of the *agr*P3 promoter.

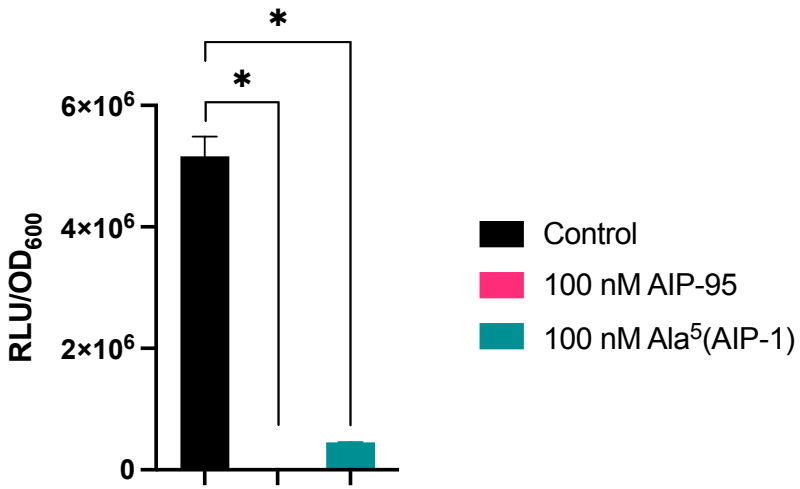


Figure 3-15. Impact of 100 nM AIP-95 and Ala^5(AIP-1) on bioluminescence output from *S. aureus* USA300 *agr*P3-SasD-NanoLuc. The data represent three technical repeats and three biological repeats for each sample with error bars displaying standard deviation. *p<0.01.

3.16 Discussion and conclusions

Antibiotic resistance in *S. aureus* is an increasing clinical problem and there is an urgent need for therapeutics which do not succumb to conventional mechanisms of antibiotic resistance. One such method is through the attenuation of the virulence of the bacteria through targeting the *agr* quorum sensing system (6, 112). To facilitate the screening of *agr* inhibitors and to

gain information about *agr* activation in infection models it is important to develop methods for monitoring *agr* activity. In this chapter we have demonstrated the use of novel luciferases GLuc and NanoLuc as secreted reporters of *agr* activation and inhibition in *S. aureus.*

In section 3.5 it was shown that production of bioluminescence from *agr*P3-GLuc correlates with growth phase and predicted *agr* activation. This could be validated further for example with quantitative reverse transcriptase PCR to detect RNAIII levels (171). This will confirm that GLuc activation occurs with activation of the *agr*P3 promoter. The correlation between GLuc bioluminescence and *agr* activation makes this a useful reporter for real time monitoring of *agr* induction and inhibition. GLuc is a useful reporter for *agr* QS as it is stable in a wide range of pH and is resistant to hydrogen peroxide and a wide range of reactive compounds (137, 140). When the *agr* system is active, the cells will release a number of toxins and the stability of GLuc means it should not be affected by these and so will be useful as an *agr* QS reporter.

This reporter was validated through demonstration of activation with exogenous cognate AIP-1 (section 3.6) and inhibition with competitive AgrC antagonists (section 3.7). The *S. aureus agr*P3 GLuc reporter was shown to be sensitive to previously reported *agr* inhibitors ambuic acid, and apicidin which target AgrB and AgrA respectively (107, 108). This demonstrates that GLuc can report on inhibition of different proteins in the *agr* system. *agr*P3-*lux* based reporters are often used to screen inhibitors of *agr* QS (61, 105, 107). However, it has been shown that QS inhibitors can interfere with the bacterial *lux* system resulting in false positive results. 3-oxo-C12 HSL is a quorum sensing molecule which is produced by *Pseudomonas aeruginosa*. This has been shown to inhibit bioluminescence produced by bacterial *lux* however has no effect on GLuc bioluminescence and has been shown, using an *agr*P3-GLuc reporter, to be an inhibitor of agr quorum sensing (152,

163). This highlights the use of GLuc as an alternative reporter to bacterial luciferase which could be used instead or as well as bacterial luciferases to report on agr inhibition.

It was shown in section 3.4 that the *agr*P3-GLuc reporter is secreted from *S. aureus* cells, with 99% of the bioluminescent signal being detected in the supernatant rather than the cell pellet after overnight growth. Some signal would be expected in the supernatant after overnight growth due to cell death and lysis releasing the luciferase however, 99% is an extremely high proportion demonstrating that the luciferase is efficiently secreted. Secreted luciferases are useful for monitoring of *in vivo* processes with minimal interference. Indeed, secreted GLuc has been shown in previous studies to be an effective reporter for *ex vivo* monitoring of *in vivo* processes including the progress of bacterial infections with the luciferase detected from blood or urine samples from murine models of infection (137, 143, 146, 172).

It is important to monitor *agr* activation *in vivo*, as *agr* quorum sensing is under tight control, influenced by many environmental factors (58). This is hard to simulate *in vitro.* Detection of GLuc from the blood or urine of mouse models of infection would inform on real time *agr* activation. The half-life of GLuc in circulation *in vivo* is 20 min therefore there would be no significant accumulation of signal meaning bioluminescence recorded would correlate with real-time activation of *agr*-dependent QS (143). This highlights another advantage over bacterial luciferase for monitoring *agr*-dependent QS. Bacterial luciferase is restricted to intracellular use which is useful for *in vivo* imaging of infection sites however the luciferase requires oxygen (173). In many *S. aureus* infection sites, oxygen is depleted therefore, the luciferase will be inactive and so will not accurately reporter on *agr* activation (87). Secreted GLuc will be detected *ex vivo* so the oxygen status at the infection site will not affect the reporter giving accurate representation of *agr* activation and inhibition. The use of secreted *agr*P3-GLuc in *in vivo* models

will give valuable insights into the dynamics of *agr* activation and the potential applications for *agr* QS inhibitors.

GLuc has been demonstrated to be an effective secreted bioreporter for *agr* QS activation and inhibition and the potential for use in *in vivo* studies has been outlined. A secreted *agr*P3-NanoLuc reporter has also been developed. NanoLuc has a number of advantages over GLuc including smaller size, brighter bioluminescence and improved optical emission for use *in vivo*. NanoLuc is an intracellular luciferase which can be secreted by adding a signal sequence to the NanoLuc sequence which is what has been done here (149). Optimisation of NanoLuc secretion has been performed with different signal peptide leaders showing that the SasD leader peptide enabled the most efficient secretion of NanoLuc. The SasD leader also promoted the highest level of bioluminescence from NanoLuc. SasD is a cell wall anchored protein containing host attachment domains (174).

Secreted NanoLuc has been shown previously to be useful for *ex vivo* analysis of *in vivo* processes in living animals showing reduced background compared to GLuc (149). Here the *agr*P3-NanoLuc signal was shown to be inhibited with competitive *agr* inhibitors AIP-95 and (Ala^5)AIP-1 confirming that this has potential to be used to screen for *agr* QS inhibitors. This demonstrates that NanoLuc could also be developed as an effective biomarker for real time *agr* activation in mouse models of infection.

Overall, the use of secreted *Gaussia* luciferase as a novel reporter of *agr* activity in *S. aureus in vitro* and the potential for use of GLuc for screening activators and inhibitors of the *agr* system has been validated. The development of a NanoLuc reporter which could be used to monitor *agr* activation and screen for inhibitors has also been demonstrated. These reporters both display good potential to be used as *in vivo* bioreporters for

agr activation and inhibition aiding in the discovery of virulence factor inhibitors against *S. aureus* infections.

4. Using bioluminescent tools to investigate AgrB and AgrD protein-protein interactions in live bacteria

4.1 Introduction

In Chapter 3 the use of bioluminescent reporters GLuc and NanoLuc to monitor the activation and inhibition of the *agr* system in *S. aureus* USA300 was described. As well as use as a bioreporter, NanoLuc has been developed for use in novel assays for monitoring protein-protein interactions in live cells.

As highlighted in the introduction (section 1.3.3), the molecular mechanism of processing of AgrD to form mature AIP is unclear. The current hypothesis is that AgrD localises to the membrane via the N-terminal amphipathic helix where is it recognised by AgrB via the negatively charged C-terminus (70). AgrB is considered to form a stable dimer in the membrane and cleave the C-terminus of AgrD before thiolactone ring formation and further processing of AgrD to form AIP (68).

Residues in AgrB which are essential for the catalytic activity and cleavage of AgrD have been identified and multiple topologies of AgrB in the membrane have been predicted (71). For example, Zhang et al. (56) in 2002 used AgrB-PhoA fusions and computer analysis to predict AgrB to have six transmembrane domains with the N- and C-termini in the cytosol (56). This was, however, disputed by Thoendel and Horswill in 2013 (72). They used substituted cysteine accessibility method (SCAM) with cysteine substitutions in AgrB in both *E. coli* and *S. aureus* to predict that AgrB has four transmembrane helices and one re-entrant loop with the N- and C-termini outside the cell (72). These topologies both place key catalytic residue C84 buried within the membrane however they disagree on the placement of other key residues. As there is no crystal structure of AgrB,

predictions such as these are useful in the understanding the function of AgrB.

The interactions between AgrB and AgrD leading to the production of mature AIP have been studied over many years often through the use of Western blots to display cleavage of AgrD and bioreporter assays to monitor production of AIP (67, 71, 72). In this chapter the development of protein-protein interaction techniques to investigate AgrBB oligomerization and AgrBD interactions in living cells is described.

As mentioned in the Introduction in section 1.3.2, there are four *agr* subgroups in *S. aureus* which have variations in AgrB (11). The work in this chapter will focus on *agr* group I proteins from *S. aureus* USA300. Work performed by Zhang et al. (56) and Thoendel et al. (72) also focussed on AgrB from *agr* group I (AgrB1) therefore this is comparable.

AgrB1 has been shown to oligomerise *in vitro* by co-immunoprecipitation, this has been hypothesised to form a pore mediating export of AIP (72). AgrB has also been reported to form stable dimers in lipid membranes which may be essential for its function (68). AgrB dimerization has not, however, been shown experimentally in live bacterial cells. In this work a NanoBRET assay has been developed to monitor AgrB1 multimerization *in vitro* in an *E. coli* expression system. NanoBRET relies on energy transfer from proteins in close proximity so will inform on AgrB multimerization.

A split luciferase assay has also been developed in *S. aureus* to monitor protein-protein interactions using NanoLuc Binary Technology (NanoBiT). NanoBiT is used to monitor protein proximity in live cells. A NanoBiT assay has been developed in *S. aureus* to identify if AgrB1B1 oligomerization can be demonstrated experimentally and which termini may be involved in this. This will also be used to identify whether the AgrB1D1 interaction can be

demonstrated experimentally in live cells and to identify which termini of AgrB and AgrD are involved in this interaction.

4.2 Aims

The aim of the work presented in this chapter was to develop and evaluate novel bioluminescent tools for investigation of the interaction of AgrB1B1 and AgrB1D1 in *S. aureus* and in an *E. coli* model. This will confirm computational modelling performed by Dr Boyan Bonev and will give insights into Agr protein-protein interactions in live cells. A NanoBRET system was developed in *E. coli* to visualise AgrB1B1 interactions. A split luciferase system using NanoBiT was also used in *S. aureus* to evaluate AgrB1B1 and AgrB1D1 interactions in live cells.

4.3 Computational modelling of AgrBB and AgrBD interactions

Computational modelling of AgrB1, analysis and interpretation was performed by Dr Boyan Bonev. As there is no structural data available for AgrB or AgrD, to understand molecular conformations, molecular dynamics annealed homology models were established. Homology modelling revealed AgrB1 to have a six transmembrane domain helical topology with both the N- and C- termini on the same side of the membrane as shown in **Figure 4-1**. The catalytic Cys84 residue was shown to be in the membrane interior, permitting contact with hydrophobic substrate, AgrD1. Other key residues which have been shown to affect AgrB1 activity during point mutagenesis, are accessible from the cytoplasmic side.

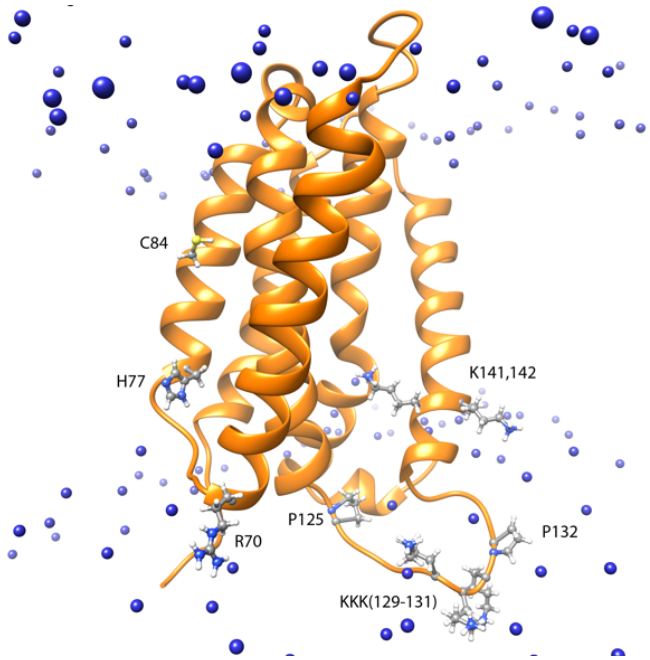


Figure 4-1. Atom MD-annealed homology model of AgrB1 in a membrane at the end of 500 ns all atom trajectory in hydrated membranes of 4:1 POPG/POPE. Membrane phospholipid phosphorus atoms (blue spheres) outline the membrane interface and show protein location in the membrane.

AgrB1 was shown to dimerize, with one monomer of AgrB1 responsible for AgrD1 pro-peptide insertion and docking in the correct orientation for catalytic processing by the other monomer of AgrB1; this is displayed in **Figure 4-2**. AgrB C84 which is responsible for cleavage of AgrD is again located in the membrane interior. C28 of AgrD is positioned in close proximity to C84.

Other residues to note include R70, G75 and H77, these have all been shown to be required for AgrB proteolytic activity (71, 72). These are located on the cytoplasmic face at the end of helix 2 and in a tighter turn towards helix 3. R70 and K139 are thought to be responsible for stabilisation of the orientation of AgrD.

Also to note are the lysines at positions 129-131 (**Figure 4-1**), mutation of these has been shown to retain AgrB peptidase activity but not AIP formation (72). These are located on a mobile cytoplasmic loop which can interact with C-terminal residues E186 and D187 on another monomer of AgrB stabilising dimerization.

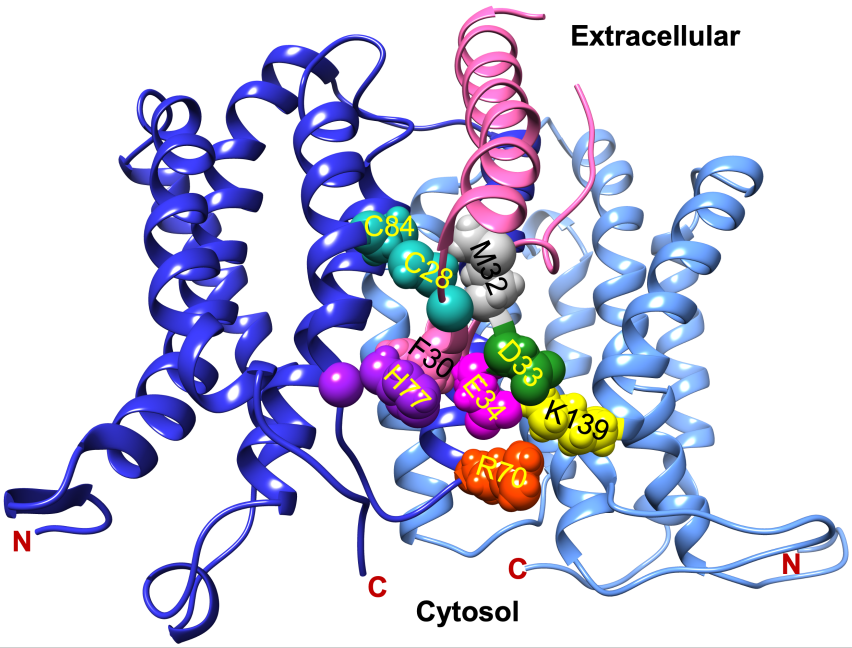


Figure 4-2. Conformation of the $(AgrB)_2$/AgrD complex at the end of 500 ns atomistic MD simulations. Annealed trajectories in hydrated membranes of POPE/POPG/CL (75/20/5) membranes, showing key residues involved in AgrD processing. The two inequivalent AgrB molecules, responsible for AgrD insertion (1, cornflower blue) and catalysis (2, blue) stabilise orientation of AgrD presenting C28 and M32 close to each other and to catalytic C84 of $AgrB_2$ via AgrB1-K139-D33 and AgrB-I R70-E34 contacts with AgrD, and *via* AgrB-II H77-F30 π-interactions. Key residues are shown in aqua (C28, C84 AgrB-II), grey (M32 AgrD), pink (F30 AgrD), purple (H77 AgrB-II), fuchsia (E34 AgrD), green (D33 AgrD), yellow (K139 AgrB-I) and orange (R70 AgrB-I). All AgrB termini are on the cytosolic side (top). The $(AgrB)_2$/AgrD complex orientation here is shown with cytosol at the bottom.

4.4 Development of a NanoBRET system to investigate presence of AgrB1 dimer in an *E. coli* expression model

Bioluminescence resonance energy transfer (BRET) is a biophysical technique used to monitor protein proximity within live cells. It relies on energy transfer from a luciferase donor to an acceptor fluorophore. Energy transfer only occurs when the donor and acceptor are in close proximity allowing protein-protein interactions to be monitored in a highly specific manner. NanoLuc is used as the energy donor for NanoBRET which allows high sensitivity of assays due to the high level of bioluminescence from NanoLuc (175).

It has been shown previously that AgrB forms stable dimers in lipid bilayers and it has also been demonstrated that AgrB oligomerises *in vitro* (68, 72). We have also shown AgrB1 dimerization is predicted using MD simulations. AgrB dimerization or multimerization has not been demonstrated, however, in live cells. To demonstrate AgrB1 dimerization in live cells, a NanoBRET system was developed in an *E. coli* expression model.

In this system NanoLuc will be linked to one copy of AgrB1 on plasmid pCDFDuet-1. This will be the energy donor. Halo-tag will be linked to another copy of AgrB1 on the same plasmid. The Halo-tag will bind covalently to a Halo-tag ligand which will be the energy acceptor. pCDFDuet-1 has two multiple cloning sites (MCS) and is designed for the co-expression of two target genes so is a suitable vector. When AgrB1 dimerises, bringing NanoLuc and Halo-tag into close proximity, and on addition of a Halo-tag ligand and NanoLuc substrate, energy will be transferred from NanoLuc to the Halo-tag ligand and fluorescence will be produced as outlined in Figure 4-3. This fluorescence can be quantified using a Tecan Infinite F200 microplate reader or visualised using confocal laser scanning microscopy.

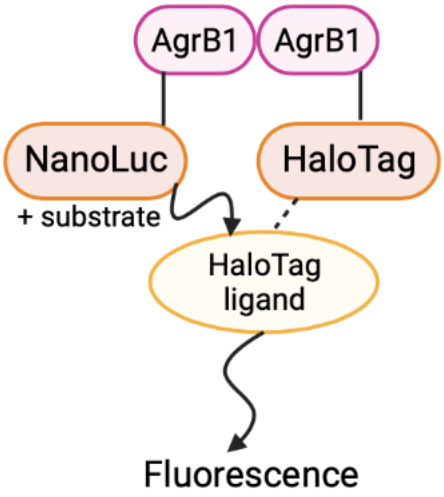


Figure 4-3. Schematic of NanoBRET used to detect AgrB1 dimer formation. NanoLuc is linked to one copy of AgrB1 and HaloTag is linked to another copy of AgrB1. When these come into close proximity in the presence of the NanoLuc substrate and HaloTag ligand, energy is transferred from NanoLuc to the HaloTag ligand which can be detected as fluorescence.

4.4.1 Creation of constructs in *E. coli* and expression of Nanoluc

Initially, to create an N-terminal translational fusion of NanoLuc to AgrB1, NanoLuc was inserted N-terminal to AgrB1 in MCS1 of expression vector pCDFDuet-1 using HiFi cloning. Protein expression from this plasmid is induced on addition of IPTG.

To determine if the construct was functional and NanoLuc was being expressed, pCDFDuet-1 *nanoluc-agrB1* was used to transform expression strain *E. coli* C41 (DE3) and streaked on LB with 100 μg/mL spectinomycin for plasmid selection and 500 μM IPTG for induction of gene expression via the T7 promoter. After overnight incubation at 37°C, plates were sprayed with 20 μM coelenterazine and imaged using a long exposure camera. As

shown in **Figure 4-4**, light was produced from this strain. This shows that NanoLuc is being expressed and is functional.

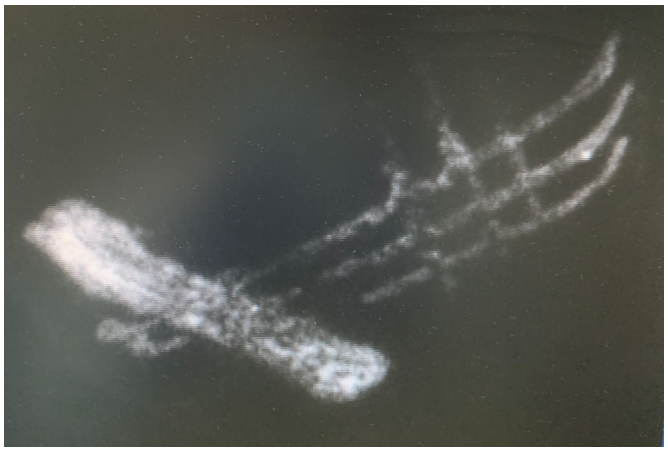


Figure 4-4. *E. coli* C41 (DE3) pCDFDuet-1 *nanoluc-agrB1* streaked on LB with 500 μM IPTG and visualised with a long exposure camera.

4.4.2 Western blot to show translational fusion of NanoLuc to AgrB1

The functional AgrB1 dimer will form at the cell membrane therefore AgrB must be linked to NanoLuc at the membrane for NanoBRET to occur. To confirm that NanoLuc was translationally fused to AgrB1 and localised to the cell membrane, pCDFDuet-1 *nanoluc-agrB1* was induced in *E. coli* C41 (DE3) and membranes separated from cytosolic fraction by ultracentrifugation. Membrane and cytosolic fractions were run on a 4-20% gradient Tris Glycine gel and probed by Western blot against AgrB and NanoLuc.

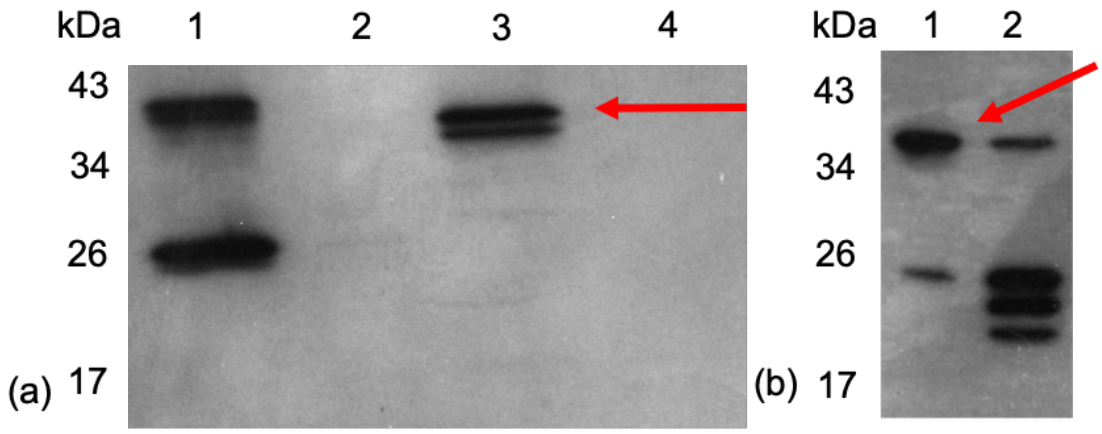


Figure 4-5. Western blots showing translational fusion of NanoLuc to AgrB1. Samples are from cultures of *E. coli* C41 (DE3) pCDFDuet-1 induced with IPTG and membrane fractions separated from cytosolic. (a) Western blot with AgrB1 specific nanobody 2ABE10. Lane 1 – pCDFDuet-1 *agr1I* membrane fraction; Lane 2 – pCDFDuet-1 *agrB1* cytosolic fraction; Lane 3 – pCDFDuet-1 *nanoluc-agrB1* membrane fraction; Lane 4 – pCDFDuet-1 *nanoluc-agrB1* cytosolic fraction. (b) Western blot with NanoLuc antibody. Lane 1 – pCDFDuet-1 *nanoluc-agrB1* membrane fraction; Lane 2 – pCDFDuet-1 *nanoluc-agrB1* cytosolic fraction. Samples were added to 2 x Novex Tris-Glycine SDS sample buffer and heated to 55°C for 5 min before running on a 4-20% Tris-Glycine gel. The gel was transferred to PVDF membrane for Western blot. The red arrows indicate translational fusion of AgrB to NanoLuc.

As shown in Figure 4-5 (a), there was an increase in the size of AgrB when expressed with NanoLuc, from 26kDa to ~43kDa. AgrB fused to NanoLuc is marked with a red arrow. This increase in size corresponds to the translational fusion of NanoLuc (19 kDa) to AgrB. AgrB localised to the membrane and when co-expressed there was no AgrB in the membrane which was not fused to NanoLuc (**Figure 4-5** (a), lane 3). The translational fusion is corroborated by the Western blot with a NanoLuc specific antibody (Figure 4-5 (b)). This showed a band at ~40 kDa corresponding to the band

on the AgrB Western blot (marked with a red arrow). This shows that AgrB and NanoLuc were present at this size. The Western blot against NanoLuc also indicates that there was NanoLuc free in the cytosol (Figure 4-5 (b), lane 2).

4.4.3 Demonstration that AgrB fused to NanoLuc is functional

To demonstrate that the addition of NanoLuc did not affect the functionality of AgrB1, *agrD1* was inserted into MCS2 of pCDFDuet-1 by HiFi cloning. AIP-1 production was determined using *S. aureus* ROJ143 as described previously after induction of protein expression in *E. coli* C41 (DE3). Expression of *agrB1D1* in *E. coli* has been shown previously to be sufficient for AIP-1 production (67).

As shown in **Figure 4-6**, bioluminescence representing AIP-1 production was detected when NanoLuc was present showing that fusion of NanoLuc to AgrB did not affect the enzyme's functionality as AgrD could still be processed to form mature AIP.

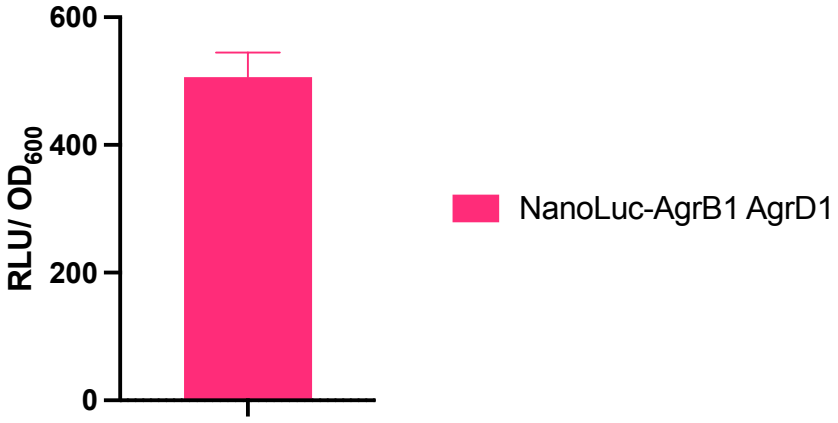


Figure 4-6. AIP-1 production from *E. coli* C41 (DE3) with pCDFDuet-1 *nanoluc-agrB1 agrD1*. *S. aureus* ROJ143 was grown in a 96 well plate in a Tecan plate reader at 37°C for 3.5 h with supernatant from induced samples. The data represent the mean with error bars displaying standard deviation of three biological repeats.

4.4.4 Bioluminescence from membrane and cytosolic fractions

AgrB1 has been shown to dimerise in lipid membranes (68). Therefore, NanoLuc linked to AgrB at the membrane must be active and producing light for BRET to occur between an AgrB dimer. To test this, expression from pCDFDuet-1 *nanoluc-agrB1 agrD1* was induced in *E. coli* C41 (DE3) and membrane fractions and cytosolic fractions were separated by ultracentrifugation. The bioluminescence from these fractions was quantified after the addition of NanoGlo substrate (Promega) using a Tecan plate reader. As displayed in **Figure 4-7**, on addition of substrate, the bioluminescence was almost 100 times higher in the cytosol than in the membrane fraction.

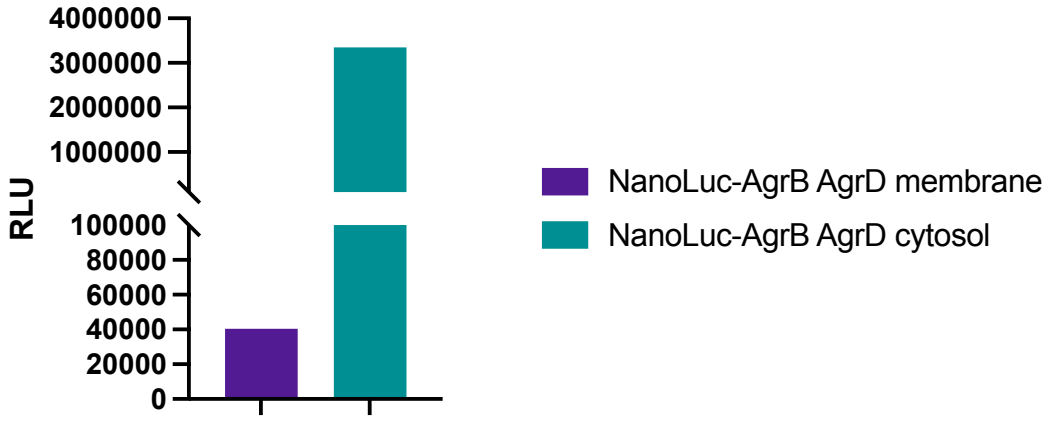


Figure 4-7. Bioluminescence produced by membrane and cytosolic fractions of *E. coli* C41 (DE3) pCDFDuet-1 *nanoluc-agrB1 agrD1*. After induction of protein expression membrane and cytosolic fractions were separated by ultracentrifugation. 100 μL sample was added to a white 96 well plate and NanoGlo substrate added before RLU was recorded.

Western blot showed that NanoLuc-AgrB1 localised to the membrane in *E. coli*, however there was unbound NanoLuc in the cytosolic fraction (Figure 4-5) which may account for the signal from this fraction. The low level of bioluminescence from the membrane fraction indicates that NanoLuc fused to AgrB1 in the membrane was not very functional although AgrB1 was shown to be. Light production from plates (**Figure 4-4**) must be

due to free NanoLuc present in the cytosol not from the membrane. NanoLuc needs to be producing light at the membrane for NanoBRET to occur therefore optimisation of this signal was performed.

4.4.5 Optimisation of signal from NanoLuc linked to AgrB

The bioluminescent signal produced by NanoLuc linked to the N-terminus of AgrB was low. For NanoBRET to occur between AgrB dimers, the bioluminescence signal from NanoLuc linked to AgrB must be high enough for energy transfer to the Halo-tag ligand. To try and improve signal, NanoLuc was fused to the C-terminus of AgrB. Additionally, the linker between AgrB and NanoLuc was increased. In the initial construct there was a 3 amino acid linker between AgrB and NanoLuc. This was increased to 15 amino acids as increased flexibility and movement of the proteins may allow increased bioluminescence output. NanoLuc may have been too close to AgrB and the cell membrane which may have decreased bioluminescence output. NanoLuc was inserted C-terminal to AgrB using HiFi cloning, and an increased linker was introduced by PCR.

agrD1 was inserted in MCS2 of pCDFDuet-1 as before to allow AIP-1 production to be assessed to confirm that AgrB1 was functional. As shown in **Figure 4-8**, AIP-1 was detected from all constructs where NanoLuc is either N- or C-terminal to AgrB with a 3 or 15 amino acid linker. This demonstrates that AgrB1 was functional in all of these constructs.

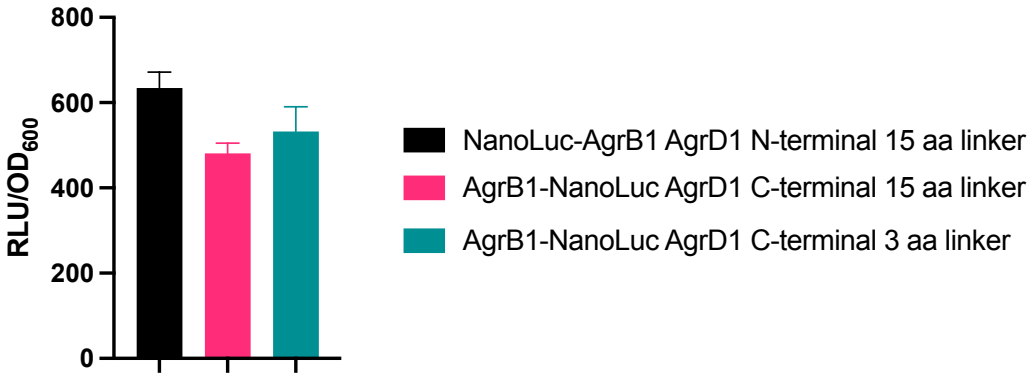


Figure 4-8. AIP-1 production from *E. coli* C41 (DE3) with pCDFDuet-1 *nanoluc-agrB1 agrD1* and pCDFDuet-1 *agrB1-nanoluc agrD1* with a 3 or 15 amino acid linker between NanoLuc and AgrB. *S. aureus* ROJ143 was grown in a 96 well plate in a Tecan plate reader at 37°C for 3.5 h with supernatant from induced samples. The data represent the mean with error bars displaying standard deviation of three biological repeats.

It was then determined whether insertion of NanoLuc C-terminal to AgrB or increasing the length of the linker improved bioluminescence from NanoLuc linked to AgrB. After induction of protein expression in *E. coli* C41 (DE3), cell membrane was separated from cytosol by ultracentrifugation and bioluminescence recorded from each fraction as before. As shown in **Figure 4-9**, bioluminescence was still highest in the cytosol for all constructs however bioluminescence from NanoLuc linked to AgrB in the membrane was greatly increased when NanoLuc was C-terminal to AgrB with a 15 amino acid linker. Therefore, this construct was used as the energy donor for NanoBRET.

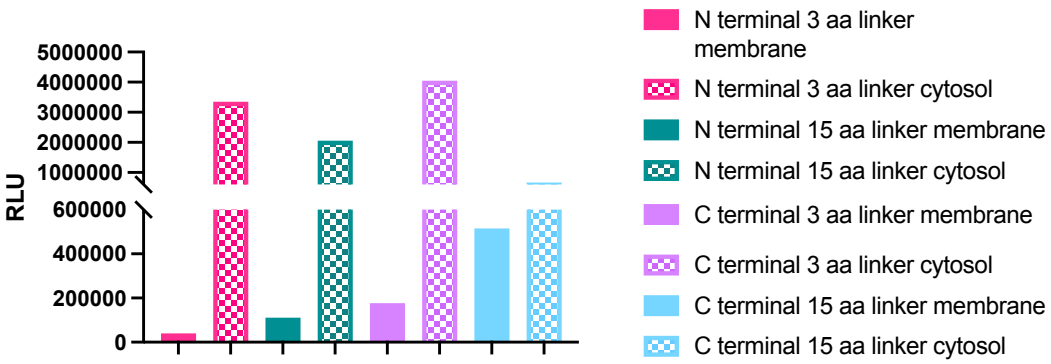


Figure 4-9. Bioluminescence produced by membrane fractions of *E. coli* C41 (DE3) pCDFDuet-1 *nanoluc-agrB1 agrD1* (N-terminal) and pCDFDuet-1 *agrB1-nanoluc agrD1* (C-terminal) with 3 or 15 amino acid linkers. After induction membrane and cytosolic fractions were separated by ultracentrifugation. 100 μL sample was added to a white 96 well plate and furimazine substrate added before bioluminescence was recorded.

4.4.6 Introduction of Halo-AgrB to MCS2 of pCDFDuet-1

AgrB1 linked to a HaloTag was the NanoBRET energy acceptor (**Figure 4-3**). Using pCDFDuet-1 as the expression construct, *HaloTag-agrB1* was inserted into MCS2 using HiFi cloning (**Figure 4-10**). The HaloTag was inserted N-terminal to AgrB. Bioluminescence from NanoLuc on one copy of AgrB transfers energy to a HaloTag ligand linked to the HaloTag on another copy of AgrB and fluorescence can be detected.

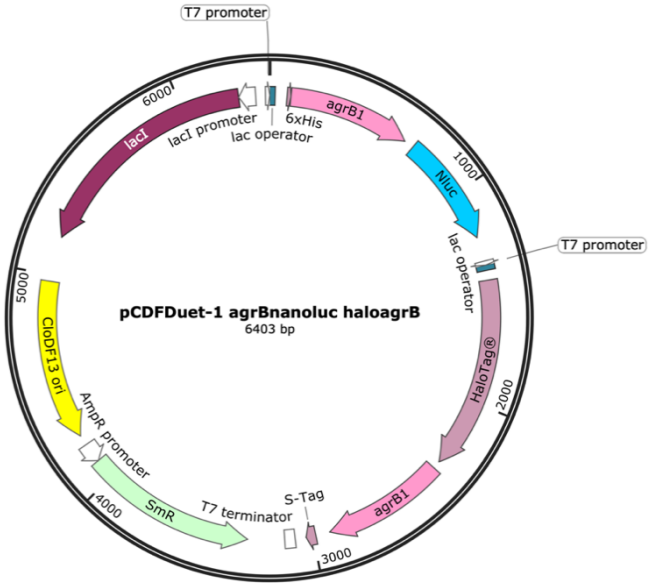


Figure 4-10. Plasmid map of pCDFDuet-1 *agrB1-nanoluc HaloTag-agrB1* used for NanoBRET. One copy of *agrB1* in MCS1 has *nanoluc* at the C-terminus, one copy of *agrB1* in MCS2 has *HaloTag* at the N-terminus.

4.4.7 Detection of NanoBRET using a Tecan plate reader

Detection of NanoBRET was first attempted using a Tecan plate reader. pCDFDuet-1 *agrB1-nanoluc HaloTag-agrB1* and control plasmid pCDFDuet-1 *HaloTag-agrB1* were expressed in *E. coli* C41 (DE3). Recommended HaloTag substrate TMRDirect was selected as it can permeate bacterial cells (176). The Förster distance is the distance between the donor and acceptor by which 50% of energy transfer occurs. For NanoBRET with NanoLuc as the donor and TMR as the acceptor this has been calculated as 6.15 ± 0.03 nm with a working range of 3.08-9.23 nm showing the proteins need to be in very close proximity for NanoBRET to occur (177).

The emission wavelength of NanoLuc is 460 nm and the emission from TMRDirect is 585 nm. To calculate NanoBRET, the bioluminescence from the donor and recipient is recorded and the ratio of receptor to donor signals is calculated. Bioluminescence was recorded using a Tecan Infinite F200

microplate reader with blue and green filters. For both strains the bioluminescence was recorded with and without incubation with TMRDirect ligand.

The raw NanoBRET ratio for each sample was calculated by dividing the acceptor emission by donor emission. The corrected BRET ratio was then calculated by subtracting the no ligand control ratio from the experimental ratio as shown below. This must be calculated to remove cross talk between the detection wavelengths.

$$NanoBRET\ corrected\ ratio = Ligand\left(\frac{585\ nm}{460\ nm}\right) - No\ ligand\ control\left(\frac{585\ nm}{460\ nm}\right)$$

Figure 4-11 displays the BRET ratio for the test strain of 16.5 milli BRET units (mBU). This ratio represents energy transfer occurring meaning energy is being transferred from one copy of AgrB to another. This demonstrates copies of AgrB are in very close proximity in at least a dimer.

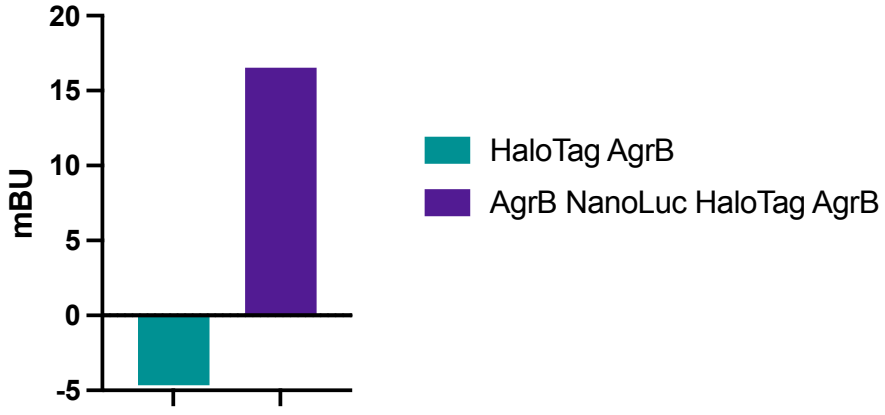


Figure 4-11. Corrected BRET ratio from test and control strain. BRET ratio is calculated using the above formula. Data represent the ratio calculated from 2 biological repeats.

4.4.8 NanoBRET detected by confocal laser scanning microscopy

As NanoBRET was detected using the Tecan Infinite F200 microplate reader we wanted to determine if the AgrB dimer could be visualised using confocal laser scanning microscopy. This would show visual evidence of the AgrB dimer at the *E. coli* membrane.

To test that fluorescence from the TMRDirect ligand bound to the HaloTag could be detected by confocal microscopy, the sample was excited by artificial excitation at 555 nm. As shown in **Figure 4-12**, with artificial excitation, fluorescence could be detected from the test and control samples. This demonstrates that the ligand could penetrate the *E. coli* cell and bind the HaloTag linked to AgrB.

When NanoGlo substrate was added, fluorescence was detected with no artificial excitation (**Figure 4-12**, bottom centre). This shows that this was the TMR ligand being excited by NanoLuc providing evidence that the AgrB monomers were in close proximity allowing energy transfer. The images with artificial excitation and excitation via NanoLuc align showing that it was the Halotag ligand which fluoresces.

No fluorescence was detected from the sample with no substrate added when there is no artificial excitation (**Figure 4-12**, top centre). This confirmed that the fluorescence observed in the sample with NanoGlo added was due to energy transfer from NanoLuc representing NanoBRET. Therefore, this represents visual evidence of AgrB1B1 interaction in the *E. coli* membrane representing at least a dimer of AgrB1.

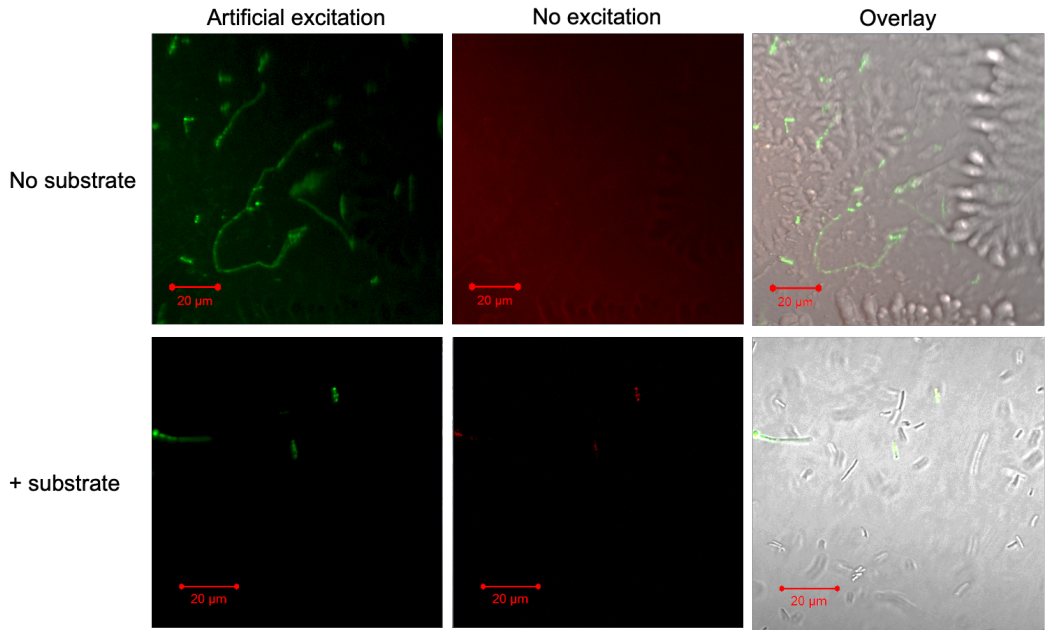


Figure 4-12. AgrB dimerization in *E. coli* C41 (DE3) visualised by NanoBRET using confocal microscopy. Images were taken on a Zeiss LSM 700 confocal laser scanning microscope controlled by the ZEN 2009 software platform and analysed using the ZEN 2009 software. 'Artificial excitation' was at 555 nm and emission captured at 585 nm. 'No excitation' was recorded using a quantum dot which excites at 350 nm, this will not excite the TMRDirect fluorophore, and emits at 585 nm. The reading from this channel is representative of no excitation of the TMRDirect ligand.

4.5 Development of a NanoBiT system to monitor AgrBB and AgrBD interactions in *S. aureus*

We have shown evidence for AgrB1 oligomerisation in *E. coli* however we also wanted to demonstrate this in *S. aureus*. NanoLuc binary technology (NanoBiT) is a novel technology which uses a split luciferase to look at protein-protein interactions. Here a NanoBiT system has been developed to investigate whether AgrB1D1 and AgrB1B1 interactions can be demonstrated experimentally in live *S. aureus* cells.

NanoBiT is a two-subunit based system where LargeBiT (156 amino acids) and SmallBiT (11 amino acids) are fused to two proteins of interest. When these proteins come into close proximity and interact, LargeBiT and SmallBiT are brought together and form a luciferase which produces bright bioluminescence on addition of NanoLuc substrate (**Figure 4-13**). This can be used to detect real time protein-protein interactions. LargeBiT and SmallBiT have a weak affinity for each other (K_D = 190 μM) so do not attract each other (178).

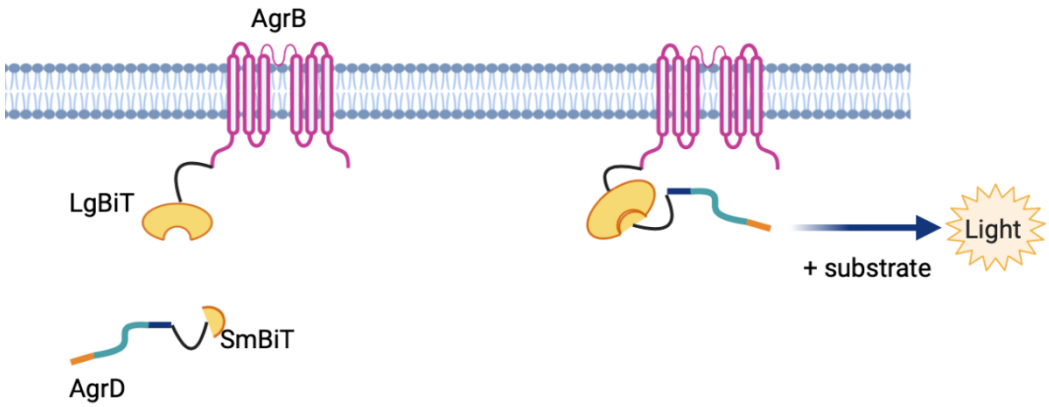


Figure 4-13. Schematic of the NanoBiT assay used to monitor AgrBD protein interaction. SmallBiT is linked to the N-terminus of AgrD and LgBiT is linked to the C-terminus of AgrB in this schematic. When these termini come into close proximity, the luciferase is formed and, on addition of NanoLuc substrate, bioluminescence is produced.

For LargeBiT and SmallBiT to interact they have to be in very close proximity therefore we have developed this technology to inform on both the interaction between AgrB1 and AgrD1 and AgrB1 multimerization. By fusing LargeBiT and SmallBiT to different termini of each protein it was possible to identify interactions and which termini are involved in interactions. Test and control strains for this investigation were created by Dr. Ewan Murray in *S. aureus* SH1000 and are outlined in the Methods section 2.10.1, **Table 2-4**.

4.5.1 AgrB1D1 interaction

NanoBiT was used to investigate AgrB1D1 interactions in live *S. aureus* cells and to determine which termini of AgrB1 and AgrD1 drive this interaction. LargeBiT or SmallBiT was fused to the N- or C-terminus of AgrB1 and this was integrated into the chromosome of *S. aureus* SH1000 under the control of the *agr*P2 promoter. Use of the *agr*P2 promoter will allow native levels of transcription of the translational fusion proteins therefore should not overwhelm the cell. LargeBiT or SmallBiT was also fused to the N- or C-terminus of AgrD1 and this was inserted into the same strain of *S. aureus* SH1000 on plasmid pSK5360 under the control of the *agr*P2 promoter. An example of this is shown in **Figure 4-14**. Each strain has a native *agr* system as well as an additional copy of AgrB1on the membrane and AgrD1 on a plasmid.



Figure 4-14. Schematic of an example NanoBiT strain used to investigate AgrB1 AgrD1 interaction. This example has LargeBiT and SmallBiT at the C-terminus of AgrB1 and AgrD1 respectively.

Constructs have LargeBiT and SmallBiT fused proteins under the control of the *agr*P2 promoter. The *agr*P2 promoter has a low level of basal expression

which increases exponentially on *agr* activation (51). This means that the translational fusion proteins will be expressed at low levels, increasing on *agr* activation which occurs in late exponential phase of growth *in vitro* (49). Therefore, overnight cultures of test and control strains were washed in TSB and regrown to OD_{600} ~1.0 when the *agr* system is active to ensure high expression of NanoBiT fusions. When the cultures reach the correct OD_{600}, NanoGlo reagent was added, and bioluminescence read in a Tecan Infinite F200 microplate reader.

As shown in **Figure 4-15**, there was high bioluminescence (~8418 RLU) from the strain with AgrB C-terminal SmallBiT and AgrD C-terminal LargeBiT (AgrBCS pAgrDCL). This shows that the C-terminus of AgrB1 interacted with the C-terminus of AgrD1. There was also low signal (~955 RLU) detected from the C-terminus of AgrD interacting with the N-terminus of AgrB. This small signal may have been due to the close proximity of the N- and C-termini of AgrB however the signal was significantly lower than for the interaction between the C-termini. There was no signal above background levels from the N-terminus of AgrD interacting either terminus of AgrB. This demonstrates that the interaction between AgrB1 and AgrD1 was via the C-terminus of AgrB and the C-terminus of AgrD. There was very low signal from all split luciferase control strains which validates that the signal detected was from the interaction of AgrBD not from the interaction of split luciferase independently.

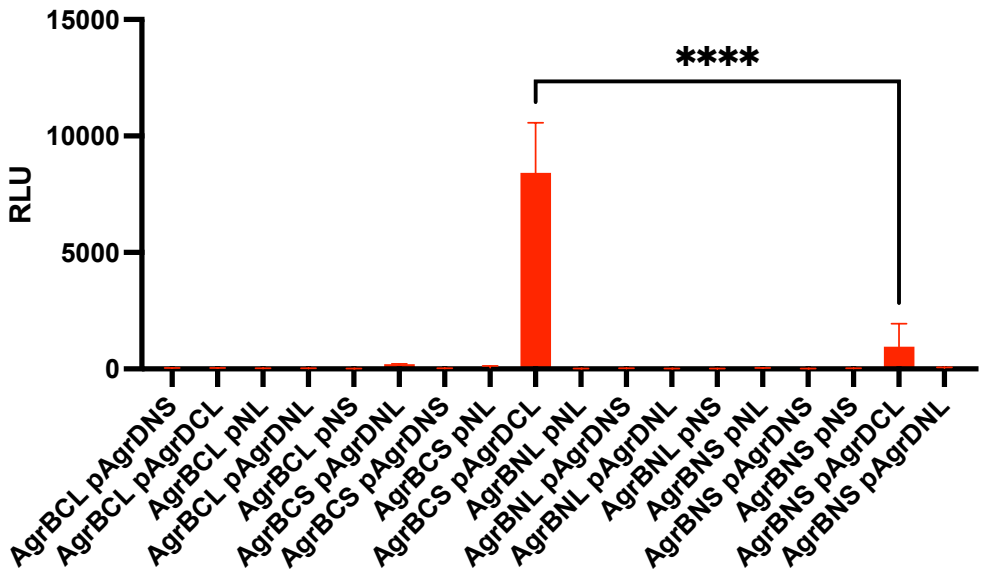


Figure 4-15. Bioluminescence from NanoBiT strains with AgrB1 on the chromosome and AgrD1 on plasmid pSK5630. x-axis labels: p, plasmid, N, N-terminal, C, C-terminal, S, SmBiT, L, LgBiT. For some experiments plasmid controls expressing the LgBiT (pNL) or SmBiT (pNS) only were included. All strains are listed in Methods section 2.10.1, **Table 2-4**. Data are representative of three technical repeats recorded for each sample with error bars displaying standard deviation. The experiment was performed in biological triplicate. ****p<0.0001

To ensure that the signal was *agr*P2 driven, AIP-95 was added to over-day culture of the strain which showed interaction between the C-terminus of AgrB and the C-terminus of AgrD. AIP-95 is a competitive AgrC inhibitor so will prevent *agr* activation and upregulation of transcription from *agr*P2.

As shown in **Figure 4-16**, bioluminescence was significantly lower when incubated with 100 nM AIP-95. This shows that the signal was driven by *agr* QS dependent upregulation of *agr*P2. The signal detected in the presence of AIP-95 was due to expression of the translational fusions from basal *agr*P2 expression. This was significantly lower than when *agr*P2

transcription was upregulated by phosphorylated AgrA when the *agr* QS system was active.

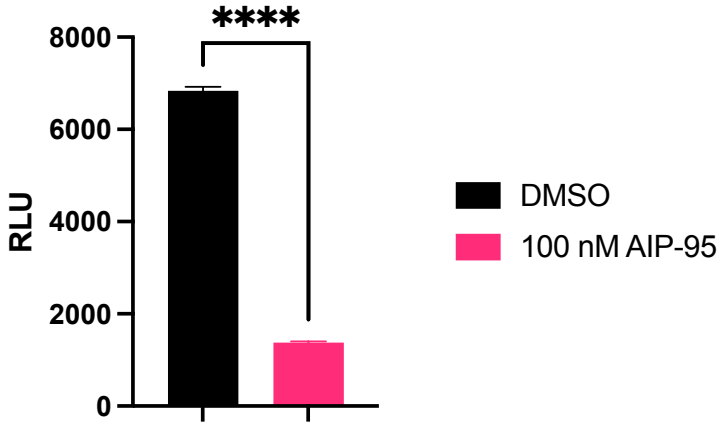


Figure 4-16. Bioluminescence from *S. aureus* SH1000 *agr*P2-AgrB1 C-terminal SmBit pSK5630 *agrD1 C-terminal LgBiT* (AgrBCS pAgrDCL) in the presence of AIP-95. AIP-95 or DMSO was added to over-day culture and grown to OD_{600}. NanoGLo was added and bioluminescence read on a Tecan plate reader. Data are representative of 3 technical repeats with error bars showing standard deviation. **** p<0.0001

4.5.2 AgrBB dimerization

NanoBiT was also used to assay AgrB1 interaction with itself in *S. aureus* and to verify which termini of AgrB1 may interact with each other. In section 4.4 AgrB dimerization was shown experimentally in *E. coli* however it was also interesting to examine this in *S. aureus*.

S. aureus SH1000 strains had LargeBiT or SmallBiT fused to the N- or C -terminus of AgrB1 integrated into the chromosome of *S. aureus* SH1000 under the control of the *agr*P2 promoter as before. They also carried plasmid pSK5630 with LargeBiT or SmallBiT fused to the N- or C-terminus of another copy of AgrB1. These strains have a native *agr* system, an additional copy

of AgrB1 on the chromosome and another copy on a plasmid. All strains were made by Dr. Ewan Murray.

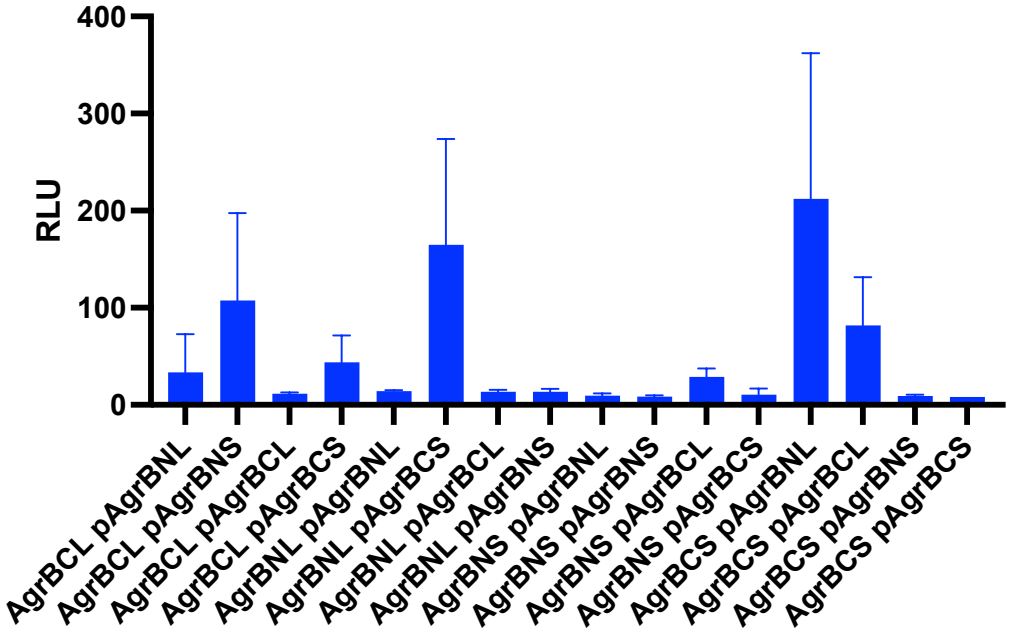


Figure 4-17. Bioluminescence from NanoBiT strains with AgrB1 on the chromosome and AgrB1 on plasmid pSK5630. x-axis labels: p, plasmid, N, N-terminal, C, C-terminal, S, SmBiT, L, LgBiT. For some experiments plasmid controls expressing the LgBiT (pNL) or SmBiT (pNS) only were included. All strains are listed in Methods section 2.10.1, **Table 2-4**. Data is representative of three technical repeats recorded for each sample with error bars displaying standard deviation. The experiment was performed in biological triplicate. ****p<0.0001

As shown in **Figure 4-17**, the highest signal was detected for strains showing interaction between the N-terminus of one copy of AgrB and the C-terminus of another copy. This indicates that AgrB1 forms a dimer interface with N- and C-termini of two monomers. This confirms what was shown in section 4.4.8 where NanoBRET was visualised between the N- and C-termini of AgrB1 in *E. coli*. This provides evidence for formation of at least an AgrB1 dimer in *S. aureus* cells. Low background signal from control

strains was due to the split luciferase associating and producing bioluminescence without fusion protein interaction.

4.6 Discussion

In this chapter the development of two novel bioluminescence-based assays for monitoring Agr protein interactions in live cells has been outlined. A NanoBRET assay was developed for demonstrating AgrB1B1 oligomerization in *E. coli* cells and a NanoBiT assay was developed to demonstrate AgrB1D1 and AgrB1B1 interactions in *S. aureus* cells. To our knowledge the use of these technologies has not been used before for monitoring of Agr protein-protein interactions. These assays have been developed to work alongside computational modelling of AgrB1B1 and AgrB1D1 interactions to provide experimental evidence of the models derived.

Computational modelling of AgrB1 indicated that AgrB1 dimerizes in a membrane and that two copies of AgrB1 are essential for the correct positioning of AgrD1 for proteolytic cleavage. In this model AgrB1 had six transmembrane domains with both termini on the same side of the membrane. This is similar to the structure outlined by Zhang et al. (56) in 2002 which also predicted AgrB1 to have six transmembrane domains with both the N- and C-terminus in the cytosol (56). This was contradicted by Thoendel and Horswill in 2013 (72), however, who used SCAM to predict that AgrB1 has four transmembrane spanning regions and one re-entrant loop with the N- and C-termini of AgrB outside the cell. They also reported that other topology prediction algorithms indicate AgrB1 has five transmembrane helices with the N-terminus outside the cell and the C-terminus inside (72). AgrB1 dimerization has also not been predicted by protein modelling before.

There are discrepancies between this most recent computational modelling and previous predicted topologies of AgrB1. To confirm the model, work in live cells was performed. Using NanoBRET it was demonstrated that AgrB1 forms at least a dimer in *E. coli* membranes. Close interaction between the N-terminus of one copy of AgrB and the C-terminus of another copy, allowed energy transfer and detection of fluorescence. NanoBiT was also used to demonstrate that AgrB1 forms at least a dimer in *S. aureus*. AgrB1 was shown to interact with itself producing bioluminescence from the split luciferase, with a putative dimer interface between the N- and C-termini of two monomers. This implies AgrB1 molecules are in the membrane as mirror images of each other. It also highlights that both the N- and C- termini of AgrB1 are inside the cell where they interact as reported previously (56). The computational model, when played as a movie, suggests that the N- and C-termini are very flexible. Taken together with the luciferase data, we demonstrate that the N- and C-termini of AgrB1 are in closest proximity in a dimer or oligomer of AgrB1. A weak interaction is also detected between the C-termini of AgrB1. This accounts for the flexibility of the terminal loops and demonstrates that this protein is dynamic in a membrane.

Formation of an AgrB1 dimer or oligomer *in vitro* has been reported by Thoendel et al. and Wang et al. (68, 72). Here, protein modelling data and bioluminescence-based assays were used to provide further evidence of AgrB1 dimerization. Protein modelling data predicted that the AgrB1 dimer enables the correct positioning of AgrD1 for processing indicating this is essential in the maturation of AIP-1. Further work must be done to characterise this dimer and assess its importance in AgrD processing.

Using the NanoBiT system strong interaction between the AgrD1 C-terminus and the AgrB1 C-terminus was also shown. One function of AgrB1 is the cleavage of the C-terminal 14 amino acids of AgrD1 and AgrD1 is thought to associate with AgrB1 via its C-terminus (68). This provides evidence of

this interaction in *S. aureus*. The AgrB C-terminus is more variable than its N-terminus, which is conserved among all staphylococcal species, this may enable group specific recognition of AgrD (71, 179). This highlights the importance of the C-terminus of AgrB in AIP processing.

The AgrD C-terminus is negatively charged, and the AgrB C-terminus contains positively charged residues such as the triple lysines at positions 129-131. The interaction between these residues could be what is detected using NanoBiT however we cannot tell if this interaction occurs before or after AgrD C-terminal cleavage. The interaction could be the C-terminus of AgrD associating with the C-terminus of AgrB after it has been cleaved, outlining a pathway for removal of this from the active site. It must also be noted that the interaction between AgrB and AgrD is via SmallBiT on AgrB and LargeBiT on AgrD. LargeBiT is 18 kDa and AgrD is ~7 kDa therefore, the addition of this to AgrD may have an effect on the peptide. More work will be done in the following chapter to characterise this interaction.

In conclusion, evidence for the interaction of AgrB1 and AgrD1 in cells via their C-termini has been provided. Two methods have been used to validate protein modelling data showing that AgrB1 forms at least a dimer at the cell membrane in both *S. aureus* and in *E. coli*. Both of these techniques could be developed further to establish screens for inhibitors of the *agr* QS system at the protein-protein interaction level. This could give insights into whether AgrB1 oligomerization is essential for processing of AgrD1 to form mature AIP-1.

5. Identification and analysis of an AgrBD intermediate required for AIP biosynthesis *in vitro*

5.1 Introduction

In the previous chapter we developed novel bioluminescent techniques to demonstrate AgrBB and AgrBD interactions in bacterial cells. In this chapter, the interaction between AgrBD will be investigated in more detail *in vitro* using proteins induced in an *E. coli* expression system. Thoendel et al. (67) demonstrated that expression of AgrB1 and AgrD1 in *E. coli* is sufficient for AIP-1 production as AgrB1 and AgrD1 are the only proteins shown to be uniquely required for AIP biosynthesis. The actions of any other components involved can be complemented by proteins in *E. coli* (67). *E. coli* is a useful expression host due to the ease of molecular manipulations therefore this organism was chosen for analysis of AgrBD interactions.

Research has been conducted over many years to try and elucidate the interaction between AgrB and AgrD and their roles in the production of mature AIP however, as outlined in the introduction in section 1.3.3, the exact mechanism of AIP processing is still unclear. The proposed mechanism of processing, nevertheless, is as follows. AgrB is an integral membrane endopeptidase which is essential for the C-terminal cleavage of AgrD and thiolactone ring formation. Residues have been identified in both AgrB and AgrD which are essential for this reaction (67, 71). After thiolactone ring formation the N-terminus of AgrD is cleaved, releasing mature AIP. Both N-terminal AgrD and mature AIP are exported from the cell either before or after N-terminal cleavage which is thought to involve proteases MroQ and potentially SpsB (46).

As the *agr* system is an interesting antivirulence target, elucidation of the interaction between AgrB and AgrD and potential other proteases will give insights into design of inhibitors. AgrB is relatively conserved compared to other *agr* proteins such as AgrC which is hypermutable. This makes it a good potential target for antivirulence inhibitors as resistance may be less quick to emerge than for bactericidal antibiotics (47, 88). Understanding the interactions between these proteins can aid in the design of alternative therapies to use against *S. aureus* infections.

5.2 Aims

The aim of this chapter was to outline the investigation of AgrBD interactions and AIP biosynthesis. This was performed using a cell free model primarily through the analysis of an AgrBD processing intermediate that can be detected by Western blot of the *E. coli* cell envelope. This intermediate is an essential step in the processing of AgrD. The formation of this intermediate was probed for *agr* subgroup cross reactivity, with inactivating mutations in active residues of AgrB and AgrD and in the presence of protease inhibitors.

5.3 Construction of an *agrB1D1* expression vector

As mentioned in the Introduction in section 1.3.2, there are four *agr* subgroups in *S. aureus.* The different subgroups have variations in AgrB, AgrD and AgrC with AIP molecules of the same group activating the system and non-self AIP molecules inhibiting the system (11). In this study, AgrB and AgrD from *S. aureus* USA300 were investigated. *S. aureus* USA300 is an *agr* group I strain which is commonly used in research and has a hyperactive *agr* system (25).

AgrB1 AgrD1 protein interactions were investigated using an *E. coli* expression construct. Previously it has been shown that expression of *agrB1* and *agrD1* are sufficient for AIP-1 production in *E. coli,* therefore this is an appropriate model for investigating AgrBD interactions (67). Expression

constructs were created in pCDFDuet-1 using HiFi cloning. pCDFDuet-1 is optimised for co-expression of two genes as it has two multiple cloning sites (MCS) both preceded by a T7 promoter, lac operator and ribosome binding site. Transcription is induced on addition of IPTG. *agrB1* and *agrD1* were amplified from *S. aureus* USA300 JE2 genomic DNA and were assembled into pCDFDuet-1 in *E. coli* DC10B. AgrB1 and AgrD1 sequences are shown in the Methods in section 2.2.3. *agrB1* was cloned into MCS1 and *agrD1* into MCS2 (Figure 5-1). Another construct was made by Dr. Ewan Murray with *agrB1D1* both in MCS1. Proteins were expressed in *E. coli* C41 (DE3) as this strain is optimised for the expression of membrane proteins.

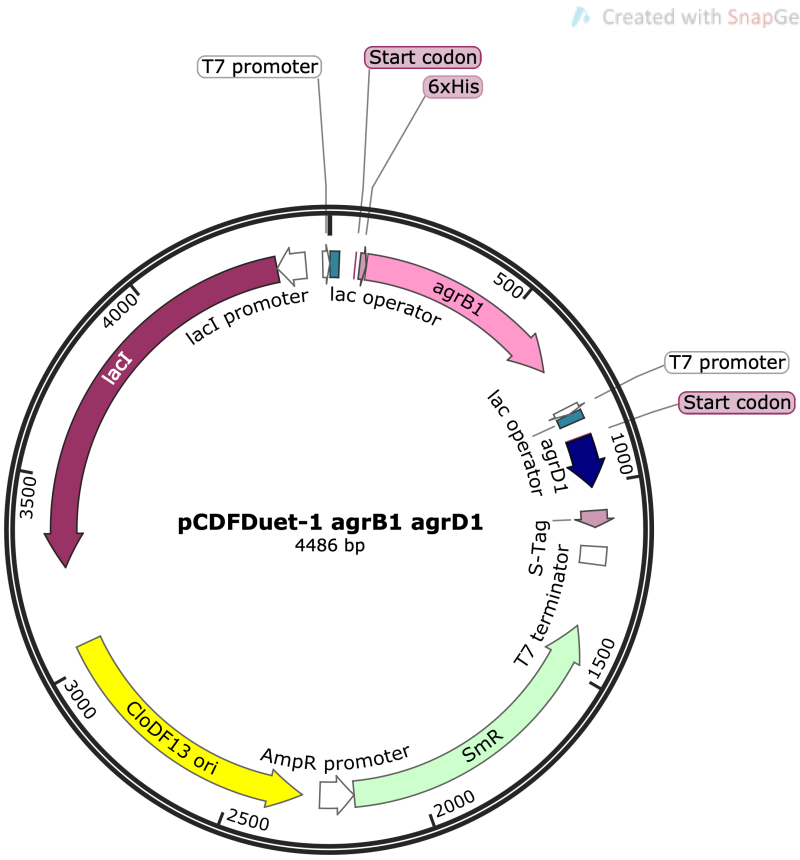


Figure 5-1. Vector map of expression vector pCDFDuet-1 *agrB1 agrD1*. *agrB1* is in MCS1 with a 6x HIS tag at the N-terminus. *agrD1* is in MCS2 with an S-tag at the C-terminus.

5.4 Expression of *agrB1D1* from *E. coli* C41 (DE3) and detection of AIP-1

To determine whether *agrB1* and *agrD1* were expressed and functional in this system the chromosomal *agr*P3-*lux* reporter *S. aureus* ROJ143 was used to detect AIP-1 expression as described previously (153).

As shown in Figure 5-2, bioluminescence representing AIP-1 production was detected when both AgrB1 and AgrD1 were present. No bioluminescence and therefore no AIP-1 production was detected when either of the proteins were expressed on their own or when protein expression was not induced. This shows that expression of both of these proteins was essential and sufficient for mature AIP-1 production in *E. coli*, confirming that this was an appropriate model for investigating AgrD1 interaction with AgrB1 and its maturation.

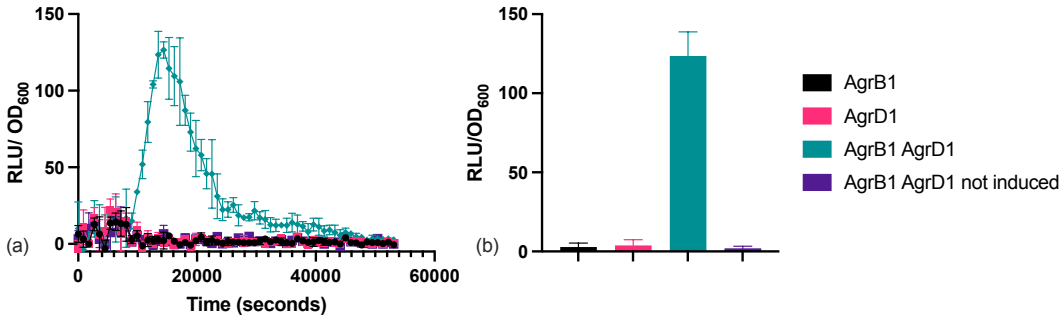


Figure 5-2. Bioluminescence from *S. aureus* ROJ143 representing AIP-1 production after induction of proteins in *E. coli* C41 (DE3). Cell free supernatants from *E. coli* following protein induction were added to *S. aureus* ROJ143 culture in a black, flat, clear bottomed 96 well plate and incubated at 37°C in a Tecan plate reader. The graphs represent bioluminescence output (as relative light units; RLU) divided by population density (OD_{600}). (a) Represents RLU/OD_{600} every 15 min over the 16 h incubation. (b) Represents a bar chart plot of RLU/OD_{600} at the peak output, after growth for 3.75 h. Data represent 3 technical repeats with error bars displaying standard deviation.

Figure 5-2 (a) outlines the RLU/OD_{600} recorded every 15 min for 16 h at 37°C, this peaked after 3.5 h growth in this assay which is displayed in **Figure 5-2** (b). Future *S. aureus* ROJ143 data in this thesis will be displayed in a bar chart representing the peak bioluminescence output which was usually after incubation for between 3-4 h.

5.5 Detection of AgrD1 by Western blot

Expression and localisation of AgrD1 was detected by Western blot against the S-tag at the C-terminus of AgrD1. After induction of protein expression in *E. coli* C41 (DE3), cell envelope and cytosolic fractions were separated by ultracentrifugation and samples were run on a 16% Tricine gel (ThermoFisher) before detection by Western blot. As shown in Figure 5-3, AgrD1 predominantly localised to the cell envelope fraction rather than the cytosol. A band was detected at ~7.5 kDa, representing AgrD1 (~5 kDa) and the S-tag (3 kDa). AgrD is directed to the cell membrane via its N-terminal region in *S. aureus* and this shows that, as in *S. aureus,* AgrD1 is primarily directed to the cell membrane in *E. coli* (67). The S-tag was at the C-terminus therefore this shows the C-terminus had not been cleaved from the AgrD peptide detected. No band was present in the non-induced control showing expression is tightly regulated and that the Western blot was specific and was detecting induced AgrD.

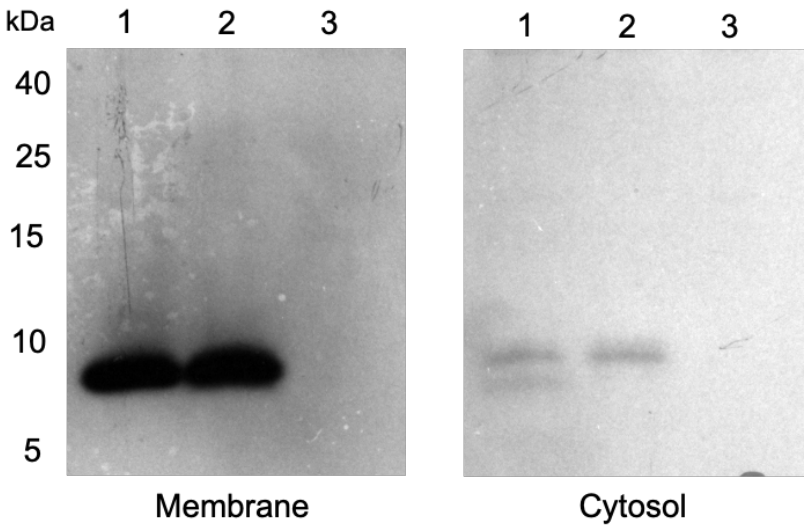


Figure 5-3. Detection of AgrD1 from *E. coli* C41 (DE3) in membrane and cytosolic fractions. Samples are from *E. coli* C41 (DE3) carrying pCDFDuet-1 encoding genes as follows; Lane 1: *agrB1 agrD1,* Lane 2: *agrD1* Lane 3: *agrB1 agrD1* not induced. Samples were added to 2 x Novex Tris-Glycine SDS sample buffer (ThermoFisher), heated to 55°C for 5 min and run on a 16% Tricine gel before transfer to PVDF 0.2 μM transfer membrane and detection with S-tag antibody.

5.6 Detection of AgrB1 by Western blot

Expression and localisation of AgrB1 was confirmed by Western blot using AgrB specific llama nanobody, following the protocol outlined in the Methods in section 2.17. Membrane fractions were separated from cytosolic by ultracentrifugation and samples were run on a 15 % acrylamide gel. As displayed in Figure 5-4, a band was detected at ~23 kDa in the membrane fraction representing AgrB1. AgrB1 localised to the membrane in this *E. coli* expression model where it interacts with AgrD1 as occurs in *S. aureus* (67). No bands were detected in the non-induced control demonstrating that the Western blot was specific for detection of AgrB. Higher order structures of AgrB can be observed in the cell membrane, with AgrB detected as a dimer and trimer in Figure 5-4 Lane 1.

Interestingly, when co-expressed with *agrD1* a shift in the size of the band representing AgrB1 was observed as shown in Figure 5-4 Lane 2. The shift in size of AgrB was observed in both the monomer (~23 kDa) and the dimer (~44 kDa), this is highlighted with red arrows in Figure 5-4. This represents a potential AgrB1D1 intermediate forming in the cell membrane. No band was detected at ~26 kDa on the Western blot against the S-tag at the C-terminus of AgrD1 (Figure 5-3), indicating that the C-terminus of AgrD1 was not present in this AgrBD complex. The C-terminus of AgrD is cleaved by AgrB and these data demonstrate that the AgrBD complex forms after cleavage of the C-terminus.

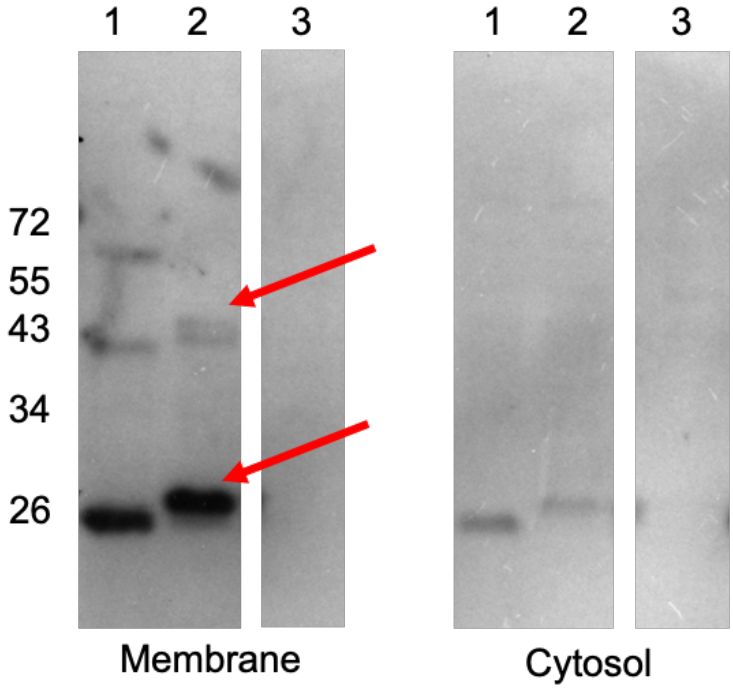


Figure 5-4. Detection of AgrB1 from *E. coli* C41 (DE3) in membrane and cytosolic fractions. Samples were added to 4 x loading buffer with SDS and BME (methods section 1.14) and heated to 55°C for 5 min before running on a 15% acrylamide gel and transfer to PVDF membrane. AgrB1 was detected with llama nanobody 2ABE15. Samples are from *E. coli* C41 (DE3) carrying pCDFDuet-1 encoding genes as follows; Lane 1: *agrB1*, Lane 2: *agrB1D1*, Lane 3: *agrB1D1* not induced. All lanes are from the same blot. Red arrows indicate AgrBD complex in the monomer and dimer.

5.7 Confirmation of AgrB1D1 complex formation with synthetic linear T7-AgrD1

To confirm that the shift in size of AgrB1 observed in Figure 5-4 was caused by the presence of AgrD1, synthetic T7-AgrD1 was used. This is linear AgrD1 with a T7-tag at the N-terminus which can be detected by Western blot, the sequence of this is displayed in the Methods in section 2.15 (Figure 5-5).

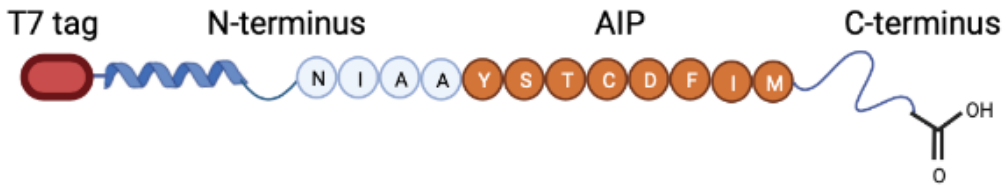


Figure 5-5. Schematic of synthetic linear T7-AgrD1. The T7 tag is at the N-terminus of the linear AgrD peptide.

A construct was made by HiFi cloning with AgrB1 in MCS1 of pCDFDuet-1. AgrB1 was expressed alone in *E. coli* C41 (DE3), membranes separated from cytosol by ultracentrifugation and incubated with T7-AgrD1. After incubation of *E. coli* membrane fraction containing AgrB1 with T7-AgrD1, samples were run on a 15% acrylamide gel. AgrB1 was detected by Western blot with 2ABE10 nanobody and the T7-tag on AgrD1 was detected by Western blot with an antibody to T7 conjugated to HRP.

On the AgrB Western blot (Figure 5-6 (a)) two bands could clearly be observed indicating the shift in size of AgrB1 when incubated with T7-AgrD1 (Lane 2). The T7-tag is 11 amino acids long so slightly increases the size of AgrD1 meaning the shift in size of AgrB1 was larger than the co-expressed form in Figure 5-4. The doublet was not detected in the absence of T7-AgrD1 (Figure 5-6 (a) Lane 1) demonstrating that it was AgrD1 causing the shift in size. On the T7 Western blot, which detects AgrD (Figure 5-6 (b)) a band can be observed in Lane 2 at the size of AgrB1D1 (indicated with a red

arrow) however no band was detected at this size when T7-AgrD1 was run alone (Lane 3). This demonstrates that the N-terminus of AgrD1 was present in the AgrB1D1 complex. T7-AgrD1 is 6.7 kDa, this can be observed at the bottom of the gel in the T7 Western ((Figure 5-6 (b), lane 2), marked with a blue arrow. T7-AgrD1 aggregates can also be observed in Figure 5-6 (b), lanes 2 and 3, marked with a green arrow.

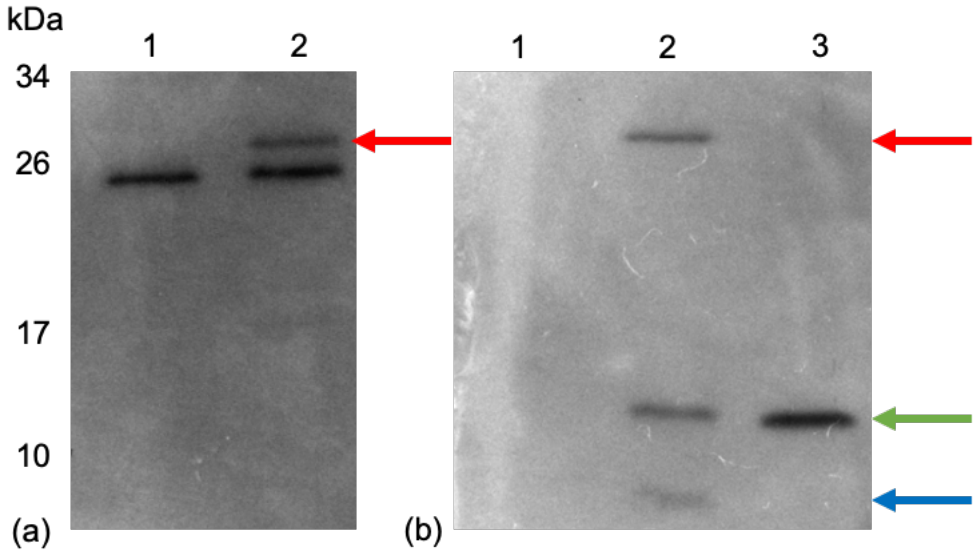


Figure 5-6. Western blots of membrane assay with AgrB1 and synthetic linear T7-AgrD1. *E. coli* C41 (DE3) pCDFDuet-1 *agrB1* was induced and membranes isolated and incubated with synthetic linear T7-AgrD1. Samples were added to 4 x loading buffer with SDS and BME, as described in the Methods in section 2.16, and heated to 55°C for 5 min before running on a 15% acrylamide gel. The gel was transferred to PVDF and probed with (a) llama nanobody 2ABE10 (b) antibody to T7 conjugated to HRP. Lane 1: AgrB1 membrane, Lane 2: AgrB1 membrane + T7-AgrD1, Lane 3: T7-AgrD1. The red arrows indicate AgrB1D1 intermediate, the blue arrow indicates T7-AgrD1 and the green arrow indicates T7-AgrD1 aggregates.

5.8 AIP-1 production from AgrB1 membrane fractions incubated with T7-AgrD1.

As shown in sections 5.6 and 5.7, AgrB1 and AgrD1 form a complex in extracted *E. coli* membranes. To determine whether AgrD1 maturation can be analysed using this model, AIP-1 production was determined using *S. aureus* ROJ143. As shown in Figure 5-7, AIP production was detected from the reaction of membrane bound AgrB1 with T7-AgrD1. This shows that the T7-tag did not interfere with AgrD1 maturation and that the presence of AgrB1 enabled the processing of AgrD1 in *E. coli* membranes. This showed that this cell-free model could be used to investigate AgrB1D1 interactions and the processing of AgrD1 to form mature AIP-1.

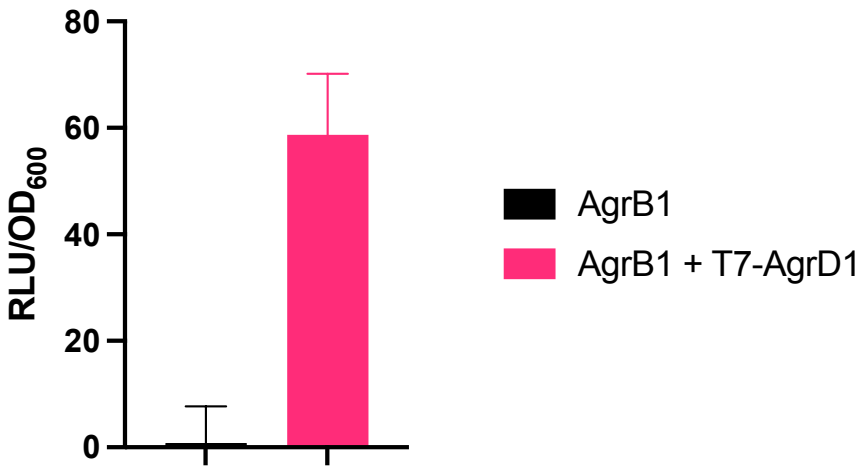


Figure 5-7. Bioluminescence output from *S. aureus* ROJ143 confirming AIP-1 production after incubation of *E. coli* C41 (DE3) pCDFDuet-1 *agrB1* membrane fractions with T7-AgrD1. *S. aureus* ROJ143 was grown overnight at 37°C, 200 rpm and was diluted 1/200. 10 μL AgrB1 membrane fraction after incubation with T7-AgrD1 was added to 190 μL diluted culture in triplicate in a 96 well, black, clear bottomed Tecan plate. The plate was placed in a Tecan plate reader and incubated at 37°C. OD_{600} and RLU were read every 15 min for 16 h. Data represent RLU divided by OD_{600} after incubation for 3 h. The data represents three technical repeats with error bars displaying standard deviation.

5.9 AgrBD complex formation with N-terminal AgrD1

We have demonstrated that the AgrB1D1 intermediate consisted of AgrB1 in complex with the N-terminus of AgrD1 but not the C-terminus. To probe the interaction between AgrB and AgrD further, a synthetic peptide was obtained consisting of linear AgrD1 without the C-terminus and with an alfa tag at the N-terminus, the sequence of this is shown in the Methods in section 2.15 (**Figure 5-8**). The alfa tag is a 15 amino acid epitope tag which forms a small alpha helix that can be used for microscopy, immunoprecipitation and Western blotting. The alfa tag is small, monovalent, hydrophilic and has no net charge resulting in minimal effects on the protein it is linked to (180). This peptide was used to identify if AgrB1 could recognise AgrD1 lacking the C-terminus. The N-terminal AgrD1 peptide was incubated with membrane fractions of *E. coli* C41 (DE3) *agrB1* and the samples probed for AgrBD complex formation by Western blot against AgrB. The samples were also tested for AIP-1 production using *S. aureus* ROJ143.

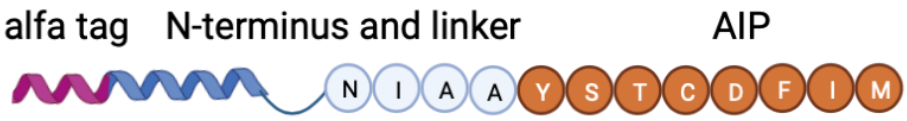


Figure 5-8. Schematic of synthetic alfa AgrD1 lacking the C-terminus

As shown in Figure 5-9 (a), there was no AgrB1D1 complex formation when *E. coli* pCDFDuet-1 *agrB1* membranes were incubated with N-terminal AgrD1. This shows that there was no recognition of AgrD1 and the C-terminus is necessary for this interaction. Additionally, as shown in **Figure 5-9** (b), no AIP-1 was produced on incubation of AgrB1 with N-terminal AgrD1. This further highlights that this version of the peptide was not recognised by AgrB1 and the C-terminus is necessary for this interaction.

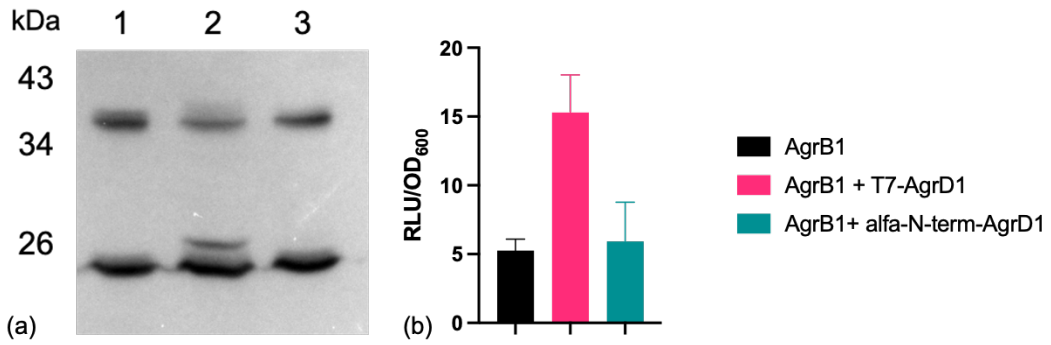


Figure 5-9. AgrB1D1 complex formation and AIP-1 production with N-terminally tagged AgrD1 peptide. (a) Western blot against AgrB1. Samples are membrane fractions of induced *E. coli* C41(DE3) pCDFDuet-1 *agrB1* incubated with T7-AgrD1 or N-terminal alfa-AgrD1 as follows; Lane 1: no AgrD peptide Lane 2: T7-AgrD1, Lane 3: N-terminal alfa-AgrD1. Samples were added to 2 x Novex Tris-Glycine SDS sample buffer and heated to 55°C for 5 min before running on a 14 % Tris-Glycine gel. The gel was transferred to PVDF and probed with AgrB nanobody 2ABE10. (b) Bioluminescence from *S. aureus* ROJ143 indicating AIP-1 production after incubation of membrane fractions of *E. coli* C41 (DE3) pCDFDuet-1 *agrB* with T7-AgrD1 or alfa-Nterm-AgrD1. Samples were added to *S. aureus* ROJ143 as described previously and OD_{600} and RLU read in a Tecan plate reader after 3.75 h incubation at 37°C. Data represent three technical repeats with error bars showing standard deviation.

5.10 Dynamics of AgrB1D1 complex formation

Recognition of AgrD by AgrB as detected here is the first step in AIP maturation. To determine the dynamics of this interaction the formation of the AgrB1D1 complex was monitored over time. *E. coli* membrane containing AgrB1 was incubated with T7-AgrD1 at 37°C and samples taken at different time points. AgrB1D1 complex formation was detected after just half an hour of incubation (**Figure 5-10**, a). Additionally, the intensity of the

upper band, and so the proportion of protein in the AgrB1D1 complex, did not change as the incubation time was increased.

Interestingly, AIP-1 production was detected after 30 min and the level of AIP-1 detected using bioreporter *S. aureus* ROJ143 decreased as the incubation time increased (**Figure 5-10**, b). This indicates the complex formed and AgrD1 was turned over to form mature AIP-1 within 30 min. The turnover of AgrD1 did not increase with increased incubation time.

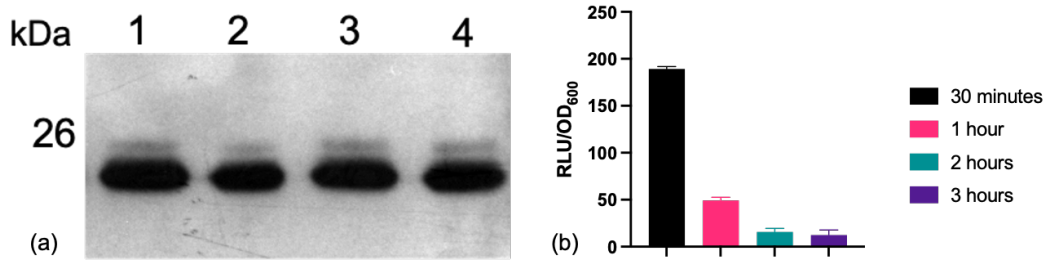


Figure 5-10. AgrB1D1 complex formation and AIP-1 production over time. (a) Western blot against AgrB. Samples were membrane fractions of induced *E. coli* C41(DE3) pCDFDuet-1 *agrB1* incubated with T7-AgrD1 at 37°C for increasing amounts of time as follows; Lane 1: 30 min, Lane 2: 1 h, Lane 3: 2 h, Lane 4: 3 h. Samples were added to 2 x Novex Tris-Glycine SDS sample buffer and heated to 55°C for 5 min before running on a 14 % Tris-Glycine gel. The gel was transferred to PVDF and probed with AgrB1 nanobody 2ABE10. (b) AIP-1 production from *E. coli* C41 (DE3) membrane with AgrB1 incubated with T7-AgrD1 for different lengths of time. Samples were added to *S. aureus* ROJ143 as described previously and OD_{600} and bioluminescence read in a Tecan plate reader after 3.25 h incubation at 37°C. Data represent three technical repeats with error bars showing standard deviation.

5.11 AgrB1D1 complex formation with increasing concentrations of T7-AgrD1

It was hypothesised that increasing the concentration of T7-AgrD1 in the *in vitro* assay would increase the intensity of the AgrB1D1 band on the Western blot. The concentration of AgrB1 was not quantified but was kept as consistent as possible between assays by keeping the induction and membrane preparation protocol the same. Increasing concentrations of T7-AgrD1 were added to the same *E. coli* AgrB1 membrane preparation and an increase in the intensity of the upper band is observed. This is representative of increasing saturation of AgrB1 as it binds more AgrD1.

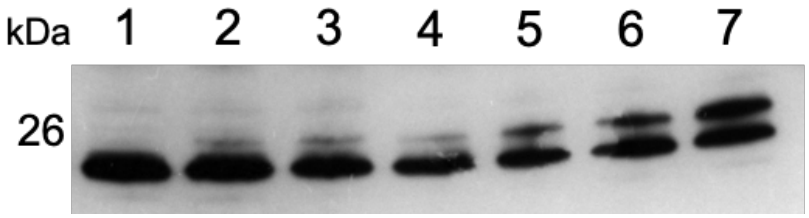


Figure 5-11. AgrB1D1 complex formation with membrane fractions of *E. coli* C41 (DE3) pCDFDuet-1 *agrB1* incubated with T7-AgrD1 at increasing concentrations. T7-AgrD1 concentration was as follows; Lane 1: 1 μM, Lane 2: 2 μM, Lane 3: 3 μM, Lane 4: 4 μM, Lane 5: 6 μM, Lane 6: 8 μM, Lane 7: 10 μM. Samples were incubated at 37°C for 2 h before being added to 2 x Novex Tris-Glycine SDS sample buffer and heated to 55°C for 5 min. Samples were run on a 14 % Tris-Glycine gel and transferred to PVDF for probing with AgrB nanobody 2ABE10.

5.12 Stability of the AgrB1D1 complex

Previously, a potential AgrBD intermediate has been shown to be resistant to attempts to separate the two components using thioester sensitive reagents such as hydroxylamine and dithiothreitol (67). We sought to determine whether the complex could be dissociated by increasing the reducing environment or by boiling. After incubation of *E. coli* membranes

containing AgrB1 with T7-AgrD1 for 2 h, samples were added to gel loading buffer with increasing concentrations of β-mercaptoethanol and run on a 15 % acrylamide gel. Increasing the concentration of β-mercaptoethanol had no effect on the intensity of the upper band indicating the AgrB1D1 intermediate. This shows this complex was resistant to a highly reducing environment.

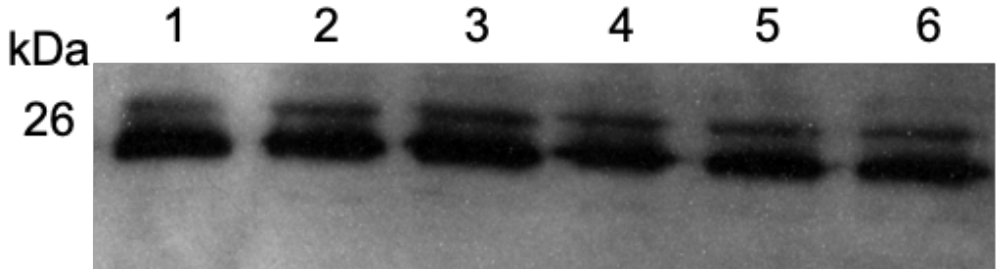


Figure 5-12. AgrB1D1 complex stability in increasing reducing environment. Samples were membrane fractions of induced *E. coli* C41(DE3) pCDFDuet-1 *agrB1* incubated with 2 μM T7-AgrD1 at 37°C. The same samples were added to loading buffer with containing SDS as outlined in methods section 2.16 with increasing concentrations of β-mercaptoethanol as follows. Lane 1: 0%, Lane 2: 1.25%, Lane 3: 2.5%, Lane 4: 5%, Lane 5: 7.5%, Lane 6: 8.75%. Samples were heated to 55°C for 5 min in sample buffer and run on a 15% acrylamide gel before transfer to PVDF and detection with AgrB nanobody 2ABE10.

Usually, samples of AgrB1 are added to SDS-PAGE sample buffer and heated to 55°C for 5 min before running on the SDS gel as boiling the sample can cause AgrB1 to aggregate at the top of the gel. To determine whether the AgrB1D1 complex was resistant to boiling, after incubation of *E. coli* membrane containing AgrB1 with T7-AgrD1 for 2 h, samples were added to 2 x Tris-Glycine sample loading buffer and heated to 100°C for 5 min before running the gel. As displayed in **Figure 5-13**, boiling the sample did not completely dissociate the complex. This shows the AgrB1D1 complex was stable after boiling.

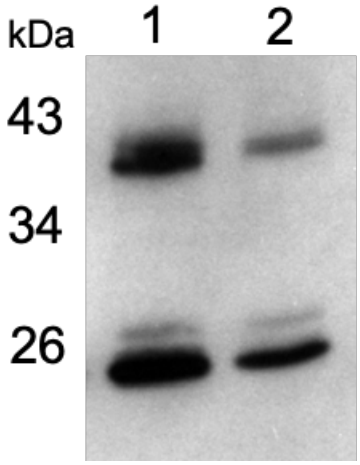


Figure 5-13. AgrB1D1 complex stability after boiling. Samples are membrane fractions of induced *E. coli* C41(DE3) pCDFDuet-1 *agrB1* incubated with T7-AgrD1 at 37°C. The same sample was added to sample buffer and either heated to 55°C or 100°C for 5 min before running on a 14% Tris-Glycine gel and transfer to PVDF for detection with AgrB nanobody 2ABE10. Lane 1: 55°C, Lane 2: 100°C.

5.13 AgrBD complex formation with different *agr* subgroups

We have demonstrated AgrBD complex formation in *agr* group I however, as mentioned previously, 4 *agr* subgroups exist in *S. aureus* which are characterised by the amino acid sequence of the pheromone AIP peptide. The sequences of the AgrD molecules of different subgroups are shown below (11). The catalytic cysteine residue is shown in red and other residues which are conserved across *Staphylococci* are shown in green. AIP molecules are highly specific for their cognate AgrC receptor, AIPs of the same subgroup activate the *agr* system whereas non-self AIPs inhibit the *agr* system (109, 181). It is known that the AgrC-AIP interaction is highly group specific. It has also been demonstrated that AgrB1 and AgrB3 can process AgrD1 and AgrD3 but not AgrD2 and AgrB2 can only process AgrD2. This was demonstrated through reporter assays detecting AIP production (60). Here we wanted to determine if the subgroup specificity between AgrB and AgrD could be detected using this model. This could give

insights into the residues in AgrD which are essential for the recognition by AgrB.

	N-terminus	AIP	C-terminus
S. aureus			
AgrD1	**MNTLFNLFFDFITGILKNIGNIAA**	**YSTCDFIM**	**DEVEVPKELTQLHE**
AgrD2	**MNTLVNMFFDFIIKLAKAIGIVG**	**GVNACSSLF**	**DEPKVPAELTNLYDK**
AgrD3	**MKKLLNKVIELLVDFFNSIGYRAAY**	**INCDFLL**	**DEAEVPKELTQLHE**
AgrD4	**MNTLLNIFFDFITGVLKNIGNVAS**	**YSTCYFIM**	**DEVEIPKELTQLHE**

Expression constructs pCDFDuet-1 *agrB2D2* and pCDFDuet-1 *agrB3* were made using HiFi cloning by Dr. Ewan Murray. *agrB2* and *agrD2* were amplified from *S. aureus* NRS149 and *agrB3* from *S. aureus* MRSA252. pCDFDuet-1 *agrB2* was constructed via inverse PCR to remove *agrD2*.

To test whether the AgrB nanobody 2ABE10 was able to detect all subgroups of AgrB, these constructs were induced in *E. coli* C41 (DE3), membranes separated from cytosolic fraction and samples run on a 14 % Tris-Glycine gel before transfer to PVDF and Western blot with nanobody 2ABE10. As displayed in **Figure 5-14**, 2ABE10 was able to detect AgrB from *E. coli* membranes from the three *agr* subgroups tested. Additionally, an AgrB2D2 complex was detected (**Figure 5-14**, Lane 4). This indicates that the AgrBD complex formation is not specific to *agr* group I. It is also to be noted that no dimer is observed for AgrB2 or AgrB3, as no band was detected at ~42 kDa as there was for AgrB1. It has been shown that AgrB2 forms a dimer in lipid membranes (68). The absence of AgrB2 and AgrB3 dimers does not mean that they do not form in *E. coli* membranes, they just may be more unstable on the SDS-PAGE gel than an AgrB1 dimer therefore the dimer could have been dissassembled.

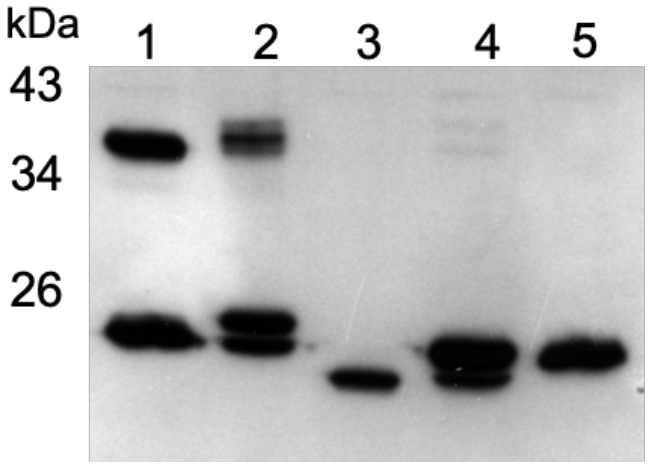


Figure 5-14. Western blot with AgrB nanobody 2ABE10 to detect AgrB1, AgrB2 and AgrB3. Samples are membrane fractions of induced *E. coli* C41 (DE3) pCDFDuet-1 encoding genes as follows; Lane 1: *agrB1*, Lane 2: *agrB1D1,* Lane 3: *agrB2,* Lane 4: *agrB2D2*, Lane 5: *agrB3.* Membrane fractions were added to 2 x Novex Tris-Glycine SDS sample buffer and heated to 55°C for 5 min before running on a 14 % Tris-Glycine gel. The gel was transferred to PVDF and probed with AgrB nanobody 2ABE10.

To check the reactivity of AgrB1 with AgrD2 and AgrD3, pCDFDuet-1 *agrB1* was induced in *E. coli* C41 (DE3), the membrane fraction separated and incubated with synthetic linear T7-AgrD1, T7-AgrD2 and T7-AgrD3. AgrB1 was able to form a complex with T7-AgrD1 and T7-AgrD3 but not T7-AgrD2 (**Figure 5-15**). There appears to be a higher proportion of AgrB1 in complex with AgrD3 than AgrD1. The peptide preparation of T7-AgrD3 was a fresher preparation and had been through fewer freeze thaw cycles than the T7-AgrD1 peptide which could have resulted in apparent increased complex formation.

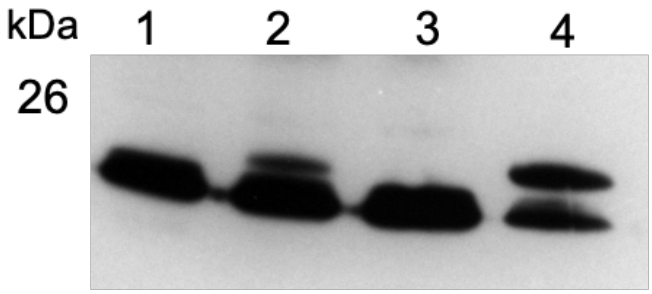


Figure 5-15. Reactivity of AgrB1 with AgrD of different subgroups. Samples were membrane fractions of *E. coli* C41 (DE3) pCDFDuet-1 *agrB1* incubated with T7-AgrD at 37°C for 2 h as follows; Lane 1: control, Lane 2: T7-AgrD1, Lane 3: T7-AgrD2, Lane 4: T7-AgrD3. Samples were added to 2 x Novex Tris-Glycine SDS sample buffer and heated to 55°C for 5 min before running on a 14 % Tris-Glycine gel. The gel was transferred to PVDF and probed with AgrB nanobody 2ABE10.

To determine whether AgrD2 forms weak or transient interactions with AgrB1 which are lost on running of the SDS-PAGE gel, the sample was also run with loading buffer containing no β-mercaptoethanol on a 15% acrylamide gel. β-mercaptoethanol will break apart the thioester bond between AgrB and AgrD therefore in the absence of this, any AgrBD complex that forms should be detected on the gel.

As shown in **Figure 5-16**, no complex was observed with AgrB1 and T7-AgrD2 in the absence of β-mercaptoethanol. This confirms that no interaction was noted between AgrB1 and T7-AgrD2 which implies that this interaction is *agr* subgroup specific.

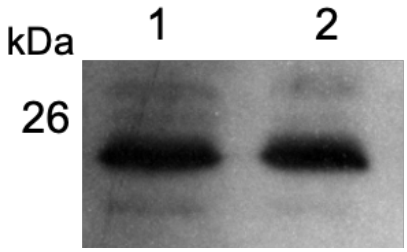


Figure 5-16. AgrB1 and T7-AgrD2 with and without β-mercaptoethanol. Samples were membrane fractions of *E. coli* C41 (DE3) pCDFDuet-1 *agrB1* incubated with T7-AgrD2. Sample buffer was added with and without BME as follows; Lane 1: 5 % BME, Lane 2: 0% BME. Samples were incubated in loading buffer at 55°C for 5 min before running on a 14 % Tris-Glycine gel. The gel was transferred to PVDF and probed with AgrB nanobody 2ABE10.

To investigate the specificity of recognition by AgrB2, pCDFDuet-1 *agrB2* was induced in *E. coli* C41 (DE3), membranes separated from cytosolic fraction and incubated with synthetic T7-AgrD1, T7-AgrD2 and T7-AgrD3. As displayed in **Figure 5-17**, AgrB2 formed a complex with T7-AgrD2 only (Lane 3). No complex formation was observed with T7-AgrD1 or T7-AgrD3.

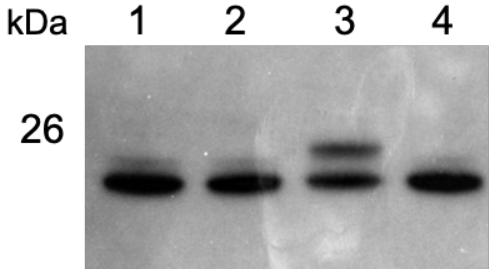


Figure 5-17. Cross reactivity of AgrB2 with AgrD of different subgroups. Samples were membrane fractions of *E. coli* C41 (DE3) pCDFDuet-1 *agrB2* incubated with T7-AgrD at 37°C for 2 h as follows; Lane 1: control, Lane 2: T7-AgrD1, Lane 3: T7-AgrD2, Lane 4: T7-AgrD3. Samples were added to 2 x Novex Tris-Glycine SDS sample buffer and heated to 55°C for 5 min before running on a 14 % Tris-Glycine gel. The gel was transferred to PVDF and probed with AgrB nanobody 2ABE10.

To examine the specificity of AgrD recognition by AgrB3, pCDFDuet-1 *agrB3* was induced in *E. coli* C41 (DE3), membranes separated and incubated with synthetic T7-AgrD1, T7-AgrD2 and T7-AgrD3. As displayed in **Figure 5-18** AgrB3 formed a complex with AgrD1 and AgrD3 but not AgrD2.

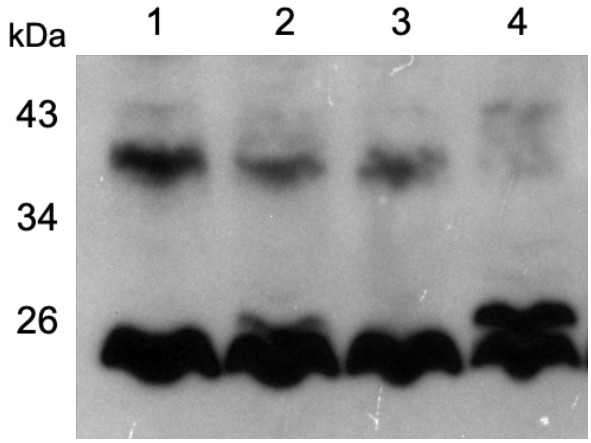


Figure 5-18. Cross reactivity of AgrB3 with AgrD of different subgroups. Samples are membrane fractions of *E. coli* C41 (DE3) pCDFDuet-1 *agrB3* incubated with T7-AgrD at 37°C for 2 h as follows; Lane 1: control, Lane 2: T7-AgrD1, Lane 3: T7-AgrD2, Lane 4: T7-AgrD3. Samples were added to 2 x Novex Tris-Glycine SDS sample buffer and heated to 55°C for 5 min before running on a 14 % Tris-Glycine gel. The gel was transferred to PVDF and probed with AgrB nanobody 2ABE10.

As there was recognition of T7-AgrD1 by AgrB3, AIP-1 production was determined using *agr* group I bioreporter *S. aureus* ROJ143. As shown in **Figure 5-19**, AIP-1 was produced on incubation of T7-AgrD1 with AgrB3 in *E. coli* membranes. This shows that AgrB3 was able to recognise and initiate turnover of AgrD1. As expected, there was no production of mature AIP-1 by AgrB2. This is due to the lack of recognition of the pro-peptide.

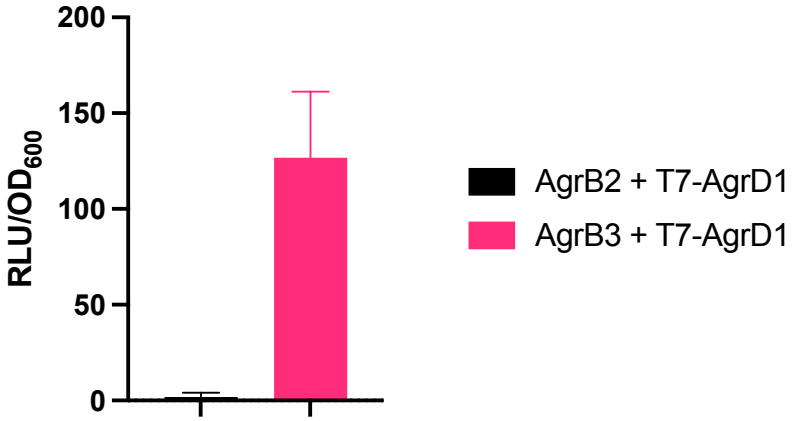


Figure 5-19. AIP-1 production from AgrB2 and AgrB3 with T7-AgrD1. Samples were added to *S. aureus* ROJ143 as described previously and OD_{600} and bioluminescence read in a Tecan plate reader after 3.25 h incubation at 37°C. Data represent three technical repeats with error bars showing standard deviation.

Overall, there was found to be inter group recognition between AgrB and AgrD of *agr* groups I and III but not group II. This is similar to what was reported by Ji et al. in 1997 (60). They detected the production of AIPs with different AgrB AgrD group combinations using a bioreporter however here we have demonstrated the formation of AgrBD complex and AIP-1 production in *E. coli* membranes. This demonstrates that AgrB1 and AgrB3 are unable to process AgrD2 and AgrB2 is unable to process AgrD1 and AgrD3 through the lack of initial recognition.

The C-terminus of AgrD has been demonstrated in this thesis to be essential for the recognition of AgrD by AgrB. The findings in this section give insights into the residues which are essential for this interaction. AgrD C-termini from the three subgroups were aligned using Clustal Omega software, this alignment is shown in **Figure 5-20** (182). As demonstrated in the alignment, the C-termini of AgrD from group I and group III are identical apart from one amino acid (V in group I, A in group II). As there is cross recognition between these groups this indicates that this amino acid position, just after the

conserved DE is not critical in recognition of AgrD by AgrB. The AgrD2 C-terminus does differ more greatly, and it has been demonstrated here that AgrD2 is not recognised by AgrB1 and AgrB3. Residues which may dictate this recognition include the proline, alanine and lysine residues indicated with a circle in **Figure 5-20**. These differ most from amino acids in AgrD1 and AgrD3 which indicates they may prevent recognition by AgrB of other subgroups.

```
AgrD1       DEVEVPKELTQLHE-       14
AgrD3       DEAEVPKELTQLHE-       14
AgrD2       DEPKVPAELTNLYDK       15
            ** :** ***:*::
```

Figure 5-20. Clustal Omega alignment of AgrD C-termini. Amino acids are colour coded by their properties as follows; blue – acidic, red – hydrophobic, magenta – basic, green – hydroxyl, sulfhydryl and amine. * indicates the same amino acids, : indicates amino acids of strongly similar properties (182).

5.14 AgrBD complex formation with AgrD2 from *Staphylococcus epidermidis*

The *agr* quorum sensing system is employed in many other Gram-positive bacteria as well as *S. aureus* such as *Staphylococcus epidermidis*. AIPs from *S. epidermidis* have been shown to be cross inhibitory to *S. aureus agr* systems and *S. epidermidis* is able to out compete *S. aureus* for colonisation (181). We wanted to determine whether AgrD from *S. epidermidis* can be recognised by AgrB1 from *S. aureus*. This will give insights into how specific this interaction is and if there is cross-reactivity between species at this stage of the signalling pathway. *S. epidermidis* has three *agr* groups. The AIP molecules have longer tails than AIPs from *S. aureus* however the AgrD molecules contain residues which are highly conserved across *Staphylococci* such as the catalytic cysteine residue (183). The sequences

of AgrD from *S. aureus* and *S. epidermidis* are outlined below, the catalytic cysteine residue is shown in red and other residues which are conserved across staphylococci are shown in green.

	N-terminus	AIP	C-terminus
S. aureus			
AgrD1	**MNTLFNLFFDFITGILKNIGNIAA**	**YSTCDFIM**	**DEVEVPKELTQLHE**
AgrD2	**MNTLVNMFFDFIIKLAKAIGIVG**	**GVNACSSLF**	**DEPKVPAELTNLYDK**
AgrD3	**MKKLLNKVIELLVDFFNSIGYRAAY**	**INCDFLL**	**DEAEVPKELTQLHE**
AgrD4	**MNTLLNIFFDFITGVLKNIGNVAS**	**YSTCYFIM**	**DEVEIPKELTQLHE**
S. epidermidis			
AgrD1	**MENIFNLFIKFFTTILEFIG**	**TVAGDSVCASYF**	**DEPEVPEELTYLYE**
AgrD2	**MNLLGGLLLKIFSNFMAVIG**	**NASKYNPCSNYL**	**DEPQVPEELTKLDE**
AgrD3	**MNLLGGLLLKLFSNFMAVIG**	**NAAKYNPCASYL**	**DEPQVPEELTKLDE**

To identify recognition between AgrD from *S. epidermidis* and AgrB from *S. aureus*, *agrD2* was amplified from *S. epidermidis* 1457 and inserted into MCS2 of pCDFDuet-1 *agrB1* using HiFi cloning. This is a biofilm forming strain which has been the focus of *agr* studies in *S. epidermidis. S. aureus* AgrB1 and *S. epidermidis* AgrD2 protein expression was induced in *E. coli* C41 (DE3) and complex formation detected using a Western blot against membrane fractions using AgrB nanobody 2ABE10.

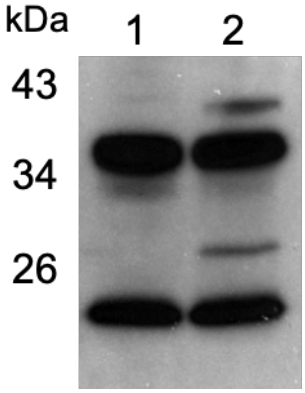


Figure 5-21. AgrBD complex formation with *S. aureus* AgrB1 and *S. epidermidis* AgrD2. Samples are induced *E. coli* C41 (DE3) pCDFDuet-1 encoding genes as follows; Lane 1: *S. aureus agrB1*, Lane 2: *S. aureus agrB1 S. epi agrD2.* Samples were added to 2 x Novex Tris-Glycine SDS sample buffer and heated to 55°C for 5 min before running on a 14 % Tris-Glycine gel. The gel was transferred to PVDF and probed with AgrB nanobody 2ABE10.

As shown in **Figure 5-21**, AgrB1 from *S. aureus* was able to recognise and form a complex with AgrD2 from *S. epidermidis* (**Figure 5-21**). Ji et al. showed in 1997 that there was no mature AIP production from AgrD of *Staphylococcus lugdunensis* with *S. aureus* AgrB group 1, 2 or 3. We have not measured mature AIP production here, however, have demonstrated that *S. aureus* AgrB1 is able to recognise AgrD of another species. Mature AIP may not be made as amino acid differences in the AIP molecule and the N-terminus may prevent further processing by AgrB of different groups.

There is high sequence homology in the C-termini of AgrD peptides as shown above. This supports the hypothesis that AgrB recognises AgrD via the C-terminus as this highly conserved region enables cross-group recognition by AgrB.

The C-terminus of AgrD2 from *S. epidermidis* was aligned with the C-terminus of AgrD1 from *S. aureus* using Clustal Omega (**Figure 5-22**) (182). Differences are seen however cross group recognition is seen between these AgrD peptides. This indicates that differences in amino acids seen here are not essential for recognition by AgrB. Taken together with the alignment of AgrD C-termini from *S. aureus* (**Figure 5-20**), this indicates that the alanine in AgrD2 and the final lysine residue may be what prevents AgrB1 and AgrB3 from recognising and binding AgrD2.



Figure 5-22. Clustal Omega alignment of AgrD C-termini from *S. aureus* group I and *S. epidermidis* group II. Amino acids are colour coded by their properties as follows; blue – acidic, red – hydrophobic, magenta – basic, green – hydroxyl, sulfhydryl and amine. * indicates the same amino acids, : indicates amino acids of strongly similar properties (182).

5.15 Identification of residues in AgrB necessary for AgrBD complex formation

In the previous section residues in the AgrD C-terminus which could be essential for recognition of AgrD by AgrB have been identified. To probe the *S. aureus* AgrB1D1 interaction further and identify residues which are essential for complex formation, site specific mutations were made in key amino acids in AgrB1 and AgrD1. Residues targeted include Cys84 and His77 which form the putative active site of AgrB and catalyse the processing of AgrD (71). Cys28 in AgrD1 was also targeted, as this is required for formation of the thiolactone macrocycle and likely catalyses thioester exchange, releasing AgrD from AgrB (**Figure 5-23**) (67).

Cys84 in AgrB1 and Cys28 in AgrD1 were converted to serine using site directed mutagenesis of pCDFDuet-1 *agrB1D1.* Creation of the mutations was confirmed by DNA sequencing carried out by Source Bioscience. These plasmids were introduced into in *E. coli* C41 (DE3), protein expression was induced, and membrane fractions isolated. Membrane fractions were run on a 14% Tris-Glycine gel and AgrB detected by Western blot with nanobody 2ABE10.

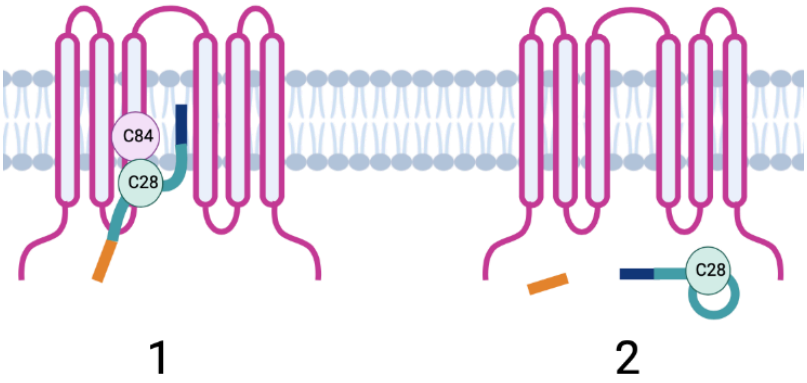


Figure 5-23. Schematic of the role of Cys84 AgrB and Cys28 AgrD. (1) AgrD binds to AgrB via Cys84 and Cys28 and Cys84 are located in close proximity. (2) After AgrD C-terminal cleavage, AgrD M33 is susceptible to nucleophilic attack by AgrD C28. This catalyses thioester exchange and thiolactone ring formation, releasing AgrD from AgrB.

As shown in **Figure 5-24** (a), with either of these mutations, no mature AIP-1 was formed. This shows that these residues are essential for the processing of AgrD1 by AgrB1 to form AIP-1. Additionally, as presented in **Figure 5-24** (b), the AgrB1D1 complex was unable to form with an inactivating mutation of AgrB Cys84 (Lane 3) however it can form with an inactivating mutation of AgrD Cys28 (Lane 4). This is expected as Cys84 is essential for recognition and binding of AgrD forming a thioester bond therefore mutation of this will prevent AgrBD complex formation. Cys28 is essential for thiolactone ring formation and release of AgrD from AgrB (**Figure 5-23**) (67). Therefore, mutation of this does not prevent recognition of AgrD by AgrB but does inhibit mature AIP-1 production as the thiolactone ring cannot be formed.

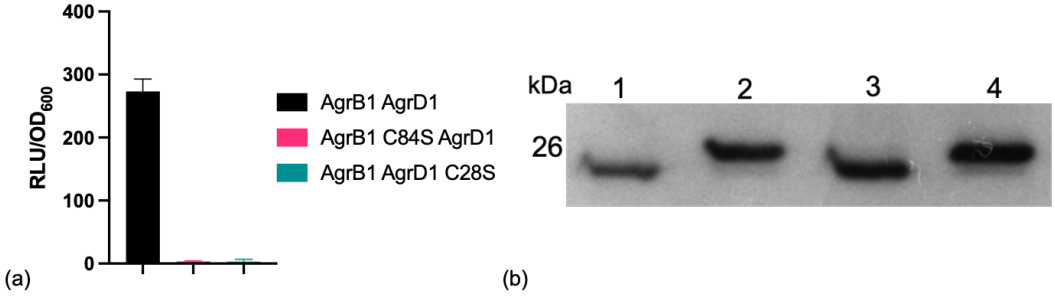


Figure 5-24. AIP-1 production and AgrB1D1 complex formation with site specific mutations in AgrB1 C84 and AgrD1 C28. (a) Cell free *E. coli* supernatants after induction were added to *S. aureus* ROJ143 as described previously and OD_{600} and RLU read in a Tecan plate reader after 3.5 h incubation at 37°C. Data represent three technical repeats with error bars showing standard deviation. (b) Western blot against AgrB. Samples were membrane fractions of *E. coli* C41 (DE3) pCDFDuet-1 with genes as follows; Lane 1: *agrB1*, Lane 2: *agrB1 agrD1* Lane 3: *agrBC84S agrD1* Lane 4: *agrB1 agrDC28S.* Samples were added to 2 x Novex Tris-Glycine SDS sample buffer and heated to 55°C for 5 min before running on a 14 % Tris-Glycine gel. The gel was transferred to PVDF and probed with AgrB nanobody 2ABE10.

Arginine 70 (R70), glycine 75 (G75) and lysines 129-131 (KKK129-131) in AgrB1 were also targeted as mutation of these residues has been shown previously to inhibit AIP production in *S. aureus* (72). Mutation of either R70 or G75 has been shown to inhibit AIP production, detected using a bioreporter, and AgrD C-terminal cleavage detected by Western blot. Mutation of KKK129-131 has been shown to inhibit AIP production but not AgrD cleavage indicating it inhibited maturation of AIP at a later stage in the pathway (72). We wanted to identify if mutating these key residues would affect the recognition of AgrD by AgrB. Each of these key active site amino acids were converted to alanine by site directed mutagenesis in pCDFDuet-1 *agrB1D1*. As previously, the expression of proteins from plasmids was induced in *E. coli* C41 (DE3) and AIP-1 production and AgrB1D1 complex formation assessed using *S. aureus* ROJ143 and Western blot against AgrB.

As shown in **Figure 5-25** (a), using group I bioreporter *S. aureus* ROJ143 to detect AIP-1 production, no AIP-1 was synthesised with G75A mutation. With a R70A mutation, AIP-1 production reduced ~3.5 fold and with mutation of the triple lysine residues surrounding K130, AIP-1 production reduced ~2.5 fold. AgrB1D1 complex formation was prevented with G75A and R70A mutations however it was able to form with mutation of the triple lysine residues surrounding K130 (**Figure 5-25**, b). This confirms what was demonstrated previously, that mutation of the lysine residues prevents AIP-1 production but does not prevent peptidase activity and recognition of AgrD by AgrB (72). Together with the findings of Thoendel et al. (72) this indicates that that these lysine residues function in processing of AgrD after recognition and C-terminal cleavage. The data also indicates that R70 and G75 are involved in the recognition of AgrD by AgrB as complex formation was prevented when they are mutated. This highlights distinct steps in the processing of AgrD including recognition and cleavage of the C-terminus followed by thiolactone ring formation and release of AgrD from AgrB.

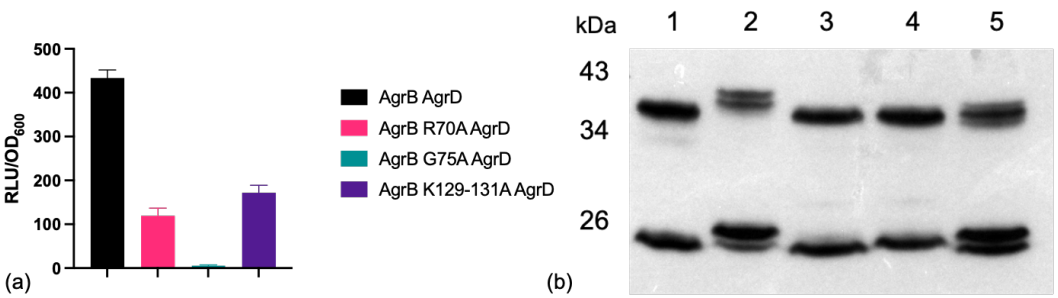


Figure 5-25. AIP-1 production and AgrBD complex formation with *E. coli* C41 (DE3) after induction of pCDFDuet-1 *agrB1D1* with inactivating point mutations. (a) Cell free supernatants of *E. coli* cultures after induction were added to *S. aureus* ROJ143 as described previously and OD_{600} and RLU read in a Tecan plate reader after 3.5 h incubation at 37°C. Data represent three technical repeats with error bars showing standard deviation. (b) Western blot against AgrB. Samples are membrane fractions of *E. coli* C41 (DE3) pCDFDuet-1 with recombinant genes as follows; Lane 1: *agrB*, Lane 2: *agrB agrD* Lane 3: *agrBR70A agrD* Lane 4: *agrBG75A agrD,* Lane 5: *agrBK129-131A agrD.* Samples were added to 2 x Novex Tris-Glycine SDS sample buffer and heated to 55°C for 5 min before running on a 14 % Tris-Glycine gel. The gel was transferred to PVDF and probed with AgrB nanobody 2ABE10.

As mentioned previously a site-specific mutation was also made in His77 in AgrB1 which is thought to be part of the active site. This mutation could not be made in the pCDFDuet-1 *agrBD* vector due to technical difficulties therefore it was made in pCDFDuet-1 *agrB.* To assay AgrBD complex formation and AIP-1 production with this mutant, pCDFDuet-1 *agrBH77A* was induced in *E. coli* C41 (DE3), membrane isolated and incubated with T7-AgrD1.

As displayed in **Figure 5-26** (a), AIP-1 production was reduced but not abolished with H77A mutation. Additionally, AgrB1D1 complex formation

was prevented with H77A mutation (**Figure 5-26**, b, Lane 2). His77 and Cys84 make up the active site and mutation of either of these residues resulted in loss of recognition of AgrD and loss of AIP-1 production showing that the catalytic activity of AgrB is essential for this.

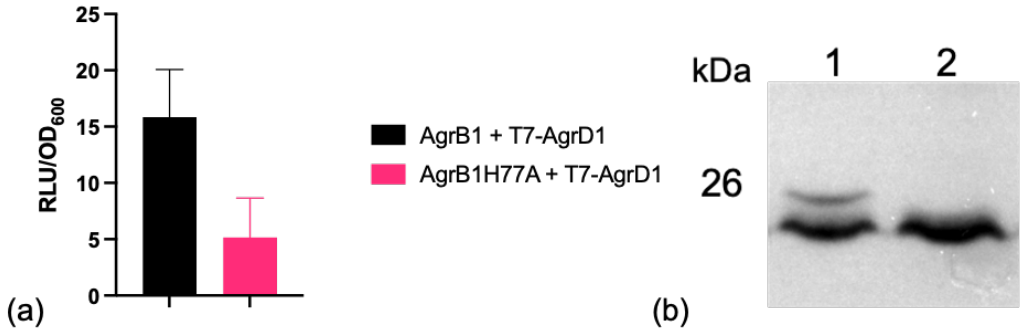


Figure 5-26. AIP-1 production and AgrBD complex formation with membrane fractions of induced *E. coli* C41(DE3) pCDFDuet-1 *agrB1D1* H77A. (a) Samples were added to *S. aureus* ROJ143 as described previously and OD_{600} and RLU read in a Tecan plate reader after 3.5 h incubation at 37°C. Data represent three technical repeats with error bars showing standard deviation. (b) Western blot against AgrB. Samples are membrane fractions of induced *E. coli* C41(DE3) pCDFDuet-1 *agrB1* incubated with T7-AgrD1. Lane 1: AgrB1 + T7-AgrD1 Lane 2: AgrB1H77A + T7-AgrD1. Samples were added to 2 x Novex Tris-Glycine SDS sample buffer and heated to 55°C for 5 min before running on a 14 % Tris-Glycine gel. The gel was transferred to PVDF and probed with AgrB nanobody 2ABE10.

5.16 Effect of protease inhibitors on AgrB1D1 complex formation

Mutation of key catalytic residues of AgrB1 was shown to prevent AgrB1D1 intermediate formation. To determine whether protease activity was necessary for AgrB1D1 complex formation, this was investigated in the presence of various protease inhibitors. Inhibitors selected had been tested

for AIP-1 biosynthesis inhibition previously using membrane extracts of *E. coli* BL21 pCold *agrB1* incubated with T7-AgrD1. Some had been shown to be AIP biosynthesis inhibitors and some had no effect (**Figure 5-27**). Inhibitors selected for use here were, ambuic acid, a known AgrB inhibitor, TPCK, an irreversible serine and cysteine protease inhibitor, E64 an irreversible cysteine protease inhibitor and pepstatin, a reversible aspartic acid protease inhibitor as well as cOmplete protease inhibitor cocktail (Sigma Aldrich).

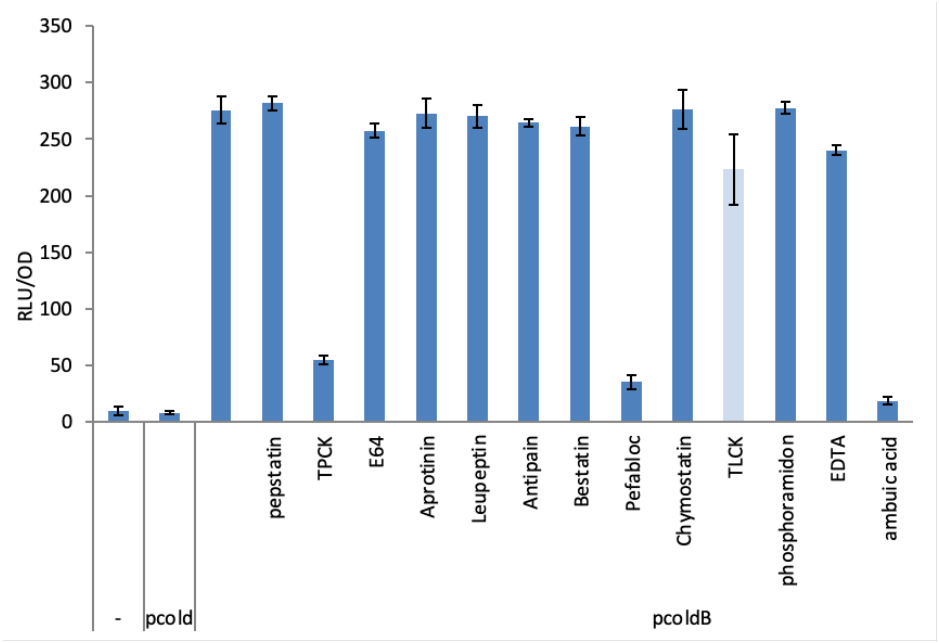


Figure 5-27. AIP-1 production from *E. coli* BL21 pCold *agrB1* incubated with T7-AgrD1. AIP-1 production was detected by addition of samples to *S. aureus* ROJ143 using the method described previously. This work was performed, and data analysed by Dr. Victoria Steele.

Protease inhibitors were tested with membrane fractions of *E. coli* C41 (DE3) *agrB1* incubated with synthetic T7-AgrD1. Protease inhibitors were incubated with AgrB1 induced *E. coli* membrane at 37°C for 1 h before addition of T7-AgrD1 and incubation at 37°C for an additional 2 h. As shown in **Figure 5-28**, ambuic acid and TPCK completely inhibited AgrB1D1 complex formation whereas cOmplete protease inhibitor, E64 and pepstatin had no effect. This confirms what was observed before by Dr. Victoria Steele who saw inhibition of AIP-1 production from cell free assays with ambuic acid and TPCK but no inhibition with pepstatin and E64 (**Figure 5-27**).

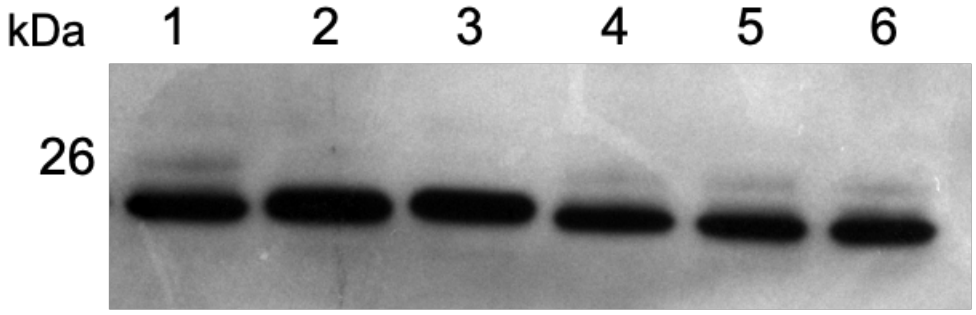


Figure 5-28. Effect of protease inhibitors on AgrB1D1 complex formation where inhibitors were added before T7-AgrD1. Samples were membrane fractions of induced *E. coli* C41(DE3) pCDFDuet-1 *agrB1* incubated with T7-AgrD1 and inhibitors as follows. Lane 1: DMSO control, Lane 2: 100 μM ambuic acid, Lane 3: 100 μM TPCK, Lane 4: 1 x cOmplete protease inhibitor cocktail, Lane 5: 10 μM E64, Lane 6: 10 μg/mL pepstatin. Samples were added to 2 x Novex Tris-Glycine SDS sample buffer and heated to 55°C for 5 min before running on a 14 % Tris-Glycine gel. The gel was transferred to PVDF and probed with AgrB nanobody 2ABE10.

Previously inhibitors were incubated with membranes for 1 h before addition of T7-AgrD1 giving them time to act before AgrB1D1 complex formation could occur. Therefore, here inhibitors were added at the same time as T7-AgrD1 and incubated at 37°C for 2 h with membrane fractions of *E. coli*

C41(DE3) pCDFDuet-1 *agrB1* to see if they acted competitively. As presented in **Figure 5-29**, the inhibition profile was the same as for when inhibitors are added first. This implies that ambuic acid and TPCK could inhibit AgrB1 competitively.

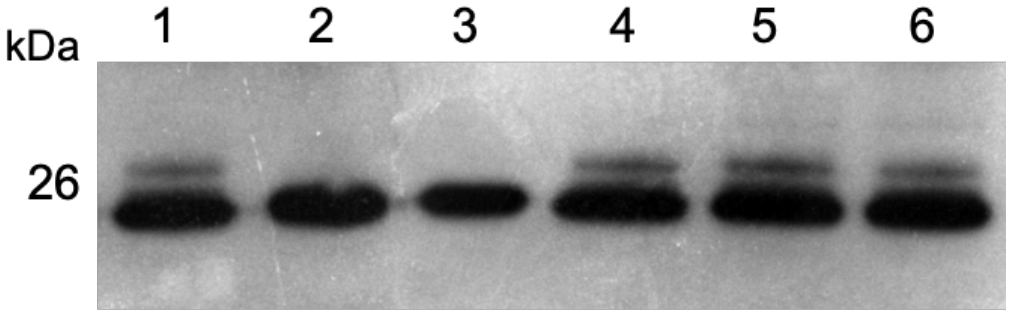


Figure 5-29. AgrB1D1 complex formation in the presence of protease inhibitors with inhibitors added simultaneously to T7-AgrD1. Samples are membrane fractions of induced *E. coli* C41(DE3) pCDFDuet-1 *agrB1* incubated with T7-AgrD1 and inhibitors as follows. Lane 1: DMSO control, Lane 2: 100 μM ambuic acid, Lane 3: 100 μM TPCK, Lane 4: cOmplete protease inhibitor cocktail, Lane 5: 10 μM E64, Lane 6: 10 μg/mL pepstatin. Samples were added to 2 x Novex Tris-Glycine SDS sample buffer and heated to 55°C for 5 min before running on a 14 % Tris-Glycine gel. The gel was transferred to PVDF and probed with AgrB nanobody 2ABE10.

Pefabloc, an irreversible serine and cysteine protease inhibitor was also tested. This was also shown to be effective in inhibiting AIP-1 production by Dr. Steele in her *in vitro* AIP biosynthesis assay (**Figure 5-27**). Interestingly, addition of 100 μM pefabloc had no effect on AgrB1D1 complex formation when added simultaneously with T7-AgrD1 to AgrB1 (**Figure 5-30**). This implies that pefabloc could inhibit AIP-1 formation but did not act at the level of AgrB1 recognition of AgrD1.

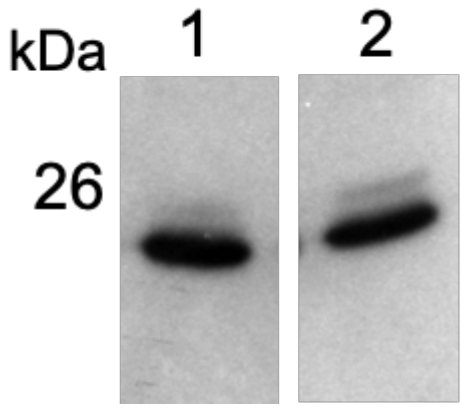


Figure 5-30. AgrB1D1 complex formation in the presence of 100 μM pefabloc. Samples are membrane fractions of induced *E. coli* C41(DE3) pCDFDuet-1 *agrB1* incubated with T7-AgrD1. Lane 1: DMSO control, Lane 2: 100 μM pefabloc. Lanes are from the same Western blot. Samples were added to 2 x Novex Tris-Glycine SDS sample buffer and heated to 55°C for 5 min before running on a 14 % Tris-Glycine gel. The gel was transferred to PVDF and probed with AgrB nanobody 2ABE10.

Finally, T7-AgrD1 was incubated with membrane fractions of *E. coli* C41 (DE3) *agrB1* for 1 h at 37°C before addition of inhibitors and incubation for a further 2 h to determine whether the inhibitors were able to dissociate the pre-formed complex. As shown in **Figure 5-10**, the AgrB1D1 complex forms within 30 min of incubation. As displayed in **Figure 5-31**, none of the inhibitors were able to dissociate the pre-formed complex.

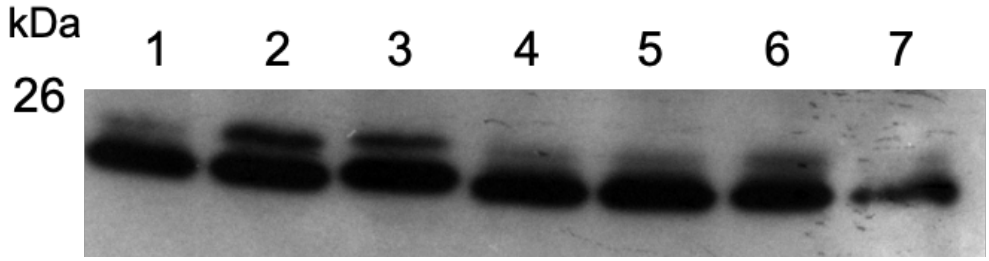


Figure 5-31. AgrB1D1 complex formation in the presence of protease inhibitors with inhibitors added after T7-AgrD1. Samples are membrane fractions of induced *E. coli* C41(DE3) pCDFDuet-1 *agrB1* incubated with T7-AgrD1 and inhibitors as follows. Lane 1: DMSO control, Lane 2: 100 μM ambuic acid, Lane 3: 100 μM TPCK, Lane 4: 10 μM E64, Lane 5: 10 μg/mL pepstatin, Lane 6: 1 mM pefabloc, Lane 7: cOmplete protease inhibitor cocktail. Samples were added to 2 x Novex Tris-Glycine SDS sample buffer and heated to 55°C for 5 min before running on a 14 % Tris-Glycine gel. The gel was transferred to PVDF and probed with AgrB nanobody 2ABE10.

5.17 Discussion

As described previously by Thoendel et al. (67) expression of AgrB1 and AgrD1 in *E. coli* was sufficient for AIP-1 production which was detectable using bioreporter *S. aureus* ROJ143 (67, 153). Co-expression of these proteins resulted in the detection of an AgrB1D1 intermediate at the cell envelope by Western blot. The formation of this AgrB1D1 complex was confirmed in section 5.7 and it was shown that AIP-1 production can be detected from membrane fractions of *E. coli* with AgrB1 incubated with synthetic AgrD1. The detection of an AgrBD intermediate by Western blot against AgrB or AgrD has been shown previously however here further work has been done to characterise this intermediate (67, 71).

It has been shown previously that the N-terminus of AgrD is essential for it's targeting to the membrane (70). It has also been shown that removal of the C-terminus of AgrD results in loss of mature AIP however the exact role of

the C-terminus was unclear (67). We showed in Chapter 4 that the C-terminus of AgrD interacts with the C-terminus of AgrB in live *S. aureus* cells. Additionally, in this chapter in section 5.9 we have demonstrated that AgrD lacking the C-terminus is not recognised by AgrB, with no AgrBD complex formation and no AIP production. Thoendel and Horswill hypothesised that the C-terminal region could be involved in mediating the interaction with AgrB (67). Our findings verify that the negatively charged C-terminus of AgrD, which is highly conserved, is essential for recognition by AgrB. AgrB has a number of positively charged residues in cytoplasmic loops which could be involved in this interaction (56). Through the evaluation of AgrBD complex formation with different *agr* subgroups we have also identified residues in the AgrD C-terminus which could be essential for this interaction. It would be interesting to mutate these residues to further validate if they are essential in this interaction. This was not performed here due to time constraints.

The AgrBD intermediate was noted by Thoendel et al. in 2008. They hypothesised that the complex was representative of AgrD peptide bound by a thioester bond to AgrB C84 (67). They showed that formation of the intermediate was pH dependent which supports the theory that it is a thioester bond. They were, however, unable to break the complex apart with thioester sensitive reagents (67). In section 5.12 it was established that the AgrB1D1 intermediate is resistant to boiling and high reducing environment. β-mercaptoethanol can disrupt thioester bonds therefore this could suggest that the complex is not held together in this way. However, taken with the findings from Thoendel et al. it is likely that the AgrBD interface is protected and is inaccessible to reducing agent and thioester disruptive agents.

On co-expression of AgrBD in *E. coli* C41 (DE3) from pCDFDuet-1, a high proportion of the protein appears to be present in an AgrBD complex (**Figure 5-4**). However, when AgrB1 is expressed alone and the cell envelope

separated and incubated with T7-AgrD1, a higher proportion of the protein appears to be unbound to AgrD1. This could be due to the unequal concentrations of protein. AgrB in the cell envelope is not quantified, indeed, when the concentration of AgrD is increased, the proportion of protein in the AgrBD complex increases (**Figure 5-11**). AgrBD are both under the *agr*P3 promoter therefore will be transcribed at a similar rate in *S. aureus* (51). However, due to differences in translation and protein degradation they will not be present at an equimolar ratio in the *S. aureus* cell. It would be interesting to quantify the levels of AgrB and AgrD in *S. aureus* and determine the proportion of AgrB present that is used for processing of AgrD. This could not be performed in this study due to the lack of antibody against native AgrD.

It was noted that the AgrB1D1 complex forms within 30 min and AIP-1 formation is highest at this time point. This is consistent with thermodynamic analysis performed by Wang et al. (68). They demonstrated that thiolactone ring formation is reversible and reaches an equilibrium with the reaction needing the rapid degradation of AgrD C-terminus by ClpP in order to progress (68). ClpP proteases exist in *E. coli* however these exist in the cytosol (184). The experiment shown here is representative of *E. coli* cell envelope with AgrB incubated with T7-AgrD1 over time, therefore ClpP will have been removed from this system. The AgrD C-terminus will not be able to be broken down in this system. Overproduction of the AgrD C-terminus leads to a decrease in AIP production as the energy from the hydrolytic degradation of the C-terminus is required to power the production of the high-energy thiolactone (46). This could explain why decrease in AIP production is observed over time as the reaction reaches equilibrium in the absence of ClpP.

In section 5.13 it was shown that there is inter group reactivity between *agr* groups I and III. AgrB1 was able to form an intermediate with AgrD3 and

AgrB3 was able to form an intermediate with AgrD1. Additionally, mature AIP-1 was made with AgrB3 turning over AgrD1. This supports work done previously which showed that the group specificity of AgrB is less stringent than the AIP-AgrC interaction which is highly group specific. Ji et al (60) in 1997 showed that AgrB1 and AgrB3 will process AgrD1 and AgrD3 with equal efficiency but neither will process AgrD2 and AgrB2 will not process AgrD1 or AgrD3 (60). It has been shown previously that different residues in AgrB1 and AgrB2 are essential for the recognition of AgrD which could lead to the group specific interactions detected here (185).

S. epidermidis AIP has been shown to be potent inhibitor of the *S. aureus agr* QS system however here we have demonstrated that *S. aureus* AgrB1 can recognise and form an intermediate with *S. epidermidis* AgrD2 (181). The C-terminal tail of *S. epidermidis* AgrD is highly conserved between the three *agr* groups with group I and III being identical and group II differing in one amino acid. The C-terminal tail contains seven amino acids which are highly conserved across staphylococcal AgrDs (183). This indicates that the C-terminus is likely to be essential for recognition of AgrD by AgrB as it is highly conserved. The sequence diversity in the AIP containing region and the N-terminus do not affect recognition of AgrD by AgrB but may affect further downstream processing.

Using alignment of the C-termini of AgrD peptides from *S. aureus* and *S. epidermidis* we have identified residues which could be essential in the recognition of AgrD by AgrB. It would be interesting to mutate these residues to confirm whether they are involved in this interaction. This would further validate that certain residues in the C-terminus of AgrD dictate recognition by AgrB.

The AgrBD intermediate was noted by Thoendel et al. (67) in 2009 with an AgrD C28A mutant however was not probed further (67). AgrBD complex

formation in the presence of an AgrD C28 mutant was also evaluated in this study. AgrD C28S was able to form a complex with AgrB but mature AIP was not formed. It is hypothesised that C28 is essential for thiolactone ring formation, therefore this intermediate consists of AgrD in complex with AgrB before thiolactone ring formation and could represent a fixed form of the intermediate (67).

Investigation into the residues of AgrB which are essential for its activity and the cleavage of AgrD has been performed previously. Qiu et al. (71) in 2005 explored residues essential for the catalytic nature of AgrB resulting in the identification of the catalytic dyad consisting of C84 and H77 (71). Thoendel et al. in 2013 (72) used random mutagenesis to identify further residues in AgrB which are essential for AIP production and AgrD processing. They observed AgrD processing through evaluation of the cleavage of AgrD detected by Western blot (72). In this study the ability of some of these mutants to produce AIP and to recognise and form an intermediate with AgrD has been investigated.

As demonstrated by Thoendel et al. (72) the AgrBD intermediate cannot form with a C84 mutation and mature AIP production is not observed. AgrD is inserted to the membrane via the N-terminal amphipathic leader. This is where C84, which is predicted to be in the membrane interior, interacts with AgrD (56). As shown in Chapter 4 section 4.3, computational modelling predicts that C84 is positioned in close proximity with C28 on AgrD and C84 cleaves between M32 and D33 on AgrD forming linear peptide before thiolactone ring formation. Mutation of C84, removes the catalytic activity and the ability of AgrB to bind and recognise AgrD.

Mutation of H77, which localises on the cytoplasmic side of AgrB, also reduced AIP production and appeared to inhibit AgrBD intermediate formation. This forms the catalytic dyad with C84 and mutation of either of

these residues inhibited efficient AIP production by inhibiting recognition of AgrD by AgrB.

Mutation of R70 and G75, which both map to a loop on the cytoplasmic side of AgrB both resulted in inhibition of AgrBD intermediate formation. Mutation of G75 resulted in complete inhibition of AIP production and mutation of R70 resulted in partial reduction of mature AIP production. This confirms what was reported by Thoendel et al. who showed that mutation of these residues blocked peptidase activity. These data imply that these residues may be essential for the recognition of AgrD by AgrB. The localisation of these residues on a cytoplasmic loop is consistent with them being involved in AgrD binding. In fact, R70 was predicted by computational modelling (section 4.3) to stabilise the orientation of AgrD in association with AgrB. This data supports that hypothesis as, with R70 mutated, AgrD is unable to remain in association with AgrB which reduces the ability to make mature AIP efficiently. G75 is among the seven residues which are conserved across all AgrB sequences from *Staphylococci*, *Clostridium* and *Listeria*, along with C84 and H77 (72). This implies a similar role for these residues in all species and implies that these residues are essential in mature AIP production.

Interestingly, mutation of the three lysine resides at positions 129-131 resulted in inhibition of AIP production but AgrBD intermediate formation was observed. This confirms what Thoendel et al. (72) reported, with AgrD cleavage observed but no AIP production. This demonstrates that these residues are essential for AIP processing after C-terminal cleavage, potentially for thiolactone ring formation or for export from the cell. These resides were previously thought to be present in the intramembrane domain however recent modelling by Dr Bonev has placed these on a cytoplasmic loop (Chapter 4, **Figure 4-1**). Protein modelling has predicted that these lysine residues may interact with C-terminal E186 and D187 residues on

another copy of AgrB to stabilise a dimer complex. We have demonstrated in Chapter 4 that AgrB forms a dimer which could be essential for its activity. Therefore, interruption of these residues could inhibit oligomer formation which may be essential for steps in the processing of AgrD after C-terminal cleavage such as thiolactone ring formation or transport across the membrane (72). Contrary to this hypothesis however, is the detection of AgrB dimer by Western blot with these residues mutated (**Figure 5-25**). This indicates that, although these residues may be important in AgrB dimerization, dimerization can still occur when these are mutated.

The data showing that AgrBD complex formation can occur with the triple lysine mutation indicates that residues in the C-terminus of AgrB are not essential for the recognition and binding of AgrD but are essential for effective AIP production. This implies that they are essential at a later stage in the pathway. One hypothesis is that these lysine residues interact with negatively charged residues in the AgrD C-terminus and are essential for the removal of AgrD C-terminus from the AgrB active site. Removal of the C-terminus is essential for efficient AIP production therefore with these residues mutated, AIP production is impaired, but not completely inhibited. We showed in Chapter 4 that there is a strong interaction between the AgrD C-terminus and the AgrB C-terminus which supports this hypothesis.

AgrB is an integral membrane protease, therefore the processing of AgrD by AgrB should be able to be inhibited with protease inhibitors. Qiu et al. showed that, in *S. aureus* cells, AIP production decreased in the presence of pefabloc (AEBSF), a serine protease inhibitor. They also showed that, in an *in vitro* assay with AgrB in purified membrane vesicles, pefabloc inhibited AgrD processing as detected by Western blot against T7-AgrD. TPCK, a serine/cysteine protease inhibitor was also shown to inhibit AgrD processing *in vitro*. Conversely, E64, a cysteine protease inhibitor, and pepstatin, an

aspartic acid inhibitor, were both shown to have no effect on AIP production or AgrD processing (71).

Using this model AgrB processing of AgrD was inhibited competitively by serine/cysteine protease inhibitor TPCK but not by cysteine protease inhibitor E64 as reported previously. Although AgrB has no sequence homology with other cysteine proteases, it has been described as a putative cysteine protease. This is because mutation of the conserved serine in AgrB has little effect on AIP production, indicating that AgrB is not a serine protease (71). Additionally, His77 and Cys84 are thought to form a catalytic centre and these most common conserved residues in the catalytic centre of cysteine proteases (71). The lack of inhibition by E64 and pepstatin could be due to the inability of the compounds to penetrate the catalytic centre rendering them ineffective.

Interestingly we showed that serine protease inhibitor pefabloc was unable to prevent AgrB1D1 intermediate formation. This was unexpected as it has been shown by Qiu et al. and by Dr Steele to inhibit AIP production and AgrD processing (71). This implies that pefabloc cannot inhibit the recognition of AgrB by AgrD but can inhibit formation of mature AIP so must be acting at a later stage in AgrD processing.

Overall, in this chapter evidence for an AgrBD intermediate which forms at the cell membrane in *E. coli* has been provided. This is essential for the production of mature AIP. It has been demonstrated using this model that recognition of AgrD by AgrB is via the C-terminus of AgrD which supports NanoBiT data outlined in Chapter 4. It has also been shown that catalytic residues of AgrB are essential for the formation of this intermediate and its formation can be inhibited with protease inhibitors.

6. Evaluating the mechanism of action of AIP biosynthesis inhibitors and the function of protease MroQ

6.1 Introduction

In the previous chapter the detection of an AgrBD intermediate which forms at the cell membrane in *E. coli* was described. The formation of this complex was shown to be essential for AIP-1 production and inhibition of this resulted in loss of AIP-1 production. We hypothesise that this assay could be used to test for inhibitors of AIP biosynthesis. Signal biosynthesis is an attractive target for QS inhibitors as AgrB is widely conserved among Gram-positive bacteria. AgrB is present in *Staphylococcus, Listeria, Enterococcus* and *Clostridium* (179). However, currently the only signal biosynthesis inhibitor identified is the fungal metabolite ambuic acid.

Ambuic acid was first identified as an inhibitor of FsrB which is an AgrB homologue in *Enterococcus faecalis* (113). It has since been identified as an inhibitor of AgrB, but the mechanism of action is unknown (107). In the previous chapter it was shown that the formation of the AgrBD intermediate can be inhibited competitively with ambuic acid. In this chapter analogues of ambuic acid which were synthesised by Dr Reekes and Dr Baldessare will be tested for inhibition of AgrBD complex formation to help elucidate their mechanism of action (186).

Additionally, in the previous chapter it was shown that AgrB and AgrD were sufficient for AIP production in an *E. coli* membrane based *in vitro* assay. However, there are many proteases in the *E. coli* membrane which are not present in *S. aureus* which could be interfering with this reaction. AgrB is known to perform C-terminal cleavage of AgrD and catalyse thiolactone ring formation (67, 71). MroQ, is another protease which is thought to perform

N-terminal cleavage of AgrD (69). The role of MroQ must be being performed by unknown proteases in the *E. coli* membrane in this model. This chapter will outline the purification of AgrB and MroQ, performed to investigate their interactions in a cell free model.

6.2 Aims

In the previous chapter evidence for an AgrBD intermediate which forms at the *E. coli* cell membrane was provided. Formation of this intermediate can be inhibited with protease inhibitors such as TPCK and the natural product, ambuic acid. In this chapter we will use AgrBD complex formation to probe the mechanism of action of AgrB inhibitor ambuic acid and its analogues.

AgrBD intermediate formation was also shown to be essential for AIP-1 production in *E. coli* membranes. There are many proteases and proteins in the *E. coli* membrane which are not present in *S. aureus* therefore AgrB will be purified to probe the AgrBD interaction and AIP production in the absence of interfering proteins.

6.3 AgrB1D1 complex formation with ambuic acid

Ambuic acid is a known AgrB inhibitor however the mechanism of action is unknown (107). As shown in the previous chapter in **Figure 5-30**, ambuic acid was able to inhibit AgrB1D1 complex formation competitively, implying that it prevented AgrB recognition of AgrD. To investigate whether inhibition was concentration dependent, increasing concentrations of ambuic acid were added to membrane fractions of induced *E. coli* C41(DE3) pCDFDuet-1 *agrB1* with T7-AgrD1 added simultaneously. These were incubated at 37°C for 2 h.

As shown in Figure 6-1 (a), the inhibition of AgrB1D1 complex formation was dose dependent, with inhibition of AgrBD complex formation increasing with increasing concentrations of ambuic acid. Surprisingly, when AIP-1

production was monitored from these reactions using *S. aureus* ROJ143 it showed that increasing the concentration of ambuic acid up to 200 μM promoted AIP-1 production (**Figure 6-1**, b).

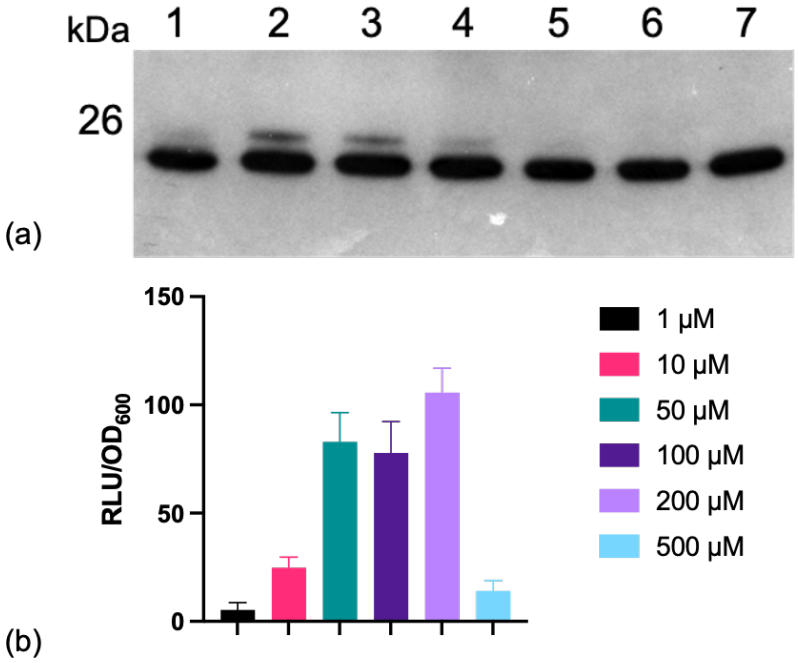


Figure 6-1. Effect of increasing concentrations of ambuic acid on (a) AgrB1D1 complex formation and (b) AIP-1 production. (a) Western blot against AgrB. Samples were membrane fractions of induced *E. coli* C41(DE3) pCDFDuet-1 *agrB1* incubated with T7-AgrD1 and increasing concentrations of ambuic acid as follows; Lane 1: DMSO control, Lane 2: 1 μM, Lane 3: 10 μM, Lane 4: 50 μM, Lane 5: 100 μM, Lane 6: 200 μM, Lane 7: 500 μM. Samples were added to 2 x Novex Tris-Glycine SDS sample buffer and heated to 55°C for 5 min before running on a 14 % Tris-Glycine gel. The gel was transferred to PVDF and probed with AgrB nanobody 2ABE10. (b) Samples were added to *S. aureus* ROJ143 as described previously and OD_{600} and bioluminescence read in a Tecan plate reader after 4 h incubation at 37°C. Data represent three technical repeats with error bars showing standard deviation.

An apparent increase in AIP-1 production in the presence of ambuic acid was unexpected. To confirm that the increase in bioluminescence observed with *S. aureus* ROJ143 was caused by an increase in AIP-1 production and not an effect of the high concentration of ambuic acid on the reporter strain, samples were sent for liquid chromatography mass spectrometry (LC-MS) to detect AIP-1. Samples for LC-MS were membrane fractions of induced *E. coli* C41(DE3) pCDFDuet-1 *agrB1* incubated with T7-AgrD1 and 200 μM ambuic acid for 2 h at 37°C. These samples were also tested for AIP-1 production using *S. aureus* ROJ143.

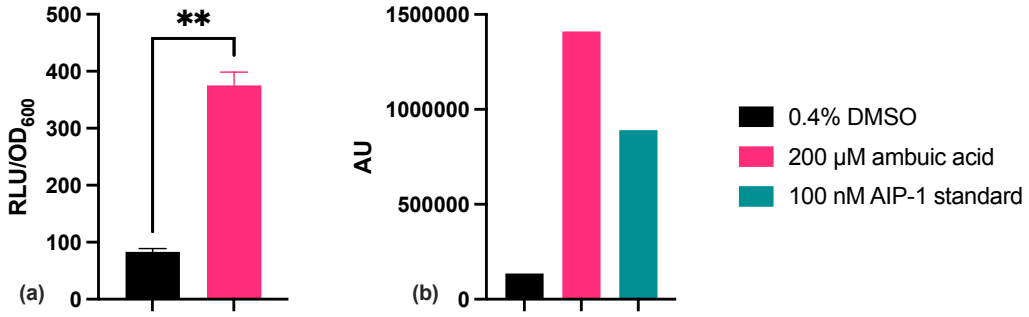


Figure 6-2. AIP-1 production from membrane fractions of induced *E. coli* C41(DE3) pCDFDuet-1 *agrB1* incubated with T7-AgrD1 and ambuic acid characterized using (a) *S. aureus* ROJ143 and (b) LC-MS. Samples were added to *S. aureus* ROJ143 as described previously and OD_{600} and bioluminescence read in a Tecan plate reader after 4 h incubation at 37°C. Data represent three technical repeats with error bars showing standard deviation. **p<0.01

As shown in **Figure 6-2**, AIP-1 production was higher in the presence of ambuic acid as detected using both the bioreporter and LC-MS. LC-MS showed a ~10-fold increase in the relative AIP-1 presence when *E. coli* C41(DE3) pCDFDuet-1 *agrB1* was incubated with T7-AgrD1 in the presence of ambuic acid compared to in the presence of DMSO which was used as a solvent control. The LC-MS data also gives insight into the turnover of T7-

AgrD1. 2 μM T7-AgrD1 was added to the initial reaction and, when compared to the AIP-1 standard, approximately 16 nM AIP-1 was produced in the presence of DMSO and 158 nM was produced in the presence of ambuic acid. This represents a 1 or 10% conversion of T7-AgrD1 to mature AIP-1. This demonstrates that the production of mature AIP-1 is inefficient. This may not mean, however that AgrBD complex formation is inefficient. The steps following C-terminal cleavage and thiolactone ring formation may be complemented by other proteases in the *E. coli* cell envelope. As these are not the native proteins from *S. aureus,* these reactions may be inefficient resulting in low turnover of AgrD to AIP.

Previously (Figure 5-18) it was shown that AgrB3 can form a complex with AgrD1 and can process AgrD1 to form mature AIP-1 (Figure 5-19). To investigate whether the addition of ambuic acid had any effect on AIP-1 production via AgrB3, *S. aureus* ROJ143 was used. *E. coli* membrane fractions with AgrB3 were incubated with T7-AgrD1 with or without ambuic acid. Reactions were added to *S. aureus* ROJ143 as previously and bioluminescence recorded using a Tecan plate reader.

As displayed in **Figure 6-3**, increased AIP-1 production was observed in the presence of ambuic acid as was shown with AgrB1. This indicated that 200 μM ambuic acid significantly increases the turn-over of AgrD1 by both AgrB1 and AgrB3 when in an *E. coli* membrane.

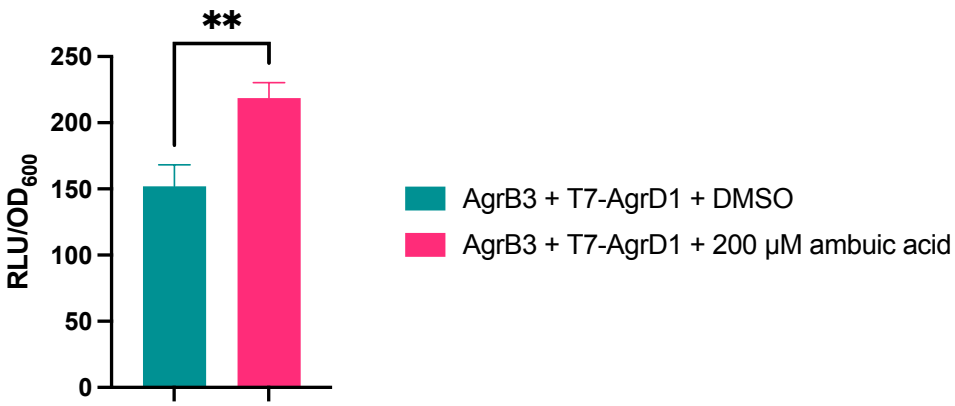


Figure 6-3. AIP-1 production from membrane fractions of induced *E. coli* C41(DE3) pCDFDuet-1 *agrB3* incubated with T7-AgrD1 and DMSO or ambuic acid. Samples were added to *S. aureus* ROJ143 as described previously and OD_{600} and bioluminescence read in a Tecan plate reader after 2.75 h incubation at 37°C. Data represent three technical repeats with error bars showing standard deviation. ** $p<0.01$.

6.4 Impact of ambuic acid analogues on AgrBD complex formation

Previous PhD students Dr James Reekes and Dr Leonardo Baldessare synthesised a number of ambuic acid analogues (186). The aims of the synthesis of these analogues were to improve the activity of the compound, to help elucidate the mechanism of action of ambuic acid and to obtain structure activity relationships. The structures of the analogues tested are shown in **Figure 6-4**. These had all been shown to be effective in inhibiting *agr* activity when tested with *agr*P3-lux based reporter *S. aureus* EJM82. This reporter is *S. aureus* SH1000 with a native *agr* system and insertion of *agrP3::luxABCDE* in the chromosome at the *attB* ectopic locus. This strain was used to calculate the IC_{50} of these compounds. The IC_{50} of ambuic acid was shown to be 0.94 ± 0.13 µM. None of the compounds tested were shown to be as potent as ambuic acid, with lower IC_{50}, except for LB276 which had a similar IC_{50} of 0.99 ± 0.46 µM (**Figure 6-4**).

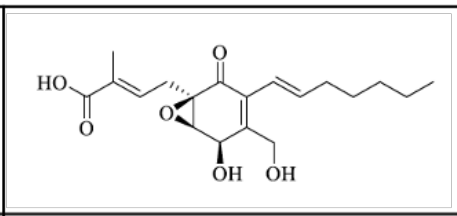
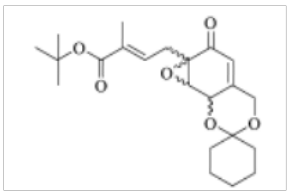
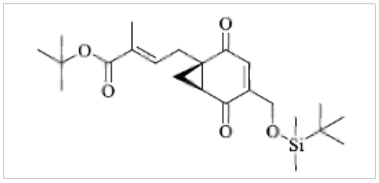
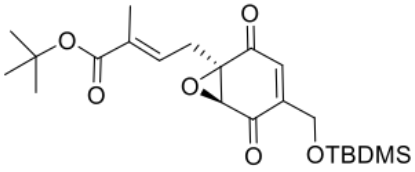
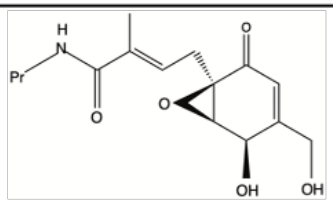
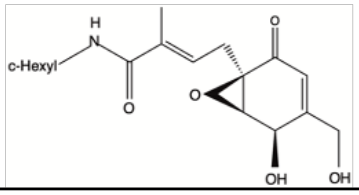
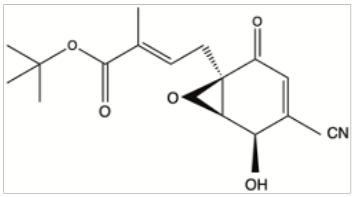
Ambuic acid (Native compound)		IC_{50} 0.94 ± 0.13 μM
JWR297 (Cyclohexyl ketal analogue)		IC_{50} 5.06 ± 3.52 μM
JWR229 (Cyclopropyl analogue)		IC_{50} 6.69 ± 0.14 μM
LB276		IC_{50} 0.99 ± 0.46 μM
LB251		IC_{50} Not calculated
LB253		IC_{50} Not calculated
LB286		IC_{50} Not calculated

Figure 6-4. Chemical structures of ambuic acid and analogues tested. Analogues were synthesised and IC_{50} determined by Dr. Leonardo Baldessare and Dr. James Reekes (186).

To further elucidate the mechanism of action of these compounds, their effect on AgrB1D1 complex formation was determined and compared with ambuic acid. This was to confirm whether the compounds also act by preventing AgrBD complex formation. Compounds were incubated with membrane fractions of *E. coli* C41 (DE3) pCDFDuet-1 *agrB1* and T7-AgrD1. Compounds and T7-AgrD1 were added simultaneously. Detection of the AgrB1D1 complex was performed by Western blot and AIP-1 production was determined using *S. aureus* ROJ143.

As shown in **Figure 6-5** (a), ambuic acid (Lane 2), LB276 (Lane 5) and LB286 (Lane 8) inhibited AgrB1D1 complex formation. As demonstrated previously, ambuic acid increased AIP-1 production as detected using *S. aureus* ROJ143 however both LB276 and LB286 inhibited AIP-1 production (**Figure 6-5**, b). This demonstrates that LB276 and LB286 inhibit AIP biosynthesis by preventing AgrB1 recognition of AgrD1. Additionally, JWR297, LB276 and LB286 appeared to inhibit AgrB dimer formation as represented by a reduction in the intensity of the band at ~40 kDa (**Figure 6-5**, a). This implies these compounds have a different mechanism of action to ambuic acid.

Of note is the lack of inhibition of complex formation by JWR229. This analogue also has no effect on AIP-1 production. This has replacement of the electrophilic epoxide centre of ambuic acid with a less reactive cyclopropyl isostere. It had been hypothesised by Dr Reekes that ambuic acid requires the epoxide moiety to covalently modify Cys84 to inhibit AgrB (186). These data suggest that the epoxide moiety is necessary for inhibition of AgrB by ambuic acid and that the interaction between AgrB and ambuic acid may be covalent.

The ketal analogue (JWR297) has increased rigidity compared to ambuic acid which may impact on AgrB inhibition. This appeared to have little effect

on AgrBD complex formation or AIP-1 production but appeared to reduce AgrB dimer formation (**Figure 6-5**).

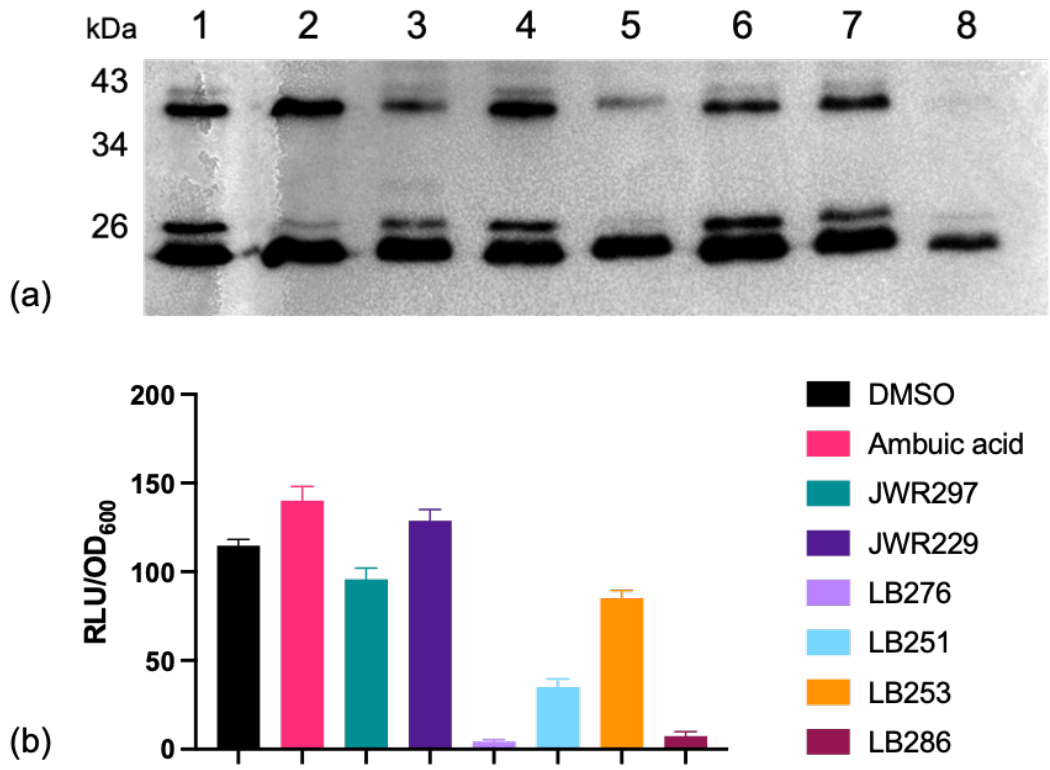


Figure 6-5. Effect of ambuic acid analogues on (a) AgrB1D1 complex formation and (b) AIP-1 production. (a) Western blot against AgrB. Samples are membrane fractions of induced *E. coli* C41(DE3) pCDFDuet-1 *agrB1* incubated with T7-AgrD1 and 200 μM ambuic acid analogues as follows; Lane 1: DMSO control, Lane 2: ambuic acid, Lane 3: JWR297, Lane 4: JWR229, Lane 5: LB276, Lane 6: LB251, Lane 7: LB253, Lane 8: LB286. Samples were added to 2 x Novex Tris-Glycine SDS sample buffer and heated to 55°C for 5 min before running on a 14 % Tris-Glycine gel. The gel was transferred to PVDF and probed with AgrB nanobody 2ABE10. (b) Samples were added to *S. aureus* ROJ143 as described previously and OD_{600} and bioluminescence read in a Tecan plate reader after 3.5 h incubation at 37°C. Data represent three technical repeats with error bars showing standard deviation.

To confirm the inhibition of AgrB1 dimer formation in the absence of AgrD, the ambuic acid analogues were tested with membrane fractions of induced *E. coli* C41(DE3) pCDFDuet-1 *agrB1*. As shown in **Figure 6-6**, dimer formation was inhibited with JWR297 (Lane 3), LB276 (Lane 5) and LB286 (Lane 8) as observed previously.

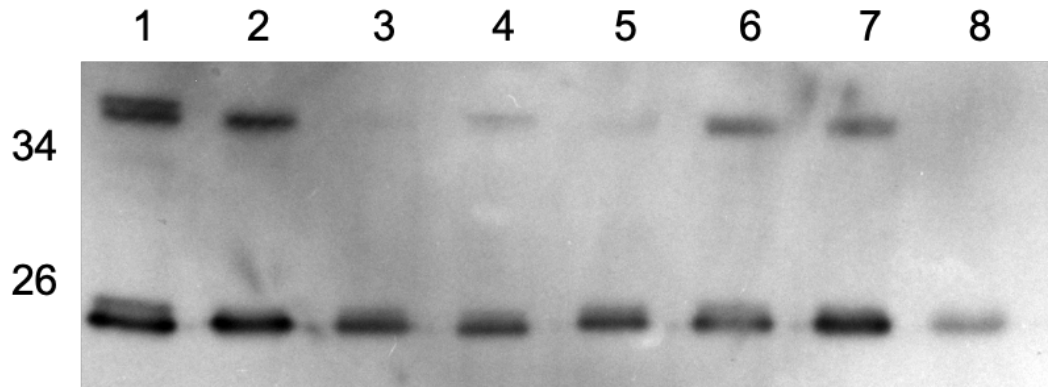


Figure 6-6. Effect of ambuic acid analogues on AgrB1 dimer formation. Samples are membrane fractions of induced *E. coli* C41(DE3) pCDFDuet-1 *agrB1* incubated with 200 μM ambuic acid analogues as follows; Lane 1: DMSO control, Lane 2: ambuic acid, Lane 3: JWR297, Lane 4: JWR229, Lane 5: LB276, Lane 6: LB251, Lane 7: LB253, Lane 8: LB286. Samples were added to 2 x Novex Tris-Glycine SDS sample buffer and heated to 55°C for 5 min before running on a 14 % Tris-Glycine gel. The gel was transferred to PVDF and probed with AgrB nanobody 2ABE10.

6.5 Purification of recombinant AgrB1

Evidence has been provided for AgrBD complex formation in *E. coli* membranes which is essential for the maturation of AgrD to form AIP. All work up until this point to probe the AgrBD complex has been performed in an *E. coli agrB* expression system. To determine which proteins are necessary for AIP-1 maturation and to probe the AgrB1D1 complex in more detail we investigated the interaction by reconstituting the *agr* QS system with purified components.

AgrB1 was purified from *E. coli* C41 (DE3) pCold *agrB1* via the His tag at the N-terminus using a Talon cobalt IMAC column. This expression construct was made by Dr. Philip Bardelang. After induction in *E. coli* the membrane and cytosolic fractions were tested for AgrB presence by Western blot with nanobody 2ABE10. As shown in **Figure 6-7**, AgrB is present in the membrane and cytosolic fractions. Interestingly no AgrB dimer was detected in the cytosol although larger aggregates are present. This indicates that AgrB may not form dimers in the cytosol. AgrB was purified from the membrane fraction.

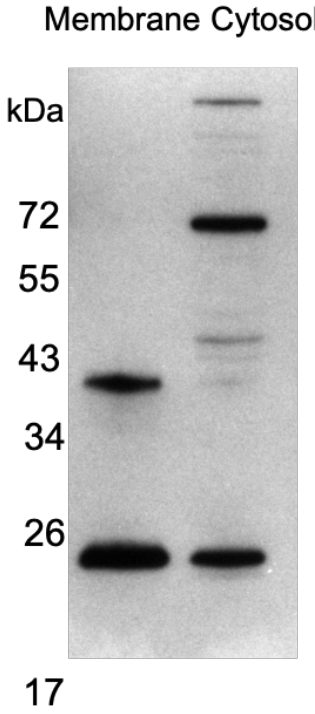


Figure 6-7. Western blot of *E. coli* C41 (DE3) after induction of AgrB1 expression from pCold *agrB1* before purification. After induction of protein expression membrane and cytosolic fractions were separated by ultracentrifugation. Samples were added to 2 x Novex Tris-Glycine SDS sample buffer and heated to 55°C for 5 min before running on a 14 % Tris-Glycine gel. The gel was transferred to PVDF and probed with AgrB nanobody 2ABE10.

Elution of AgrB1 was performed over three columns with two elutions per column (**Figure 6-8**). After purification the elution fractions were spin concentrated and desalted with EDTA to prevent aggregation of the purified protein via the His tag. Two desalting columns were used, and the protein eluted in four fractions (**Figure 6-9**). Monomeric AgrB1 is present at ~26kDa (blue arrow) however a greater proportion is in the dimeric state as shown at ~36 kDa (lowest red arrow). Multimers of AgrB1 are observed up the gel (red arrows). Smaller bands are also present, these are likely to be breakdown products of AgrB caused by the running of the denaturing gel or small contaminants which are difficult to remove as AgrB has been purified from the membrane. Elution fractions after desalting were pooled and spin concentrated, and the concentration was determined using a NanoDrop spectrophotometer. AgrB1 at 50.8 μM was stored at -80 °C prior to use.

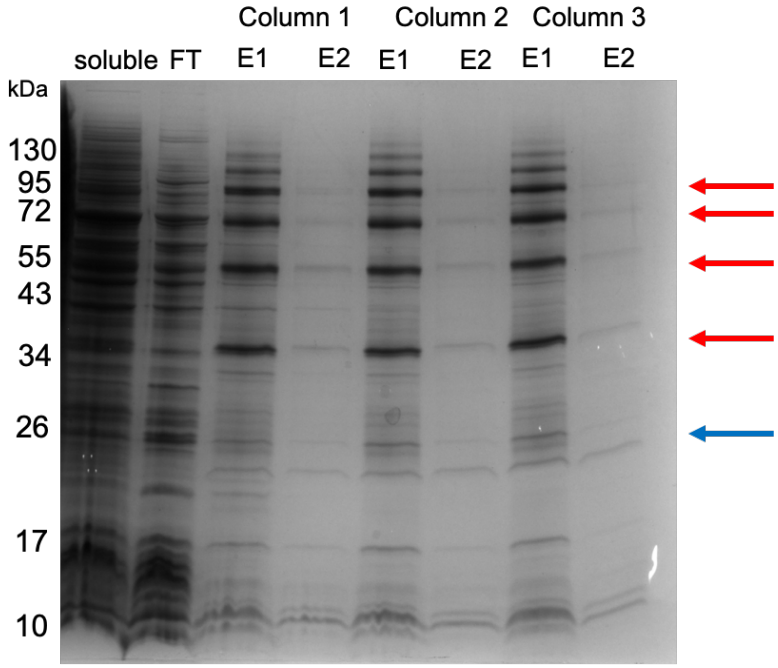


Figure 6-8. Coomassie stained gel showing AgrB1 purification. Samples were run on a 14% Tris-Glycine gel and stained with Coomassie blue. Soluble: soluble fraction, FT: flow through from column 1, E1: Elution 1, E2: Elution 2. Two elutions were collected and run from each of three columns. The blue arrow indicates monomeric AgrB1 and red arrows indicate AgrB1 higher order structures.

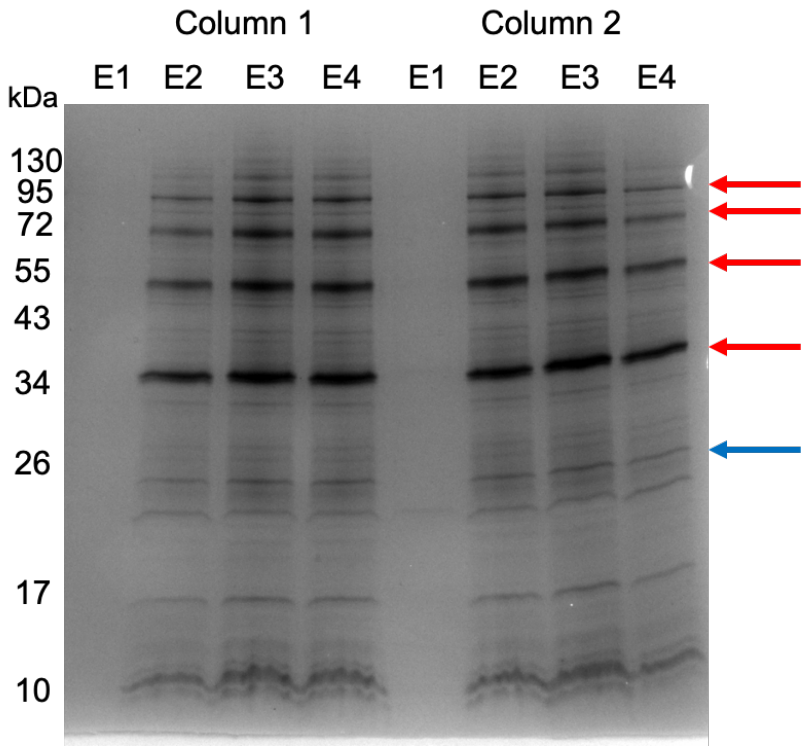


Figure 6-9. Coomassie stained gel of AgrB1 purification after desalting. Two desalting columns were used. E1-4 represents elution fractions 1-4 collected from each column. The blue arrow indicates monomeric AgrB1 and red arrows indicate AgrB1 higher order structures.

6.6 Incubation of purified AgrB1 with T7-AgrD1

To determine AgrB1D1 complex formation with purified AgrB1, a reaction was set up with AgrB1, T7-AgrD1 and synthetic lipid DOPG. It has been shown that lipid is essential for the peptidase activity of AgrB1 and Dr Steele demonstrated that addition of DOPG facilitated the most efficient cleavage of AgrD1 by AgrB1 (68). Samples were incubated at 37°C for 2 h to allow the complex to form, samples were then added to 2 x Novex Tris-Glycine SDS sample buffer and heated to 55°C for 5 min before running on a 14 % Tris-Glycine gel. As marked with an arrow in **Figure 6-10**, a Coomassie blue stained band migrating at the expected mass for an AgrB1D1 complex was observed. This band was excised and sent to the University of York for mass spectrometry analysis by MALDI-MS and MS/MS. The presence of AgrB

peptide fragments were confirmed but not the presence of T7-AgrD1. This is a small peptide at a low concentration and is so the lack of detection by mass spectrometry does not mean that it was not present.

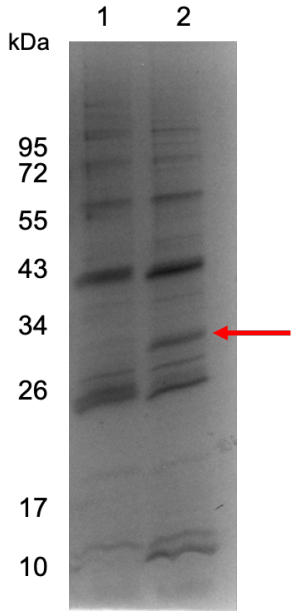


Figure 6-10. Coomassie stained gel of purified AgrB1 incubated with T7-AgrD1. Lane 1: AgrB1, Lane 2: AgrB1 + T7-AgrD1. Samples were added to 2 x Novex Tris-Glycine SDS sample buffer and heated to 55°C for 5 min before running on a 14 % Tris-Glycine gel and visualisation by Coomassie blue staining. Red arrow indicates the AgrBD complex.

To confirm that the band observed on the Coomassie stained gel was the AgrBD complex, a Western blot was performed against AgrB and against the T7 tag at the N-terminus of AgrD. As shown in **Figure 6-11** (a), AgrB1 was detected as a monomer and dimer and when incubated with T7-AgrD1. A third band (lane 3) was detected at ~30 kDa indicating the AgrBD complex, this is marked with a red arrow. The presence of AgrD in this complex was confirmed with the T7 Western **Figure 6-11** (b) which shows a band in lane 3 containing the N-terminus of AgrD at ~30 kDa, this is also marked with a red arrow. There was no band in lane 2 with T7-AgrD run alone indicating

this is not an aggregate. The linear peptide (6.7kDa) and aggregates of AgrD can be detected at the bottom of the blot (**Figure 6-11**, b).

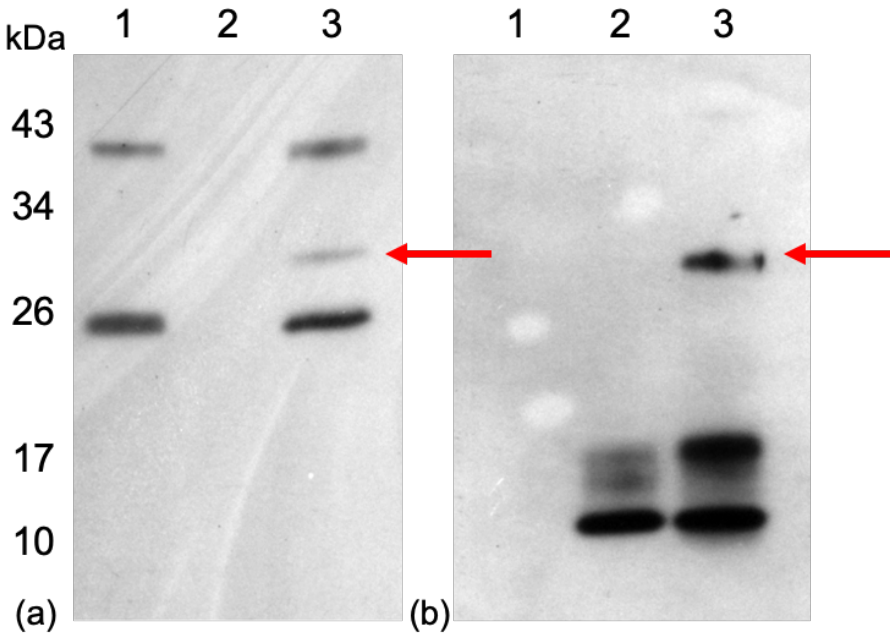


Figure 6-11. Western blot of purified AgrB1 incubated with T7-AgrD1. Blot against (a) AgrB, (b) T7 tag. Lane 1: AgrB1, Lane 2: T7-AgrD1, Lane 3: AgrB1 + T7-AgrD1. Samples were added to 2 x Novex Tris-Glycine SDS sample buffer and heated to 55°C for 5 min before running on a 14 % Tris-Glycine gel. The gel was transferred to PVDF and probed with AgrB nanobody 2ABE10 or T7 antibody conjugated to HRP. Red arrows indicate the AgrBD complex.

Interestingly, when these reactions were tested for AIP-1 production, no AIP-1 was detected above the background level (**Figure 6-12**). This shows that AgrB1 is not sufficient alone to process AgrD1 to mature AIP-1. There must be proteases in the *E. coli* membrane which can perform the later stages of AgrD processing to form mature AIP-1.

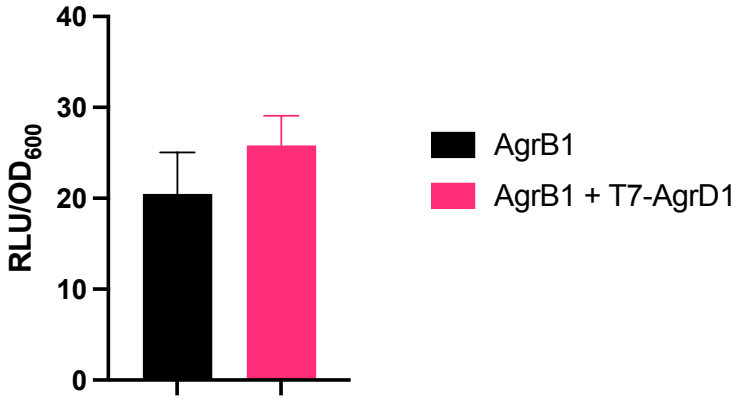


Figure 6-12. AIP-1 production from purified AgrB1 incubated with T7-AgrD1. Reactions were added to *S. aureus* ROJ143 as described previously and OD_{600} and bioluminescence read in a Tecan plate reader after 3.25 h incubation at 37°C. Data represent three technical repeats with error bars showing standard deviation.

6.7 Incubation of purified AgrB1 with T7-AgrD1 and ambuic acid

Ambuic acid was shown previously to reduce AgrB1D1 complex formation but increase AIP-1 production when AgrB1 was expressed in *E. coli* membranes therefore the effect of ambuic acid on purified AgrB1 was tested. The effect of the ambuic acid analogue LB276 was also tested. This was selected as, in section 6.4 it was shown that LB276 could inhibit AgrB1D1 complex formation in *E. coli* membranes and inhibit AIP-1 production. It was also shown previously to have the lowest IC_{50} of the analogues tested (**Figure 6-4**).

Interestingly, as shown in **Figure 6-13**, the shift in size of AgrB in complex with AgrD when using the purified protein was larger than the shift in size when AgrB is in an *E. coli* membrane. This is demonstrated by the red and green arrows in **Figure 6-13**.

The addition of ambuic acid and LB276 reduced AgrB1D1 complex formation when AgrB is in an *E. coli* membrane as expected (**Figure 6-13**, lane 5, 7, red arrow). Both compounds also reduced complex formation with purified AgrB in DOPG (**Figure 6-13**, lane 6, 8, green arrow). Furthermore, as observed before, LB276 reduced AgrB dimer formation in both the membrane bound and purified forms of the protein (**Figure 6-13**, lane 7, 8, purple arrow).

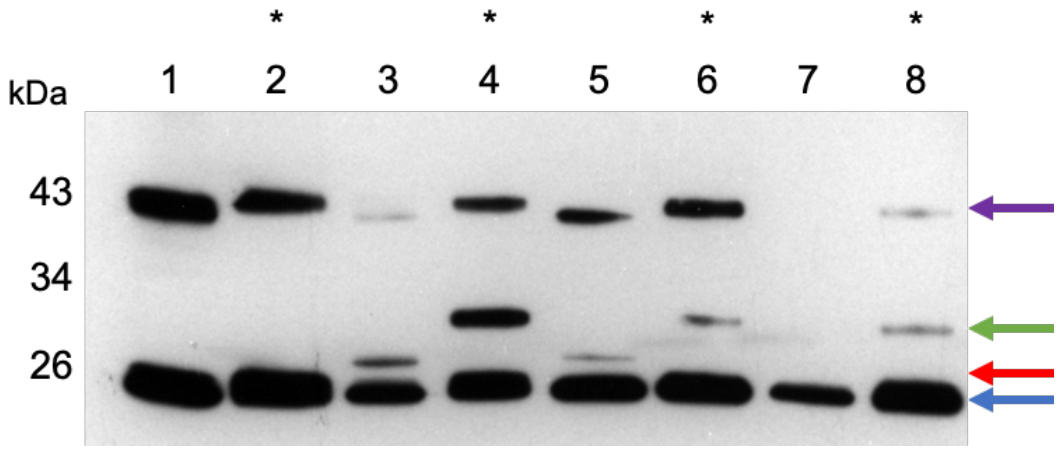


Figure 6-13. Impact of the addition of ambuic acid and LB276 on complex formation of AgrB in *E. coli* membrane and purified (*) AgrB with T7-AgrD. Lane 1: membrane AgrB1, Lane 2: purified AgrB1, Lane 3: membrane AgrB1 + T7-AgrD1, Lane 4: purified AgrB1 + T7-AgrD1, Lane 5: membrane AgrB1 + T7-AgrD1 + 200 μM ambuic acid, Lane 6: purified AgrB1 + T7-AgrD1 200 μM ambuic acid, Lane 7: membrane AgrB1 + T7-AgrD1 + 200 μM LB276, Lane 8: purified AgrB1 + T7-AgrD1 200 μM LB276. Samples were run on a 14% Tris-Glycine gel and detected by Western blot with 2ABE10 nanobody. The blue arrow indicates AgrB monomer, the red arrow indicates AgrBD complex with membrane inserted AgrB, the green arrow indicates AgrBD complex with purified AgrB and the purple arrow indicates AgrB dimer.

As shown previously, addition of ambuic acid to AgrB1 in *E. coli* membrane incubated with T7-AgrD1 increased AIP-1 production as detected with

S. aureus ROJ143 (**Figure 6-14**). However, interestingly, there was no increase in AIP-1 production with purified AgrB1 incubated with T7-AgrD1 in the presence of ambuic acid. This implies that the increase in AIP-1 production was due to the effect of ambuic acid on other proteases in the *E. coli* membrane which may be facilitating the turnover of AgrD. This highlights the necessity to investigate AgrBD interaction with purified proteins.

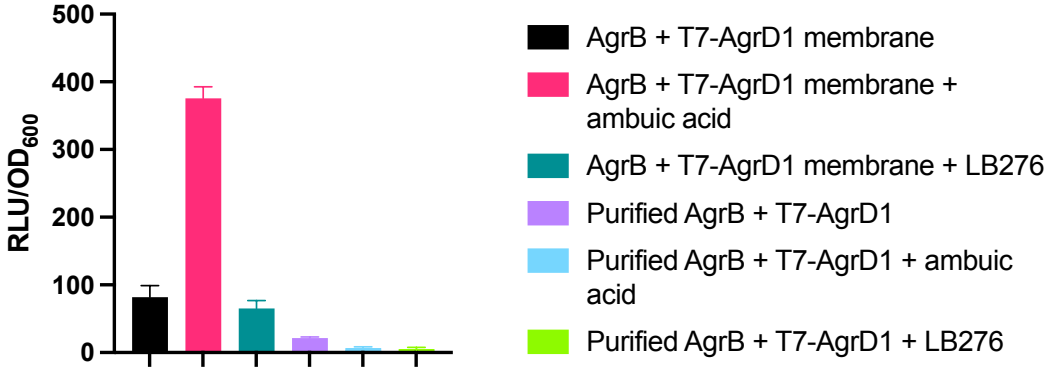


Figure 6-14. AIP-1 production from *E. coli* membrane fractions with AgrB1 and purified AgrB1 incubated with T7-AgrD1 in the presence and of ambuic acid. Samples were added to *S. aureus* ROJ143 as described previously and OD_{600} and bioluminescence read in a Tecan plate reader after 3.75 h incubation at 37°C. Data represent three technical repeats with error bars showing standard deviation.

6.8 Purification of MroQ

When testing purified AgrB1 with T7-AgrD1, no mature AIP-1 was produced (**Figure 6-12**), indicating another protease is necessary for full processing of AgrD. MroQ, a putative type II CAAX peptidase, has been reporterd to be necessary for maturation of AIP-1 in *S. aureus* (69, 76). MroQ was therefore expressed and purified as a maltose binding fusion protein following a previously described technique (69). Purification was performed via the His tag using an Ni-NTA resin. Three elution fractions were collected and MBP-

MroQ can be observed on a Coomassie stained gel at ~70 kDa, this is marked with a red arrow in **Figure 6-15**.

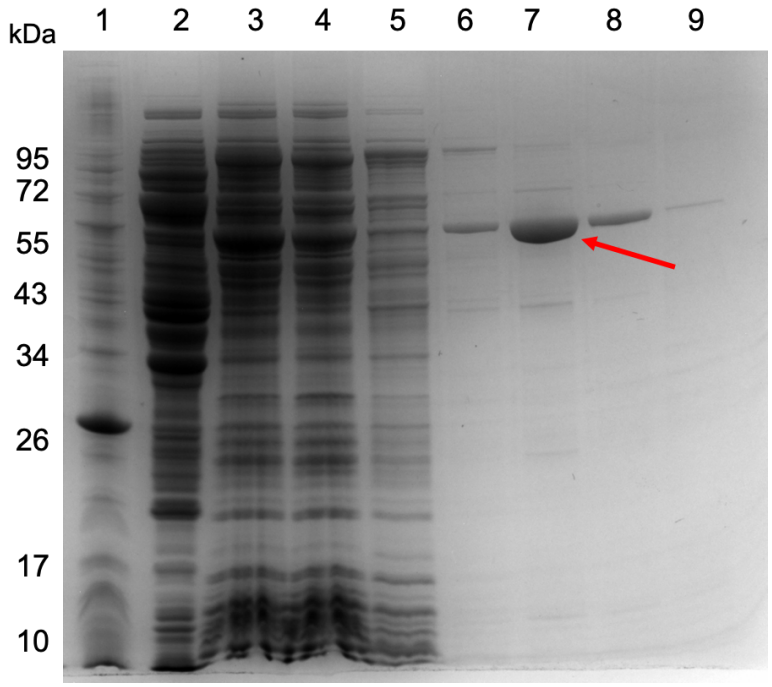


Figure 6-15. Coomassie stained gel showing MBP-MroQ purification. Lane 1: unextracted cell pellet, Lane 2: cytosolic fraction, Lane 3: soluble fraction, Lane 4: flow through, Lane 5: wash 1, Lane 6: wash 2, Lane 7: elution 1, Lane 8: elution 2, Lane 9: elution 3. Samples were added to 2 x Novex Tris-Glycine SDS sample buffer and heated to 55°C for 5 min before running on a 14 % Tris-Glycine gel and visualisation with Coomassie blue staining. The red arrow indicates MBP-MroQ.

Size exclusion chromatography was carried out to remove small contaminants such as proteases which may break down MBP-MroQ. As shown in **Figure 6-16**, a peak was observed at 62.10 representing MBP-MroQ. Fractions 10-17 were collected and run on a 14% Tris-Glycine gel and stained with Coomassie blue (**Figure 6-17**). The purity of the MBP-MroQ purification was confirmed by SEC and contaminating bands decreased in concentration after SEC as shown in **Figure 6-17**. The smaller bands present on the Coomassie gel may be breakdown products caused

by the running of the denaturing gel. Fractions 11 to 16 were spin concentrated and the concentration determined using a NanoDrop spectrophotometer.

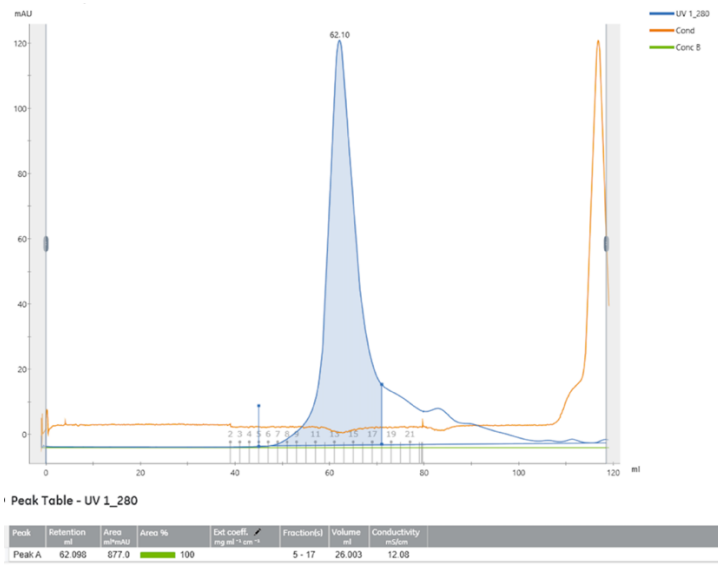


Figure 6-16. Size exclusion chromatography peak from AKTApure.

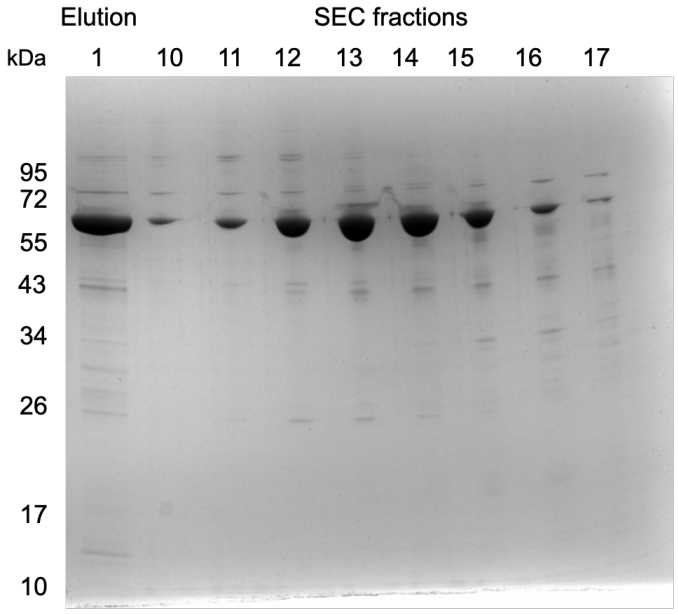


Figure 6-17. Coomassie stained gel of MBP-MroQ purification after size exclusion chromatography. Elution 1 was from purification before SEC. Fractions 10-17 were collected from the AKTApure.

6.9 AIP-1 production with purified AgrB1 and MroQ

MroQ was added to purified AgrB1, 2 μM T7-AgrD1 and DOPG to determine if mature AIP-1 could be synthesised. AgrB1 and T7-AgrD1 were both added at 2 μM as previously and MroQ was added at 0.2 μM, 2 μM and 10 μM. Reactions were incubated at 37°C for 2 h.

As shown in **Figure 6-18** (a), AIP-1 was produced on addition of MroQ. An equimolar concentration of AgrB1, T7-AgrD1 and MroQ produced the most AIP-1. Additionally, AgrB1D1 complex formation decreased with increasing concentration of MroQ (**Figure 6-18**, a). This is due to the turnover of AgrD1 and release from AgrB1 facilitated by MroQ which leads to a reduction in AgrB1D1 complex.

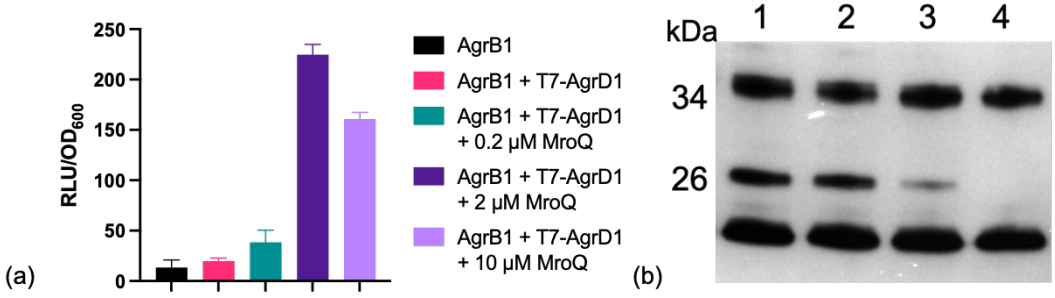


Figure 6-18. AIP-1 production and AgrB1D1 complex formation with purified AgrB1 and T7-AgrD1 with increasing concentrations of MroQ. (a) Samples were added to *S. aureus* ROJ143 as described previously and OD_{600} and bioluminescence read in a Tecan plate reader after 4 h incubation at 37°C. Data represent three technical repeats with error bars showing standard deviation. (b) Western blot against AgrB. Samples were purified AgrB1 incubated with T7-AgrD1 and MroQ at increasing concentrations as follows; Lane 1, 0 μM, Lane 2, 0.2 μM, Lane 3, 2μM, Lane 4, 10 μM. Samples were added to 2 x Novex Tris-Glycine SDS sample buffer and heated to 55°C for 5 min before running on a 14 % Tris-Glycine gel. The gel was transferred to PVDF and probed with AgrB nanobody 2ABE10.

N-acetyl-S-farnesyl-L-cysteine (AFC), the minimal analogue of farnesylated peptides, is a CAAX protease inhibitor, shown to inhibit CAAX proteases such as Rce1, a prenyl endopeptidase first identified in *Saccharomyces cerevisiae* (187). As MroQ is a putative CAAX protease, AFC was added to determine if CAAX protease activity is essential for processing of AgrD1. In the presence of AFC, AIP-1 production was measured using LC-MS and bioreporter *S. aureus* ROJ143. As shown in **Figure 6-19** (b), AIP-1 production was slightly lower with the addition of 20 or 100 μM AFC as detected using *S. aureus* ROJ143. However, no difference in AIP-1 production was observed in the presence or absence of AFC when detected using LC-MS **Figure 6-19** (a). Additionally, as shown in **Figure 6-20**, there was no difference in AgrBD complex formation in the presence of AFC. If MroQ was inhibited by AFC, an increase in the presence of AgrBD intermediate would be expected to be detected as less AgrD would be turned over to form mature AIP-1 when MroQ is inhibited. This implies that either the CAAX protease activity is not required for MroQ driven proteolysis or that AFC is ineffective against MroQ.

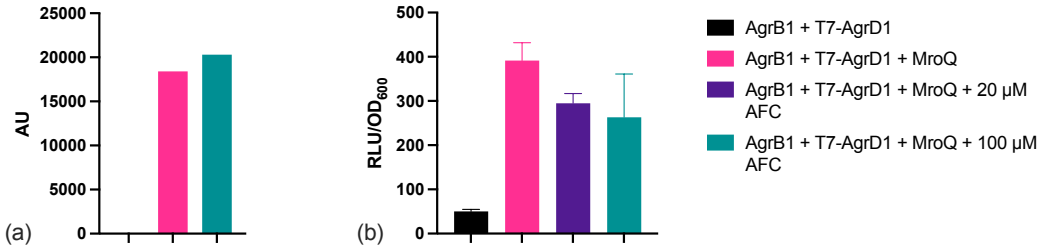


Figure 6-19. AIP-1 production from purified AgrB1 with T7-AgrD1 and MroQ in the presence of AFC characterized using (a) LC-MS and (b) *S. aureus* ROJ143. LC-MS arbitrary units represent relative AIP-1 concentration compared to an AIP-1 control. Samples were added to *S. aureus* ROJ143 as described previously and OD_{600} and bioluminescence read in a Tecan plate reader after 3.5 h incubation at 37°C. Data represent three technical repeats and two biological repeats with error bars showing standard deviation. The experiment was repeated twice.

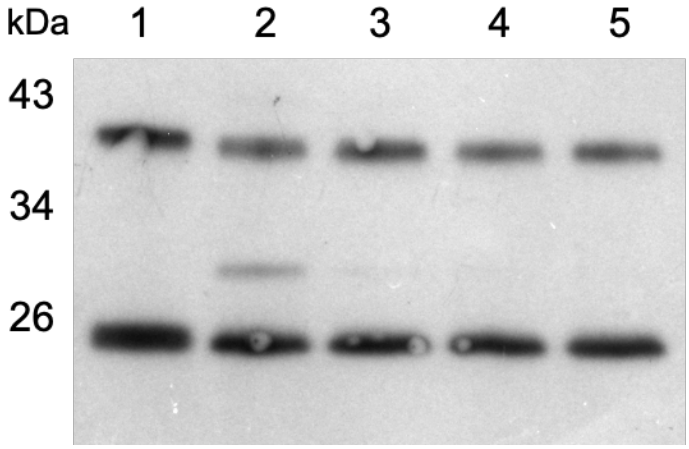


Figure 6-20. AgrBD complex formation with purified AgrB1, T7-AgrD1 and 2 μM MroQ in the presence of AFC. Samples are purified AgrB1 incubated with T7-AgrD1, MroQ and AFC as follows; Lane 1: AgrB1, Lane 2: AgrB1 + T7-AgrD1, Lane 3: AgrB1 + T7-AgrD1 + MroQ, Lane 4: AgrB1 + T7-AgrD1 + MroQ + 20 μM AFC, Lane 5: AgrB1 + T7-AgrD1 + MroQ + 100 μM AFC. Samples were added to 2 x Novex Tris-Glycine SDS sample buffer and heated to 55°C for 5 min before running on a 14 % Tris-Glycine gel. The gel was transferred to PVDF and probed with AgrB nanobody 2ABE10.

6.10 Analysis of the processing of T7-AgrD1 by AgrB1 and MroQ

To establish the processing of T7-AgrD1 by AgrB1 and MroQ, samples were run on a 16% Tricine gel and transferred to PVDF before Western blot with T7 antibody. The T7 tag is at the N-terminus of AgrD so this will give insight into the cleavage of AgrD.

As shown in Figure 6-21, a band was detected at ~25 kDa in Lane 3, this is indicated by a red arrow. This represents the AgrB1D1 complex which is detected when T7-AgrD1 is incubated with purified AgrB1. This band was lost in the presence of MroQ which confirms the loss of visualisation of the AgrB1D1 complex on the AgrB nanobody Western (**Figure 6-20**).

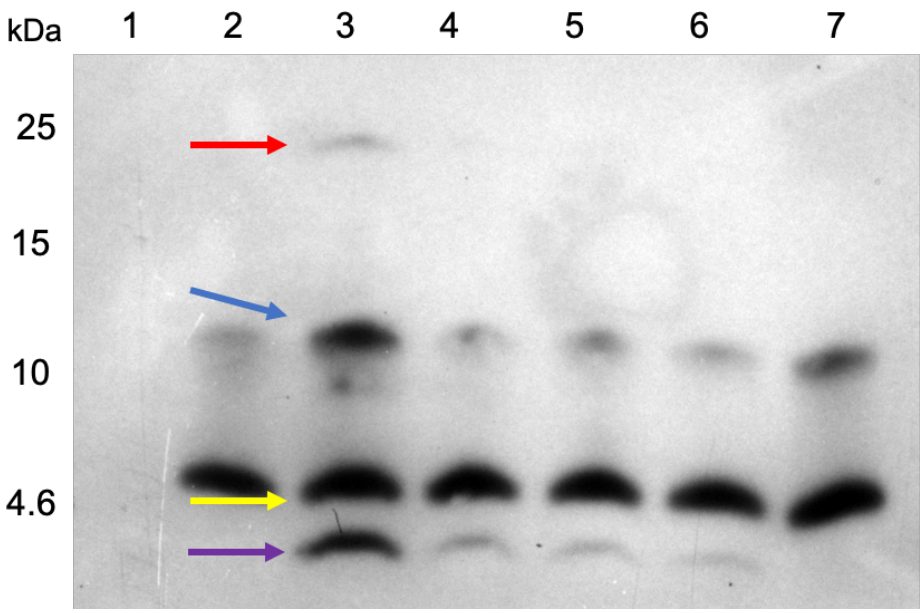


Figure 6-21. Processing of T7-AgrD1 by AgrB1 and MroQ. Samples are purified AgrB1 incubated with T7-AgrD1, MroQ and AFC as follows; Lane 1: AgrB1, Lane 2: T7-AgrD1, Lane 3: AgrB1 + T7-AgrD1, Lane 4: AgrB1 + T7-AgrD1 + MroQ, Lane 5: AgrB1 + T7-AgrD1 + MroQ + 20 μM AFC, Lane 6: AgrB1 + T7-AgrD1 + MroQ + 100 μM AFC, Lane 7: MroQ + T7-AgrD1. Samples were added to 2 x Novex Tricine SDS sample buffer and heated to 55°C for 5 min before running on a 16 % Tricine gel. The gel was transferred to PVDF and probed with T7 antibody linked to HRP. The red arrow indicates AgrB1D1 complex, the blue arrow indicated T7-AgrD1 aggregate, the yellow arrow represents T7-AgrD1 and the purple arrow represents C-terminally cleaved T7-AgrD1.

Cleavage of T7-AgrD1 by AgrB1 can be observed in Lane 3 of **Figure 6-21**, this is represented by two bands ~4.6 kDa, marked with a yellow arrow and purple arrow. The upper band represents unprocessed T7-AgrD1 and the lower band represents C-terminally cleaved T7-AgrD1. This demonstrates that AgrB1 is performing C-terminal cleavage of T7-AgrD1. The concentration of the AgrD cleavage product decreases in the presence of MroQ. This is due to the turnover of this intermediate by MroQ to form

mature AIP as detected with bioreporter *S. aureus* ROJ143 (Figure 6-19). No cleavage is observed in the absence of AgrB (Lane 7), this represents the inability of MroQ to cleave full length AgrD1. The bands observed at ~12 kDa, indicated with a blue arrow in lane 3, represent aggregates of T7-AgrD1.

6.11 AIP-1 production from MroQ with N-terminal AgrD1

In the previous chapter, in section 5.9 it was shown that AgrB1 was unable to recognise and process synthetic AgrD1 which is lacking the C-terminus. The role of AgrB is to recognise and cleave the AgrD1 C-terminus and in this chapter, it has been demonstrated that MroQ is necessary and sufficient for further processing of AgrD1 to form mature AIP-1 in a cell free protein system. In section 6.10 it was also shown that MroQ was unable to cleave full length AgrD1. Therefore, we hypothesise that AgrD1 lacking the C-terminus is the substrate for MroQ.

MroQ was incubated with linear alpha-AgrD1 which lacks the C-terminus and samples were tested for AIP-1 production using *S. aureus* ROJ143 and LC-MS. As shown in Figure 6-22, AIP-1 was detected by bioreporter and LC-MS when AgrD1 lacking the C-terminus (alfa-AgrD1) was incubated with MroQ. This shows MroQ was able to cleave the N-terminus of truncated AgrD. However, the alfa-AgrD peptide is linear, with no thiolactone ring. Therefore, it is surprising that AIP-1 was able to activate the bioreporter (**Figure 6-22**, a) as the thiolactone ring is essential for AIP activity. It is also surprising that AIP-1 was detectable by LC-MS (**Figure 6-22**, b).

MroQ was expected to cleave the N-terminus however the peptide will still be linear, not containing the thiolactone which is present in AIP-1. When the peptide was acquired from Peptide Synthetics, the company had attempted to form the thiolactone ring but were unsuccessful. The reason for the detection of AIP-1 could be that part of the peptide had formed the

thiolactone ring meaning that on cleavage of the N-terminus by MroQ, AIP-1 was produced. Additionally, MroQ may facilitate thiolactone ring formation. This data shows that MroQ was able to cleave the N-terminus of the truncated peptide but not the full-length peptide.

A higher level of AIP-1 was detected using the bioreporter when AgrB was present (**Figure 6-22**, a). This is because AgrB was able to form the thiolactone in the linear peptide before N-terminal cleavage and release of mature AIP-1. No bioreporter activation was observed with the alfa-AgrD peptide on its own showing that N-terminal cleavage by MroQ is essential for AIP formation. Additionally, no bioreporter activation was observed with AgrB and truncated AgrD showing that AgrB is unable to perform N-terminal cleavage.

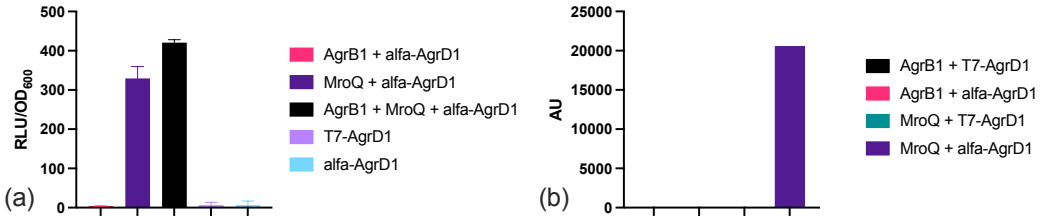


Figure 6-22. AIP-1 production from purified MroQ and AgrB1 with alfa-AgrD1 characterized using (a) *S. aureus* ROJ143 and (b) LC-MSLC-MS arbitrary units represent relative AIP-1 concentration compared to an AIP-1 control. Samples were added to *S. aureus* ROJ143 as described previously and OD_{600} and bioluminescence read in a Tecan plate reader after 3.5 h incubation at 37°C. Data represent three technical repeats and two biological repeats with error bars showing standard deviation. The experiment was repeated twice.

6.12 Discussion and conclusions

Ambuic acid is a known AgrB inhibitor however the mechanism of action is unknown (107, 113). It was noted in section 6.3 that ambuic acid can inhibit

AgrBD intermediate formation *in vitro* in *E. coli* membranes. It was also noted that, addition of up to 200 μM ambuic acid to *E. coli* membranes with AgrB1 and T7-AgrD1 increased mature AIP-1 production. In section 6.7 we showed that this phenomenon was not observed with purified AgrB1 incubated with T7-AgrD1 in synthetic lipid in the presence of ambuic acid. This shows that this was an unanticipated side effect due to using *E. coli* as an expression host and may be due to interaction of ambuic acid with other proteases in the *E. coli* membrane. This could be investigated further by testing the effect of ambuic acid on AIP-1 production with the AgrB triple lysine mutant created in section 5.15. This mutant showed no decrease in AgrBD complex formation but did show reduced AIP production. We hypothesise that this mutant retains AgrB catalytic activity, but AIP production is prevented due to inhibition of AIP processing after cleavage by AgrB. If addition of ambuic acid to this mutant increased AIP production, it may demonstrate that ambuic acid is affecting AgrD processing by interaction with another protease.

Ambuic acid analogues were synthesised by Dr James Reekes and Dr Leonardo Baldessare. These were synthesised both to try and increase potency and to elucidate the mechanism of action of ambuic acid. Ambuic acid has an epoxy moiety which is shared with other known cysteine protease inhibitors. A proposed mechanism of action of ambuic acid is the covalent interaction of the epoxide electrophilic centre with AgrB, irreversibly alkylating the active cysteine residue, resulting in loss of activity (186). JWR229 has replacement of the epoxide centre with a cyclopropyl ring. The lack of inhibition of AgrBD intermediate formation and AIP biosynthesis in this model with this analogue suggests that the covalent interaction is necessary for inhibition of AgrB. It was shown previously that JWR229 reduced AIP formation in *S. aureus* cells (186). The disparity in these results could be due to the differences analysing these compounds in *S. aureus* cells and in *E. coli* membranes. Analysis in a system employing the purified

proteins will give better insights into the interactions of ambuic acid analogues and AgrB. This was not performed here due to limitations on the quantity of analogue compounds available.

The mechanism of action of each of the compounds appears to be different which gives interesting insights into the moieties required for inhibition of AgrBD interactions. Of interest is the inhibition of AgrB dimerization in *E. coli* membrane fractions by LB276 and LB286. Inhibition of dimerization of purified AgrB was also observed with LB276. This implies that these analogues have a different mechanism of action to ambuic acid. AgrB oligomerisation is thought to be necessary for AgrD processing and, as outlined in Chapter 4, protein modelling work indicates that two copies of AgrB are necessary for the correct positioning of AgrD for cleavage (72).. Therefore, inhibition of oligomerisation of AgrB by these compounds may prevent the correct positioning of AgrD for cleavage meaning that production of mature AIP is inhibited

To investigate Agr protein interactions without interfering proteases present in *E. coli* membranes, AgrB1 was purified. Purified AgrB1 was shown to be able to form a complex with T7-AgrD1 in the presence of DOPG lipid, and to be able to cleave the AgrD1 C-terminus, however mature AIP-1 was not formed. This is consistent with the knowledge that another protease performs N-terminal cleavage of AgrD to form mature AIP. Originally it was hypothesised that SpsB performs N-terminal cleavage of AgrD outside the cell releasing mature AIP (73). Recent studies have, however argued against a major role for SpsB in N-terminal cleavage instead putting forward a different protease, MroQ, for this role (69). Indeed, here it was demonstrated that incubation of purified AgrB1, T7-AgrD1 and MroQ in the presence of synthetic lipid was sufficient for mature AIP-1 production (section 6.9). Moreover, the addition of MroQ to this reaction caused a reduction in AgrB1D1 complex formation detected by Western blot. This

demonstrated the ability of MroQ to facilitate the release of AgrD1 from AgrB1 and to catalyse N-terminal cleavage and links the release of AgrD1 from AgrB1 to the cleavage of the N-terminus (**Figure 6-23**). This confirms what was reported by Zhao et al who showed that MroQ was able to cleave the AgrD thiolactone, recognising the AgrD linker motif to release mature AIP (69).

MroQ is a putative CAAX protease however addition of AFC, a CAAX protease inhibitor did not have any apparent effect on MroQ proteolysis. AFC could be ineffective against MroQ however this could also imply that MroQ has a different mechanism of action for cleavage of the N-terminus of AgrD. This corresponds with what Cosgriff et al. suggested. They noted that conserved active site residues in MroQ are important for it's activity, which is not observed in other CAAX proteases. They hypothesised that MroQ may act differently to other CAAX proteases and may act more similarly to proteases which perform intramembrane proteolysis (74).

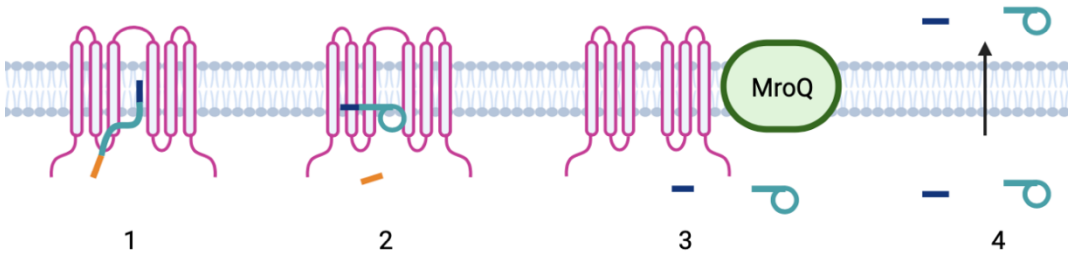


Figure 6-23. Schematic of processing of AgrD by AgrB and MroQ. 1: AgrD associates with AgrB in the membrane and the N-terminus inserts to the membrane. 2: AgrB cleaves AgrD C-terminus and the thiolactone ring is formed giving the enzyme bound intermediate. 3: MroQ catalyses cleavage of the N-terminus and release of AgrD from AgrB. 4: AgrD N-terminus and AIP leave the cell. Step 4 may occur before or in tandem with step 3.

Overall, this outlines clear steps in the AgrD processing pathway of C-terminal cleavage followed by thiolactone ring formation and the formation

of the AgrBD intermediate. The presence of MroQ then facilitates removal of AgrD from AgrB and N-terminal cleavage releasing mature AIP. This is outlined in **Figure 6-23**. Here this has been performed in a cell free model therefore no insight is given into the export of AIP from the cell however one theory is that an AgrB-MroQ complex processes AgrD within the membrane before it's passive diffusion outside the cell (76). More work must be done to characterise the interaction between AgrB and MroQ to confirm this hypothesis.

7. Summary and Future Directions

S. aureus is able to cause infection due to the production of a range of tightly controlled virulence factors. Due to the emergence and clinical significance of antibiotic resistant strains of *S. aureus* alternative therapies are being investigated (33). One method is through the attenuation of the virulence of the bacterium through interfering with virulence factor production controlled by *agr* quorum sensing. Attenuation of the virulence of the bacteria will not inhibit growth or kill the bacteria therefore will provide less selective pressure for resistance to emerge (15, 46). To be able to design inhibitors and screen for these it is important to have reporters to monitor *agr* activation and inhibition. Additionally, it is important to have a good understanding of the mechanisms behind the *agr* quorum sensing system. In this thesis, the development of reporters for *agr* QS has been demonstrated as well as an investigation into the production of the signalling molecule, AIP.

7.1 Development of *agr* QS reporters

In this study, it was shown that *Gaussia* luciferase, a naturally secreted luciferase from *Gaussia princeps*, can be expressed in *S. aureus* and used as a secreted bioreporter for *agr* QS. It was also shown that NanoLuc, from *Oplophorus gracilirostris,* can be expressed in *S. aureus* and used as a reporter for *agr* QS. This is the first report of either of these luciferases being used in *S. aureus.*

It was demonstrated here that GLuc can be used to quantitatively report on temporal *agr* activation as well as *agr* inhibition. As the GLuc signal has been reported previously not to accumulate over time *in vivo* we propose that this could be useful as a reporter for *agr* activation and inhibition in animal models of infection (143). Bacterial luciferases are often used to screen for *agr* system inhibitors *in vitro* and *in vivo* (109, 162). It has, however, been demonstrated that *agr* inhibitors can interfere with the *lux* signal giving false results (152, 163). The GLuc reporter has been shown

here to be useful for monitoring *agr* activation therefore we recommend this as an alternative reporter or counter screen for *agr* inhibitors enabling the removal of false positive or negative results.

The *agr*P3-GLuc reporter represented an excellent candidate for trialling in mouse models of infection. It is secreted efficiently from the *S. aureus* cell and has been demonstrated previously to be useful as an *ex vivo* reporter in mouse models (137, 143, 146, 172). This reporter would give real-time information on *agr* activation and inhibition which is essential in the design of inhibitors. Developing this reporter for use in *S. aureus* would inform on the timing of *agr* activation with respect to the infection stage and when or if inhibition of *agr* QS is appropriate as a therapy.

NanoLuc was also developed as a reporter for *agr* quorum sensing. This has a number of advantages over GLuc as outlined in the introduction however was not secreted as efficiently. The purpose of this work was to develop secreted reporters for *agr* activation to use as *ex vivo* reporters for *in vivo* processes. It is also useful, however, to develop intracellular luciferases, these are useful for *in vivo* imaging which can be used to localise infection (148). We have established that NanoLuc is expressed and functional in *S. aureus* in response to *agr* activation. It could, therefore, be beneficial to develop NanoLuc as an intracellular reporter for *agr* activation. NanoLuc has been shown previously to be useful for *in vivo* bioluminescence-based imaging therefore has the potential to be used in this way as a reporter for *agr* activation (149). This would give information on the spatial localisation of *agr* activation and inhibition within an infection site which could be used alongside temporal activation information from the secreted GLuc reporter.

Overall, the use of two novel bioluminescent reporters for monitoring *agr* QS *in vitro* has been demonstrated. These could both be developed further for

in vivo studies. This will give valuable insights into the timing of *agr* activation and whether *agr* QS inhibitors could be used as therapies against *S. aureus* infections.

7.2 AgrB oligomerization and AgrBD interactions

In this thesis, in chapter 4 evidence was provided for AgrB1 multimerization. This was demonstrated through protein modelling data from Dr. Boyan Bonev and through the use of novel bioluminescence-based techniques in *E. coli* and *S. aureus* cells. This confirmed what reported by Thoendel et al. (72) and Wang et al. (68) *in vitro*. The function this dimer has in AgrD1 processing, however, is still to be elucidated. Thoendel et al. predicted that an oligomer of AgrB forms a pore which is used for export of AIP from the cell (72). Protein modelling data from Dr Bonev also demonstrated the formation of a water channel across the membrane within an AgrB dimer in the presence of an AgrD propeptide. This implies that the AgrB1 oligomer could potentially have functionality in the transfer of AgrD across the membrane.

AgrB oligomerization can be observed on SDS-PAGE gels and on Western blots against AgrB, for example in **Figure 6-10** and **Figure 6-11**. These AgrB aggregates on an SDS gel may have been thought to be an artefact of the running of the gel. Proof of AgrB oligomerization in live cells, however, suggests these are not. Further work is required to determine how many monomers of AgrB aggregate in live cells in membranes and whether this oligomerization is essential for the processing of AgrD.

In this work, AgrBD complex formation has been shown to be an essential step in AIP production. Complex formation is usually displayed in the monomer at ~26 kDa however it is also observed in the dimer. Protein modelling data suggests that one monomer of AgrB in a dimer is responsible for pro-peptide insertion and docking of AgrD in the correct orientation for

catalytic processing by another AgrB monomer. The AgrBD intermediate observed at the size of a monomer could represent AgrD in complex with the catalytic monomer of AgrB as the monomer responsible for orienting the peptide has been removed due to the reducing nature of the gel. This supports the hypothesis that the function of the AgrB dimer could be to correctly position AgrD for processing.

In Chapter 5 section 5.15, site specific mutations were made in AgrB to identify residues which are essential for AgrBD complex formation. This work could be taken forward with site specific mutants used in the NanoBiT assay. This could be used to support protein modelling work to identify amino acids which are essential for both AgrB oligomerization and AgrBD complex formation. For example, mutation of lysines 129-131 in the NanoBiT assays would inform if these residues are essential for dimerization or for the interaction of AgrB with the AgrD C-terminus.

The AgrBD intermediate has been shown to be very stable in this work and previously by Thoendel et al. (67). This could be exploited for crystallization of AgrB as currently there is no structure available. Crystallization of membrane proteins can be difficult due to the extraction of the protein from it's native phospholipid environment and placement in detergents which is essential for crystallization (188). Having the protein in complex with a peptide partner may stabilise its structure and therefore assist in crystallization attempts. Elucidation of the structure of AgrB or AgrD would give further insights into the mechanisms of AIP processing and would enable the design of inhibitors through analysis of structural relationships.

The formation and detection of an AgrBD intermediate was probed in the presence of ambuic acid and a number of analogues. Of interest was the activity of LB276 and LB286. These both appeared to inhibit AgrB dimerization as well as AgrBD interactions. This hints that the mechanism

of action of these compounds could be to prevent AgrB dimerization which prevents association of AgrD. This would corroborate the protein modelling data which suggests that two monomers of AgrB are essential for the correct docking of AgrD to AgrB. To test this hypothesis these compounds should be tested for inhibition of AgrB dimerization in the NanoBRET or NanoBiT assays developed in Chapter 4.

In this work it has been shown that MroQ can perform N-terminal cleavage of AgrD1, releasing it from AgrB1 and producing mature AIP-1. This provides evidence for a role of MroQ in the maturation of AIP-1. Interestingly, it has been reported previously that MroQ is essential for the production of AIP-1 and AIP-2 but not AIP-3 (69, 76). MroQ is conserved in all sequence variants, therefore it is thought that the differences in the linker region between the AgrD N-terminus and AIP region are what dictates the *agr* group cleavage specificity (69, 76). AgrD3 has a positively charged arginine in this region which is in the place of isoleucine or valine in other groups. This is thought to be essential for recognition and cleavage by MroQ although the mechanism of action of MroQ is unknown (69). There must be another, as yet unidentified protease which is responsible for the cleavage of the N-terminus of AgrD3. Zhao et al. (69) hypothesised that AgrD3 may interact with the membrane differently from the other subgroups which may lead to processing via a different pathway. We have shown, however, that AgrD3 is able to interact with AgrB1 at the membrane and be processed to form AIP-3. This indicates that it is able to interact with the membrane in a similar way to AgrD1. More work must be done here to identify other proteases involved in the processing of AgrD3.

Finally, the mechanism of transport of AIP and N-terminal AgrD across the membrane is still unknown. It has been hypothesised by Zhao et al. (69) that the AgrD substrate may enter the MroQ active size from the extracellular side meaning cleavage releases AIP directly outside the cell. This means

that AgrD with the N-terminus must be transported across the cell prior to cleavage. Another proposed mechanism of transport involves cleavage of AgrD inside the cell and active or passive transport of mature AIP and N-terminal AgrD across the membrane. Further work must be done to identify the interactions between AgrB, MroQ and AgrD. This could include direct binding assays such as thermal shift assays or development of further *in vivo* assays such as NanoBiT to identify interactions between AgrB and MroQ. This will give insights into the transport of AIP across the membrane and the mechanism of action of MroQ. Knowledge and understanding of how these proteins interact and function will aid in the design of alternative therapies to use against *S. aureus* infections.

7.3 Development of screening pathway for AgrB inhibitors

As outlined in this thesis, the inhibition of *agr* QS is a potential antivirulence strategy to control *S. aureus* infections. Inhibition of the biosynthesis of AIP through targeting AgrB is one way in which the *agr* system can be controlled and design of AIP biosynthesis inhibitors is facilitated by research into the processing of AgrD. Currently the only known AgrB inhibitor is the natural product ambuic acid however the methods described in this thesis could be developed further for the screening of AgrB inhibitors. A flow diagram outlining a proposed screening pathway is shown in **Figure 7-1**.

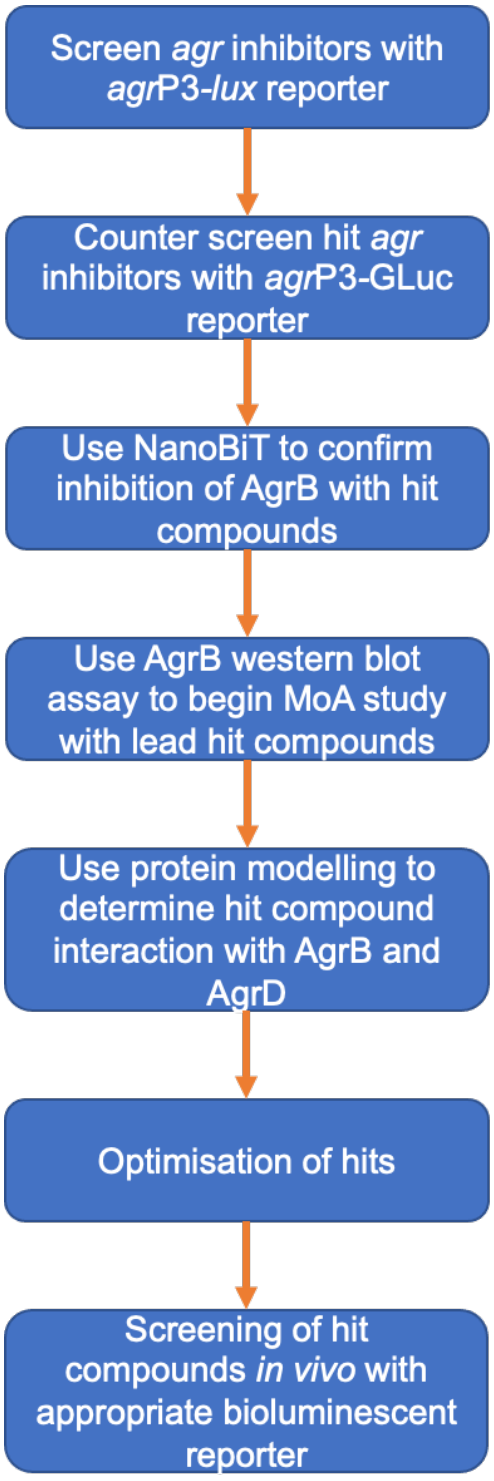


Figure 7-1. Flow chart demonstrating screening pathway for AgrB inhibitors using methods developed in this thesis.

Potential AgrB inhibitor compounds could be initially screened using cell-based assays with an *agr*P3-*lux* based reporter. This has been used previously and would identify compounds which inhibit *agr* signalling in *S. aureus* cells. Hit compounds would then be used in an orthogonal screen using the *agr*P3-GLuc reporter, the development and validation of which is described in Chapter 3 of this thesis. This would remove any false positive results and would validate hits which inhibit *agr* QS in *S. aureus*.

The NanoBiT assay described in Chapter 4 of this thesis could then be used to screen hit compounds. This would determine if the compounds inhibit the interaction between AgrB and AgrD or if they interfere with AgrB oligomerisation. This will begin the elucidation of the mechanism of action of the compounds.

Hit compounds which are shown to inhibit AgrBD interactions can then be tested for the ability to inhibit AgrB recognition of AgrD using Western blot against AgrB as detailed in Chapter 5. This will inform on whether the compounds inhibit recognition of AgrD or whether they act at a later stage in the AIP processing pathway, giving further insight into the mechanism of action.

Protein modelling could also be used to simulate the docking of the compound to the AgrBD complex. This would inform on the mechanism of action of the compound. If crystallization of AgrB was successful, this would be useful in modelling to give more accurate predictions of the molecular dynamics. Information from protein modelling can then give insights into optimisation of the hit inhibitor compounds.

Finally, once hit compounds have been optimised, lead hit compounds could be used in *in vivo* studies using murine models of *S. aureus* infection with bioluminescent reporter strains. The *agr*P3-GLuc reporter strain can be

used as a secreted reporter to monitor real time inhibition of *agr* QS. As well as this an *agr*P3-*lux* reporter or the *agr*P3-NanoLuc reporter described in Chapter 3 can be used as an intracellular reporter for imaging of the infection site. This will give information on the real time and spatial inhibition of *agr* and will help determine if the compounds could have potential use clinically.

Overall, this outlines a potential screening pathway which could be used to identify inhibitors of the biosynthesis of AIP through inhibition of AgrB processing of AgrD. These could have applications as alternative therapies against *S. aureus* infections.

8. References

1. Sengupta S, Chattopadhyay MK, Grossart HP. The multifaceted roles of antibiotics and antibiotic resistance in nature. Frontiers in Microbiology. 2013;4:47.

2. Martinez JL, Baquero F. Emergence and spread of antibiotic resistance: setting a parameter space. Upsala Journal of Medical Sciences. 2014;119(2):68-77.

3. Ventola CL. The antibiotic resistance crisis: part 1: causes and threats. P t. 2015;40(4):277-83.

4. Gould K. Antibiotics: from prehistory to the present day. Journal of Antimicrobial Chemotherapy. 2016;71(3):572-5.

5. Spellberg B, Gilbert DN. The future of antibiotics and resistance: a tribute to a career of leadership by John Bartlett. Clinical Infectious Diseases. 2014;59 Suppl 2:S71-5.

6. Gordon CP, Williams P, Chan WC. Attenuating *Staphylococcus aureus* virulence gene regulation: a medicinal chemistry perspective. Journal of Medicinal Chemistry. 2013;56(4):1389-404.

7. Clatworthy AE, Pierson E, Hung DT. Targeting virulence: a new paradigm for antimicrobial therapy. Nature Chemical Biology. 2007;3(9):541-8.

8. Aminov RI. A brief history of the antibiotic era: lessons learned and challenges for the future. Frontiers in Microbiology. 2010;1:134.

9. Asokan GV, Ramadhan T, Ahmed E, Sanad H. WHO Global Priority Pathogens List: A Bibliometric Analysis of Medline-PubMed for Knowledge Mobilization to Infection Prevention and Control Practices in Bahrain. Oman Medical Journal. 2019;34(3):184-93.

10. Tong SY, Davis JS, Eichenberger E, Holland TL, Fowler VG, Jr. *Staphylococcus aureus* infections: epidemiology, pathophysiology, clinical manifestations, and management. Clinical Microbiology Reviews. 2015;28(3):603-61.

11. Novick RP. Autoinduction and signal transduction in the regulation of staphylococcal virulence. Molecular Microbiology. 2003;48(6):1429-49.
12. Queck SY, Jameson-Lee M, Villaruz AE, Bach TH, Khan BA, Sturdevant DE, Ricklets S, Otto M. RNAIII-independent target gene control by the *agr* quorum-sensing system: insight into the evolution of virulence regulation in *Staphylococcus aureus*. Molecular Cell. 2008;32(1):150-8.
13. Bhattacharya M, Wozniak DJ, Stoodley P, Hall-Stoodley L. Prevention and treatment of *Staphylococcus aureus* biofilms. Expert Review of Anti Infective Therapy. 2015;13(12):1499-516.
14. Frank DN, Feazel LM, Bessesen MT, Price CS, Janoff EN, Pace NR. The human nasal microbiota and *Staphylococcus* aureus carriage. PLoS One. 2010;5(5):e10598.
15. Otto M. Quorum-sensing control in Staphylococci -- a target for antimicrobial drug therapy? FEMS Microbiology Letters. 2004;241(2):135-41.
16. Bronner S, Monteil H, Prevost G. Regulation of virulence determinants in *Staphylococcus aureus*: complexity and applications. FEMS Microbiology Review. 2004;28(2):183-200.
17. Olaniyi R, Pozzi C, Grimaldi L, Bagnoli F. *Staphylococcus aureus*-Associated Skin and Soft Tissue Infections: Anatomical Localization, Epidemiology, Therapy and Potential Prophylaxis. Current Topics in Microbiology and Immunology. 2017;409:199-227.
18. Thomas O, Ramsay A, Yiasemidou M, Hardie C, Ashmore D, Macklin C, z. The surgical management of cutaneous abscesses: A UK cross-sectional survey. Annals of Medicine and Surgery (Lond). 2020;60:654-9.
19. Kobayashi SD, Malachowa N, DeLeo FR. Pathogenesis of *Staphylococcus aureus* abscesses. The American Journal of Pathology. 2015;185(6):1518-27.
20. McGuinness WA, Malachowa N, DeLeo FR. Vancomycin Resistance in *Staphylococcus aureus*. Yale Journal of Biology and Medicine. 2017;90(2):269-81.

21. Boles BR, Horswill AR. *agr*-mediated dispersal of *Staphylococcus aureus* biofilms. PLoS Pathogens. 2008;4(4):e1000052.

22. Foster TJ. Antibiotic resistance in *Staphylococcus aureus*. Current status and future prospects. FEMS Microbiology Reviews. 2017;41(3):430-49.

23. Kavanaugh JS, Horswill AR. Impact of Environmental Cues on Staphylococcal Quorum Sensing and Biofilm Development. Journal of Biological Chemistry. 2016;291(24):12556-64.

24. Klevens RM, Morrison MA, Nadle J, Petit S, Gershman K, Ray S, et al. Invasive methicillin-resistant *Staphylococcus aureus* infections in the United States. Jama. 2007;298(15):1763-71.

25. Thurlow LR, Joshi GS, Richardson AR. Virulence strategies of the dominant USA300 lineage of community-associated methicillin-resistant *Staphylococcus aureus* (CA-MRSA). FEMS Immunology and Medical Microbiol. 2012;65(1):5-22.

26. van Hal SJ, Jensen SO, Vaska VL, Espedido BA, Paterson DL, Gosbell IB. Predictors of mortality in *Staphylococcus aureus* Bacteremia. Clinical Microbiology Reviews. 2012;25(2):362-86.

27. Salam AM, Quave CL. Targeting Virulence in *Staphylococcus aureus* by Chemical Inhibition of the Accessory Gene Regulator System In Vivo. mSphere. 2018;3(1).

28. Rae N, Jarchow-MacDonald A, Nathwani D, Marwick CA. MRSA: treating people with infection. BMJ Clinical Evidence. 2016;2016.

29. Appelbaum PC. The emergence of vancomycin-intermediate and vancomycin-resistant *Staphylococcus aureus*. Clinical Microbiology and Infection. 2006;12 Suppl 1:16-23.

30. Kirby WM. Extraction of a highly potent penicillin inactivator from penicillin resistant Staphylococci. Science. 1944;99(2579):452-3.

31. Rammelkamp CH, Maxon T. Resistance of *Staphylococcus aureus* to the Action of Penicillin. Proceedings of the Society for Experimental Biology and Medicine. 1942;51(3):386-9.

32. Peacock SJ, Paterson GK. Mechanisms of Methicillin Resistance in *Staphylococcus aureus.* Annual Review of Biochemistry. 2015;84:577-601.
33. Lowy FD. Antimicrobial resistance: the example of *Staphylococcus aureus*. Journal of Clinical Investigation. 2003;111(9):1265-73.
34. Hartman BJ, Tomasz A. Low-affinity penicillin-binding protein associated with beta-lactam resistance in *Staphylococcus aureus*. Journal of Bacteriology. 1984;158(2):513-6.
35. Utsui Y, Yokota T. Role of an altered penicillin-binding protein in methicillin- and cephem-resistant *Staphylococcus aureus*. Antimicrobial Agents and Chemotherapy. 1985;28(3):397-403.
36. Cong Y, Yang S, Rao X. Vancomycin resistant *Staphylococcus aureus* infections: A review of case updating and clinical features. Journal of Advanced Research. 2020;21:169-76.
37. Kim C, Milheiriço C, Gardete S, Holmes MA, Holden MT, de Lencastre H, et al. Properties of a novel PBP2A protein homolog from *Staphylococcus aureus* strain LGA251 and its contribution to the β-lactam-resistant phenotype. Journal of Biological Chemistry. 2012;287(44):36854-63.
38. Long SW, Olsen RJ, Mehta SC, Palzkill T, Cernoch PL, Perez KK, et al. PBP2a mutations causing high-level ceftaroline resistance in clinical methicillin-resistant *Staphylococcus aureus* isolates. Antimicrobial agents and chemotherapy. 2014;58(11):6668-74.
39. Smith TL, Pearson ML, Wilcox KR, Cruz C, Lancaster MV, Robinson-Dunn B, et al. Emergence of vancomycin resistance in *Staphylococcus aureus*. Glycopeptide-Intermediate *Staphylococcus aureus* Working Group. The New England Journal of Medicine. 1999;340(7):493-501.
40. Chambers HF, Deleo FR. Waves of resistance: *Staphylococcus aureus* in the antibiotic era. Nature Reviews Microbiology. 2009;7(9):629-41.
41. Plumet L, Ahmad-Mansour N, Dunyach-Remy C, Kissa K, Sotto A, Lavigne JP, et al. Bacteriophage Therapy for *Staphylococcus aureus*

Infections: A Review of Animal Models, Treatments, and Clinical Trials. Frontiers in Cellular and Infection Microbiology. 2022;12:907314.

42. Clegg J, Soldaini E, McLoughlin RM, Rittenhouse S, Bagnoli F, Phogat S. *Staphylococcus aureus* Vaccine Research and Development: The Past, Present and Future, Including Novel Therapeutic Strategies. Frontiers in Immunology. 2021;12:705360.

43. Dhand A, Bayer AS, Pogliano J, Yang SJ, Bolaris M, Nizet V, et al. Use of antistaphylococcal beta-lactams to increase daptomycin activity in eradicating persistent bacteremia due to methicillin-resistant *Staphylococcus aureus*: role of enhanced daptomycin binding. Clinical Infectious Diseases. 2011;53(2):158-63.

44. Kong KF, Vuong C, Otto M. Staphylococcus quorum sensing in biofilm formation and infection. International Journal of Medical Microbiology. 2006;296(2-3):133-9.

45. Dinges MM, Orwin PM, Schlievert PM. Exotoxins of *Staphylococcus aureus.* Clinical Microbiology Reviews. 2000;13(1):16-34.

46. Wang B, Muir TW. Regulation of Virulence in *Staphylococcus aureus*: Molecular Mechanisms and Remaining Puzzles. Cell Chemical Biology. 2016;23(2):214-24.

47. Gray B, Hall P, Gresham H. Targeting *agr*- and *agr*-Like quorum sensing systems for development of common therapeutics to treat multiple gram-positive bacterial infections. Sensors (Basel). 2013;13(4):5130-66.

48. Rutherford ST, Bassler BL. Bacterial quorum sensing: its role in virulence and possibilities for its control. Cold Spring Harbor perspectives in medicine. 2012;2(11):a012427.

49. Sloan TJ, Murray E, Yokoyama M, Massey RC, Chan WC, Bonev BB, et al. Timing Is Everything: Impact of Naturally Occurring *Staphylococcus aureus* AgrC Cytoplasmic Domain Adaptive Mutations on Autoinduction. Journal of Bacteriology. 2019;201(20).

50. Traber KE, Lee E, Benson S, Corrigan R, Cantera M, Shopsin B, et al. agr function in clinical *Staphylococcus aureus* isolates. Microbiology (Reading). 2008;154(Pt 8):2265-74.

51. Novick RP, Projan SJ, Kornblum J, Ross HF, Ji G, Kreiswirth B, et al. The agr P2 operon: an autocatalytic sensory transduction system in *Staphylococcus aureus*. Molecular Genetics and Genomics. 1995;248(4):446-58.

52. Morfeldt E, Taylor Dv, Von Gabain A, Arvidson S. Activation of alpha-toxin translation in *Staphylococcus aureus* by the trans-encoded antisense RNA, RNAIII. The EMBO journal. 1995;14(18):4569-77.

53. Novick RP, Ross HF, Projan SJ, Kornblum J, Kreiswirth B, Moghazeh S. Synthesis of staphylococcal virulence factors is controlled by a regulatory RNA molecule. Embo Journal. 1993;12(10):3967-75.

54. Novick RP, Geisinger E. Quorum sensing in staphylococci. Annual Review of Genetics. 2008;42:541-64.

55. Saenz HL, Augsburger V, Vuong C, Jack RW, Götz F, Otto M. Inducible expression and cellular location of AgrB, a protein involved in the maturation of the staphylococcal quorum-sensing pheromone. Archives of Microbiology. 2000;174(6):452-5.

56. Zhang L, Gray L, Novick RP, Ji G. Transmembrane topology of AgrB, the protein involved in the post-translational modification of AgrD in *Staphylococcus aureus*. Journal of Biological Chemistry. 2002;277(38):34736-42.

57. Lina G, Jarraud S, Ji G, Greenland T, Pedraza A, Etienne J, et al. Transmembrane topology and histidine protein kinase activity of AgrC, the agr signal receptor in *Staphylococcus aureus*. Molecular microbiology. 1998;28(3):655-62.

58. Tan L, Huang Y, Shang W, Yang Y, Peng H, Hu Z, et al. Accessory Gene Regulator (agr) Allelic Variants in Cognate *Staphylococcus aureus* Strain Display Similar Phenotypes. Frontiers in Microbiology. 2022;13:700894.

59. Tal-Gan Y, Ivancic M, Cornilescu G, Cornilescu CC, Blackwell HE. Structural characterization of native autoinducing peptides and abiotic analogues reveals key features essential for activation and inhibition of an AgrC quorum sensing receptor in *Staphylococcus aureus*. Journal of the American Chemical Society. 2013;135(49):18436-44.
60. Ji G, Beavis R, Novick RP. Bacterial interference caused by autoinducing peptide variants. Science. 1997;276(5321):2027-30.
61. Paharik AE, Parlet CP, Chung N, Todd DA, Rodriguez EI, Van Dyke MJ, et al. Coagulase-Negative Staphylococcal Strain Prevents *Staphylococcus aureus* Colonization and Skin Infection by Blocking Quorum Sensing. Cell Host Microbe. 2017;22(6):746-56.e5.
62. van Leeuwen W, van Nieuwenhuizen W, Gijzen C, Verbrugh H, van Belkum A. Population studies of methicillin-resistant and-sensitive *Staphylococcus aureus* strains reveal a lack of variability in the agrD gene, encoding a staphylococcal autoinducer peptide. Journal of Bacteriology. 2000;182(20):5721-9.
63. Javdan S, Narimani T, Shahini Shams Abadi M, Gholipour A. Agr typing of *Staphylococcus aureus* species isolated from clinical samples in training hospitals of Isfahan and Shahrekord. BMC Research Notes. 2019;12(1):363.
64. Gillet Y, Issartel B, Vanhems P, Fournet JC, Lina G, Bes M, et al. Association between *Staphylococcus aureus* strains carrying gene for Panton-Valentine leukocidin and highly lethal necrotising pneumonia in young immunocompetent patients. Lancet. 2002;359(9308):753-9.
65. Sakoulas G, Eliopoulos GM, Moellering RC, Jr., Wennersten C, Venkataraman L, Novick RP, et al. Accessory gene regulator (*agr*) locus in geographically diverse *Staphylococcus aureus* isolates with reduced susceptibility to vancomycin. Antimicrobial Agents and Chemotherapy. 2002;46(5):1492-502.
66. P MD, Affas Z, Reynolds C, Holden MT, Wood SJ, Saint S, et al. Structure, activity and evolution of the group I thiolactone peptide quorum-

sensing system of *Staphylococcus aureus*. Molecular Microbiology. 2001;41(2):503-12.

67. Thoendel M, Horswill AR. Identification of *Staphylococcus aureus* AgrD residues required for autoinducing peptide biosynthesis. Journal of Biological Chemistry. 2009;284(33):21828-38.

68. Wang B, Zhao A, Novick RP, Muir TW. Key driving forces in the biosynthesis of autoinducing peptides required for staphylococcal virulence. PNAS. 2015;112(34):10679-84.

69. Zhao A, Bodine SP, Xie Q, Wang B, Ram G, Novick RP, et al. Reconstitution of the *Staphylococcus aureus* agr quorum sensing pathway reveals a direct role for the integral membrane protease MroQ in pheromone biosynthesis. PNAS. 2022;119(33):e2202661119.

70. Zhang L, Lin J, Ji G. Membrane anchoring of the AgrD N-terminal amphipathic region is required for its processing to produce a quorum-sensing pheromone in *Staphylococcus aureus*. Journal of Biological Chemistry. 2004;279(19):19448-56.

71. Qiu R, Pei W, Zhang L, Lin J, Ji G. Identification of the putative staphylococcal AgrB catalytic residues involving the proteolytic cleavage of AgrD to generate autoinducing peptide. Journal of Biological Chemistry. 2005;280(17):16695-704.

72. Thoendel M, Horswill AR. Random mutagenesis and topology analysis of the autoinducing peptide biosynthesis proteins in *Staphylococcus aureus*. Molecular Microbiology. 2013;87(2):318-37.

73. Kavanaugh JS, Thoendel M, Horswill AR. A role for type I signal peptidase in *Staphylococcus aureus* quorum sensing. Molecular Microbiology. 2007;65(3):780-98.

74. Cosgriff CJ, White CR, Teoh WP, Grayczyk JP, Alonzo F, 3rd. Control of *Staphylococcus aureus* Quorum Sensing by a Membrane-Embedded Peptidase. Infection and Immunity. 2019;87(5).

75. Marroquin S, Gimza B, Tomlinson B, Stein M, Frey A, Keogh RA, et al. MroQ is a novel Abi-domain protein that influences virulence gene

expression in *Staphylococcus aureus* via modulation of *agr* activity. Infection and Immunity. 2019;87(5):e00002-19.

76. Stock MR, Fang L, Johnson KR, Cosgriff C, Teoh WP, Alonzo F, 3rd. Characterization of MroQ-Dependent Maturation and Export of the *Staphylococcus aureus* Accessory Gene Regulatory System Autoinducing Peptide. Infection and Immunity. 2022;90(10):e0026322.

77. Schwartz K, Sekedat MD, Syed AK, O'Hara B, Payne DE, Lamb A, et al. The AgrD N-terminal leader peptide of *Staphylococcus aureus* has cytolytic and amyloidogenic properties. Infection and Immunity. 2014;82(9):3837-44.

78. Gonzalez DJ, Corriden R, Akong-Moore K, Olson J, Dorrestein PC, Nizet V. N-terminal ArgD peptides from the classical *Staphylococcus aureus* Agr system have cytotoxic and proinflammatory activities. Chemical Biology. 2014;21(11):1457-62.

79. Balaban N, Novick RP. Translation of RNAIII, the *Staphylococcus aureus agr* regulatory RNA molecule, can be activated by a 3′-end deletion. FEMS microbiology letters. 1995;133(1-2):155-61.

80. Jenul C, Horswill AR. Regulation of *Staphylococcus aureus* Virulence. Microbiol Spectr. 2019;7(2).

81. Morfeldt E, Taylor D, von Gabain A, Arvidson S. Activation of alpha-toxin translation in *Staphylococcus aureus* by the trans-encoded antisense RNA, RNAIII. Embo Journal. 1995;14(18):4569-77.

82. Huntzinger E, Boisset S, Saveanu C, Benito Y, Geissmann T, Namane A, et al. *Staphylococcus aureus* RNAIII and the endoribonuclease III coordinately regulate spa gene expression. Embo Journal. 2005;24(4):824-35.

83. McNamara PJ, Milligan-Monroe KC, Khalili S, Proctor RA. Identification, cloning, and initial characterization of *rot*, a locus encoding a regulator of virulence factor expression in *Staphylococcus aureus*. Journal of Bacteriology. 2000;182(11):3197-203.

84. Yarwood JM, Schlievert PM. Quorum sensing in *Staphylococcus* infections. Journal of Clinical Investigation. 2003;112(11):1620-5.

85. Cheng AG, DeDent AC, Schneewind O, Missiakas D. A play in four acts: *Staphylococcus aureus* abscess formation. Trends in Microbiology. 2011;19(5):225-32.

86. Pollitt EJG, Szkuta PT, Burns N, Foster SJ. *Staphylococcus aureus* infection dynamics. PLoS Pathogens. 2018;14(6):e1007112.

87. Balasubramanian D, Harper L, Shopsin B, Torres VJ. *Staphylococcus aureus* pathogenesis in diverse host environments. Pathogens and Disease. 2017;75(1).

88. Tan L, Li SR, Jiang B, Hu XM, Li S. Therapeutic Targeting of the *Staphylococcus aureus* Accessory Gene Regulator (*agr*) System. Frontiers in Microbiology. 2018;9:55.

89. Sun F, Liang H, Kong X, Xie S, Cho H, Deng X, et al. Quorum-sensing *agr* mediates bacterial oxidation response via an intramolecular disulfide redox switch in the response regulator AgrA. PNAS. 2012;109(23):9095-100.

90. Reynolds J, Wigneshweraraj S. Molecular insights into the control of transcription initiation at the *Staphylococcus aureus agr* operon. Journal of Molecular Biology. 2011;412(5):862-81.

91. Reyes D, Andrey DO, Monod A, Kelley WL, Zhang G, Cheung AL. Coordinated regulation by AgrA, SarA, and SarR to control *agr* expression in *Staphylococcus aureus*. Journal of Bacteriology. 2011;193(21):6020-31.

92. Chien Y, Manna AC, Cheung AL. SarA level is a determinant of *agr* activation in *Staphylococcus aureus*. Molecular Microbiology. 1998;30(5):991-1001.

93. Manna AC, Cheung AL. *sarU*, a *sarA* homolog, is repressed by SarT and regulates virulence genes in *Staphylococcus aureus*. Infection and Immunity. 2003;71(1):343-53.

94. Manna AC, Cheung AL. Expression of SarX, a negative regulator of *agr* and exoprotein synthesis, is activated by MgrA in *Staphylococcus aureus.* Journal of Bacteriology. 2006;188(12):4288-99.

95. Roux A, Todd DA, Velazquez JV, Cech NB, Sonenshein AL. CodY-mediated regulation of the *Staphylococcus aureus agr* system integrates nutritional and population density signals. Journal of Bacteriology. 2014;196(6):1184-96.

96. Wang J, Li H, Pan J, Dong J, Zhou X, Niu X, et al. Oligopeptide Targeting Sortase A as Potential Anti-infective Therapy for *Staphylococcus aureus.* Frontiers in Microbiology. 2018;9:245.

97. Cascioferro S, Raffa D, Maggio B, Raimondi MV, Schillaci D, Daidone G. Sortase A Inhibitors: Recent Advances and Future Perspectives. Journal of Medicinal Chemistry. 2015;58(23):9108-23.

98. Gao P, Ho PL, Yan B, Sze KH, Davies J, Kao RYT. Suppression of *Staphylococcus aureus* virulence by a small-molecule compound. PNAS. 2018;115(31):8003-8.

99. Wei B, Zhang T, Wang P, Pan Y, Li J, Chen W, et al. Anti-infective therapy using species-specific activators of *Staphylococcus aureus* ClpP. Nature Communications. 2022;13(1):6909.

100. McCormick CC, Caballero AR, Balzli CL, Tang A, O'Callaghan RJ. Chemical inhibition of alpha-toxin, a key corneal virulence factor of *Staphylococcus aureus*. Investigative Ophthalmology & Visual Science. 2009;50(6):2848-54.

101. Ford CA, Hurford IM, Cassat JE. Antivirulence Strategies for the Treatment of *Staphylococcus aureus* Infections: A Mini Review. Frontiers in Microbiology. 2020;11:632706.

102. Gao P, Davies J, Kao RYT. Dehydrosqualene Desaturase as a Novel Target for Anti-Virulence Therapy against *Staphylococcus aureus*. mBio. 2017;8(5).

103. Liu CI, Liu GY, Song Y, Yin F, Hensler ME, Jeng WY, et al. A cholesterol biosynthesis inhibitor blocks *Staphylococcus aureus* virulence. Science. 2008;319(5868):1391-4.
104. Sun F, Zhou L, Zhao BC, Deng X, Cho H, Yi C, et al. Targeting MgrA-mediated virulence regulation in *Staphylococcus aureus*. Chemical Biology. 2011;18(8):1032-41.
105. Sully EK, Malachowa N, Elmore BO, Alexander SM, Femling JK, Gray BM, et al. Selective chemical inhibition of *agr* quorum sensing in *Staphylococcus aureus* promotes host defense with minimal impact on resistance. PLoS Pathogens. 2014;10(6):e1004174.
106. Mahdally NH, George RF, Kashef MT, Al-Ghobashy M, Murad FE, Attia AS. Staquorsin: A Novel *Staphylococcus aureus agr*-Mediated Quorum Sensing Inhibitor Impairing Virulence *in vivo* Without Notable Resistance Development. Frontiers in Microbiology. 2021;12:700494.
107. Todd DA, Parlet CP, Crosby HA, Malone CL, Heilmann KP, Horswill AR, et al. Signal Biosynthesis Inhibition with Ambuic Acid as a Strategy To Target Antibiotic-Resistant Infections. Antimicrobial Agents and Chemotherapy. 2017;61(8).
108. Parlet CP, Kavanaugh JS, Crosby HA, Raja HA, El-Elimat T, Todd DA, et al. Apicidin Attenuates MRSA Virulence through Quorum-Sensing Inhibition and Enhanced Host Defense. Cell Reports. 2019;27(1):187-98.e6.
109. Wright JS, 3rd, Jin R, Novick RP. Transient interference with staphylococcal quorum sensing blocks abscess formation. PNAS. 2005;102(5):1691-6.
110. Daly SM, Elmore BO, Kavanaugh JS, Triplett KD, Figueroa M, Raja HA, et al. omega-Hydroxyemodin limits *Staphylococcus aureus* quorum sensing-mediated pathogenesis and inflammation. Antimicrobial Agents and Chemotherapy. 2015;59(4):2223-35.
111. Matsumoto M, Nakagawa S, Zhang L, Nakamura Y, Villaruz AE, Otto M, et al. Interaction between Staphylococcus *agr* virulence and neutrophils

regulates pathogen expansion in the skin. Cell Host Microbe. 2021;29(6):930-40.e4.

112. Baldry M, Kitir B, Frokiaer H, Christensen SB, Taverne N, Meijerink M, et al. The *agr* Inhibitors Solonamide B and Analogues alter Immune Responses to *Staphylococccus aureus* but do not exhibit adverse effects on Immune Cell Functions. PLoS One. 2016;11(1):e0145618.

113. Nakayama J, Uemura Y, Nishiguchi K, Yoshimura N, Igarashi Y, Sonomoto K. Ambuic acid inhibits the biosynthesis of cyclic peptide quormones in gram-positive bacteria. Antimicrobial Agents and Chemotherapy. 2009;53(2):580-6.

114. Yarwood JM, McCormick JK, Paustian ML, Kapur V, Schlievert PM. Repression of the *Staphylococcus aureus* accessory gene regulator in serum and *in viv*o. Journal of Bacteriology. 2002;184(4):1095-101.

115. Vuong C, Saenz HL, Gotz F, Otto M. Impact of the *agr* quorum-sensing system on adherence to polystyrene in *Staphylococcus aureus*. Journal of Infectious Diseases. 2000;182(6):1688-93.

116. Alksne LE, Projan SJ. Bacterial virulence as a target for antimicrobial chemotherapy. Current Opinions in Biotechnology. 2000;11(6):625-36.

117. Shopsin B, Eaton C, Wasserman GA, Mathema B, Adhikari RP, Agolory S, et al. Mutations in *agr* do not persist in natural populations of methicillin-resistant *Staphylococcus aureus.* Journal of Infectious Diseases. 2010;202(10):1593-9.

118. Paulander W, Varming AN, Bojer MS, Friberg C, Bæk K, Ingmer H. The *agr* quorum sensing system in *Staphylococcus aureus* cells mediates death of sub-population. BMC Research Notes. 2018;11(1):503.

119. Shopsin B, Drlica-Wagner A, Mathema B, Adhikari RP, Kreiswirth BN, Novick RP. Prevalence of *agr* dysfunction among colonizing *Staphylococcus aureus* strains. Journal of Infectious Diseases. 2008;198(8):1171-4.

120. Bezar IF, Mashruwala AA, Boyd JM, Stock AM. Drug-like Fragments Inhibit *agr*-Mediated Virulence Expression in *Staphylococcus aureus*. Science Reports. 2019;9(1):6786.

121. Tal-Gan Y, Ivancic M, Cornilescu G, Yang T, Blackwell HE. Highly Stable, Amide-Bridged Autoinducing Peptide Analogues that Strongly Inhibit the AgrC Quorum Sensing Receptor in *Staphylococcus aureus*. Angew Chem Int Ed Engl. 2016;55(31):8913-7.

122. Nielsen A, Månsson M, Bojer MS, Gram L, Larsen TO, Novick RP, et al. Solonamide B inhibits quorum sensing and reduces *Staphylococcus aureus* mediated killing of human neutrophils. PLoS One. 2014;9(1):e84992.

123. Peterson MM, Mack JL, Hall PR, Alsup AA, Alexander SM, Sully EK, et al. Apolipoprotein B Is an innate barrier against invasive *Staphylococcus aureus* infection. Cell Host Microbe. 2008;4(6):555-66.

124. Rothfork JM, Timmins GS, Harris MN, Chen X, Lusis AJ, Otto M, et al. Inactivation of a bacterial virulence pheromone by phagocyte-derived oxidants: new role for the NADPH oxidase in host defense. PNAS;101(38):13867-72.

125. Park S, Classen A, Gohou HM, Maldonado R, Kretschmann E, Duvernay C, et al. A new, reliable, and high-throughput strategy to screen bacteria for antagonistic activity against *Staphylococcus aureus*. BMC Microbiology. 2021;21(1):189.

126. Malone CL, Boles BR, Lauderdale KJ, Thoendel M, Kavanaugh JS, Horswill AR. Fluorescent reporters for *Staphylococcus aureus*. Journal of Microbiological Methods. 2009;77(3):251-60.

127. Avci P, Karimi M, Sadasivam M, Antunes-Melo WC, Carrasco E, Hamblin MR. *In-vivo* monitoring of infectious diseases in living animals using bioluminescence imaging. Virulence. 2018;9(1):28-63.

128. Kaskova ZM, Tsarkova AS, Yampolsky IV. 1001 lights: luciferins, luciferases, their mechanisms of action and applications in chemical

analysis, biology and medicine. Chemical Society Reviews. 2016;45(21):6048-77.
129. Hall MP, Unch J, Binkowski BF, Valley MP, Butler BL, Wood MG, et al. Engineered luciferase reporter from a deep sea shrimp utilizing a novel imidazopyrazinone substrate. ACS Chemical Biology. 2012;7(11):1848-57.
130. Yan Y, Shi P, Song W, Bi S. Chemiluminescence and Bioluminescence Imaging for Biosensing and Therapy: *In Vitro* and *In Vivo* Perspectives. Theranostics. 2019;9(14):4047-65.
131. Neefjes M, Housmans BAC, van den Akker GGH, van Rhijn LW, Welting TJM, van der Kraan PM. Reporter gene comparison demonstrates interference of complex body fluids with secreted luciferase activity. Scientific Reports. 2021;11(1):1359.
132. Hutchens M, Luker GD. Applications of bioluminescence imaging to the study of infectious diseases. Cell Microbiology. 2007;9(10):2315-22.
133. Tung JK, Berglund K, Gutekunst CA, Hochgeschwender U, Gross RE. Bioluminescence imaging in live cells and animals. Neurophotonics. 2016;3(2):025001.
134. Choy G, O'Connor S, Diehn FE, Costouros N, Alexander HR, Choyke P, et al. Comparison of noninvasive fluorescent and bioluminescent small animal optical imaging. Biotechniques. 2003;35(5):1022-6, 8-30.
135. Troy T, Jekic-McMullen D, Sambucetti L, Rice B. Quantitative comparison of the sensitivity of detection of fluorescent and bioluminescent reporters in animal models. Molecular imaging. 2004;3(1):15353500200403196.
136. He L, Binari R, Huang J, Falo-Sanjuan J, Perrimon N. *In vivo* study of gene expression with an enhanced dual-color fluorescent transcriptional timer. Elife. 2019;8.
137. Maguire CA, Deliolanis NC, Pike L, Niers JM, Tjon-Kon-Fat LA, Sena-Esteves M, et al. *Gaussia* luciferase variant for high-throughput functional screening applications. Analytical Chemistry. 2009;81(16):7102-6.

138. Rathnayaka T, Tawa M, Sohya S, Yohda M, Kuroda Y. Biophysical characterization of highly active recombinant *Gaussia* luciferase expressed in *Escherichia coli.* Biochimica et Biophysica Acta. 2010;1804(9):1902-7.
139. Tannous BA, Kim DE, Fernandez JL, Weissleder R, Breakefield XO. Codon-optimized *Gaussia* luciferase cDNA for mammalian gene expression in culture and in vivo. Molecular Therapy. 2005;11(3):435-43.
140. Wiles S, Ferguson K, Stefanidou M, Young DB, Robertson BD. Alternative luciferase for monitoring bacterial cells under adverse conditions. Applied and Environmental Microbiology. 2005;71(7):3427-32.
141. Wu N, Rathnayaka T, Kuroda Y. Bacterial expression and re-engineering of *Gaussia princeps* luciferase and its use as a reporter protein. Biochimica et Biophysica Acta. 2015;1854(10 Pt A):1392-9.
142. Biotechnology A. *Gaussia* Luciferase Assay Kit - Luminometric 2022 [Available from: https://www.assaybiotechnology.com/Gaussia-Luciferase-Assay-Kit-Luminometric.
143. Wurdinger T, Badr C, Pike L, de Kleine R, Weissleder R, Breakefield XO, et al. A secreted luciferase for *ex vivo* monitoring of *in vivo* processes. Nature Methods. 2008;5(2):171-3.
144. Bovenberg MS, Degeling MH, Tannous BA. Enhanced *Gaussia* luciferase blood assay for monitoring of *in vivo* biological processes. Analytical Chemistry. 2012;84(2):1189-92.
145. Wille T, Blank K, Schmidt C, Vogt V, Gerlach RG. *Gaussia princeps* luciferase as a reporter for transcriptional activity, protein secretion, and protein-protein interactions in *Salmonella enterica* serovar Typhimurium. Applied and Environmental Microbiology. 2012;78(1):250-7.
146. Tannous BA. *Gaussia* luciferase reporter assay for monitoring biological processes in culture and *in vivo*. Nature Protocols. 2009;4(4):582-91.
147. Li J, Guo Z, Sato T, Yuan B, Ma Y, Qian D, et al. Optimized application of the secreted Nano-luciferase reporter system using an affinity purification strategy. PLoS One. 2018;13(5):e0196617.

148. England CG, Ehlerding EB, Cai W. NanoLuc: A Small Luciferase Is Brightening Up the Field of Bioluminescence. Bioconjugugate Chemistry. 2016;27(5):1175-87.
149. Stacer AC, Nyati S, Moudgil P, Iyengar R, Luker KE, Rehemtulla A, et al. NanoLuc reporter for dual luciferase imaging in living animals. Molecular Imaging. 2013;12(7):1-13.
150. Loh JM, Proft T. Comparison of firefly luciferase and NanoLuc luciferase for biophotonic labeling of group A *Streptococcus*. Biotechnology Letters. 2014;36(4):829-34.
151. McDougal LK, Steward CD, Killgore GE, Chaitram JM, McAllister SK, Tenover FC. Pulsed-field gel electrophoresis typing of oxacillin-resistant *Staphylococcus aureus* isolates from the United States: establishing a national database. Journal of Clinical Microbiology. 2003;41(11):5113-20.
152. Tong C. Screening for inhibitors of Staphylococcal Sortase A as novel anti-infective agents University of Nottingham; 2018.
153. Jensen RO, Winzer K, Clarke SR, Chan WC, Williams P. Differential recognition of *Staphylococcus aureus* quorum-sensing signals depends on both extracellular loops 1 and 2 of the transmembrane sensor AgrC. Journal of Molular Biology. 2008;381(2):300-9.
154. Lei MG, Cue D, Alba J, Junecko J, Graham JW, Lee CY. A single copy integration vector that integrates at an engineered site on the *Staphylococcus aureus* chromosome. BMC Research Notes. 2012;5:5.
155. Horsburgh MJ, Aish JL, White IJ, Shaw L, Lithgow JK, Foster SJ. sigmaB modulates virulence determinant expression and stress resistance: characterization of a functional rsbU strain derived from *Staphylococcus aureus* 8325-4. Journal of Bacteriology. 2002;184(19):5457-67.
156. Galac MR, Stam J, Maybank R, Hinkle M, Mack D, Rohde H, et al. Complete Genome Sequence of *Staphylococcus epidermidis* 1457. Genome Announcements. 2017;5(22).
157. Monk IR, Shah IM, Xu M, Tan MW, Foster TJ. Transforming the untransformable: application of direct transformation to manipulate

genetically *Staphylococcus aureus* and *Staphylococcus epidermidis*. mBio. 2012;3(2).

158. Miroux B, Walker JE. Over-production of proteins in *Escherichia coli*: mutant hosts that allow synthesis of some membrane proteins and globular proteins at high levels. Journal of Molecular Biology. 1996;260(3):289-98.

159. Biolabs NE. NEBuilder Assembly Tool 2022 [Available from: https://nebuilder.neb.com/#!/.]

160. Ubeda C, Olivarez NP, Barry P, Wang H, Kong X, Matthews A, et al. Specificity of staphylococcal phage and SaPI DNA packaging as revealed by integrase and terminase mutations. Molecular Microbiology. 2009;72(1):98-108.

161. Wider D, Picard D. Secreted dual reporter assay with *Gaussia* luciferase and the red fluorescent protein mCherry. PLoS One. 2017;12(12):e0189403.

162. Francis KP, Joh D, Bellinger-Kawahara C, Hawkinson MJ, Purchio TF, Contag PR. Monitoring bioluminescent *Staphylococcus aureus* infections in living mice using a novel luxABCDE construct. Infection and Immunity. 2000;68(6):3594-600.

163. Blower I, Tong C, Sun X, Murray E, Luckett J, Chan W, et al. *Gaussia* Luciferase as a Reporter for Quorum Sensing in Staphylococcus aureus. Sensors (Basel). 2020;20(15).

164. Murray EJ, Williams P. Detection of *agr*-Type Autoinducing Peptides Produced by *Staphylococcus aureus*. Methods in Molecular Biology. 2018;1673:89-96.

165. Brockmeier U, Caspers M, Freudl R, Jockwer A, Noll T, Eggert T. Systematic screening of all signal peptides from Bacillus subtilis: a powerful strategy in optimizing heterologous protein secretion in Gram-positive bacteria. Journal of Molecular Biology. 2006;362(3):393-402.

166. Mathiesen G, Sveen A, Brurberg MB, Fredriksen L, Axelsson L, Eijsink VG. Genome-wide analysis of signal peptide functionality in Lactobacillus plantarum WCFS1. BMC Genomics. 2009;10:425.

167. DeDent A, Bae T, Missiakas DM, Schneewind O. Signal peptides direct surface proteins to two distinct envelope locations of *Staphylococcus aureus.* Embo Journal. 2008;27(20):2656-68.

168. Yu W, Missiakas D, Schneewind O. Septal secretion of protein A in *Staphylococcus aureus* requires SecA and lipoteichoic acid synthesis. Elife. 2018;7.

169. Centre for Biological Sequence Analysis TUoD. SignalP-5.0 2020 [Available from: http://www.cbs.dtu.dk/services/SignalP/index.php.]

170. Nielsen H. Predicting Secretory Proteins with SignalP. Methods Mol Biol. 2017;1611:59-73.

171. Sawires Y, Gresham H. Improves probe-based assay for the quantification of *Staphylococcus aureus* virulene regulator, RNAIII, both *in vitro* and *in vivo.* Journal of Rapid Methods & Automation in Microbiology. 2008;16(2):140-53.

172. Liu M, Blinn C, McLeod SM, Wiseman JW, Newman JV, Fisher SL, et al. Secreted *Gaussia princeps* luciferase as a reporter of *Escherichia coli* replication in a mouse tissue cage model of infection. PLoS One. 2014;9(3):e90382.

173. Doyle TC, Burns SM, Contag CH. Technoreview: *In vivo* bioluminescence imaging for integrated studies of infection. Cellular microbiology. 2004;6(4):303-17.

174. Muthukrishnan G, Quinn GA, Lamers RP, Diaz C, Cole AL, Chen S, et al. Exoproteome *of Staphylococcus* aureus reveals putative determinants of nasal carriage. Journal of Proteome Ressearch. 2011;10(4):2064-78.

175. Dale NC, Johnstone EKM, White CW, Pfleger KDG. NanoBRET: The Bright Future of Proximity-Based Assays. Frontiers in Bioengineering and Biotechnology. 2019;7:56.

176. Yang Z, Weisshaar JC. HaloTag Assay Suggests Common Mechanism of *Escherichia coli* Membrane Permeabilization Induced by Cationic Peptides. ACS Chemical Biology. 2018;13(8):2161-9.

177. Weihs F, Wang J, Pfleger KDG, Dacres H. Experimental determination of the bioluminescence resonance energy transfer (BRET) Förster distances of NanoBRET and red-shifted BRET pairs. Analytica Chimica Acta X. 2020;6:100059.
178. Promega. NanoBiT® Protein:Protein Interaction System Technical Manual 2022 [Available from: https://www.promega.co.uk/resources/protocols/technical-manuals/101/nanobit-protein-protein-interaction-system-protocol/.]
179. Thoendel M, Kavanaugh JS, Flack CE, Horswill AR. Peptide signaling in the staphylococci. Chemical Reviews. 2011;111(1):117-51.
180. Götzke H, Kilisch M, Martínez-Carranza M, Sograte-Idrissi S, Rajavel A, Schlichthaerle T, et al. The ALFA-tag is a highly versatile tool for nanobody-based bioscience applications. Nature Communications. 2019;10(1):4403.
181. Otto M, Echner H, Voelter W, Gotz F. Pheromone cross-inhibition between *Staphylococcus aureus* and *Staphylococcus epidermidis*. Infection and Immunity. 2001;69(3):1957-60.
182. EMBL-EBI. Clustal Omega 2023 [Available from: https://www.ebi.ac.uk/Tools/msa/clustalo/.]
183. Olson ME, Todd DA, Schaeffer CR, Paharik AE, Van Dyke MJ, Büttner H, et al. *Staphylococcus epidermidis agr* quorum-sensing system: signal identification, cross talk, and importance in colonization. Journal of Bacteriology. 2014;196(19):3482-93.
184. Michel A, Agerer F, Hauck CR, Herrmann M, Ullrich J, Hacker J, et al. Global regulatory impact of ClpP protease of *Staphylococcus aureus* on regulons involved in virulence, oxidative stress response, autolysis, and DNA repair. Journal of Bacteriology. 2006;188(16):5783-96.
185. Zhang L, Ji G. Identification of a staphylococcal AgrB segment(s) responsible for group-specific processing of AgrD by gene swapping. Journal of Bacteriology. 2004;186(20):6706-13.

186. Reekes J. The synthesis and testing of novel analogues of (+)-ambuic acid as inhibitors of staphylococcal virulence: University of Nottingham; 2020.
187. Manolaridis I, Kulkarni K, Dodd RB, Ogasawara S, Zhang Z, Bineva G, et al. Mechanism of farnesylated CAAX protein processing by the intramembrane protease Rce1. Nature. 2013;504(7479):301-5.
188. Kermani AA. A guide to membrane protein X-ray crystallography. Febs Journal. 2021;288(20):5788-804.